RELATIONSHIPS BETWEEN MEASURED ROCK MAGNETIZATIONS AND INTERPRETATIONS OF LONGER WAVELENGTH ANOMALIES IN THE SUPERIOR PROVINCE OF THE CANADIAN SHIELD

A THESIS

PRESENTED TO

THE FACULTY OF GRADUATE STUDIES

UNIVERSITY OF MANITOBA

IN PARTIAL FULFILLMENT

OF THE REQUIREMENTS FOR THE DEGREE

DOCTOR OF PHILOSOPHY

BY

RICHARD L. COLES

AUGUST 1973

RELATIONSHIPS BETWEEN MEASURED ROCK MAGNETIZATIONS AND INTERPRETATIONS OF LONGER WAVELENGTH ANOMALIES IN THE SUPERIOR PROVINCE OF THE CANADIAN SHIELD

By

Richard L. Coles

A dissertation submitted to the Faculty of Graduate Studies of the University of Manitoba in partial fulfillment of the requirements of the degree of

DOCTOR OF PHILOSOPHY

ABSTRACT

Rock magnetism measurements have demonstrated that, in part of the western Superior Province of the Canadian Shield, definite long wavelength variations in shallow magnetizations are present. For a depth extent of several kilometres for these magnetizations, significant long wavelength contributions to the total magnetic anomaly field appear. In situations where prominent, large-scale, nearer-surface magnetic units are evident, filtering of selected wavelength anomalies may not be a suitable means of separating anomalies caused by deep sources. Provided sufficient information is available, subtraction of the field due to shallower units (both shorter and longer wavelengths) may be the more satisfactory method.

Remanent magnetizations in the sampled area are dominated by soft components, and significant reversed magnetizations are not found. In part of the area, remanent and induced magnetizations are comparable in magnitude. Several magnetic units have been delineated at the surface, which correlate with major geological units. Magnetic minerals are dominated by large-grained, optically homogeneous magnetite.

Model studies show that although the shallow magnetizations may produce a significant contribution, they do not account fully for the longer wavelength anomaly field in the sampled region, and deeper magnetizations are therefore implied.

The signal-to-noise ratios between various model magnetic units, in the frequency domain, are used with information theory concepts to indicate the reliability of detecting anomalies from particular magnetic units at depth, and to show how frequency filters may be selected to enhance signals from groups of anomaly sources, under given conditions of generalized magnetic structure.

Spectra and filtered anomaly maps show good correlations with major surface geological features in a part of the Superior Province. The spectra are compatible with broad shallow gradational magnetizations, but the presence of deeper magnetizations, which may be related to both shallow magnetizations and surface geology, is not excluded.

ACKNOWLEDGEMENTS

The writer wishes to express his many thanks to Dr. D.H. Hall of the Department of Earth Sciences, University of Manitoba, for his supervision, and for his advice and encouragement during the period of this work.

The author thanks Drs. P. Cerny, A.C. Turnock, and H.D.B. Wilson for their advice on opaque mineralogy.

The help and advice provided by Messrs. J. Coyle and B. Riley from Delro Industries Ltd. in the program of drilling is much appreciated. Mr. E.M. Shemeluk is thanked for his help as party chief in the field during difficult times, and the efforts of the several members of drilling crews are gratefully acknowledged.

This study would not have been possible without the contributions to construction of equipment from Messrs. Gerson and Uzat, and the Staff of the University Central Instrument Service.

The author wishes to thank the Manitoba Mines Branch and the Geological Survey of Canada for providing digitized data. Mr. P.H. McGrath kindly allowed the use of some of his digitized data and his filter program.

The work was made possible by support from the National Research Council and the Geological Survey of Canada. The author gratefully acknowledges the receipt of a University of Manitoba

Fellowship and a National Research Council Postgraduate Scholarship.

This work could not have been achieved without the encouragement and moral support of my wife. I would like to dedicate these efforts to the memory of my late father, whose keen interest in his total environment provided the initial stimulus.

TABLE OF CONTENTS

LIST OF ILLUSTRATIONS

LIST OF TABLES

LIST OF PLATES

CHAPTER I

INTRODUCTION

1.1 Statement

The existence of large-scale spatial anomalies in the magnetic field measured above the earth's surface has been known for some years. Anomalies of long wavelength have been found in data obtained both at low altitudes and up to satellite altitudes of several hundred kilometers. This present work is concerned mainly with the features observed in data measured at low altitudes (500 and 1000 feet; 0.15 and 0.3 km.), of wavelengths approximately in the range 12 to 1000 km. Such anomalies have been observed in maps produced by Bhattacharyya and Morley (1965), Morley et al. (1967), McGrath and Hall (1969), Hall and Dagley (1970), Hall (1971, 1973). Similar features have been observed in data obtained at other altitudes (e.g. Haines et al., 1971; Riddihough, 1972; Riddihough et al., 1973; Krutikhovskaya et al., 1973).

A major question is to what extent are long wavelength anomalies caused by deep-lying bodies, or to what extent by shallower more gradational variations in magnetization. It has been shown that in some areas, the long wavelength components of the anomalies cannot be explained by the effects of near-surface geological bodies (e.g. Hall, 1968; Krutikhovskaya et al., 1973). This must be examined more closely in relation

to other areas. The problem of the separation of effects of sources in different depth regions is one which is ever present. The extent to which this separation is possible must be considered in the light of prior knowledge of the region.

McGrath and Hall (1969) and Hall (1971, 1973) have produced maps of filtered magnetic anomalies over parts of Manitoba and Northwestern Ontario, within the Superior Province of the Canadian Precambrian Shield. The present work extends this coverage and considers the surface magnetizations in part of the previously mapped region.

The problems to be considered are: (1) what is the nature of the surface magnetizations; (2) to what extent do shallow magnetizations contribute to the regional anomaly field; (3) is it possible to obtain some indication of the reliability of detecting an anomaly which originates from a certain depth range, under given conditions; (4) to what extent do the longer wavelength anomalies correlate with major geological features.

1.2 Outline of Approach

The earth has been described as a noisy channel for information transfer (e.g. Sax, 1966). The information theory concept of the capacity of a noisy channel is used to demonstrate a way of estimating the likelihood of accurately detecting anomalies under various conditions. A method of selecting

possible filter bandwidths is also considered.

To obtain information on shallow magnetizations, magnetic property measurements are necessary on samples taken from the region. Details of the samplings and results are given in Chapters 3 and 4.

Using the detailed magnetization properties from the sampling area, modelling of the magnetic anomaly field is performed, using multiple application of discrete bodies, to gain some indication of relations between shallow magnetic units and longer wavelength anomalies in the region sampled.

By considering the spectrum of the anomaly field in several areas, together with filtered anomaly maps, a discussion of the anomalies in relation to major geologic features is given.

1.3 Geology

The area of study lies almost wholly within the Superior Province of the Canadian Shield (e.g. Wilson, 1971), Fig. 1.1. A small area in the extreme south-east is within the limits of the Southern Province as defined by Stockwell et al. (1970). Wilson (1971) has shown that the western Superior province may be subdivided into major blocks of contrasting geologic styles and metamorphic grades. The contrasting styles consist of a volcanic-sedimentary-granitic diapir type and a sedimentary gneiss-

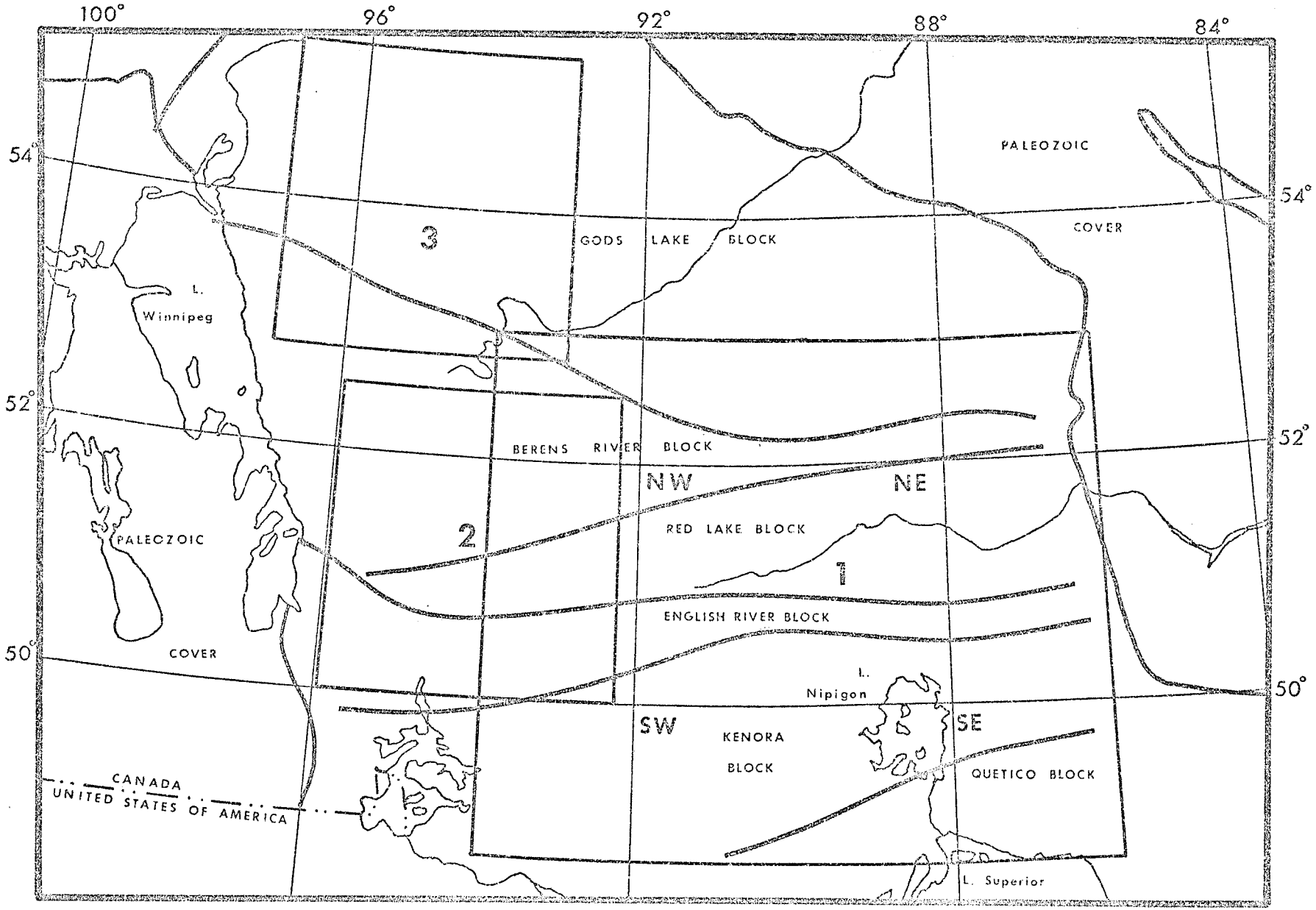

Figure 1.1 Location map, with major subdivisions of the western Superior Province (after Wilson, 1971).

concordant granitic intrusion type.

The Kenora block (Figure 1 of Wilson, 1971) underlies much of the southern part of the present area of study, and is characterized by volcanic and sedimentary belts intruded by granitic diapirs. The volcanic-sedimentary rocks are regionally metamorphosed mainly to the greenschist metamorphic facies. Higher grade metamorphism and partial breakup of the volcanic-sedimentary belts by increased granitic intrusion occur towards the east within the block. Metamorphism also increases in a zone along the northern edge of the block close to the English River Gneiss block.

The English River Gneiss block (Wilson and Brisbin, 1963; Wilson, 1971) is composed almost entirely of sedimentary gneiss and interlayered granitic rocks. Gneiss domes are prominent in the southern part of the block. Regional metamorphism is high grade, in the amphibolite or granulite metamorphic facies. The presence of anatectic melting is inferred from compositions of the granitic rocks (Dwibedi, 1966; McRitchie, 1971). Partial mobilization has occurred in the gneiss dome areas. In the west, the block widens and the metamorphic grade changes from amphibolite to greenschist facies in the centre of the block. To the north and south, higher grade metamorphism persists (McRitchie, 1971).

To the north, the Red Lake block (Wilson, 1971) is similar to the Kenora block both in style and metamorphic grade. The Berens River block (Wilson, 1971; Ermanovics, 1971, 1972) has been shown to be similar to the Red Lake and Kenora blocks, but to have undergone a greater intensity of granitic intrusion and to have experienced a higher grade of metamorphism.

The God's Lake block (Wilson, 1971) further to the north is complex in structure and may represent several narrower blocks. Volcanic belts are present at metamorphic grades intermediate between those of the Berens River and Kenora blocks. In addition, sedimentary-granitic gneiss occurs in two major elongated belts.

In the south-east of the area of study, a large region is covered by the Nipigon plate, which is of Helikian age, and consists of conglomerate, sandstone, shale, and dolomite, overlain by basalts with interbedded sedimentary rocks; these rocks overlap the Archean rocks of the Superior Province (Stockwell et al. 1970; Ontario Dept. of Mines, 1971). In the extreme south-east, partly overlain by the Nipigon plate and other younger rocks, is the Archean Quetico block (Wilson, 1971) which contains abundant sedimentary gneiss and migmatites.

Throughout the whole area, there are numerous late carbonatite-alkalic intrusions and some late granitic intrusions

(sometimes with associated mafic bodies). Prominent trends pervade the whole region. North-easterly, north-westerly and east-west trends are apparent in the volcanic-sedimentary belts. A system of late east-west faults accentuates this pattern.

A more detailed dicussion of some of the geological and geochemical features of the western end of the English River block is given in Chapter 3, which deals with the more localized study of the rock magnetizations in this region.

CHAPTER 2

INTERPRETATION TECHNIQUES

2.1 Introduction

In the interpretation of magnetic field data, there is the ever present problem of ambiguity. For a given magnetization, there is always a unique predictable magnetic field, but the reverse is not in general true; a given magnetic field may be caused by any one of an infinite number of different magnetization distributions. General discussions of the ambiguity of potential field interpretations have been given by Skeels (1947), and by Roy (1962), who also discussed the problem of ambiguity in relation to other geophysical methods.

In presenting interpretations of magnetic fields, one is relying on additional information such as the magnetic properties of rocks, geologic information (both compositional and structural), and geophysical information from other methods. In the more accessible near-surface, one may have quite a good knowledge of these features, but at greater depths, on the scale of total crustal thicknesses or greater, information is much more scanty and indirect.

An attempt is made here to indicate in a semi-quantitative manner to what extent reliance may be placed on an interpretation, in a particular magnetic environment. In recent years, several departures have been made from the traditional space-

domain deterministic approach of curve-fitting to individual anomalies. One of these, Fourier spectrum analysis, will be considered here, together with some basic ideas of information theory. Model fitting is still a very necessary part of the interpretation, but is done in the frequency domain in the present thesis and often in terms of many anomalies.

Traditional space-domain model-fitting to individual or groups of anomalies will be returned to later.

2.2 Information Theory and Probability

Sax (1966) has discussed the application of filter theory and information theory to the interpretation of gravity measurements. The development which follows is based in part on that of Sax, but considers a magnetic analog to this gravity case.

Seismic evidence (e.g. Hall, 1971), previous work in magnetic interpretations (e.g. Mundt, 1969) and geologic considerations suggest that a horizontally layered model for at least some areas of the earth's continental crust and upper mantle may be useful from the point of view of magnetic anomaly interpretation.

Consider a layered earth model, Fig. 2.1. A flat earth model is adequate for this purpose. Consider that the magnetic

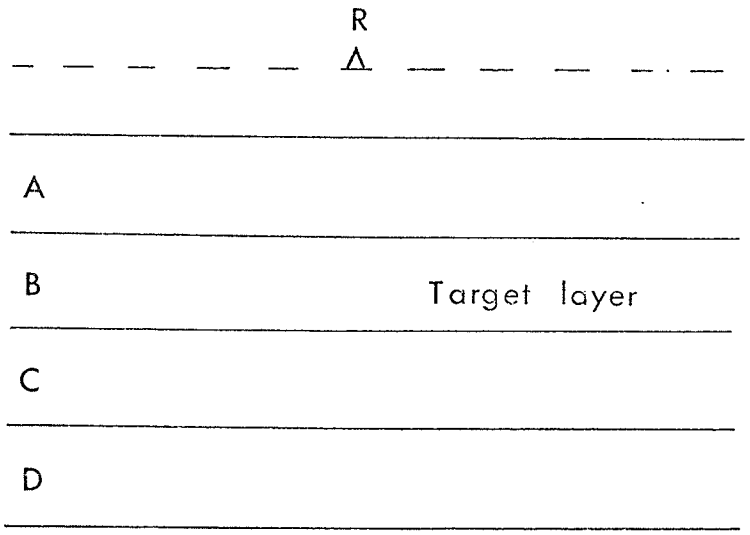

Figure 2.1 Simple layered Earth.

signals from sources in layer B, say, as measured at the surface, are of interest. The magnetometer R responds to the total field at each of its sites, being the summation of effects from sources in layers A, B, C, D, etc.

If B is the 'target layer', the part of the field due to sources in B is the 'signal', the rest is 'noise'. If the layers A, C, D, etc., were non-magnetic (or uniformly magnetized, of infinite extent), the field would unambiguously result from layer B, but if layers A, C, D, etc., also contain magnetic inhomogeneities, ambiguities are present. The extent of ambiguity is dependent on the noise levels, i.e. on the relative magnetization contrasts between the layers.

The message to be conveyed to the detector carries the characteristics of the magnetization at points within the layer. The encoding process which converts this information into a transmissable form is potential theory, which determines the field in space received by the detector (in the analog with conventional communication theory, space becomes the equivalent of time). The same message can be produced in an indefinite number of ways, i.e. the same field can be produced by the encoding of a multitude of different magnetization distributions from different parts of the sub-surface. If the message originates wholly from the target layer, it is considered 'signal', if from elsewhere, it is 'noise'.

In transmitting information over a communication channel there is a technical problem of devising a set of symbols suitable to the information and to the medium of the channel. For the present purposes, consider the contours of the two-dimensional map as the symbols; the channel here is the earth structure, magnetometer and the processing leading to the final map.

Assume for the moment that the symbols are independent of each other and are uncorrelated, (this is not strictly true for magnetic anomalies, as discussed below). An arbitrary succession of symbols is assumed capable of representing a certain message. The total duration T (in space) of a message is the sum of individual durations of the symbols contained in the message (i.e. the contour spacings). Consider all possible distinct messages having a total duration T, corresponding to all the possible combinations of the symbols, with no restriction, no correlation in the use of the different symbols (see below). Let the number of such distinct messages be N(T). All of the N messages of total duration T are considered as equally probable a priori.

In selecting one of the messages, information I is obtained,

$$I = k \ln N ,$$

where k is constant (Brillouin 1956).

The rate of transmission of information in the channel is I/T; this varies with T but approaches a limit as T becomes larger. The capacity of the channel is defined as

$$C = k \lim_{T \to \infty} \frac{\ln N(T)}{T}$$

(Brillouin 1956).

In the case of magnetic anomalies, there exist certain correlations and restrictions on the sequences of contours that are permissible. As a result, redundancies are present in the information and the channel capacity is reduced; in addition, the message length is not infinite, and the contours are not equally likely. The above definition then gives an upper limit.

Thus far the channel is noiseless. However, in the presence of noise, a given unperturbed signal may be displaced, and the noise may constitute a message identical with the 'signal' message.

The channel capacity in the presence of noise has been given by the Hartly-Tuller-Shannon formula (e.g. Brillouin 1956).

$$C \leq k \, \Delta\upsilon \ln (1 + P/Pn) \quad \text{bits/unit distance} \qquad (1)$$

where C is the channel capacity, k constant, $\Delta\upsilon$ the bandwidth

of the channel, P the average signal power and P_n the average noise power; the equality holds for white noise. If the quantities on the right hand side of equation (1) can be estimated, an upper limit for C may be determined.

Shannon (1963) showed that, for a noisy channel, the maximum rate of transmission for an arbitrary small frequency of errors is given by equation (1). If information is transmitted at rates greater than this, a definite positive frequency of errors occurs. Sax (1966) defined a resolving power $1/\Delta s$, to provide an estimate of the spatial density of contours which can resolve signals with minimum error.

The number of bits of information per symbol, assuming that contours (symbols) have equal a priori probability is

$$B = \log_2 \left(\frac{Imax - Imin}{\Delta I}\right) \text{ bits/contour} \qquad (2)$$

where ΔI is the contour interval, and Imax and Imin are the highest and lowest contours, respectively, in the map.

The resolving power is obtained from

$$\Delta S = \frac{B}{C} \geq \frac{1}{\Delta \nu} \cdot \frac{\log \left(\frac{Imax - Imin}{\Delta I}\right)}{\log (1 + P/P_n)} \text{ unit distance/contour} \qquad (3)$$

If the distance ΔA represents the mean distance observed between contours in an area of the map, one may consider that the number of false changes is proportional to $1/\Delta A$, and the number of true messages is proportional to $1/\Delta S$.

Thus, using an information channel approach, one may make estimates of probabilities of seeing true, uncontaminated anomalies from given depth ranges, assuming that there are anomaly sources there. This is not the same as a determination of the probability that a given anomaly originates from a certain layer, in the sense that even if the anomaly has been contaminated with noise, it may basically originate from that layer. What is implied, however, is that in many situations caution must be applied in the interpretation of anomalies attributed to certain levels in the sub-surface. An estimate of reliability, or 'confidence parameter' might be considered along with an interpretation.

A mathematical description is necessary for the model referred to above, and this is developed in Section 2.3. Examples of possible crustal magnetic situations are modelled in Section 2.4.

2.3 Theory of Model

Several versions of layered models in the frequency domain have been presented (e.g. Spector and Grant 1970, Naidu 1968, 1970),

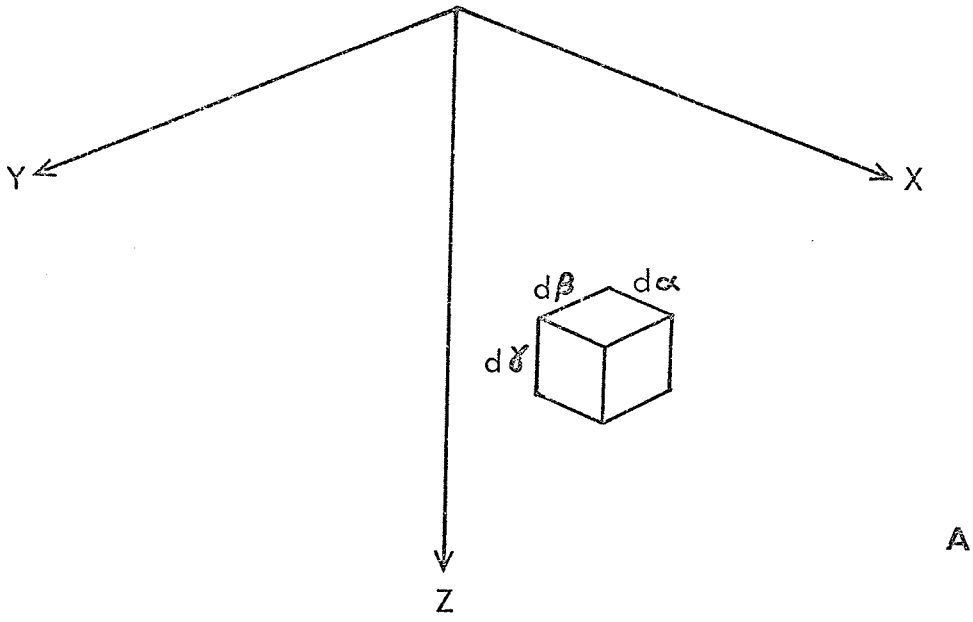

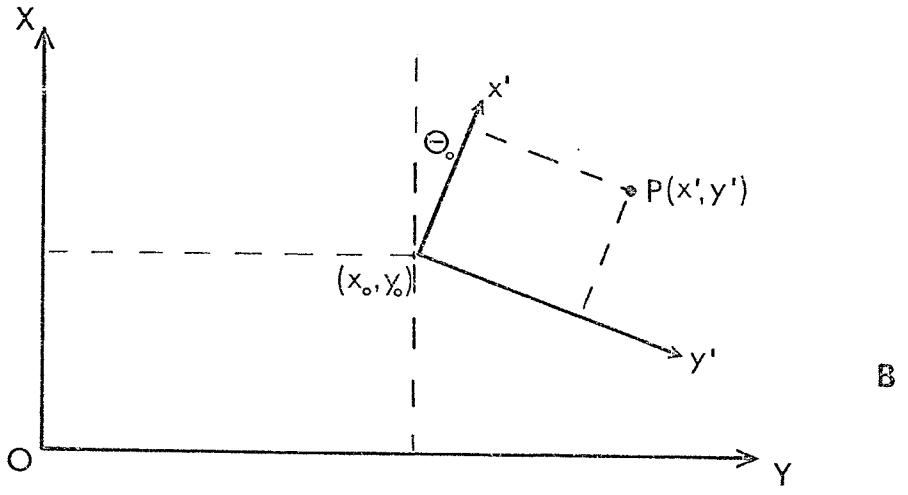

Figure 2.2 Coordinate axes for models.

but have been applied mainly to near surface magnetizations. The development which follows differs from those of Naidu in that magnetizations do not vary in the vertical direction, within a layer of finite thickness. In this respect, the model is analogous to that developed for the gravity case by Sax (1966); it also has some affinity to the model of Spector and Grant. The restriction of constant magnetization with depth within a layer may not be unreasonable geologically, in many areas.

Consider an element of magnetized material of volume $d\alpha d\beta d\gamma$ at position $(\alpha,\beta,\gamma,)$ relative to coordinate axes, as shown in Fig. 2.2(A). Let the polarization vector be characterized by the direction cosines L,M,N, and its magnitude by I.

The magnetic potential dV at a point P(x,y,z), distant r from the element is given by

$$dV = I \frac{\partial}{\partial s} \left(\frac{1}{r} \right) d\alpha d\beta d\gamma \qquad (1)$$

where

$$\frac{\partial}{\partial s} = L \frac{\partial}{\partial \alpha} + M \frac{\partial}{\partial \beta} + N \frac{\partial}{\partial \gamma}$$

The magnetic field at this point P in the direction (l,m,n) is

$$dF = I \frac{\partial^2}{\partial s \partial t} \left(\frac{1}{r} \right) \quad d\alpha d\beta d\gamma$$

where

$$\frac{\partial}{\partial t} = l \frac{\partial}{\partial x} + m \frac{\partial}{\partial y} + n \frac{\partial}{\partial z}$$

and

$$r^2 = (\alpha - x)^2 + (\beta - y)^2 + (\gamma - z)^2 \quad .$$

Consider I to be a function only of (α,β) within a layer of finite thickness, i.e. $I(\alpha,\beta)$. This suggests a system of variable sized, variable magnetization blocks within the layers, not unreasonable geologically. A further assumption that will be made is that the direction of magnetization can be considered constant throughout the layer. The layer will be considered infinite in extent, and between depths L_1 and L_2 below the plane of measurement ($z = 0$).

The total potential at the point $P(x,y,0)$ due to the layer is given by

$$V(x,y,0) = \int_{-\infty}^{\infty} \int_{-\infty}^{\infty} \int_{L_1}^{L_2} I(\alpha,\beta) \frac{\partial}{\partial s} \left(\frac{1}{r} \right) d\alpha d\beta d\gamma \qquad (4)$$

Consider the Fourier pair: (with u,v the component frequencies in x,y directions, respectively)

$$I(\alpha,\beta) = \frac{1}{4\pi^2} \iint_{-\infty}^{\infty} \hat{I}(u,v)\, e^{i(u\alpha + v\beta)}\, du\, dv \qquad (5a)$$

$$\hat{I}(u,v) = \iint_{-\infty}^{\infty} I(\alpha,\beta)\, e^{-i(u\alpha + v\beta)}\, d\alpha\, d\beta \qquad (5b)$$

Substituting for $I(\alpha,\beta)$ in equation (4),

$$v(x,y,0) = \frac{1}{4\pi^2} \iint_{-\infty}^{\infty} \iint_{-\infty}^{\infty} \hat{I}(u,v) \int_{L_1}^{L_2} \frac{\partial}{\partial s}\left(\frac{1}{r}\right) e^{i(u\alpha + v\beta)}\, d\gamma\, du\, dv\, d\alpha\, d\beta$$

$$= \frac{1}{4\pi^2} \iint_{-\infty}^{\infty} \hat{I}(u,v) \int_{L_1}^{L_2} \iint_{-\infty}^{\infty} \frac{\partial}{\partial s}\left(\frac{1}{r}\right) e^{i(u\alpha + v\beta)}\, d\alpha\, d\beta\, d\gamma\, du\, dv$$

$$= \frac{1}{4\pi^2} \iint_{-\infty}^{\infty} \hat{I}(u,v) \int_{L_1}^{L_2} \iint_{-\infty}^{\infty} \frac{\partial}{\partial s}\left(\frac{1}{r}\right) e^{i(u(\alpha-x)+v(\beta-y))}\, d\alpha\, d\beta\, d\gamma\, .$$

$$. e^{i(ux + vy)}\, du\, dv$$

Let $X = \alpha - x$, $Y = \beta - y$, $Z = \gamma - z$, and $k = (u^2 + v^2)^{\frac{1}{2}}$.

Then,

$$V(x,y,0) = \frac{1}{4\pi^2} \iint_{-\infty}^{\infty} \hat{I}(u,v) \int_{L_1}^{L_2} \left\{ -(Liu + Miv) \iint_{-\infty}^{\infty} \frac{1}{r} e^{i(uX+vY)}\, dX\, dY + \right.$$

$$+ \int_{-\infty}^{\infty}\int N \frac{\partial}{\partial\gamma}\left(\frac{1}{r}\right) e^{i(uX + vY)}\, dXdY \Bigg] d\gamma .\ e^{i(ux + vy)} dudv$$

$$= \frac{1}{4\pi^2} \int_{-\infty}^{\infty}\int \hat{I}(u,v) \int_{L_2}^{L_1} -(Liu + Miv + Nk).\frac{2\pi}{k} e^{-(\gamma - z)k} d\gamma .e^{i(ux+vy)} dudv \Bigg|_{z=0}$$

$$= \frac{1}{4\pi^2} \int_{-\infty}^{\infty}\int \hat{I}(u,v).(Liu + Miv + Nk).\left(\frac{+2\pi}{k^2}\right).\left(e^{-L_2 k} - e^{-L_1 k}\right).e^{i(ux+vy)} dudv$$

(6)

using the integral transforms given by Erdelyi (1954), in equations (7), p. 11, and equation (44), p. 56, and noting that $\nabla^2 V = 0$ in free space.

Consider the Fourier pair:

$$V(x,y) = \frac{1}{4\pi^2} \int_{-\infty}^{\infty}\int \hat{V}(u,v)\, e^{i(ux + vy)}\, du\, dv \qquad (7a)$$

$$\hat{V}(u,v) = \int_{-\infty}^{\infty}\int V(x,y)\, e^{-i(ux + vy)}\, dx\, dy \qquad (7b)$$

Comparing equations (6) and (7a), for z = 0,

$$\hat{V}(u,v) = -2\pi \hat{I}(u,v).(Liu + Miv + Nk).\left(e^{-L_1 k} - e^{-L_2 k}\right) / k^2 \quad .$$

The magnetic field is given by

$$F(x,y) = \frac{\partial}{\partial t} V(x,y)$$

and its Fourier transform by

$$\hat{F}(u,v) = -(liu + miv + nk).\hat{V}(u,v) \quad .$$

Thus,

$$\hat{F}(u,v) = 2\pi \hat{I}(u,v).(Liu + Miv + Nk).(liu + miv + nk).\left(e^{-L_1 k} - e^{-L_2 k}\right) / k^2 \qquad (8)$$

and for the energy spectrum,

$$\hat{P}(u,v) = \hat{F}(u,v).\hat{F}^*(u,v)$$

$$= 4\pi^2\, Q(u,v).\left[(Lu + Mv)^2 + N^2k^2\right].\left[(lu + mv)^2 + n^2k^2\right].\left[\frac{e^{-L_1k} - e^{-L_2k}}{k^2}\right]^2 \qquad (9)$$

$$= S(u,v).Q(u,v)$$

where

$$Q(u,v) = \hat{I}(u,v).\hat{I}^*(u,v)$$

The total spectral energy content observed at the surface $z = 0$ is obtained by linear summation of the energies from all the layers, assuming that the anomalies in the layers are statistically independent, and that cross-power terms are negligible.

Some assumptions regarding the spectra of magnetization variations in the layers must be made. Various forms have been proposed (Mundt 1969, Naidu 1968, Spector and Grant 1970).

Initially, one might consider the situation of a constant mean square magnetization contrast for all frequencies. However, trends which are apparent in the field spectrum may be related to magnetization trends in the various layers. The level of magnetization contrast may differ in different directions within

a layer.

Another simple form for the magnetization spectrum is

$$|\hat{I}| = A^2 \exp(-B^2 k) \quad , \quad k = |(u^2 + v^2)^{\frac{1}{2}}|$$

A is a measure of the magnetization intensity contrasts in the layer, and B is a measure of the spatial frequency distribution of the contrasts. B may be directional; however, unless independent information is available, assumptions must be made regarding the parameter B. Furthermore, the exponential factor is indistinguishable from the exponential factors in the earth structure terms. Thus, there is a certain latitude in the depth estimates, depending upon the nature of the magnetization spectrum used. For the surface layers, sampling of rocks may give an indication of spectral variations.

There is another form of model which may be more applicable to studies of large scale magnetic anomaly fields. In the above models, no explicit consideration has been given to the physical dimensions of the anomaly sources within a layer; merely attempts to describe the magnetization spectrum in simple mathematical form. It may be more useful to consider source sizes. In the layered model previously described, it is convenient to consider the sources as rectangular blocks of

various lateral dimensions, but constrained to have the depth extent of the layer. A simple rectangular distribution of lateral block sizes will be considered (cf. Spector and Grant 1970), (other distributions are possible, but more complex).

It is now possible to consider the spectral contribution of such sources. The Fourier transform of a single areal region of constant magnetization is of the form

$$A. \frac{2\ \sin(au)}{u} \cdot \frac{2\ \sin(bv)}{b}$$

where a, b are the half-lengths and u, v the frequencies in the x, y directions, respectively; A is an amplitude constant.

This transform, when squared and multiplied by the structure term for the layer (from equation 9) gives the field spectrum of the finite block of magnetization, for block axes coincident with x, y, z, axes.

Therefore, if a number of blocks of varying lateral dimensions are present, the areal magnetization spectrum will be of the form, for many blocks

$$\text{Ave} \left| A^2 \left(\frac{2\ \sin(au)}{u} \cdot \frac{2\ \sin(bv)}{v} \right) \right| \Bigg|_{a_{min}}^{a_{max}} \Bigg|_{b_{min}}^{b_{max}}$$

In addition, if the blocks are randomly oriented with

respect to the x, y axes, it is useful to express u and v as $k.\cos\theta$ and $k.\sin\theta$, where

$$k^2 = u^2 + v^2 \quad , \qquad \theta = \tan^{-1} v/u \quad ,$$

and averaging is also done over θ, from 0 to π radians.

Performing the averaging over the lateral dimensions gives the expression, for constant A,

$$\frac{\dfrac{1}{k^2\cos^2\theta}\left[2a - \dfrac{\sin(2ak.\cos\theta)}{k.\cos\theta}\right]_{a_{min}}^{a_{max}}}{(a_{max} - a_{min})} \cdot \frac{\dfrac{1}{k^2\sin^2\theta}\left[2b - \dfrac{\sin(2bk.\sin\theta)}{k.\sin\theta}\right]_{b_{min}}^{b_{max}}}{(b_{max} - b_{min})} \qquad (10)$$

This is then averaged over θ. This is done most readily by numerical methods; series expansions of the terms $\sin(2ak\cos\theta)$ and $\sin(2bk\sin\theta)$ are necessary for small values of a, b, and k.

These expressions are very significant, especially at lower frequencies, if the sizes of blocks depart from the infinitesimal. In fact, the simplest assumption of a flat magnetization spectrum is the case of zero lateral dimensions.

As examples, plots of the expression (10), averaged over θ also, are given in Fig. 2.3, for the special case where

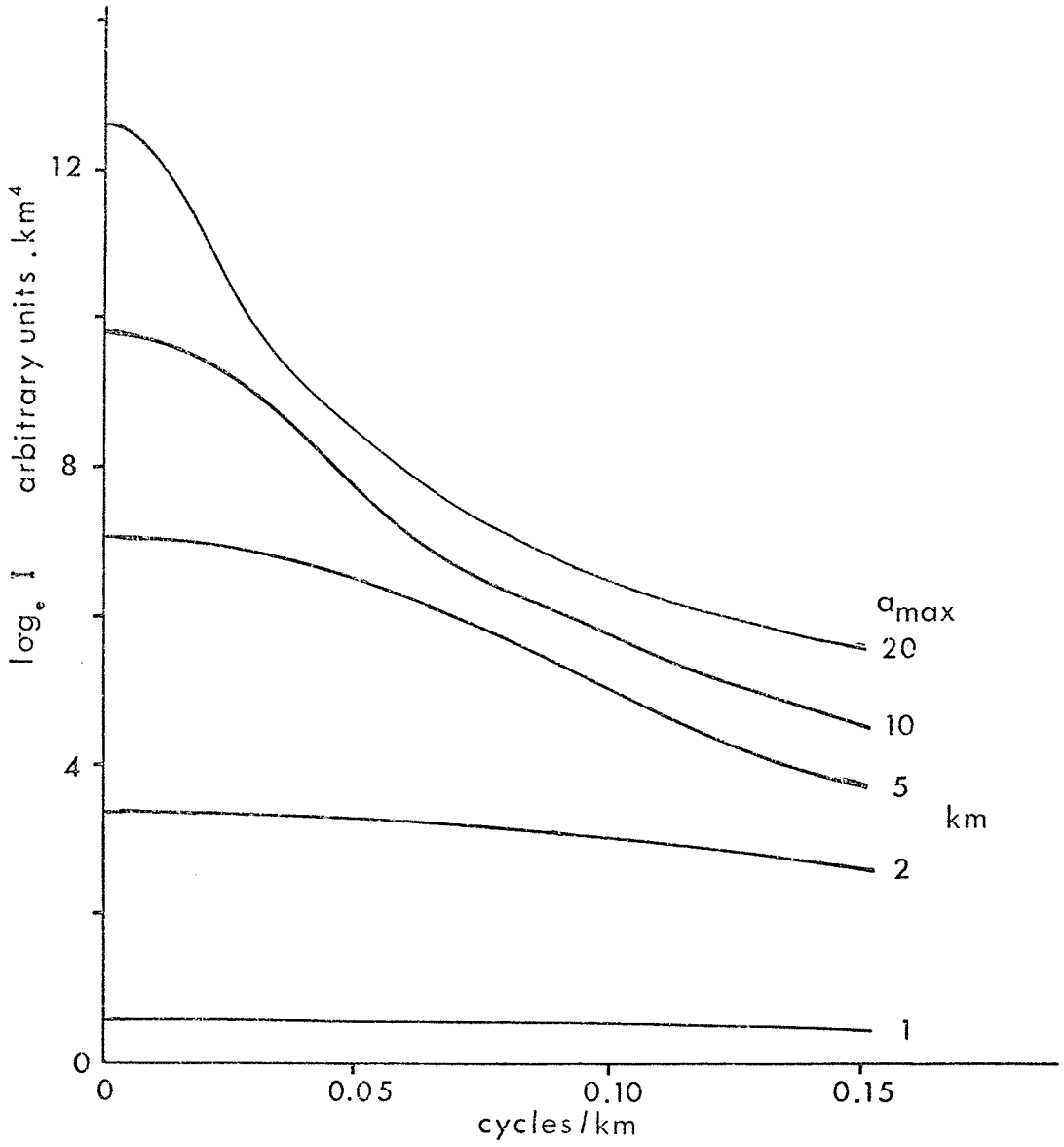

Figure 2.3 Effects of size on magnetization spectrum for randomly oriented rectangular blocks.

$a_{max} = b_{max}$, and $a_{min} = b_{min} = 0$, for several values of a_{max}. It is seen that for dimension limits less than about 1 km, the spectrum approaches zero slope for frequencies less than about 0.15 cycles/km. It is in this range of frequencies that one is mainly interested, in large scale studies. However, as the block sizes increase, the slope of the curves increases rapidly at lower frequencies, with a relative increase in amplitude, and the general amplitude of the whole curve increases. (These curves are similar to those given by Spector and Grant (1970), but differ by a factor containing the dimensions as a result of a different definition of parameters.) Therefore, when multiplied by the structure terms (equation 9), the effect of block size is very significant in shaping the anomaly field spectrum.

In other situations, block axes may be aligned, and it is useful then to consider the spectrum perpendicular to the strike direction, say in the x, u direction, for v = 0. In this case, expression (10) reduces to

$$\frac{\frac{1}{k^2}\left[2a - \frac{\sin(2ak)}{k}\right]_{a_{min}}^{a_{max}} \cdot \frac{4}{3}\left[b_{max}^2 + b_{max}b_{min} + b_{min}^2\right]}{(a_{max} - a_{min})} \qquad (11)$$

There are many other mathematical forms which might be used in this context. One other relatively simple one is the triangle pulse. This corresponds, physically, to a gradually increasing magnetization to a peak value over a certain distance, followed by a similar decrease beyond the peak. One might associate this with say, a gradational variation in magnetite content as a result of changing metamorphic grades in the rocks. In two-dimensions, consider a triangle form (of semi-dimension a) in, say, the x-direction, and a rectangular form (of semi-dimension b) in the y-direction. The spectral form for this is (Papoulis 1962)

$$\left(A \cdot \frac{4 \sin^2(au/2)}{au^2} \cdot \frac{2 \sin(bv)}{v} \right)^2$$

and again one could consider averaging over lateral dimensions, and θ, if necessary.

More complicated variations, in attempts to model changes in magnetization more closely, will in general result in very involved spectra, often not readily calculable. Furthermore, it may be that no real gain in information would be achieved.

Another simplifying assumption might be made in many cases. If, on the statistical scale, the effective directions of magnetization may be considered to be the same as, or close to,

that of the ambient field, then a 'reduction to the pole' may be made (Baranov 1957, Baranov and Naudy 1964, Spector and Grant 1970). In terms of equation (9), the transformation may be made in the frequency domain by changing the direction cosine terms. The expression for $\hat{p}(u,v)$ in equation (9) is divided by

$$\left[(L\cos\theta + M\sin\theta)^2 + N^2 \right]\left[(l\cos\theta + m\sin\theta)^2 + n^2 \right]$$

where

$$\theta = \tan^{-1}(v/u) \quad .$$

If the parameters for the layers are known or estimated from some other independent information, such as seismic data along with geologic interpretations and rock magnetic data, then these may be used to determine the contributions due to the different layers to the spectrum. The energies due to the layers other than the 'target layer' are summed to give the 'noise', and the ratio of this noise to the energy of the target layer gives the signal to noise ratios over the frequency range of interest.

It is possible to consider the same types of models in relation to spectra of real data, to obtain some estimates of possible structures and magnetizations. However, certain assumptions regarding the nature of the magnetization spectra

are again inevitable; some of these may be suggested by the form of the actual anomaly field.

To demonstrate the ways in which the several terms affect the shape of the theoretical spectrum, a series of standard curves is given. In Fig. 2.4, structure factors S(u,v) for layers of several depths and thicknesses are shown. This structure factor is the right hand side of equation (9), 'reduced to the pole' and excluding the factor Q(u,v). If the magnetization spectrum Q(u,v) is flat, these curves also represent the shape of the total anomaly field spectrum. These curves were calculated with an implicit amplitude factor of 10^4, which is to be considered if estimates of relative levels are needed in comparing spectra.

In Fig. 2.5, curves are given for magnetized blocks all aligned and viewed across-strike (v = 0), for b_{max} = 100 km. and b_{min} = 0. By reference to equation (11), different values for these parameters simply involve recalculation of a constant multiplicative factor. Effects of varying a_{min} for constant a_{max} are shown.

In Fig. 2.6, curves are shown for 'triangular' magnetization variations, all aligned, for v = 0, and b_{max} = 100 km., b_{min} = 0.

The curves are plotted in logarithmic form, and since

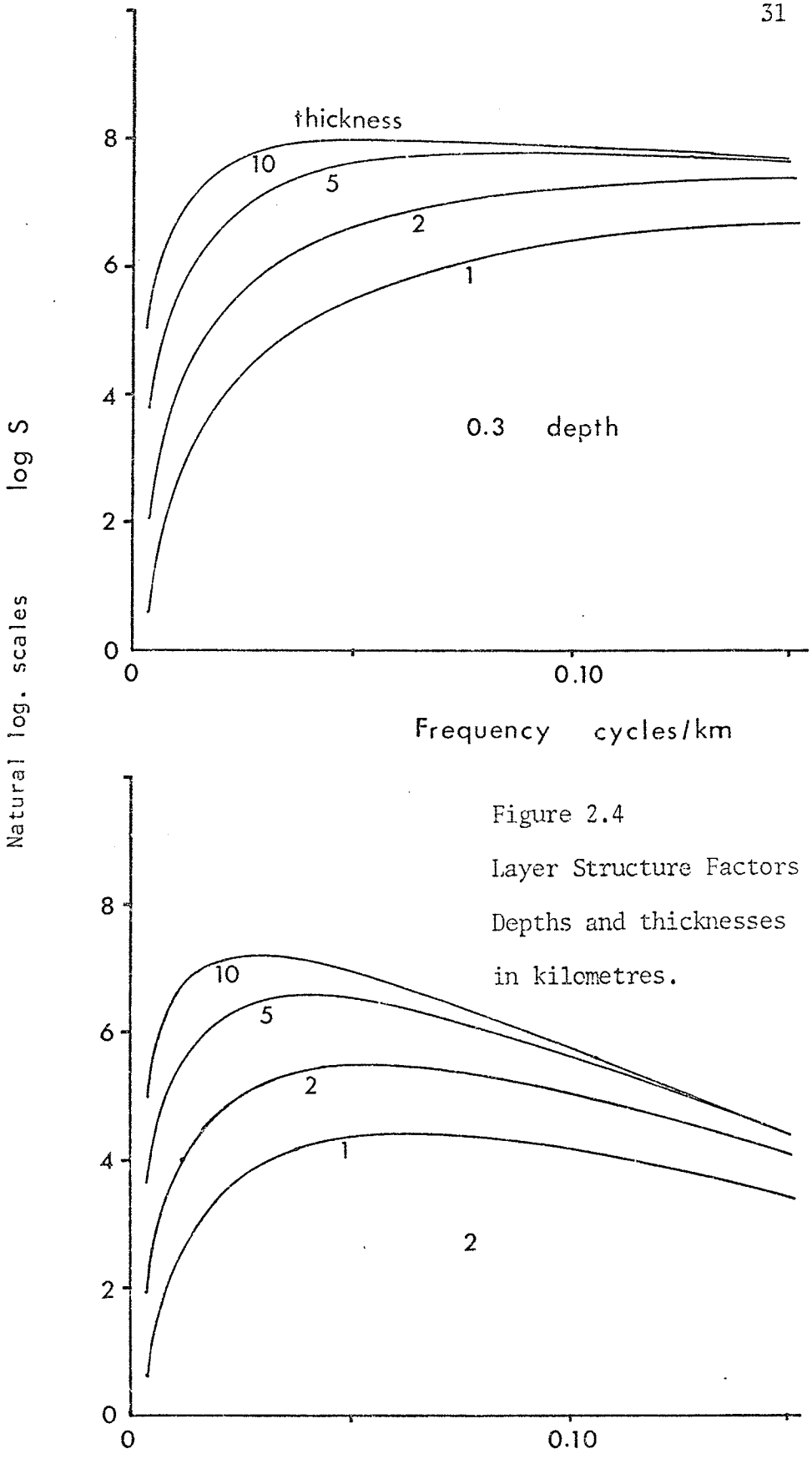

Figure 2.4

Layer Structure Factors

Depths and thicknesses

in kilometres.

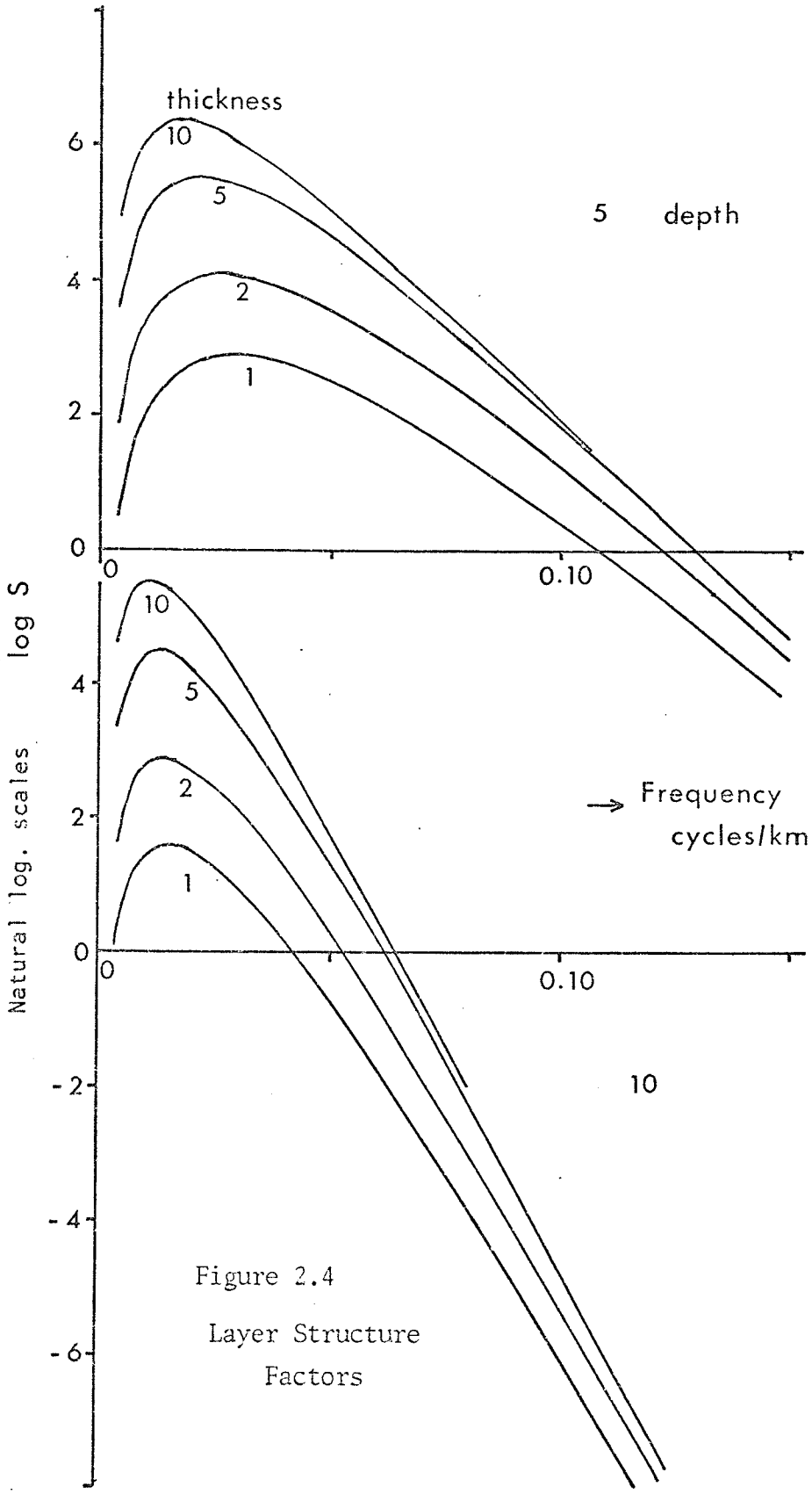

Figure 2.4

Layer Structure Factors

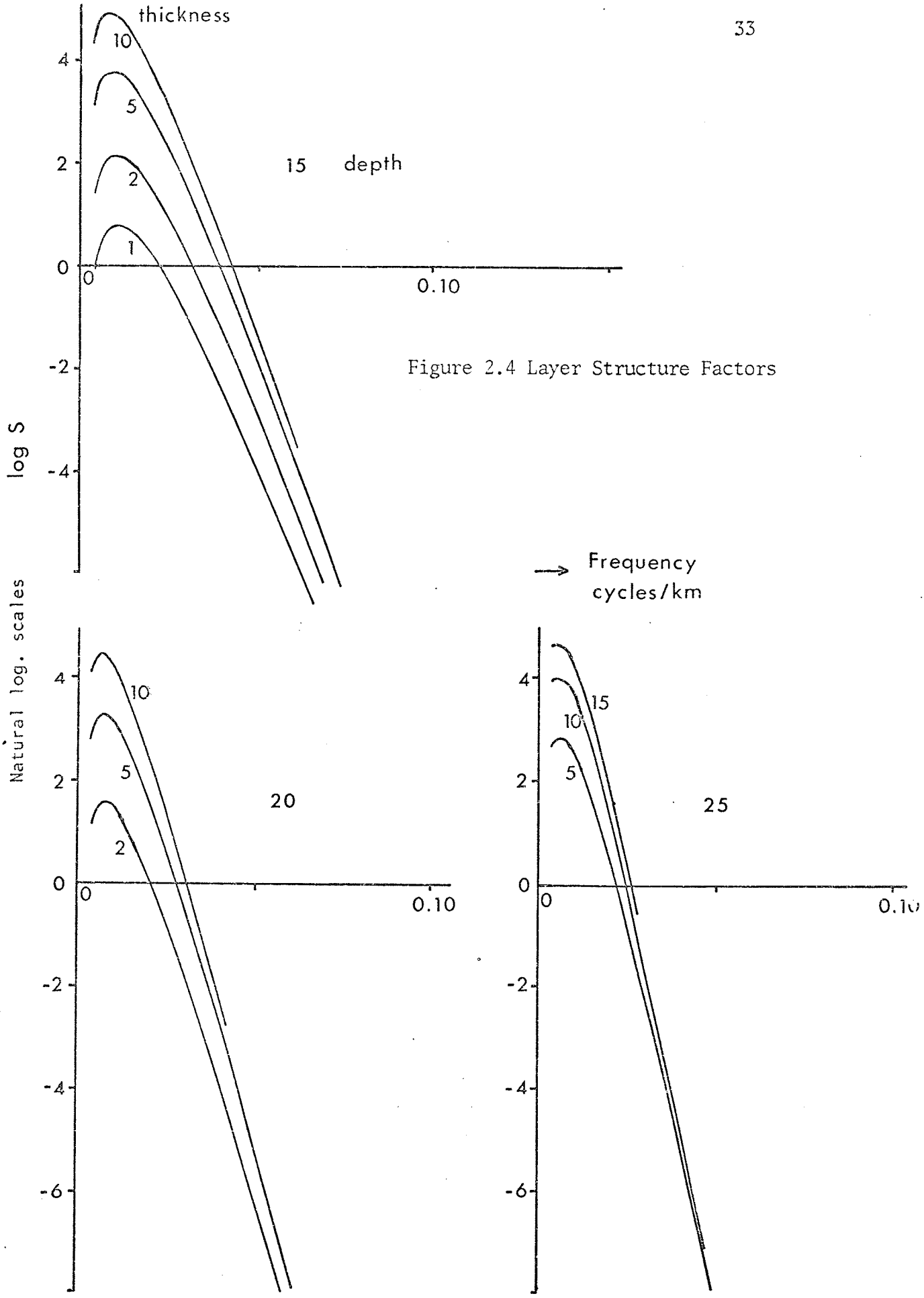

Figure 2.4 Layer Structure Factors

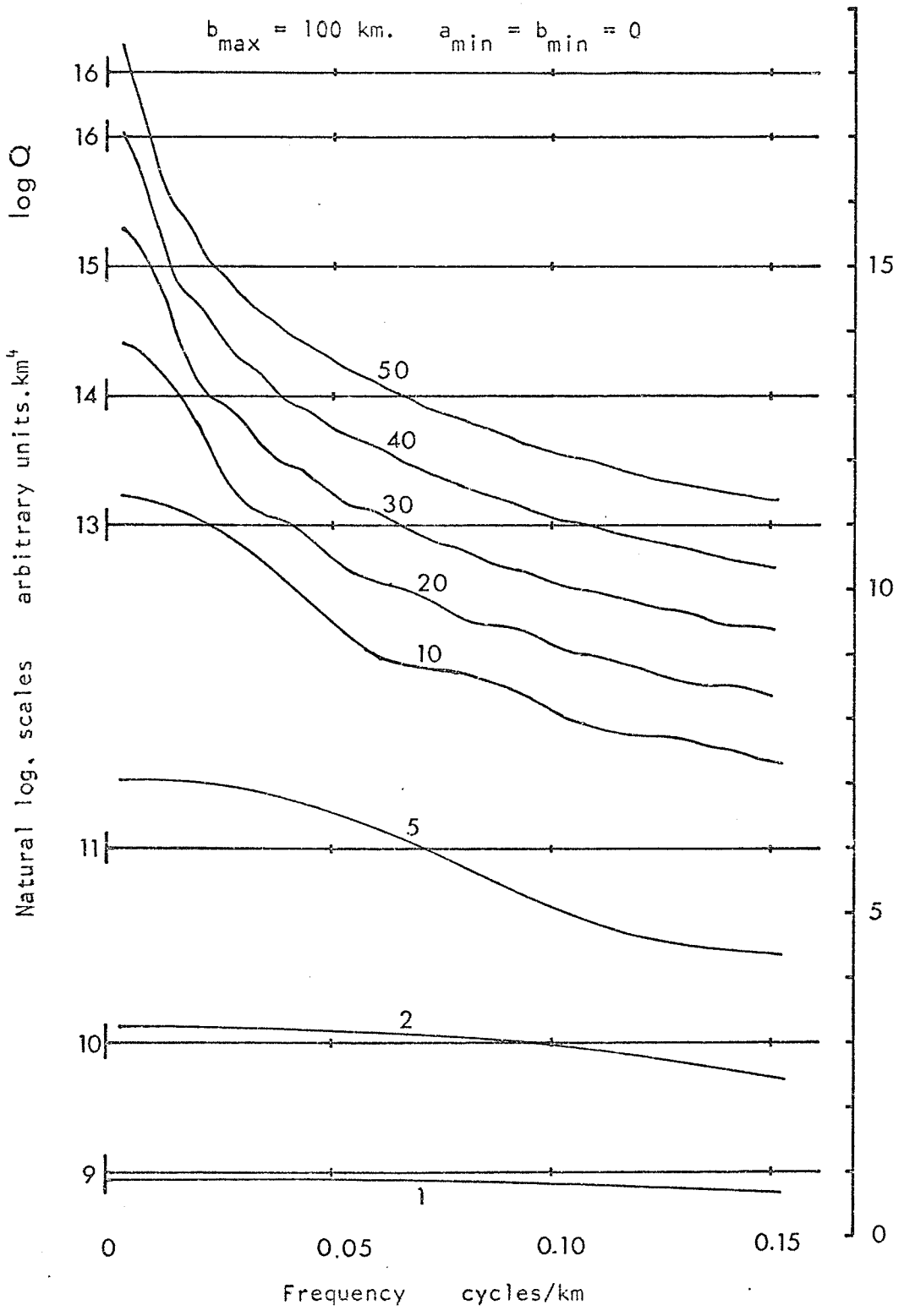

Figure 2.5 Magnetization spectra for rectangular block magnetizations - aligned.
Varying a_{max}. Dimensions in kilometres

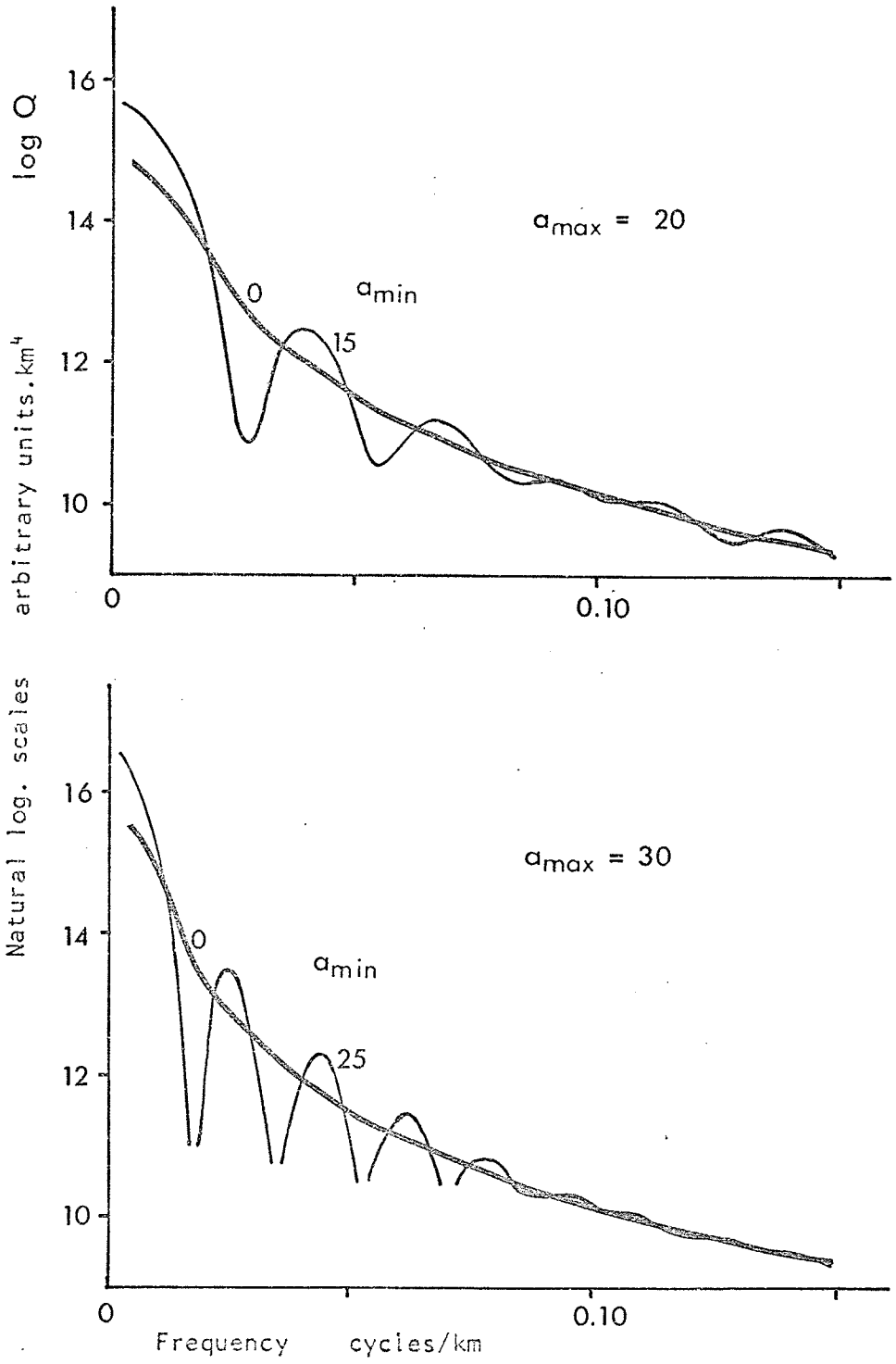

Figure 2.5 Magnetization spectra for rectangular block magnetizations - aligned. Effect of varying a_{min}. Dimensions in kilometres.

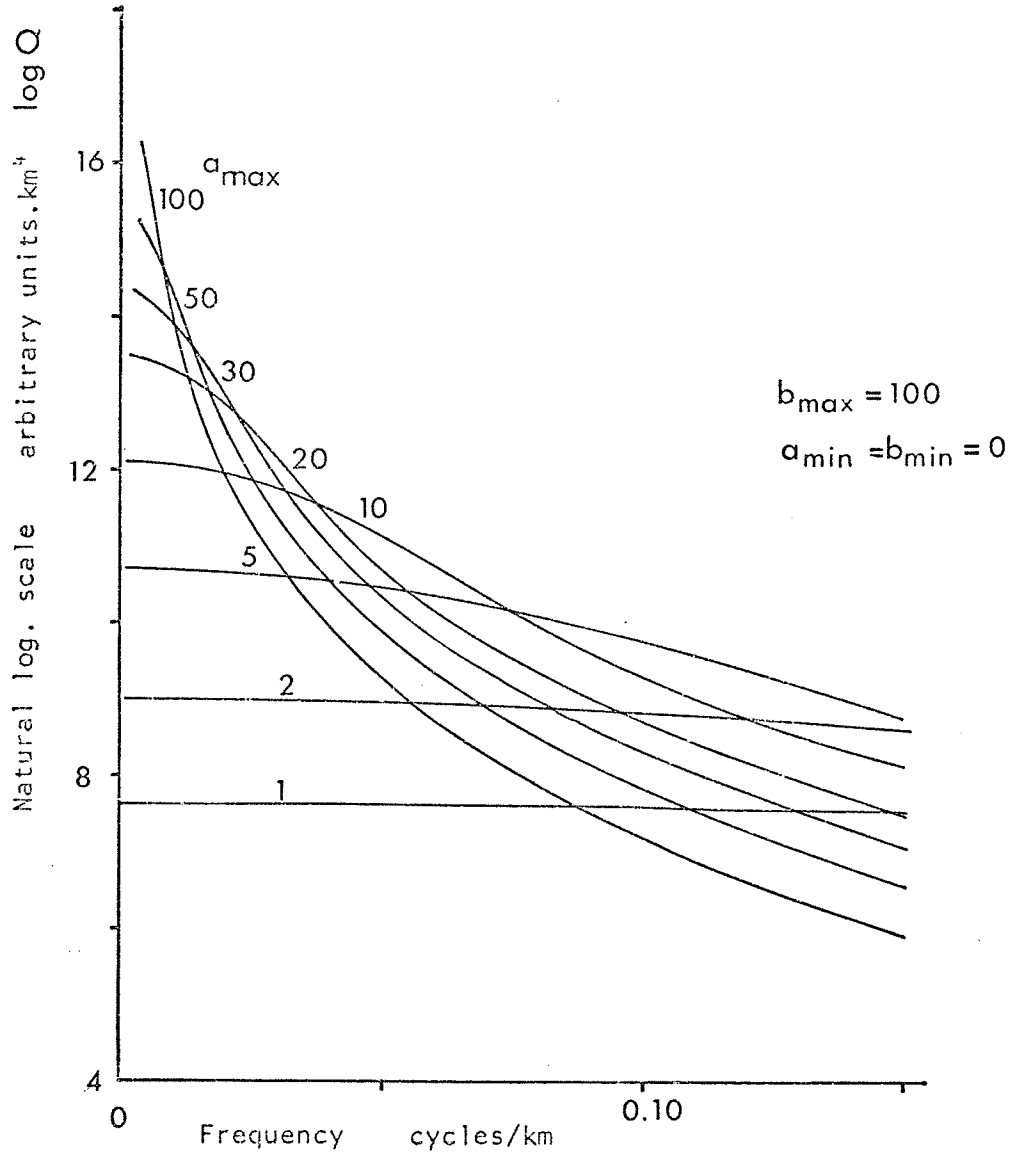

Figure 2.6 Magnetization Spectra for 'Triangular' gradational magnetizations - aligned. Effect of varying a_{max}. Dimensions in kilometres.

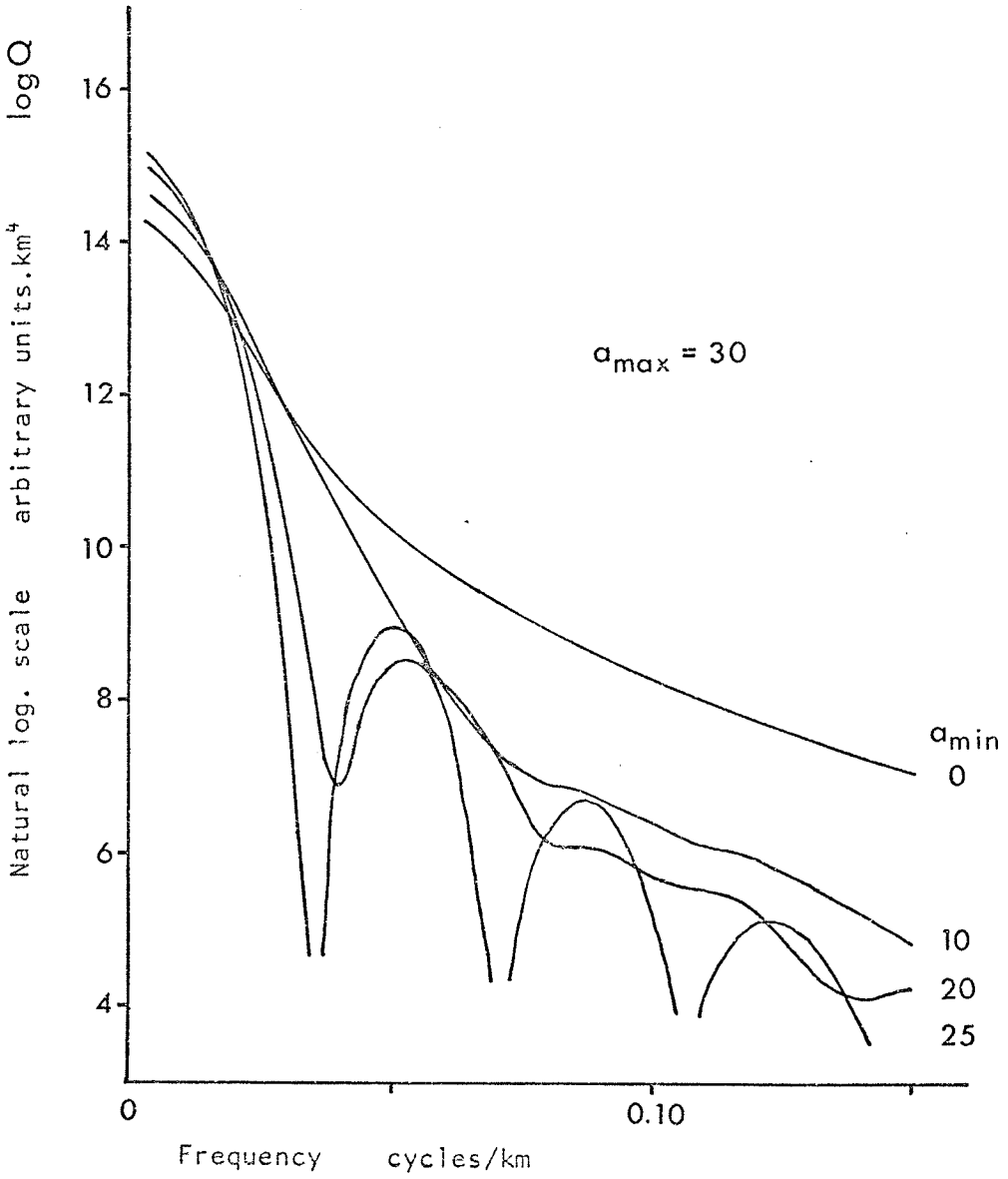

Figure 2.6 Magnetization spectra for 'triangular' gradational magnetizations - effect of varying a_{min}. Dimensions in kilometres.

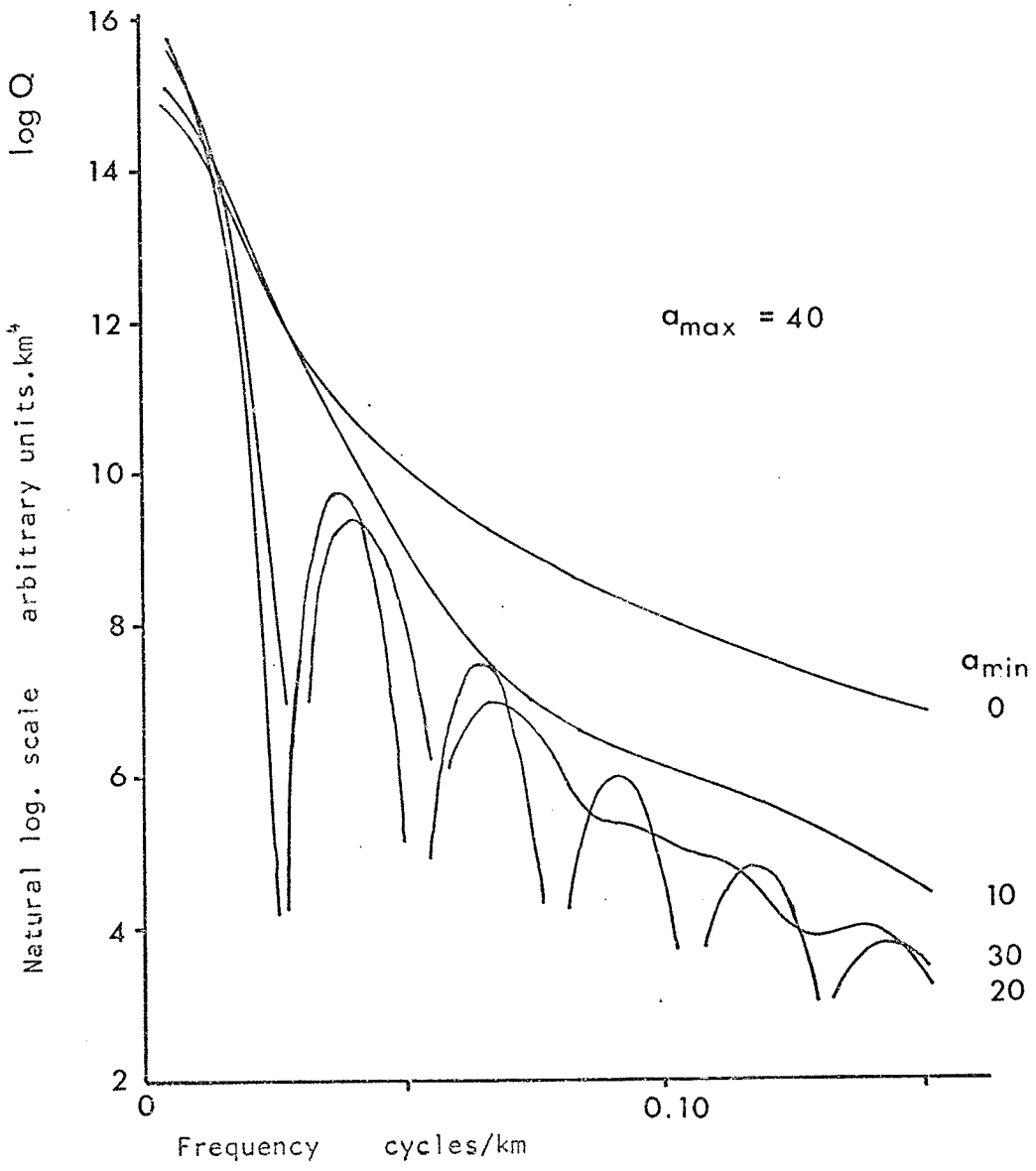

Figure 2.6 Magnetization spectra for 'triangular' gradational magnetizations - effect of varying a_{min}. Dimensions in kilometres.

the factors are multiplied in the equation (9), model spectra may be readily constructed by adding the values obtained from the curves in Fig. 2.4 to those taken from Figs. 2.3, 2.5, or 2.6, as appropriate, together with an amplitude factor.

Only a selection of curves is shown here. Curves for other parameter values have been, and may be, readily obtained from the basic formulas. A point to be noted is that the foregoing has assumed a sufficiently large number of individual bodies for the averaging to be valid. In some instances, this may imply a very large area of study. In attempting to interpret measured spectra, this may not be realizable, and the form of the models may require that the simple averaging be replaced by another process, such as straightforward summation of discrete body contributions - this, however, brings one back to individual interpretations. Experimentation with the formulas has indicated that, in most cases, a small statistical population does not drastically affect the curves shown, for semi-dimension 'a' less than about 50 km. in the frequency range of interest here.

2.4 Models

As an example, consider the situation of a two-layer crust, with structure on the interface between the layers. For a simple model, assume that the structures are laterally

equidimensional, vertical-sided, and all of the same depth extent. In this way, a three-layer magnetic model, of the type discussed in section 2.3, may be considered, if a magnetic contrast exists between the crustal layers.

Suppose that both upper and lower layers are magnetized, and further that in the main body of each layer, only small (semi-dimension less than 1 km.) magnetization blocks are present, and that they are randomly distributed, i.e. a near flat spectrum of magnetization exists.

In the 'interface' layer, the blocks of magnetization will alternate between the mean magnetization of the upper layer and that of the lower layer, but consider that the structures are much larger, say of the order of 20 to 30 km. semi-dimension. Superimposed on this one should also consider the smaller scale variations within the major structural blocks, appropriate to the upper or lower layers.

The problem now is the choice of magnetization levels. It has been proposed (e.g. Hall 1973) that the deeper crust may be more highly magnetic than the upper crust. Consider a model with mean upper layer magnetization 1000 units, and for the lower layer 5000 units. The block magnetizations will be taken to be of the same order as the mean levels.

There is also the question of how many blocks in each

layer. This must be considered in order to compare the layer spectra. The average number per unit area is sufficient for this estimate. To allow for random lateral distribution, one might assume a mean separation of 10 times the mean block semi-dimension in a layer. Thus, for upper and lower layers, the mean semi-dimension is 0.5 km. and the mean separation 5 km. The number per unit area may be taken as $0.04/km^2$. For the middle layer, with larger structural blocks of mean semi-dimension 25 km., the mean separation is taken as 250 km., and the number per unit area is $1.6 \times 10^{-5}/km^2$.

The number per unit area is multiplied by the square of the block magnetization and by the total area of concern to give the amplitude factor in the spectrum. For the upper layer, the factor is $0.04 \times 10^6 = 4 \times 10^4$ $units^2/km^2$; for the lower layer, 10^6 $units^2/km^2$; and for the middle layer, 256 $units^2/km^2$.

There are indications (Chapter 4, following; Puranen et al. 1968) that the standard deviation of magnetization is of the order of the mean, for surface layers, but the model distribution above would result in lower standard deviations (lower relative dispersions) for upper and lower model layers, i.e. the layers are more homogeneous magnetically. This might be so for lower layers, but in any case, the number of, or intensities of magnetization of, blocks in a layer may be greater than those considered above.

Consider relief on the crustal interface of the order of 4 km., from 18 to 22 km., with the base of magnetization at 35 km. The spectral contributions of the individual block units, with others yet to be discussed, are shown in Fig. 2.7. The total model spectra are given in Fig. 2.8. The signal-to-noise ratios for the several units are shown in Fig. 2.9.

A similar model, but with a different form of block structure in the middle layer, is also worthy of note. Consider a series of long blocks of order 160 to 200 km. length and 30 to 40 km. width, all aligned in the strike (lengthwise) direction; consider that they may be fairly closely spaced along strike, but may be separated by the order of 250 km. between centres, across strike. On average, assume 1 block in an area 250 km. x 250 km., and the number per unit area becomes $1.6 \times 10^{-5}/km^2$.

For these simple models, the signal-to-noise ratios show that to isolate the anomalies caused by the structures on the interface between upper and lower crust, the application of a filter of short wavelength cut-off of about 40 km. will provide good separation from shallower effects. The power contribution of other deep sources is very small in comparison.

Using the ideas of section 2.2, an estimate of the resolving power of the filtered map for such anomalies may be

Magnetic Unit	Depth to Top	Thickness	Amplitude	Semi-dimensions amax / amin	bmax / bmin
	km.	km.	units^2/km^2	km.	km.
1	0.3	17.7	$4x10^4$	1	1
				0	0
2	0.3	6.0	16	50	120
				30	80
3	6.0	10.0	712	10	10
				5	5
4	18.0	4.0	256	20	100
				15	80
5	18.0	4.0	256	30	30
				20	20
6	18.0	4.0	$1x10^6$	1	1
				0	0
7	22.0	13.0	$1x10^6$	1	1
				0	0

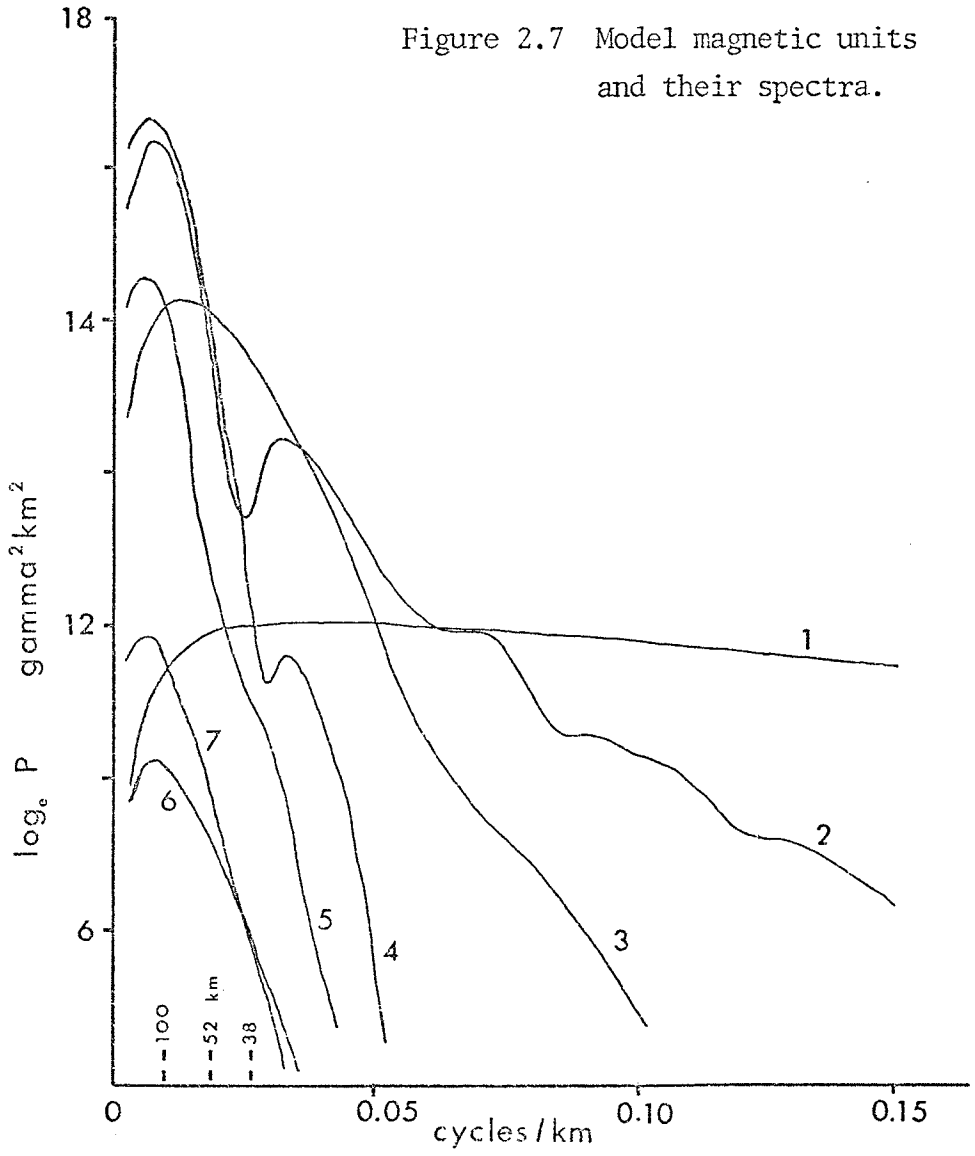

Figure 2.7 Model magnetic units and their spectra.

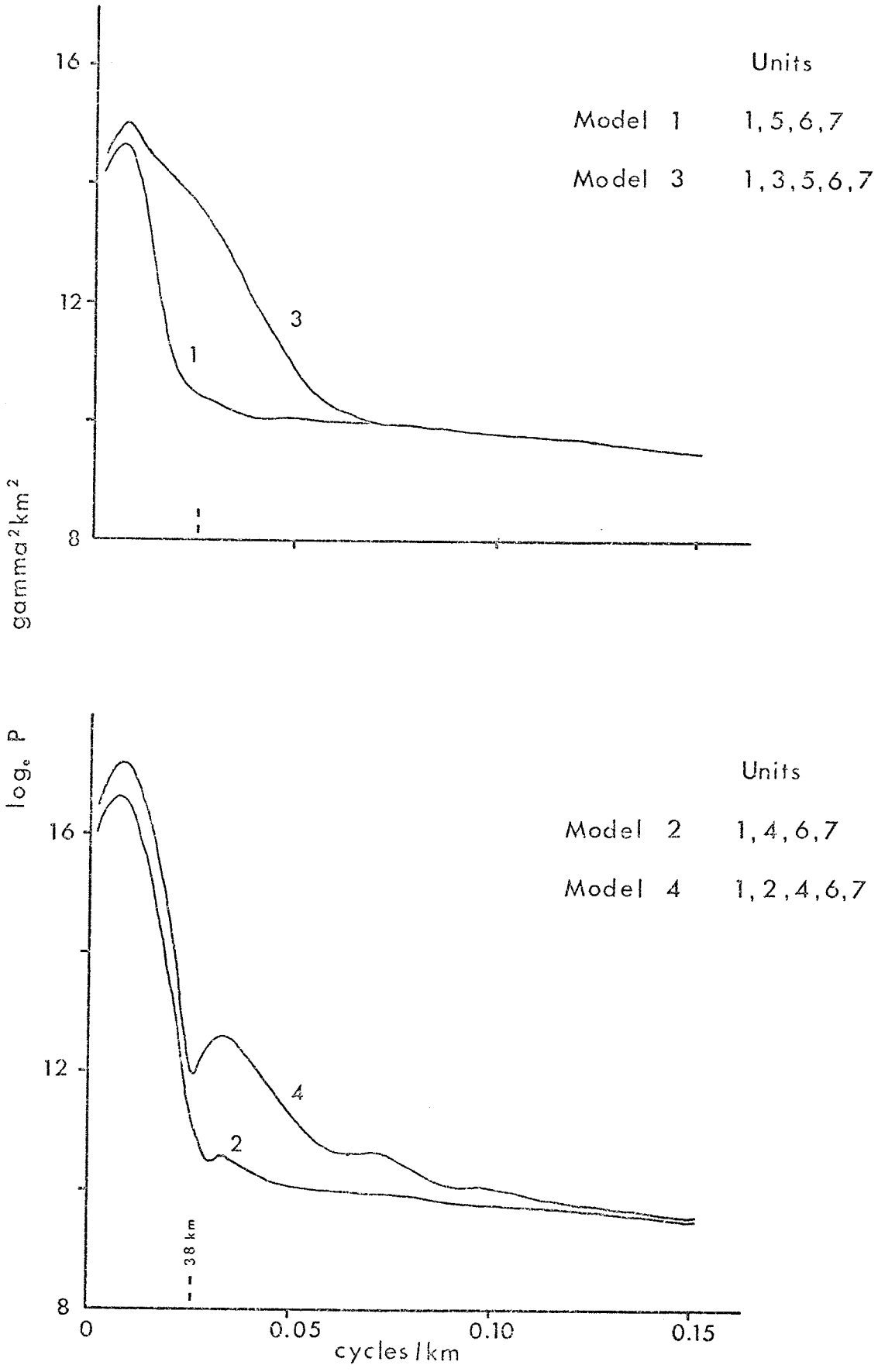

Figure 2.8 Model Spectra.

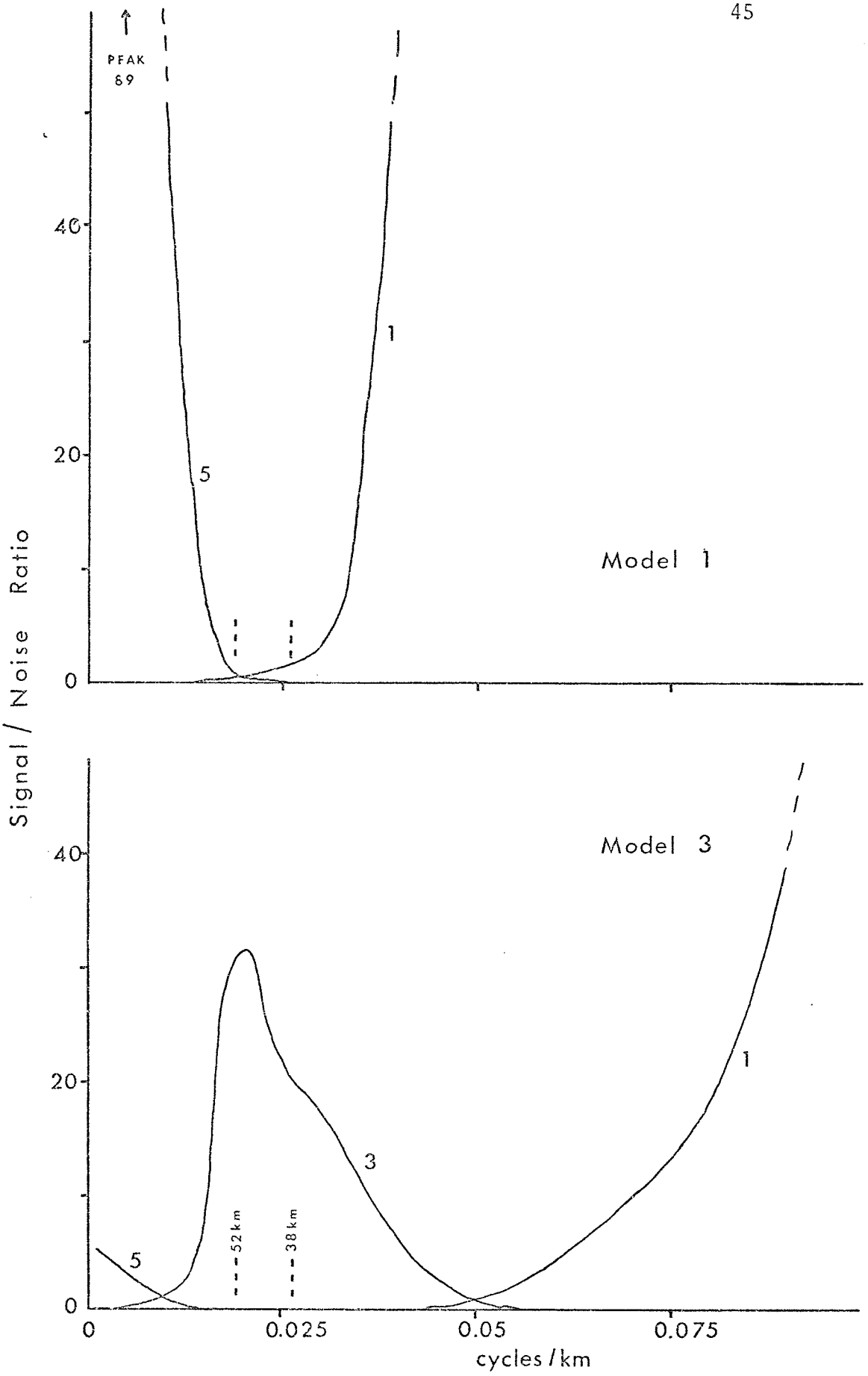

Figure 2.9 a Signal-to-noise ratios for models.

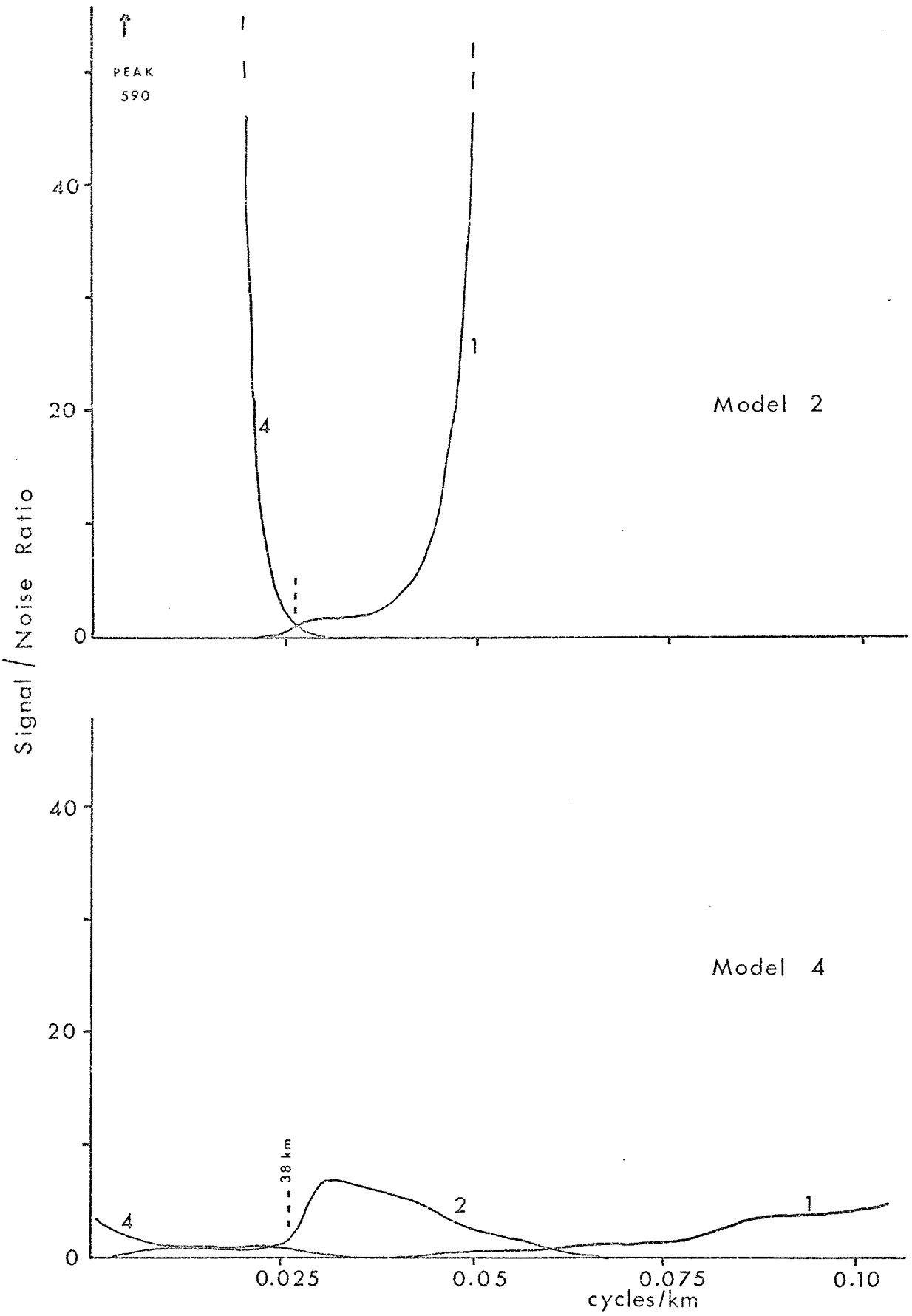

Figure 2.9b Signal-to-noise ratios for models.

obtained, with an estimate of the probability, or 'confidence parameter', for accurate, uncontaminated detection. The mean signal-to-noise ratio in the appropriate filter bandwidth is obtained; this, with the filter bandwidth, map contour interval, and map contour range will give the resolving power, ΔS. The mean actual contour spacing is estimated from the map, ΔA. The probability is obtained from

$$P = \frac{1}{1 + \Delta S/\Delta A} \quad .$$

For example, when filtered at 38 km. cut-off wavelength, for a contour interval of 200 gammas (nanotesla), contour range of 800 gammas and assuming a typical contour spacing of 10 km., the 'confidence parameter', or probability, for Model 1 is 0.39, and for Model 2 is 0.51. In these cases, the estimated resolving power is approached; detailed comparisons are not possible, in view of the underlying assumptions, but a high reliability is indicated here.

This is not always the case, however; a simply structured upper layer is unlikely. A large variety of models might be considered in this context, but two additional ensembles will be given as examples.

Model 3 reconsiders the Model 1 situation, but with an additional ensemble of blocks, of semi-dimensions 5 to 10 km.,

say, at depth 6 to 16 km.; suppose the same relative spacing as before, 1 block in 75 km. x 75 km. or $1.78 \times 10^{-4}/km^2$. Consider that these blocks have magnetizations of 2000 units, the amplitude factor being 712, Fig. 2.7.

Model 4 reconsiders Model 2, with near-surface shallow large scale structures within which the magnetization increases linearly to a peak and then decreases again, in the cross-strike direction; the semi-dimensions range from 30 to 50 km. cross-strike and 80 to 120 km. along strike. All the blocks are aligned along the major trend direction. Assume 1 block in 250 km., and an amplitude factor of 16, for a peak magnetization of 1000 units, Fig. 2.7.

The chances of accurately detecting anomalies due to the structures on the original crustal interface are now much reduced; for the same specifications as before, the 'confidence parameters' are now, for Model 3 - 0.12, and for Model 4 - 0.13. However, for Model 3 especially, the 38 km. filter cut-off is not optimum. For a cut-off at, say, 52 km., there is slightly better enhancement of the required anomaly group, but still a decrease in 'confidence parameter' to 0.10, owing to the loss of higher frequency content; i.e. a further loss of information from the map. There is still a major contribution from the unwanted sources. To filter further to, say, 100 km. cut-

off, will remove the effects of these sources, but as seen from Fig. 2.7, will seriously affect the required anomaly form by removing major components from the wanted anomalies. For Model 4, further filtering will not improve the situation.

These examples, though of course artificial and somewhat arbitrary, serve to indicate the relative contributions to the total spectrum of different groups of magnetized blocks. Geologic structures similar to these forms are not uncommon, at least at the surface and, by inference and by geophysical interpretations of various kinds, probably at depth.

The examples also show how possible filter bandwidths for attempting to enhance particular groups of anomalies might be obtained, and from these, estimates of the 'confidence parameters' that observed anomalies are true manifestations of the effects of sources in a particular group.

It is evident that when there is considerable magnetic structure in the upper layers, the chances of observing a true anomaly from a deeper region become small. Therefore, in any interpretation, it is of the utmost importance that the possible contributions of surface and near-surface magnetization distributions be accounted for, before interpretations in terms of deep distributions may be taken too far.

2.5 Model-fitting using Multiple Right Rectangular Prisms

Many simple geometric forms have been used to model magnetic anomaly fields; some of these, e.g. the vertical or inclined two-dimensional slab, have been particularly successful, especially in near-surface exploration work. More complicated shapes are often difficult to model exactly. Talwani (1965) has produced a method for three-dimensional arbitrary shapes involving the stacking of polygonal laminas. A simple geometric form which is readily applicable to multiple close-spaced stacking in order to model anomalies, and also to allow for variations of magnetization, is the finite-depth vertical-sided rectangular prism. Bhattacharyya (1964) gave the expression for the total field anomaly at a general point above such a prism. Sharma (1966) has also produced formulas for the prism, giving vertical and horizontal anomaly fields. Sharma applied his method to the computation of anomalies caused by bodies of arbitrary shape, and to the discussion of demagnetization effects.

In the present work, Bhattacharyya's expression has been programmed for the computer, so that the total anomaly field caused by a number of prisms, of differing sizes and polarizations, may be calculated, Bhattacharyya's expression is analytical, and similar in form to that of Sharma. Remanence

effects are included in both cases.

The expression for the total field anomaly for an infinite depth vertical-sided prism is given by equation (10) from Bhattacharyya (1964),

$$\frac{F(x,y,0)}{I_p} = \left[\frac{\alpha_{23}}{2} \log\left(\frac{r_0-\alpha_1}{r_0+\alpha_1}\right) + \frac{\alpha_{13}}{2} \log\left(\frac{r_0-\beta_1}{r_0+\beta_1}\right) - \alpha_{12} \log(r_0+h) \right.$$

$$- 1L \tan^{-1}\left(\frac{\alpha_1\beta_1}{\alpha_1^2+r_0h+h^2}\right) - mM \tan^{-1}\left(\frac{\alpha_1\beta_1}{\beta_1^2+r_0h+h^2}\right)$$

$$\left. + nN \tan^{-1}\left(\frac{\alpha_1\beta_1}{r_0h}\right) \right] \Bigg|_{\alpha_1}^{\alpha_u} \Bigg|_{\beta_1}^{\beta_u} \qquad (12)$$

where α_u, β_u are the upper limits and α_1, β_1 the lower limits of α_1 and β_1 respectively; α, β and γ are the coordinates of the volume element $d\alpha d\beta d\gamma$ in the prism (Fig. 2.2) and $(x,y,0)$ are the coordinates of the measurement point.

$$\alpha_1 = \alpha - x$$

$$\beta_1 = \beta - y$$

$$r_0^2 = \alpha_1^2 + \beta_1^2 + h^2$$

The direction cosines for the polarization vector are L, M, N and for the direction of the earth's total field, 1, m, n.

The inclination and declination of the earth's field are I_o and D_o, respectively, and for the polarization vector, I and D, respectively.

$$\alpha_{12} = Lm + Ml , \qquad \alpha_{13} = Ln + Nl, \qquad \alpha_{23} = Mn + Nm .$$

To obtain the field for a prism of finite vertical extent, the fields due to two bodies of infinite vertical extent, with depths equal to the top and bottom, respectively, of the finite prism are calculated. The latter field is subtracted from the former to give the resultant field of the finite prism.

Details of the computer program BLOCK are given in Appendix 3. It is designed for the computation of the resultant total field anomaly caused by any number of right prisms, with arbitrary dimensions, directions and intensities of magnetization.

The direction of the x-axis is chosen perpendicular to the predominant strike direction of the anomaly field. The declinations of the geomagnetic field and prism polarizations are measured relative to the x-axis. The facility in the program whereby a previously computed field may be modified is useful in modelling a complex anomaly pattern; a simple prism configuration may be used initially, with refinements added

subsequently. In many cases, the main features of an anomaly field are represented by a few large prisms, whereas in order to model the smaller scale detail, numerous smaller blocks may be needed. Herein lies a possible disadvantage in the use of right prisms; if the depths of the prisms are small, unwanted residuals may occur at the edges of the prisms. However, with careful choice of prism dimensions, these effects may usually be made insignificant. In modifying an anomaly field, in order to subtract an unwanted prism, the prism is given a polarization of opposite sign to that previously carried. It is important, where prisms overlap, to ensure that the correct polarization is obtained in the overlap (a summation effect will occur).

This type of modelling is very useful in attempting to explain anomalies caused by deep-seated bodies (Hall, 1973), where residuals at block boundaries become less evident. It is also valuable in modelling anomaly fields in terms of known surface magnetizations (see Chapter 5).

As indicated by Sharma (1966), demagnetization effects may become significant at high magnetization intensities; also interactions between the secondary fields of blocks and the geomagnetic field may have a significant effect on the anomalies generated. However, in the application to large-scale crustal anomaly modelling, these are not likely to be impor-

tant factors.

2.6 A Least Squares Approach to Finite Prisms

In appropriate circumstances, space-domain model-fitting of magnetic anomalies by the least squares techniques has some advantages over other interpretation methods; many data values are used to obtain the solution and the solution may take into account known geological or geophysical constraints. The least-squares method which has been used here in modelling right rectangular finite prisms to total field anomalies is due to Marquardt (1963), described in its application to two-dimensional structures by Johnson (1969) and McGrath and Hood (1970). McGrath and Hood (1973) have used a combination of Marquardt and Powell algorithms in a different approach to the problem.

Consider that the total magnetic anomaly $\hat{T}(i,j,)$ is measured at a constant level of Z and at the points (x,y) denoted by (x(i), y(j), i = 1, 2.....m; j = 1,2.....n).

The condition of least squares requires that

$$S(\xi_1,\xi_2,\ldots\xi_q) = \sum_{i=1}^{m}\sum_{j=1}^{n}\left[\hat{T}(i,j) - T(\xi_1,\xi_2,\ldots\xi_q,x(i),y(j))\right]^2 \qquad (13)$$

be a minimum. T is the theoretical computed field and the

symbol ξ_q denotes a general parameter of T.

The expression for T (equation 12) is nonlinear with respect to the body parameters. T is expanded in a first order Taylor series about initial values of the ξ parameters to obtain an approximation of equation (13). The approximate sum of squares is minimized for the changes of the parameter values; the ξ values are corrected and the process is iterated with the hope of minimizing S. The least square values of the changes $\Delta\xi_q$ are given, following Johnson (1969), by the p linear equations,

$$\sum_{i=1}^{m}\sum_{j=1}^{n}\sum_{l=1}^{p}\left(\left|\left(\frac{\partial T(\xi,x(i),y(j))}{\partial \xi_k}\right)\left(\frac{\partial T(\xi,x(i),y(j))}{\partial \xi_l}\right)\right|_{\xi=\xi_{(r)}} .(1 + \delta_{kl}\lambda)\Delta\xi_l\right)$$

$$= \sum_{i=1}^{m}\sum_{j=1}^{n}\left(\left|\frac{\partial T(\xi,x(i),y(j))}{\partial \xi_k}\right|_{\xi=\xi_{(r)}} . \left[\, T(\xi_{(r)},x(i),y(j)) - \hat{T}(i,j)\right]\right) \qquad (14)$$

where k = 1,2,.....p

and $\delta_{kl} = 1$ if k = l; otherwise $\delta_{kl} = 0$

The value of parameter ξ at the r iteration is denoted by $\xi_{(r)}$.

It is seen from equations (14) that the first derivatives of the expression for T with respect to all the variables are required. The analytical determination of the derivatives of (12) is tedious but quite straightforward, and many of the terms involved are very similar to one another. Particular terms are often used in several different derivatives. As a result of this, the programming of the method could be simplified considerably.

The form of equation (12) as used in this section is modified slightly from that described in the previous section. In order to permit the direction of the x-axis to vary in relation to the sides of the prism, x and y are replaced with the forms

$$x' = (y - y_0) \sin\theta_0 + (x - x_0) \cos\theta_0$$
$$y' = (y - y_0) \cos\theta_0 - (x - x_0) \sin\theta_0$$

where x_0, y_0 are the coordinates of the centre of the top of the block relative to the fixed x, y axes, and x', y' are coordinates of points relative to axes parallel to the prism sides. θ_0 is the angle between the x-axis and the x'axis (Fig. 2.2).

Also,

$$\alpha_1 = -\alpha_u \quad , \quad \beta_1 = -\beta_u \quad .$$

The subtraction involved to produce a finite depth extent is also incorporated into the derivative calculation. The parameters which are incorporated into this part of the solution are the following: length, width; depth to top, depth to bottom; x-coordinate of centre, y-coordinate of centre, angle between x-axis and x'-axis; declination and inclination of polarization, intensity of polarization.

One of the problems encountered in model fitting is the correct choice of base level. In the present method, this choice is made separately from the solution for the other parameters. The kernel of the computer program is the iterative solution for the ten prism parameters. This kernel is itself incorporated into an iterative scheme using a selection of base level values. The best fit choice is taken from the series of sets of parameter values obtained for the various base levels. A facility for constraining parameters within certain ranges is also available.

The anomaly field is fed to the program, along with initial guesses of parameter values and a sequence of control codes to define which parameter values, if any, are to remain unchanged in the solution. The lowest, incremental, and highest base levels to be tried are also given.

Many of the terms required in the calculation of the

derivatives are independent of x and y; these are computed first. Following this, further terms, the full derivatives and then the total field are obtained. The normal equations are set up, and a solution obtained. Any suitable subroutine may be used for this solution. The parameters are modified according to the solutions of the normal equations, and a check on the sum of squares of differences is made. If this has decreased, λ (equation 14) is reduced and the process repeated. If the sum of squares has not decreased, λ is increased and the process repeated using the previous set of parameters, until a decrease in the sum occurs or the iteration limit is exceeded.

When all variable parameters have ceased changing significantly, a procedure is available to restart the iterative process, which normally moves to an improved convergence.

A good choice of initial parameters is sometimes important but in many cases, some of the parameters, such as the coordinates of the prism centre and angle to the x-axis may be suggested by the anomaly field. Good choice of base level increments is often very important, but usually a repeat run centred around a previous 'best fit' base level will produce a satisfactory result.

A choice of an acceptable minimum value of the sum of squares of errors should be made. When this limit, or the iteration limit,

is reached, execution will stop.

The facility whereby parameters may be constrained within limits is often useful as an interpretation technique. Independent information, geological or geophysical, may be available, which enables restrictions to be placed on one or more of the parameters.

The method is most reliable when the anomaly to be interpreted is isolated, as applies in all interpretation methods. However, provided that anomalies do not overlap to a great extent, it is successful. Careful choice of the extent of the grid of data values is sometimes very important.

The most critical inter-parameter relationship appears between the base-level, depth to bottom, and intensity of polarization. It was for this reason that the base-level iteration was kept separate from the rest. The human interpreter is very important in the selection of optimum values of these parameters.

Details of the use of the computer program PRISM are given in Appendix 3.

CHAPTER 3

ROCK MAGNETISM - INTRODUCTION

3.1 Rock Magnetism and Anomaly Interpretation

A knowledge of the magnetization characteristics of rocks is essential to the meaningful interpretation of magnetic anomaly fields measured above, or below, the earth's surface. The more that is known about the rock magnetizations in a locality, the more valuable may be anomaly interpretations. As discussed in the previous chapter, interpretation of magnetic field data is inherently ambiguous and any information from other sources helps to reduce the uncertainties. A knowledge of the spatial variations of magnetizations, of the relative contributions of induced and remanent magnetizations to anomaly fields, of the directions of resultant polarizations, is of great value in using some of the recent semi-statistical interpretation methods, and also, of course, in any interpretation method.

Several studies of the distributions of and variations in the magnetizations of rocks and their relations with magnetic anomaly systems have been made. Puranen et al. (1968) studied the induced, and some remanent, magnetizations of a large number of samples from Precambrian rocks in the Virrat area of Finland. Kornik (1968) has conducted a survey of induced and remanent magnetizations of samples from sites scattered over a large area of Precambrian rocks in northern Manitoba and Saskatchewan. Hall (1968) made an extensive survey of rock magnetism in the Kenora area, northwestern Ontario, and

showed some correlations between regional magnetic anomalies, surface magnetizations, and deeper magnetizations. Lidiak (1973) has studied the relations between magnetic anomalies and rock types in selected basement areas of the United States.

In attempting to assess the significance of surface rock magnetizations to the production of magnetic anomalies over a large region, several types of measurement should be made on a representative series of rock samples from the region.

To determine the effect of induced magnetization, magnetic susceptibility measurements are needed. To determine the effects of remanent magnetization, a more complex series of measurements is necessary. The magnitudes and directions of the remanences of the samples are needed, and in addition, a knowledge of the stabilities of these remanences must be obtained by a series of tests involving progressive demagnetization of the remanences.

A rock unit cannot contribute significantly to an anomaly field if its magnetic minerals are above their Curie temperatures. Accordingly, this parameter should be determined. The comparison of the measured Curie temperatures with estimates of temperatures in the earth's crust and upper mantle is useful.

To further define the significance of magnetizations and the relations of magnetic minerals with other minerals of the rocks, microscope studies are also very useful.

3.2 Location and Details of Field Work

In order that the study of the rock magnetizations in Southeastern Manitoba could be made, a program of rock sampling has been carried out. Samples were obtained from 279 sites along roads and trails, as indicated on the map in Fig. 3.2, (Fig. 3.1 is an index map). The work was carried out during parts of three field seasons, 1970, 1971, 1972.

The spacing between sites averaged about 0.8 kilometre, being governed in many areas by occurrences of rock outcrop. In areas of abundant outcrop, the site spacing was about 0.4 kilometre. Magnetizations often change considerably from one site to the next, and to achieve a reasonable representation of magnetization variations on a regional scale, such a small spacing between sites was necessary.

Two oriented cores were generally obtained from each site, the two cores being several feet apart, chosen to represent the rock type at the site as well as possible. In a relatively small number of sites, the outcrops were badly shattered or difficult of access, and oriented cores were not obtained; grab samples were taken and remanence measurements were not made in these cases.

Cores were obtained by diamond drilling using, at different times, two drill systems. The G.S.C. type sampling drill (Truco Ltd.) operates with a gravity feed water supply, is portable, and can be readily used in areas where vehicle access is not possible.

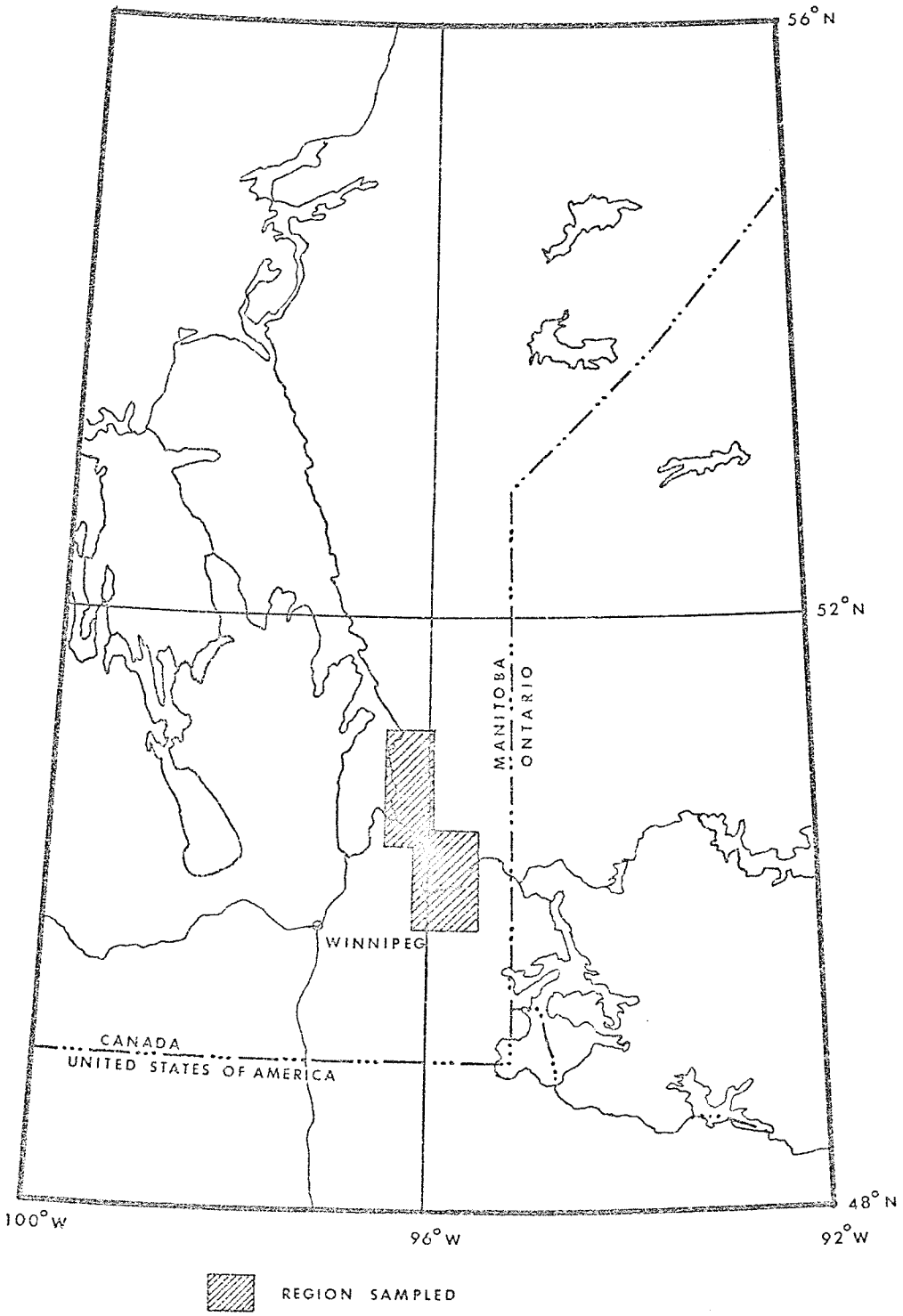

Figure 3.1 Index map for sampling location.

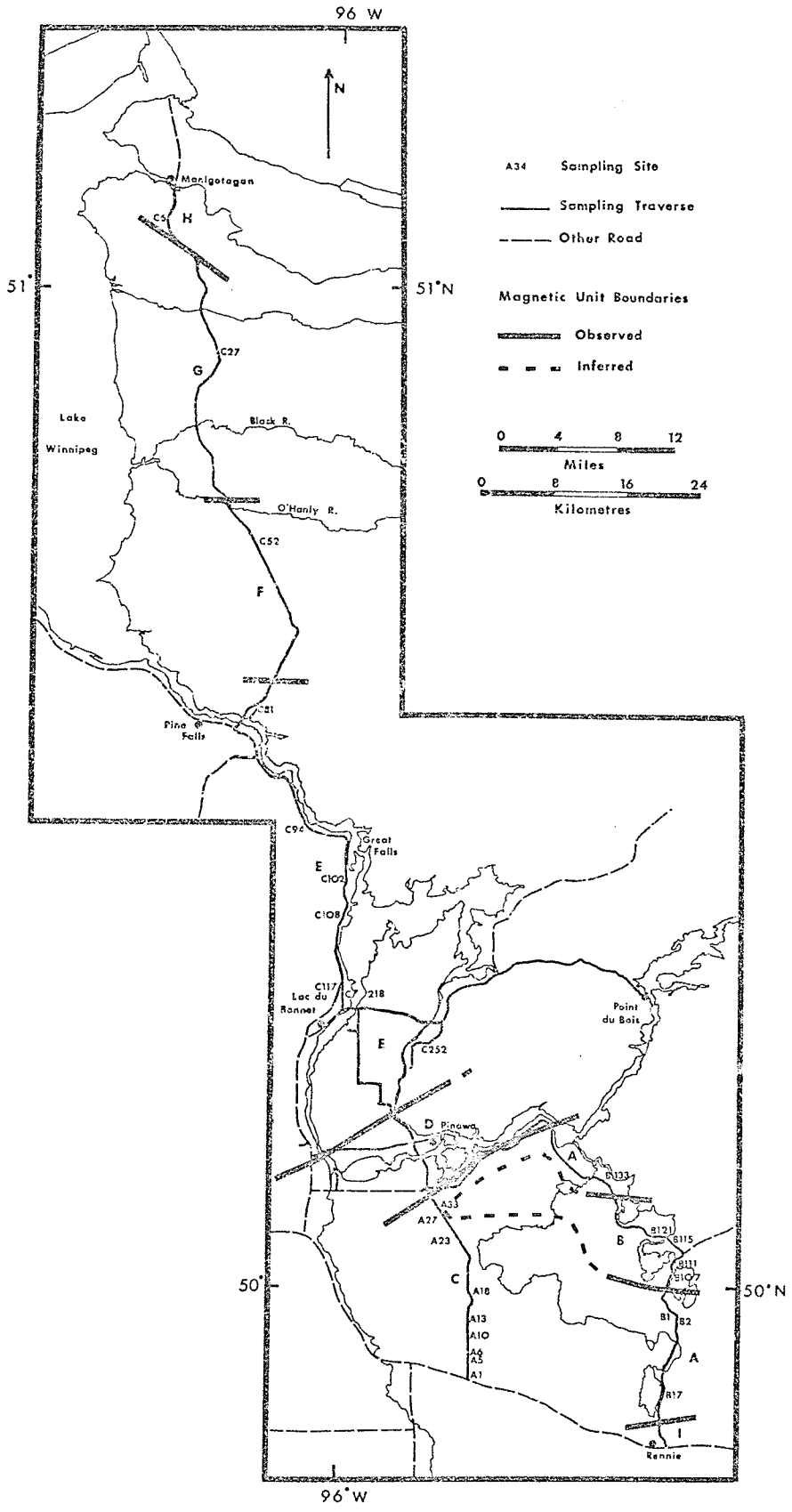

Figure 3.2 Sampling locations and magnetic units.

This drill was used for about 50% of the sites. The drill is a converted chain saw, and has a high speed 2-stroke motor. Bits which allow the development of a high speed, and yet are adequate for cutting in granitic gneiss terrain, are needed. Cores of 1 inch (2.54 centimetre) nominal diameter were produced, initially using thin-walled high-speed bits which proved inadequate for these rocks, and later with modified industrial bits (Delro Industries Ltd.) which though slower were more robust and longer lasting. A factor of some importance in selecting bits is that a left-hand thread is needed for this machine.

The other drilling system was based on the Model 4M Packsack drill (Truco Ltd.). Water was provided by a truck based centrifugal pump, driven by a gasoline engine. The pump was arranged either to draw water direct from a lake or pond, or to take it from a 45 gallon (0.2 metre^3) tank carried in the truck. In this way, the tank could be replenished periodically using the pump, enabling drilling to be done in areas of no natural water supply. Enough water could be carried for about 5 or 6 average sites. Cores of 29/32 inch (2.30 centimetre) nominal diameter were produced using standard EXT straight-wall bits (Delro Industries Ltd.). Core lengths from both systems varied but were typically 3.5 inch (9 centimetre). This length was used in order to sample below the topmost, often fractured region, and to provide sufficient length for susceptibility measurements and the cutting of more than one

specimen, if needed.

In the application of these drills to this type of work, it is sometimes difficult to obtain good cores still attached to the outcrop (for orientation purposes), in view of the hardness, and often fractured nature of the rocks. However, in almost all cases, it is possible to rematch the core, if broken, to its stub on the outcrop and to fix it with a quick-setting (5 minutes) epoxy adhesive. There is no loss of orientation accuracy in this operation. The drills are normally hand-held, and as a result, the life of the diamond bits is relatively short, though this may be extended slightly, with easier drilling and cleaner cores, by the addition of cutting oil (soluble oil) to the cooling water. As an alternative, a frame or jo-bar attachment might be used, to steady the drill, but this normally involves a second hole.

The early cores (codes begin with A) were oriented by magnetic compass held at head height with careful alignment of marks on the core top and outcrop. Inclement weather and a lack of identifiable major features precluded sun and topographic sightings. The later series of cores were oriented by using a special sighting tube and head (similar to those described by Helsley, 1967; Brown and Kahn, 1967; Opdyke, 1967) with a Brunton transit to obtain sun sightings (Creer and Sanver, 1967). Magnetic compass readings taken with the instrument close to the rock surface were not reliable in areas of high localized magnetizations, but if held at head height, the compass deviated

at most by no more than 3 or 4° from the general magnetic north in the area. This observation cannot be assumed valid in other areas (for example, where iron formations are known to exist, or in greenstone areas). Orientation accuracies for the bulk of the A-series of cores are ± 5° in declination, and ± 6° in dip angle; for the later series of cores, accuracies are ± 2° in declination, and ± 1° in dip angle.

3.3 General Geology and Geochemistry of the Area

The geologic mapping in the area of the sampling survey, Fig. 3.2, has been uneven in coverage and in scale. Until recent times, studies of the 'granitic' rocks of the Precambrian Shield have been neglected as a result of the common association of economic mineralization with metasedimentary and metavolcanic rocks. A recent extended project which has included in part a study of acid 'plutonic' rocks is Project Pioneer (McRitchie and Weber, 1971). The Project Pioneer area covered parts of the Red Lake block and the English River block (see Section 1.3, Chapter 1) in Manitoba, and as an extension, to place the study in the context of the surrounding regions, a reconnaissance survey was made by McRitchie (1971) of the region to the south and west of the main Project Pioneer study area. It is in this region that part of the present work was carried out.

Early geologic work in the southern part of the present area

of interest was done on a reconnaissance scale by Delury (1946), Wright (1932), and Springer (1952). More recently, geochronological work has been carried out in the region east of Lac du Bonnet (Penner and Clark, 1971) and south of the Winnipeg River (Farquharson and Clark, 1971).

The area of study lies almost wholly within the confines of the western extension of the English River gneiss block as defined by Wilson (1971). It extends from Rennie in the south, close to the southern boundary of the gneissic block (H.D.B. Wilson, personal communication 1973), to Manigotagan in the north, which lies just within the Rice Lake greenstone belt of the Red Lake block.

Major rock divisions are discussed by McRitchie (1971) and Farquharson and Clark (1971), and are in agreement with summary examinations of outcrops and handspecimens during the present study.

In the north of the area, near Manigotagan, greenstones are found, with granodiorite-quartz diorite intrusions in a few places. Southward to the Black River, (Fig. 3.2), the predominant rocks are paragneisses and grey granodioritic gneisses, with some pink granitic phases. Near the Black and O'Hanly Rivers, porphyroblastic quartz dioritic and granodioritic gneisses occur. Between the O'Hanly River and the Pine Falls area is a grey granitized gneiss tract; it is heterogeneous and contains

abundant discontinuous amphibolitic dykes, and quartz dioritic intrusions and skialiths.

To the south of Pine Falls, the abundance of quartz dioritic and quartz monzonitic intrusive phases increases, until between Great Falls and Lac du Bonnet, a fairly homogeneous unit is found, which extends to within about 5 kilometres north of Pinawa and eastward towards Point du Bois. Its westward extension disappears beneath glacial and Paleozoic cover. This unit has been described by McRitchie as the Lac du Bonnet quartz monzonite, and it represents the youngest and largest distinct pluton in the area.

South of the Lac du Bonnet pluton is a grey granitized gneiss region which continues to just south of the Winnipeg River. In the western part of the area to the south of the river, a rapid transition to a pink granodioritic unit takes place. In the transition zone, some xenoliths of amphibolite are found, together with skialiths of mafic inclusions. This pink granodioritic unit is heterogeneous in character, sometimes showing compositional layering, sometimes foliated, often massive, hypautomorphic granular to porphyritic and often crosscut by pink pegmatitic phases. Schlieren of more mafic composition are common. The unit extends at least to the southern limit of the survey, at Highway 44.

In the eastern part immediately south of the Winnipeg River, a pink granodioritic unit is present, which may be the same unit as that described above, but definite continuity has not been

established. However, the transitional zone of xenoliths and skialiths is present. A few kilometres south of the river, abundant large (1-2 cm.) microcline prophyroblasts appear in a coarse grained granodioritic matrix. Farquharson and Clark (1971) have termed this the Whiteshell Porphyritic Granodiorite. Its full extent is not known, but as observed during the present work, it extends southward to Jessica Lake. McRitchie (1971) has described a rock type in the area extending towards the west and southward from the contact zone with the grey gneissic unit, as a massive porphyroblastic granodiorite. With the whole area are several locally porphyritic quartz monzonitic phases.

Centred around Red Rock Lake is a medium grained pink granitic unit. Immediately to the south, a small area of grey granodioritic material is found, followed to the south by heterogeneous pink granodioritic material, similar in appearance to that described for the western part of the region. South of Brereton Lake, to Rennie, migmatite becomes the dominant rock type. A number of amphibolite xenoliths occur in the pink granodiorite and the migmatite.

Penner and Clark (1971) have given an Rb-Sr age for the Lac du Bonnet quartz monzonite as 2495$\pm$ 130 m.y., and for the quartz dioritic material to the north, 2640$\pm$ 135 m.y. This tends to support the geological interpretation of age relations by McRitchie (1971). A high initial Sr^{87}/Sr^{86} ratio for the quartz monzonite suggests that it originated from pre-existing crustal material, or was contaminated by Rb-rich material during emplacement.

Farquharson and Clark (1971) have determined Rb-Sr ages for the major units south of the Winnipeg River. They consider that the pink granodiorite was emplaced about 2665± 50 m.y. followed by the emplacement of the Whiteshell prophyritic granodiorite about 2610 m.y. Allanite, an indicator of late-stage intrusive phases, was noted by these workers in the porphyritic granodiorite, and they suggest that this unit may be a mobilized margin of the pink granodiorite. The initial Sr^{87}/Sr^{86} ratio for the pink granodiorite is low, indicating that it was derived from primitive material, not enriched in Rb through crustal fractionation processes. In contrast, the initial ratio for the porphyritic granodiorite is higher, which may reflect derivation from a crustal source. Alternatively, Farquharson and Clark suggest that the higher initial ratio may be a result of the time lapse, if the porphyritic unit is a late stage phase of the pink granodiorite. As another possibility, they consider that contamination of granodioritic material by pre-existing metasedimentary or metavolcanic rocks may have produced the high initial ratio.

McRitchie (1971) has pointed out similarities between the porphyritic unit and that found near the Black and O'Hanly Rivers, but considers that whereas metasomatic origins may be true for this latter unit, the Whiteshell unit is probably magmatic and intrusive in origin.

CHAPTER 4

MAGNETIC MEASUREMENTS

4.1 Introduction

Physical measurements have been made on the samples collected during the field work described in Chapter 3. The measurements made were those indicated in Section 3.1, namely, susceptibility, remanence (before and after magnetic cleaning) and Curie temperature determinations. In some series of measurements, only selected samples were used. In addition, microscope studies of the opaque minerals in some polished sections from cores are described in this chapter. A discussion of the results of the measurements and observations is given at the end of the chapter.

4.2 Induced Magnetization

Magnetic susceptibility measurements have been made on all core and grab samples, using a Geophysical Specialties MS-3 susceptibility bridge. For the cores, two measurements were made, the second one with the core inverted from the first position. These two measurements sometimes differed by several percent due to inhomogeneities, and an average of the two values was taken as a representative value for the core. Some but not all of the grab samples were repeated; the samples were crushed to pea-sized fragments for the measurements, and no significant differences were found on remeasuring.

A histogram of susceptibilities of all the samples is presented in Fig. 4.1. A bimodal distribution is evident, with the bulk of samples in the 3×10^{-4} to 3×10^{-3} emu/cm.^{3} (3.8×10^{-3} to 3.8×10^{-2} SIU) range, but with a second peak at the low end of the scale, below 10^{-5} emu/cm.^{3} (1.3×10^{-4} SIU.).

A susceptibility profile along an approximately linear traverse over the whole region is presented in Fig. 4.2. The position of this traverse is within 2 kilometres of the line XX' marked on Fig. 4.3. The traverse extends from the regional magnetic anomaly low into the anomalous high region to the south. A second profile is shown in Fig. 4.2, and its position is approximately along the line YY' in Fig. 4.3. This profile extends only over part of the high anomaly field region. It is immediately evident that there exist considerable differences in the levels and patterns of induced magnetizations between the several regions.

Along most of its length, the profile XX' was sampled at 0.8 kilometre intervals or closer. Using a third order polynomial, the data were interpolated on to a 1 kilometre spacing; the differences between this interpolated profile and Fig. 4.2 are minor. Using the regularly spaced interpolated values, a cumulative induced magnetization profile was determined and is shown in Fig. 4.4. A similar determination using the original data showed the same general features. Distinct changes of slope are apparent at several points along the profile, indicating changes in the mean level and character of magnetization.

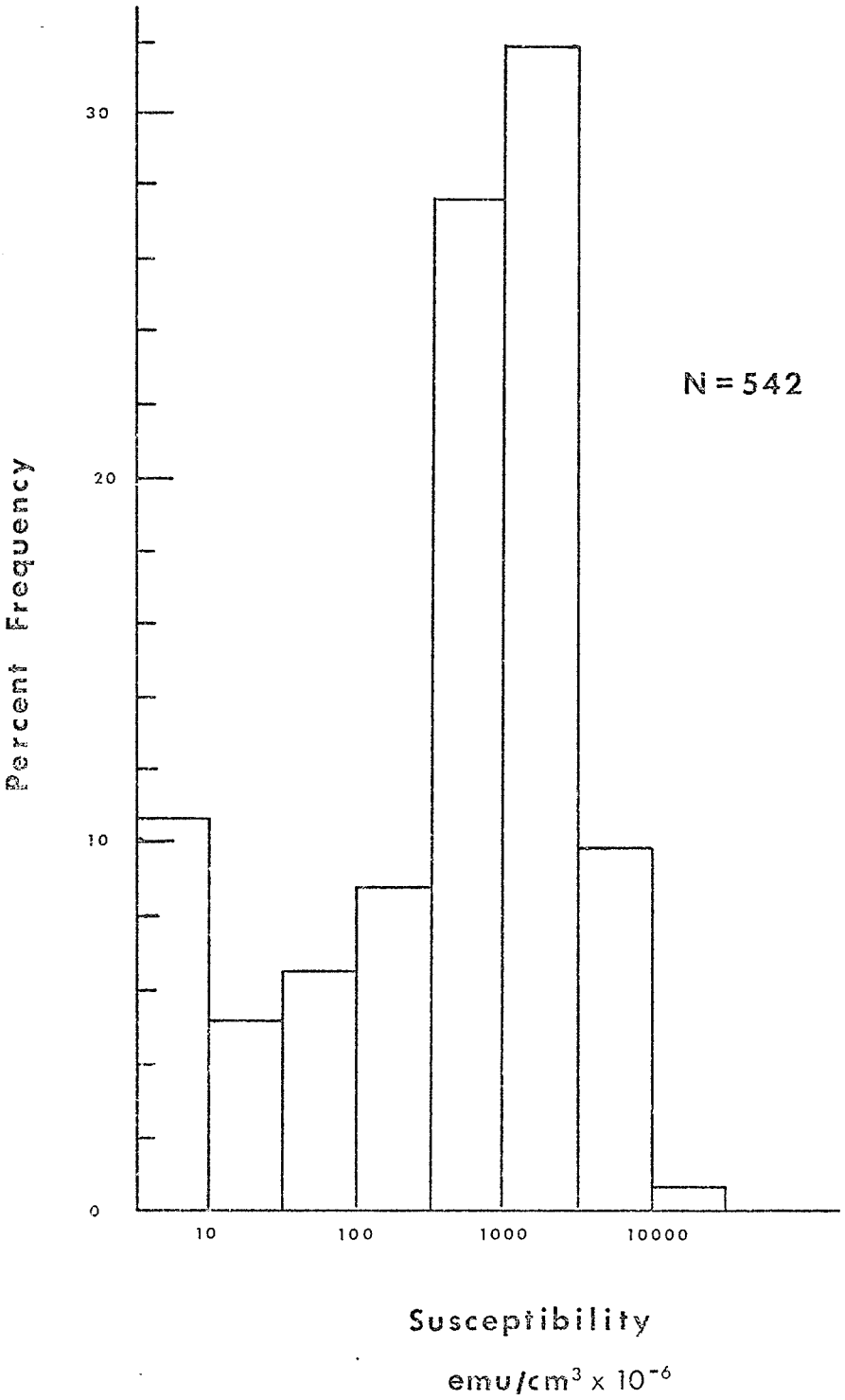

Figure 4.1 Histogram of susceptibilities - all samples.

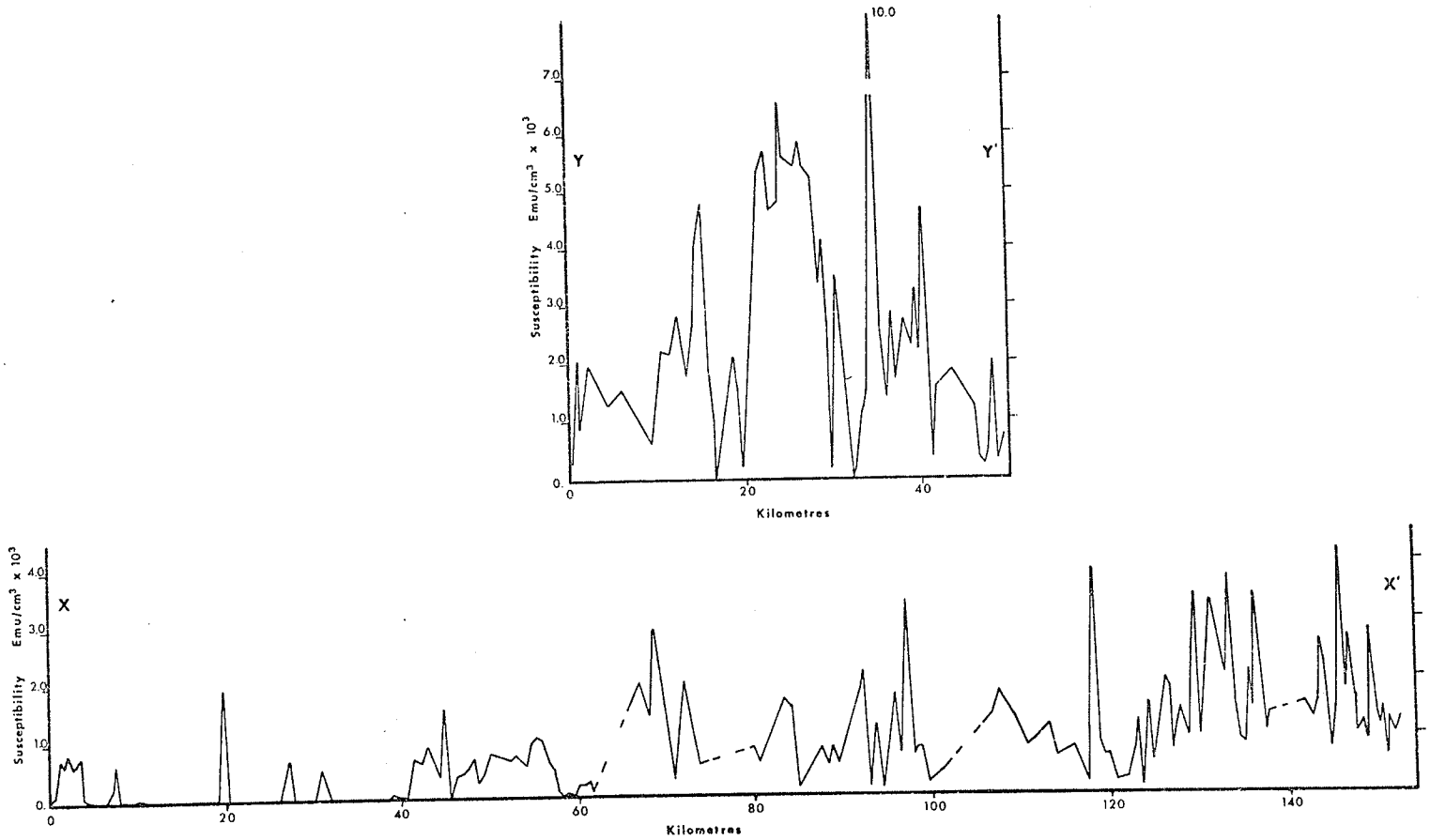

Figure 4.2 Susceptibility profiles.

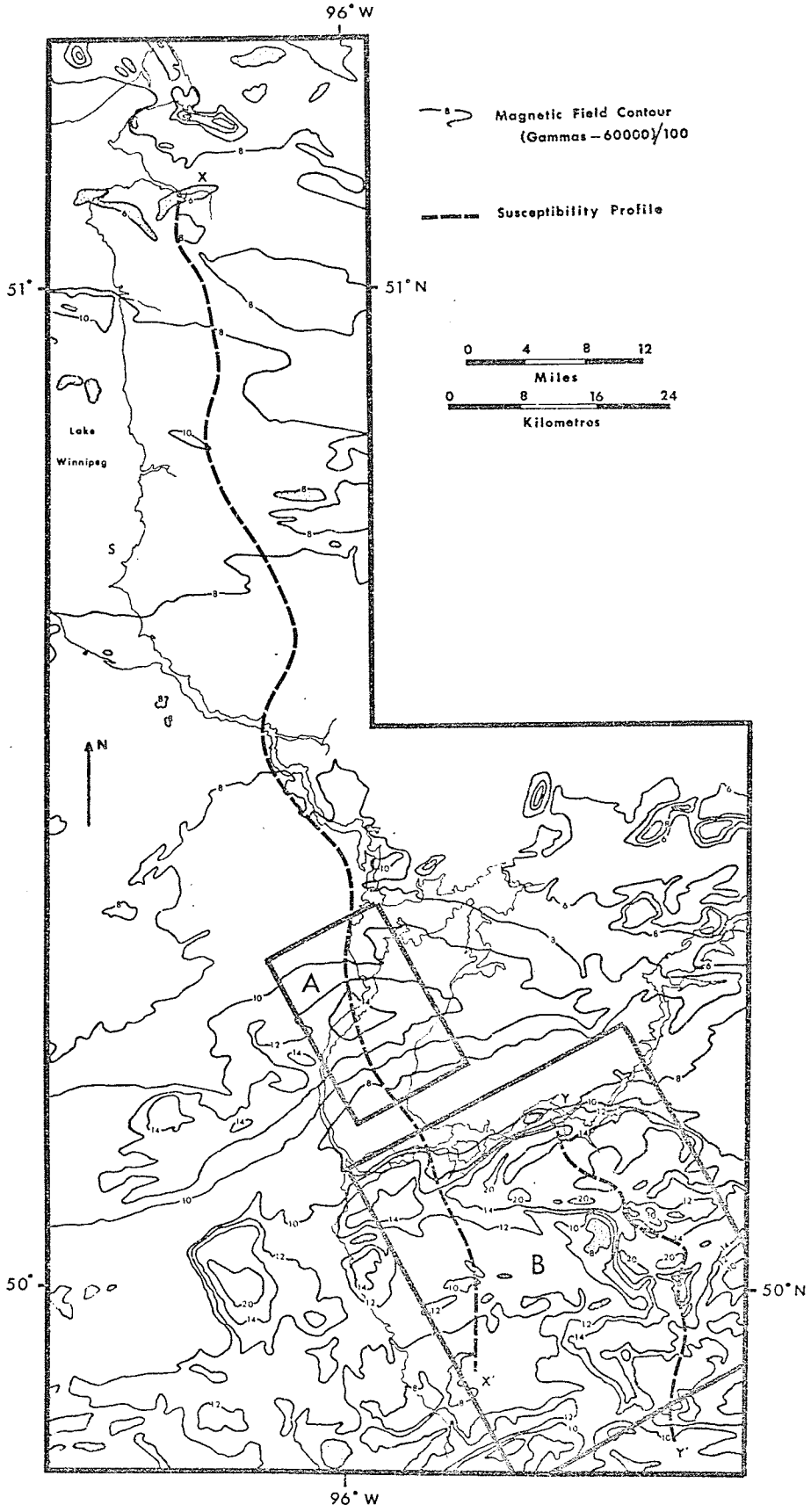

Figure 4.3 Simplified magnetic anomaly map.

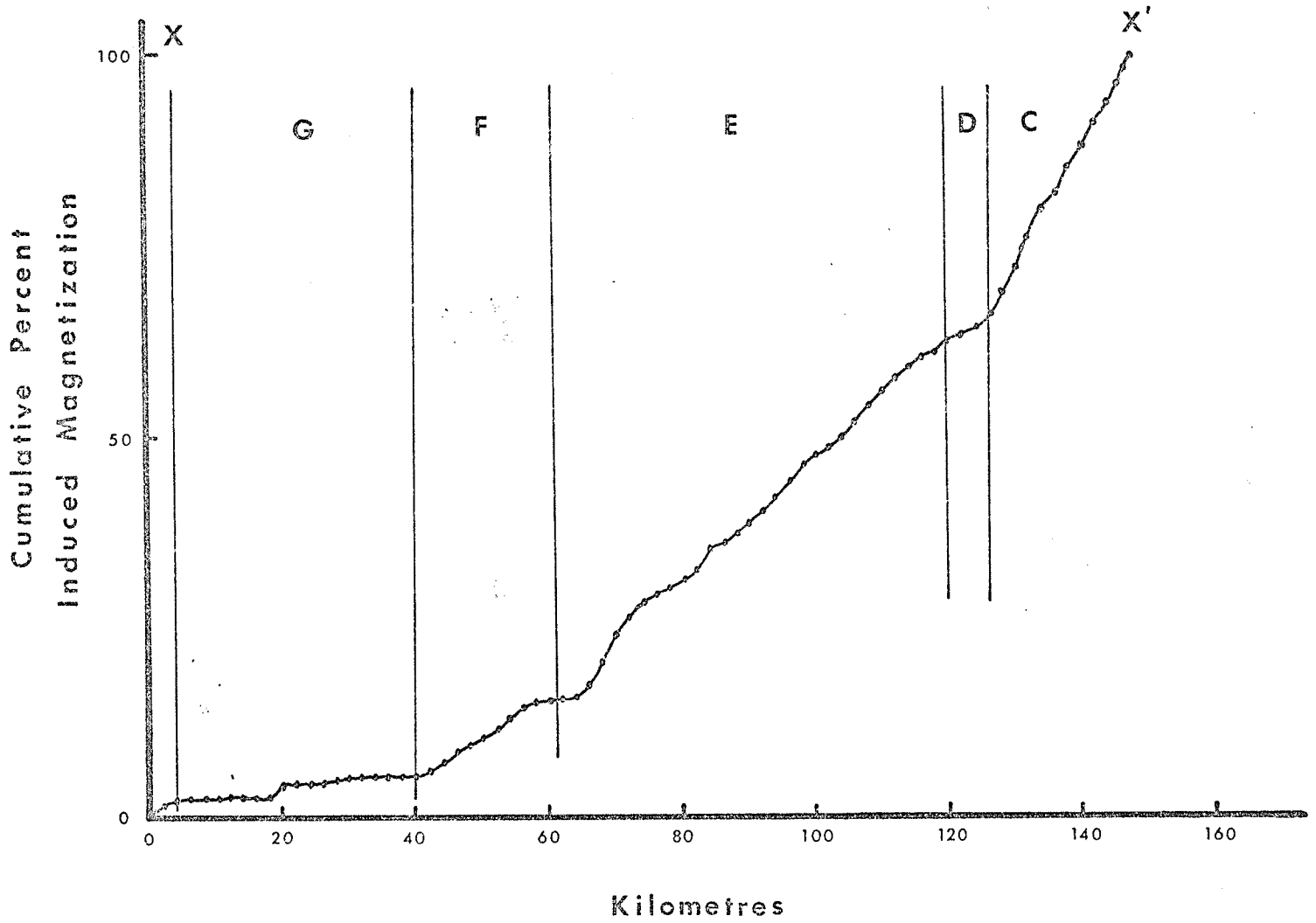

Figure 4.4 Cumulative induced magnetization along Profile XX'.

In Fig. 4.5, the susceptibility data have been contoured to delineate major changes in the level of magnetization. Within each of the areas, there is considerable variation in detail, but the contouring was done on the basis of broad features. The contour levels are 0.5, 1.0, 2.0, and 3.0 x 10^{-3} emu/cm^3. The 3.0 contour encloses areas of much higher susceptibility.

4.3 Remanent Magnetization.

Remanence measurements have been made on most core samples taken in the field survey. The magnetometer used was developed as part of this project, and is described in detail in Appendix 1. A discussion of the measurement procedures is also given in this Appendix. The limit of measurability for the magnetometer is about 6 x 10^{-6} emu/cm^3. (7.5 x 10^{-10} Wb/m^2.). This is well below the minimum level of significance for aeromagnetic anomalies.

A group of samples which had no remanence greater than this was found; these also, in many cases, had induced magnetizations of less than 6 x 10^{-6} emu/cm^3. In other more highly magnetic samples, remanent intensities also ranged as high as about 10^{-2} emu/cm^3. (1.3 x 10^{-6} Wb/m^2.). The distribution of remanent intensities for all samples measured is described in the histogram in Fig. 4.6. The distribution is bimodal, but the peak at higher intensities is broader than the corresponding peak in the histogram of susceptibilities, Fig. 4.1.

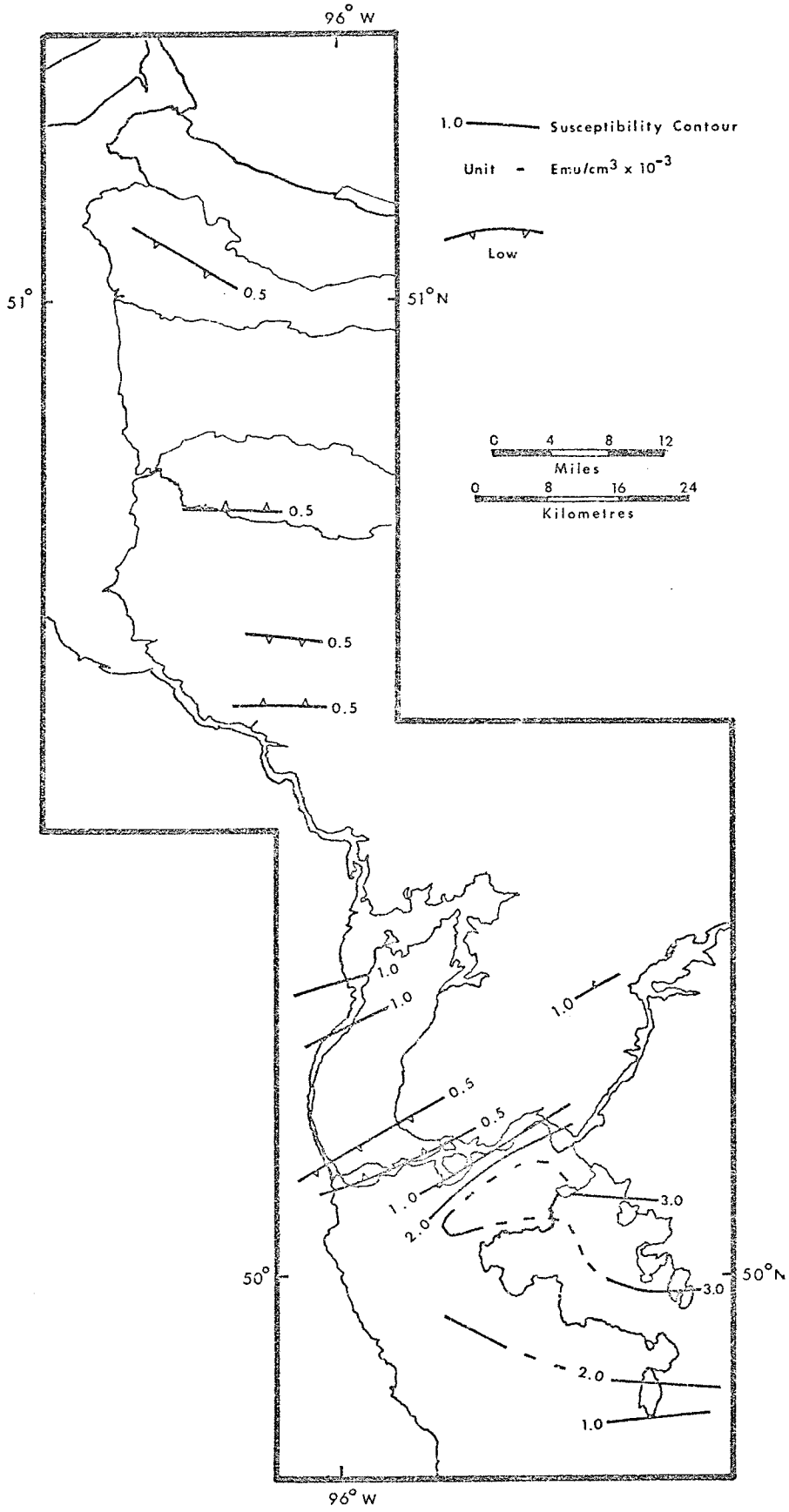

Figure 4.5 Contoured susceptibilities.

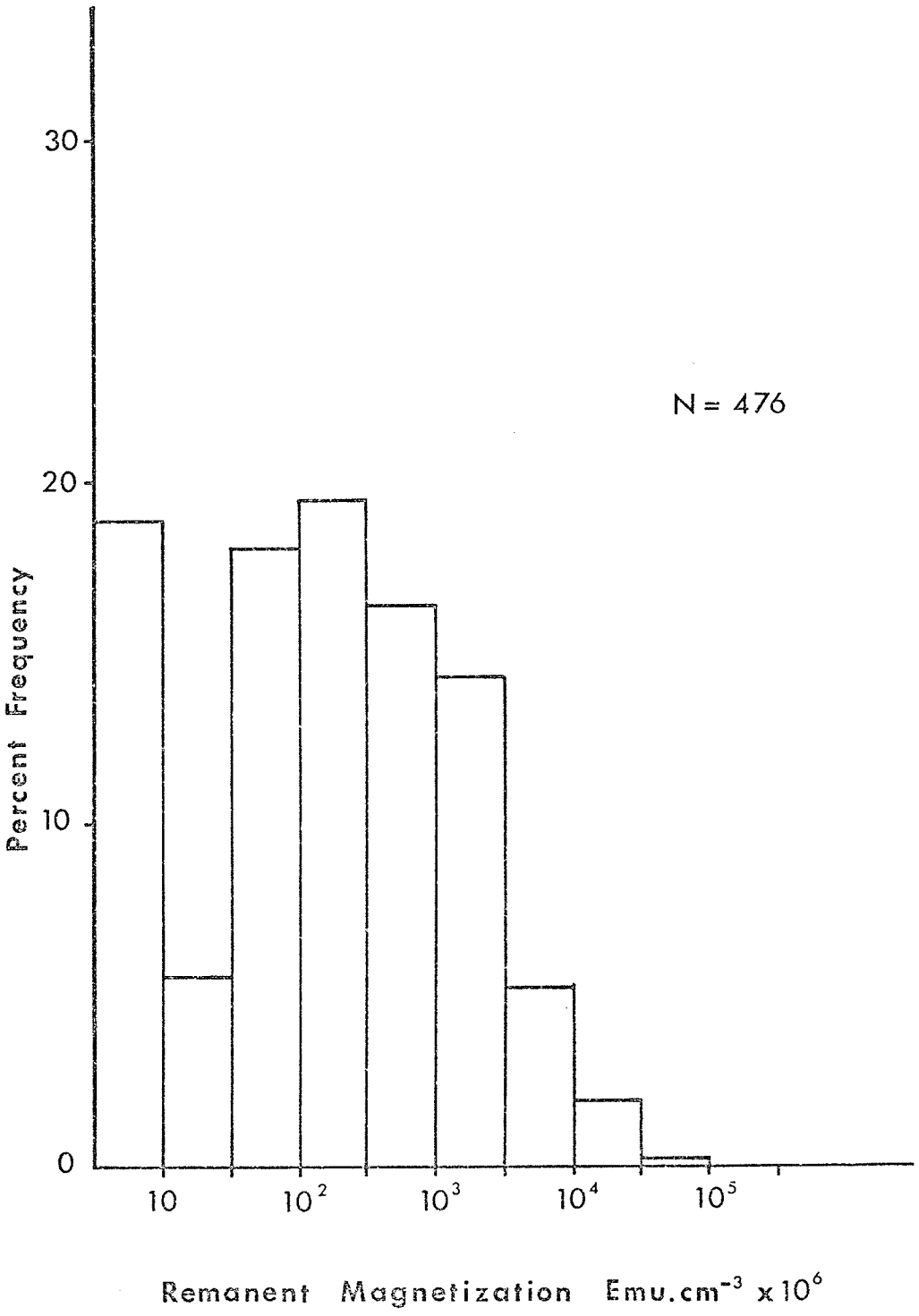

Figure 4.6 Histogram of remanent magnetization intensities - all samples.

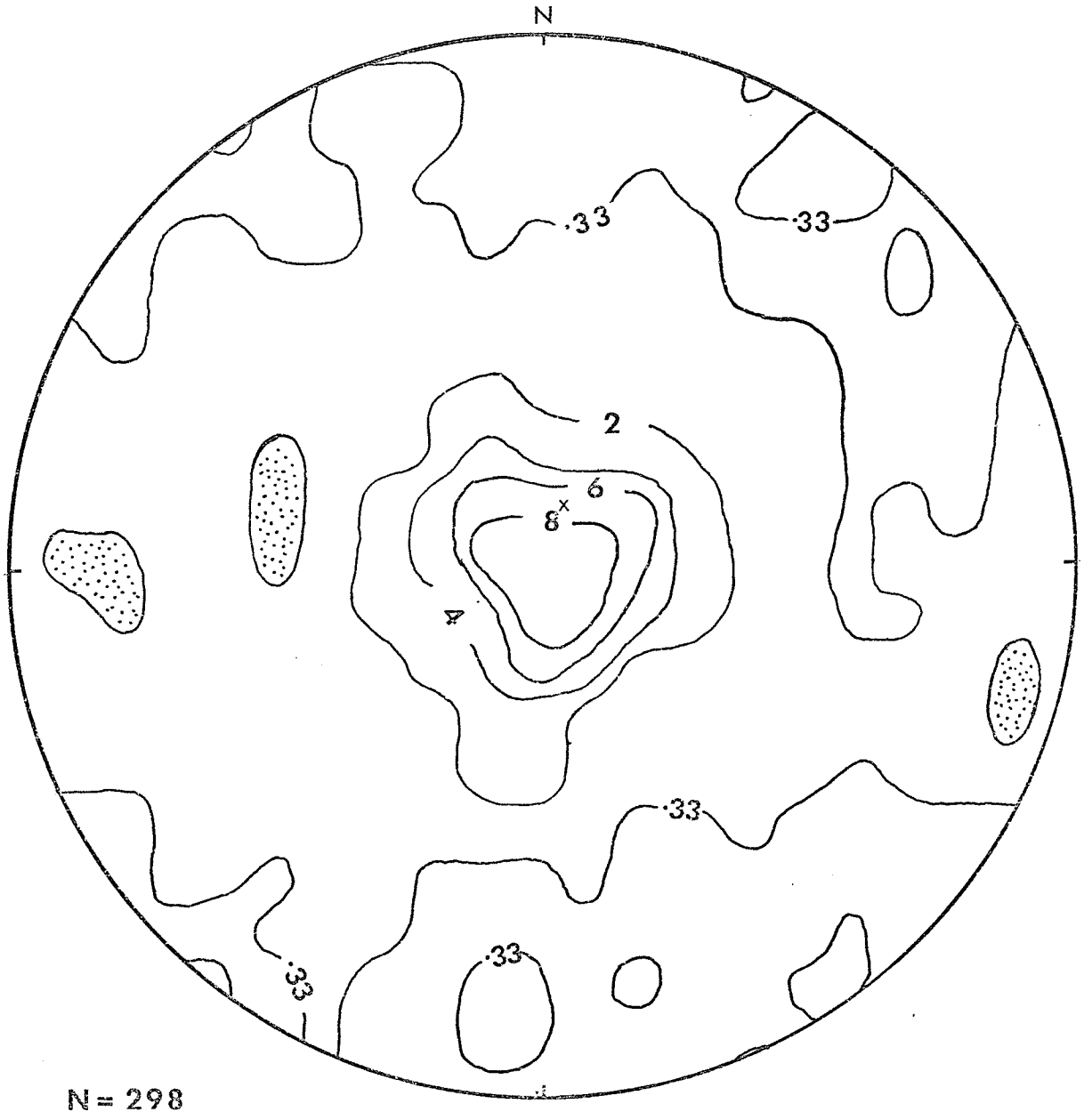

Figure 4.7 Contoured equal-area projection plot of 'normally' directed remanences (some with very low intensities are not included).

The remanence directions for the whole area are summarized in Fig. 4.7, which is a contoured plot of the directions on a lower hemisphere equal-area projection, using standard techniques (Turner and Weiss, 1963). Upper hemisphere directions are not included on the plot; as shown later (Fig. 4.9 and Section 4.5) they are subordinate in numbers, and very scattered in directions. Although there is scatter present in the directions which are 'normally' directed, there is a prominent peak, not centred around the geomagnetic field direction but about the centre of the net, (Fig. 4.7).

4.4 Curie Temperatures

Curie temperatures have been determined for many of the samples taken in the survey. The instrumentation, methods and techniques used have been described and the results for the A-series of samples have been presented previously (Coles, 1970). The Curie temperatures for all these samples were found to be within a few degrees of 573°C (846K). The measurements are made in air, with rapid heating of whole rock samples, in subsaturation magnetic fields.

A representative selection of samples from the other areas were subjected to the same kind of analysis. A total of 42 additional samples were measured. With one exception, the Curie temperatures may be quoted as 575 $\pm$ 5°C. (848 $\pm$ 5K).

The exception was a very weak sample, C48A, which gave a just

detectable indication of a Curie point at about 320°C (593 K), but the sample appeared to undergo alteration and disintegration above about 400°C. (673 K). The sample occurred near the O'Hanly River (Fig. 3.2).

4.5 Magnetic Units

It is evident from an examination of the spatial distributions of magnetic properties that there are several distinct magnetic units in the region. These magnetic units have been defined primarily in terms of induced magnetization, because it is the susceptibility property that shows the distinctions most clearly. Magnetic units defined in terms of other properties may or may not coincide with the present ones; for example, a definition based on Curie temperatures would not be a useful one in this context. In fact, an examination of the character of the magnetizations within the units shows that, in general, remanences do tend to suggest units similar to those based on susceptibility. The units as chosen would then appear to be reasonable ones.

The areal distribution of the magnetic units is given in Fig. 3.2. Susceptibility histograms are shown in Fig. 4.8, and some statistical parameters are presented in Table 4.1. The remanence directions are summarized in Fig. 4.9, where they are divided into the same units as for the susceptibilities. Only six major units are shown; in the other units, remanences are mainly very weak, often

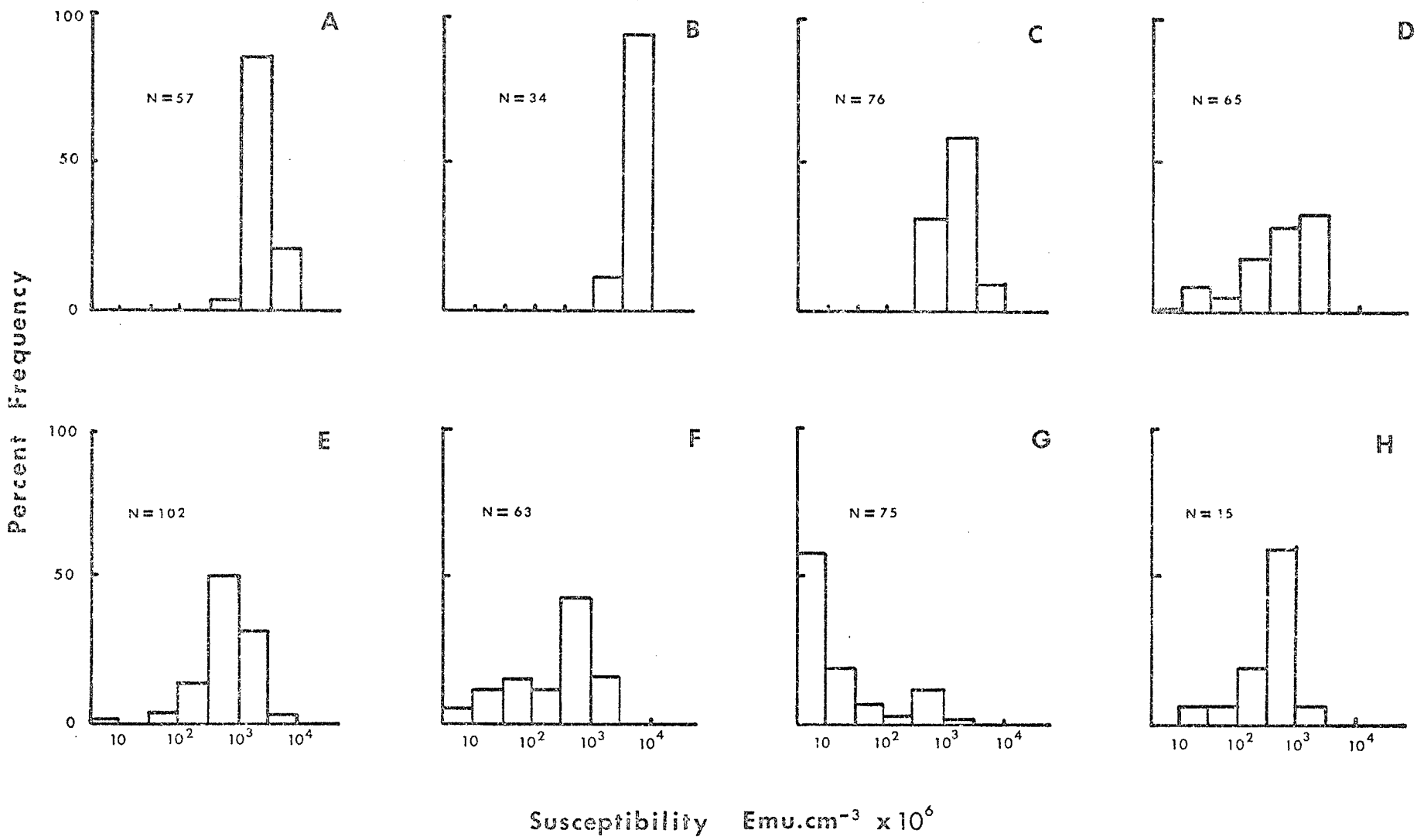

Figure 4.8 Histograms of susceptibilities for the major magnetic units.

TABLE 4.1

STATISTICAL PARAMETERS OF SUSCEPTIBILITIES

OF MAGNETIC UNITS

UNIT	N	MEAN m	STANDARD DEVIATION s	s/m	LOG. MEAN m_1	LOG. S.D. s_1
A	57	2052	831	0.41	3.28	0.16
B	34	4809	1055	0.22	3.67	0.10
C	76	1633	1130	0.69	3.13	0.23
A+C	133	1813	1030	0.57	3.20	0.22
A+B+C	167	2423	1591	0.66	3.30	0.28
D	65	802	721	0.90	2.61	0.63
E	102	972	815	0.84	2.81	0.45
F	63	479	450	0.94	2.36	0.66
G	75	96	203	2.11	1.18	0.72
H	15	551	355	0.64	2.57	0.48
ALL SAMPLES	542	1278	1608	1.26	2.61	0.88

IN UNITS OF $EMU/CM^3 \times 10^{-6}$

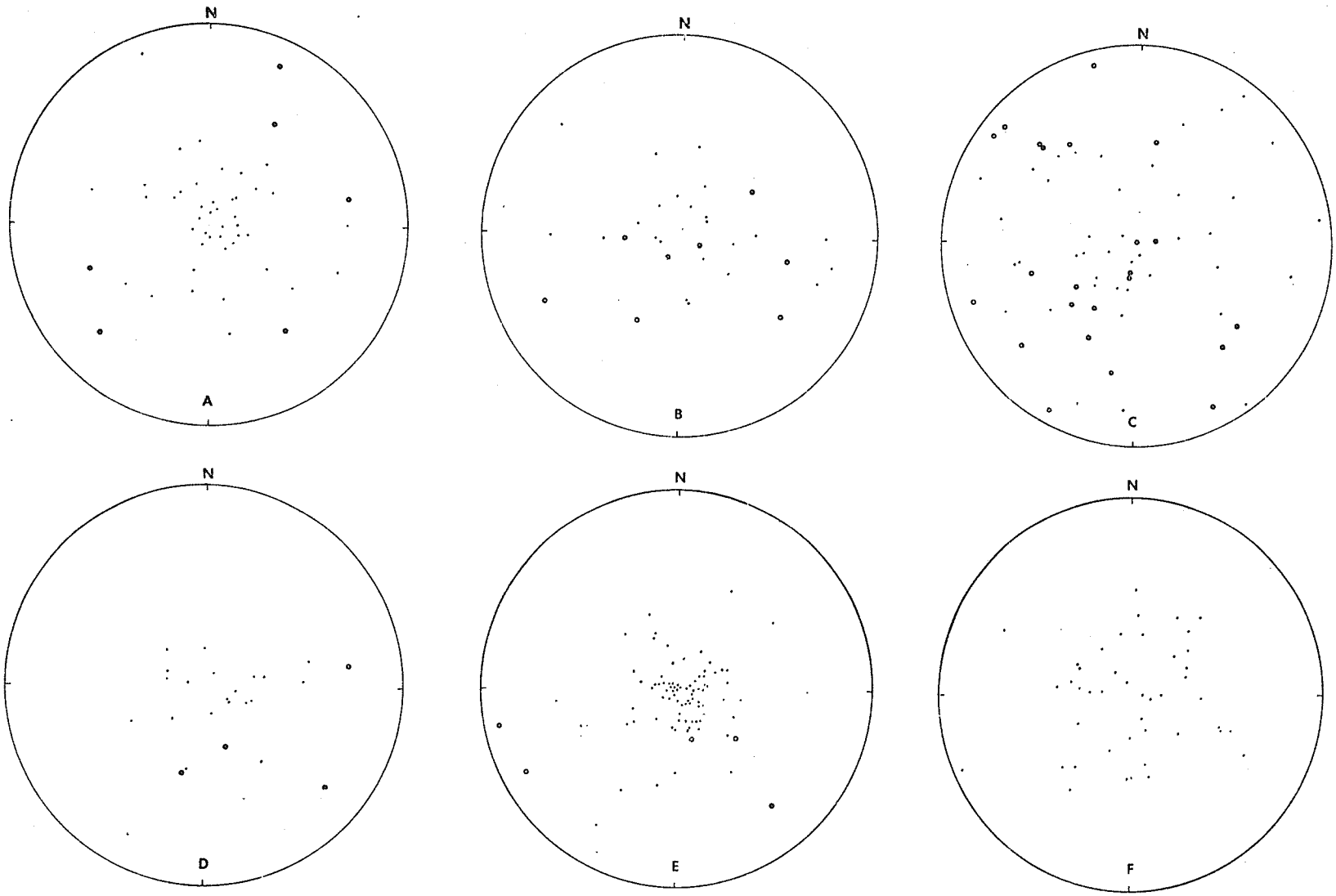

Figure 4.9 Equal-area plots of remanence directions in major magnetic units.

unmeasurable, with a few higher ones, widely scattered in direction. Remanence intensity histograms for Units A+B+C and D+E+F+G+H are shown in Fig. 4.10, which may be compared with corresponding histograms of induced magnetization in Fig. 4.11.

In order to express the several units in another manner, which serves again to indicate the relative contributions to induced and remanent magnetizations to the anomaly field over the area, plots are presented in Fig. 4.12, of the remanent magnetization versus induced magnetization for samples in the several units.

Although there is overlap in properties between the different units, separate distribution centroids and spatial discreteness justify the delineation of the units. There is a distinct change in character between Units A, B, C on the one hand, and Units D, E, F, G, H on the other. Boundaries between Units A, B, C are less clear, as are those between Units D, E, F, G, H, but differences are present.

The divisions into Units A, B, C, may not be exact, and it is considered that some samples in Units A, C, have properties effectively the same as some of those in Unit B. However, the spatial discreteness and the distinctly higher magnetizations in Unit B tend to set it apart. The general level of magnetization in Unit A is higher than that of Unit C, from which it is separated in space. Furthermore, the remanence directions in these two units appear to have different characters.

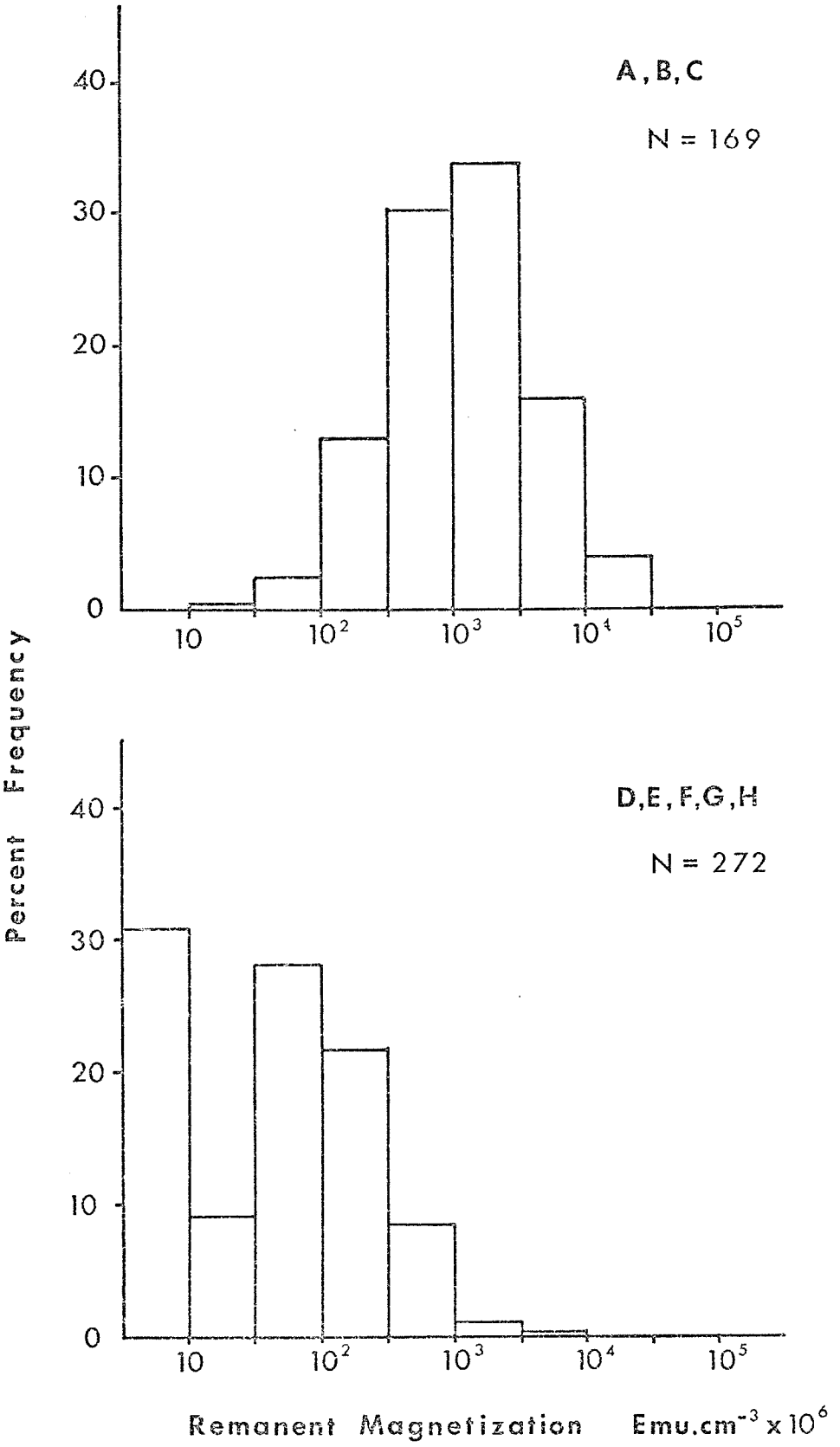

Figure 4.10 Remanent magnetization histograms for major subdivisions.

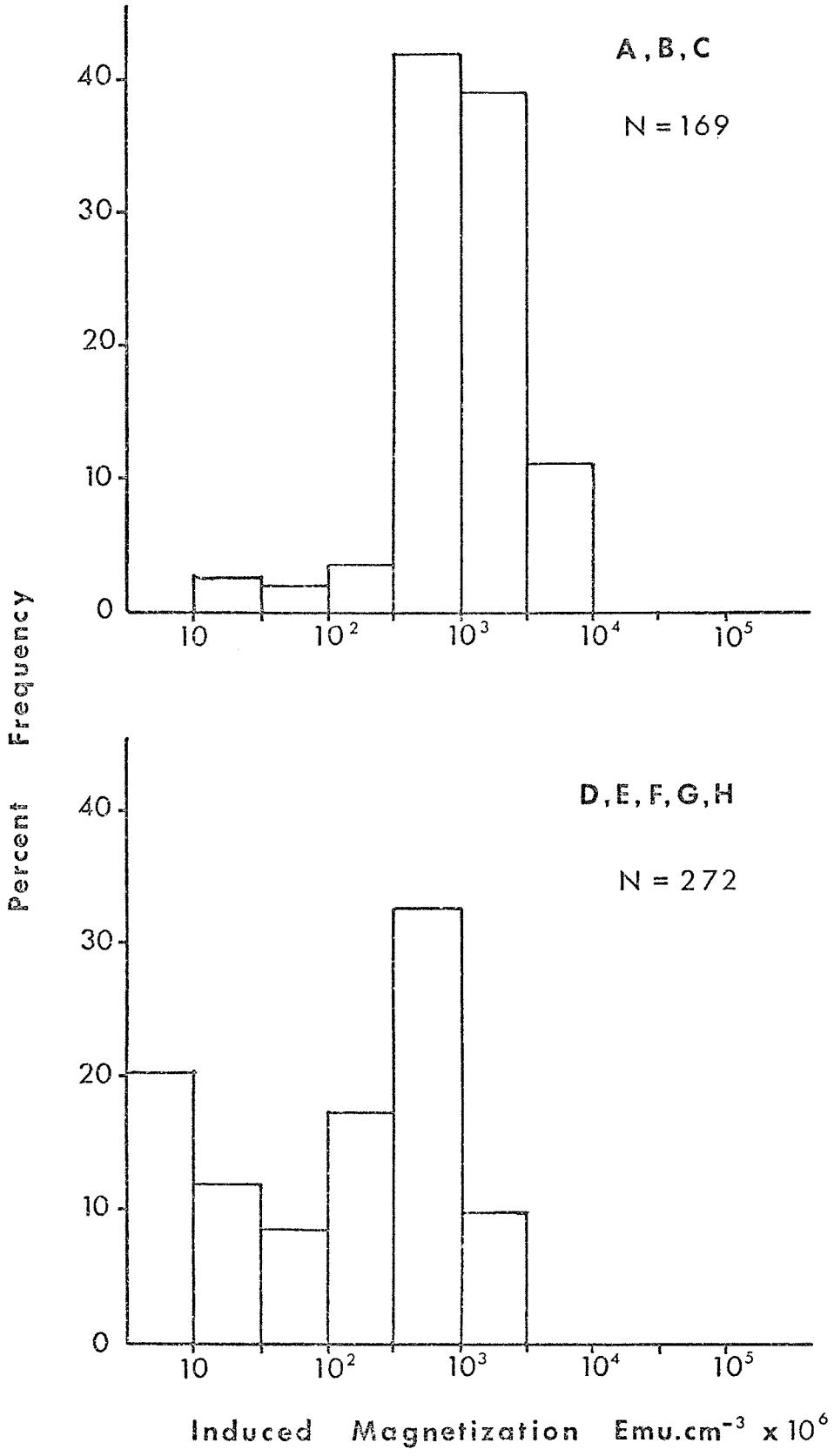

Figure 4.11 Induced magnetization histograms for major subdivisions.

Figure 4.12 Comparison of Remanent and Induced Magnetizations for Magnetic Units

Remanent magnetization (R) in emu/cm^3.

Induced magnetization (I) in emu/cm^3.

Logarithmic scales.

The dashed line on the plots for Units D, E, F represents the limit of measurability for remanences.

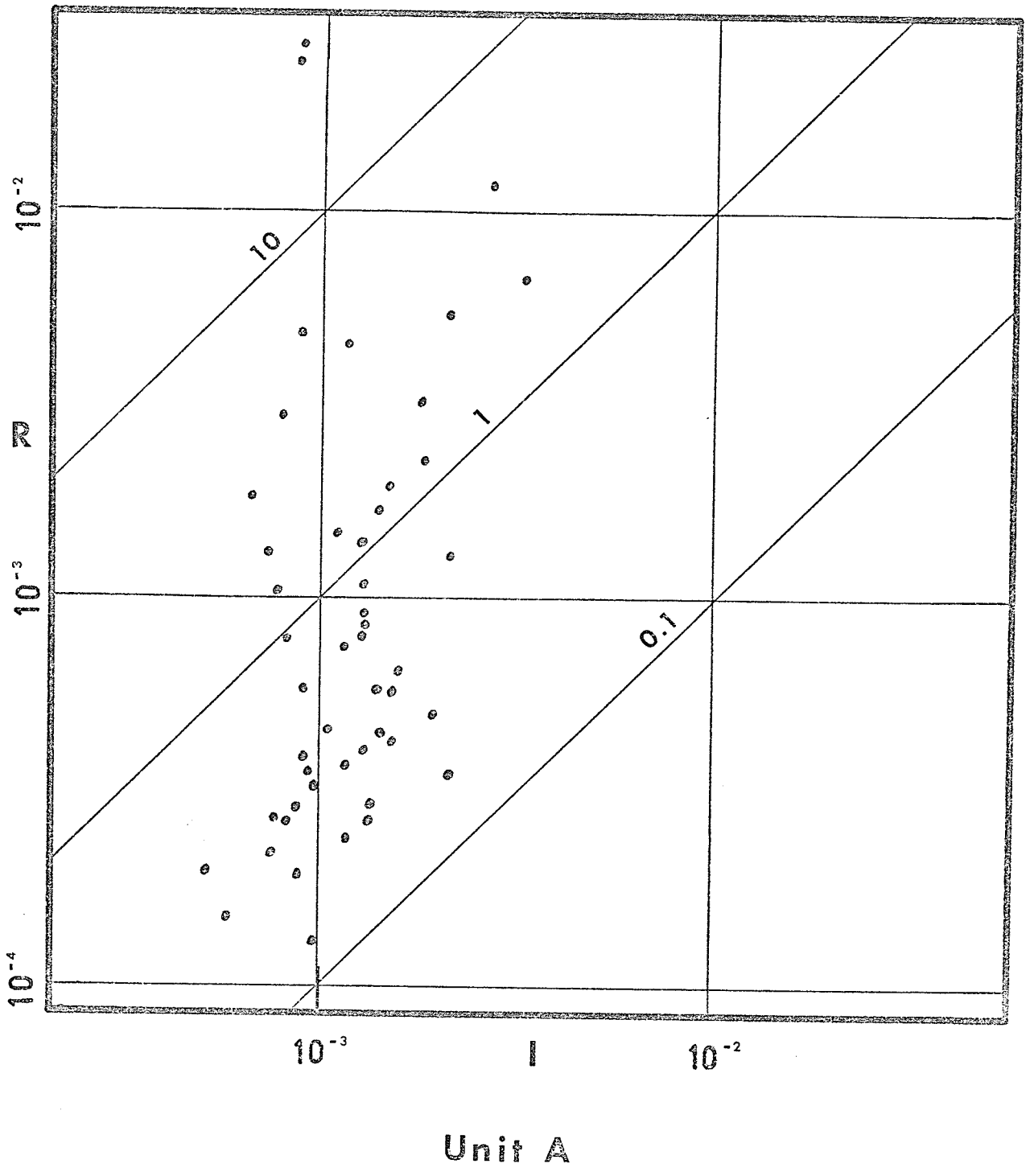

Figure 4.12 Remanent/induced magnetizations.

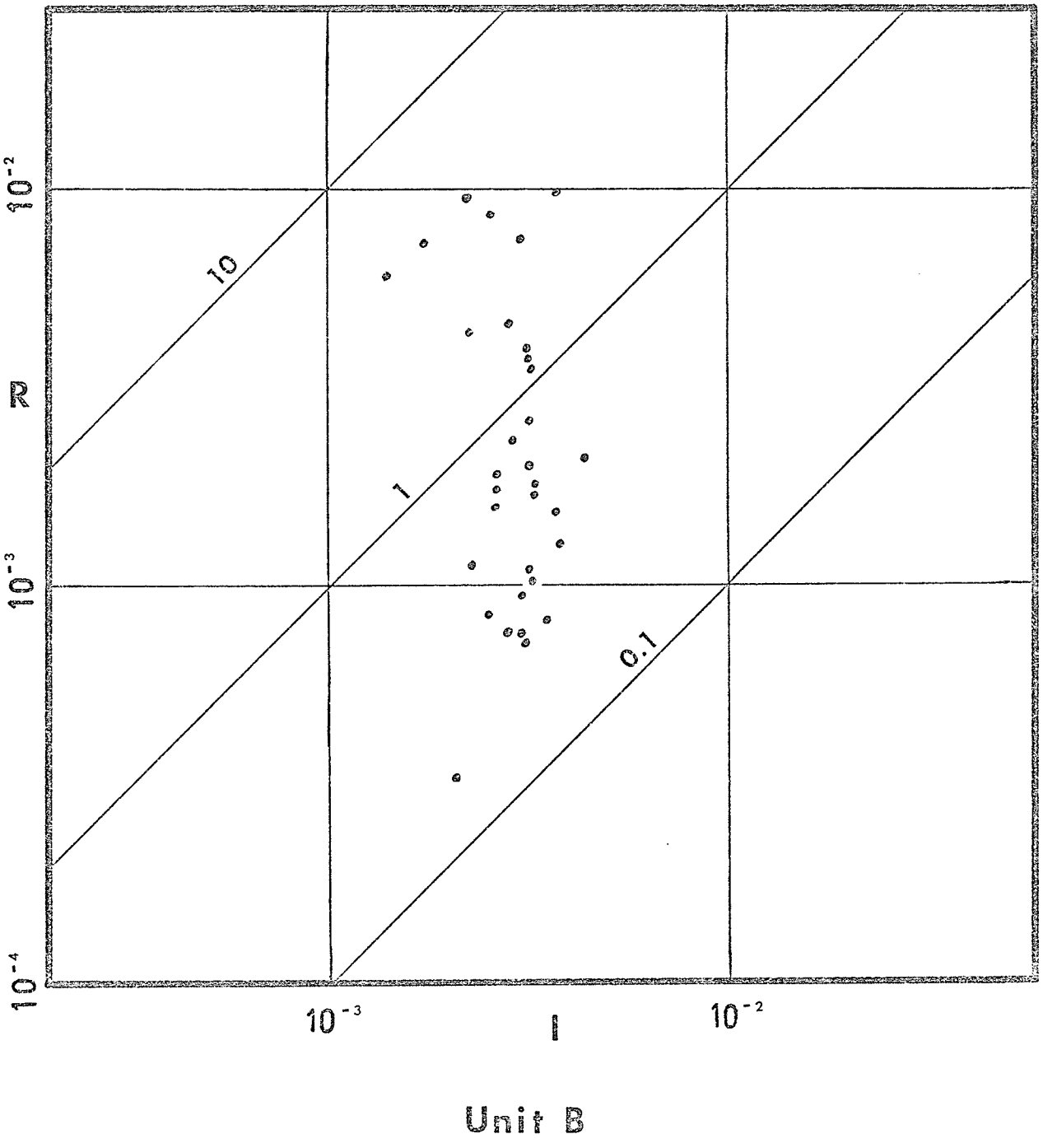

Figure 4.12 Remanent/induced magnetizations.

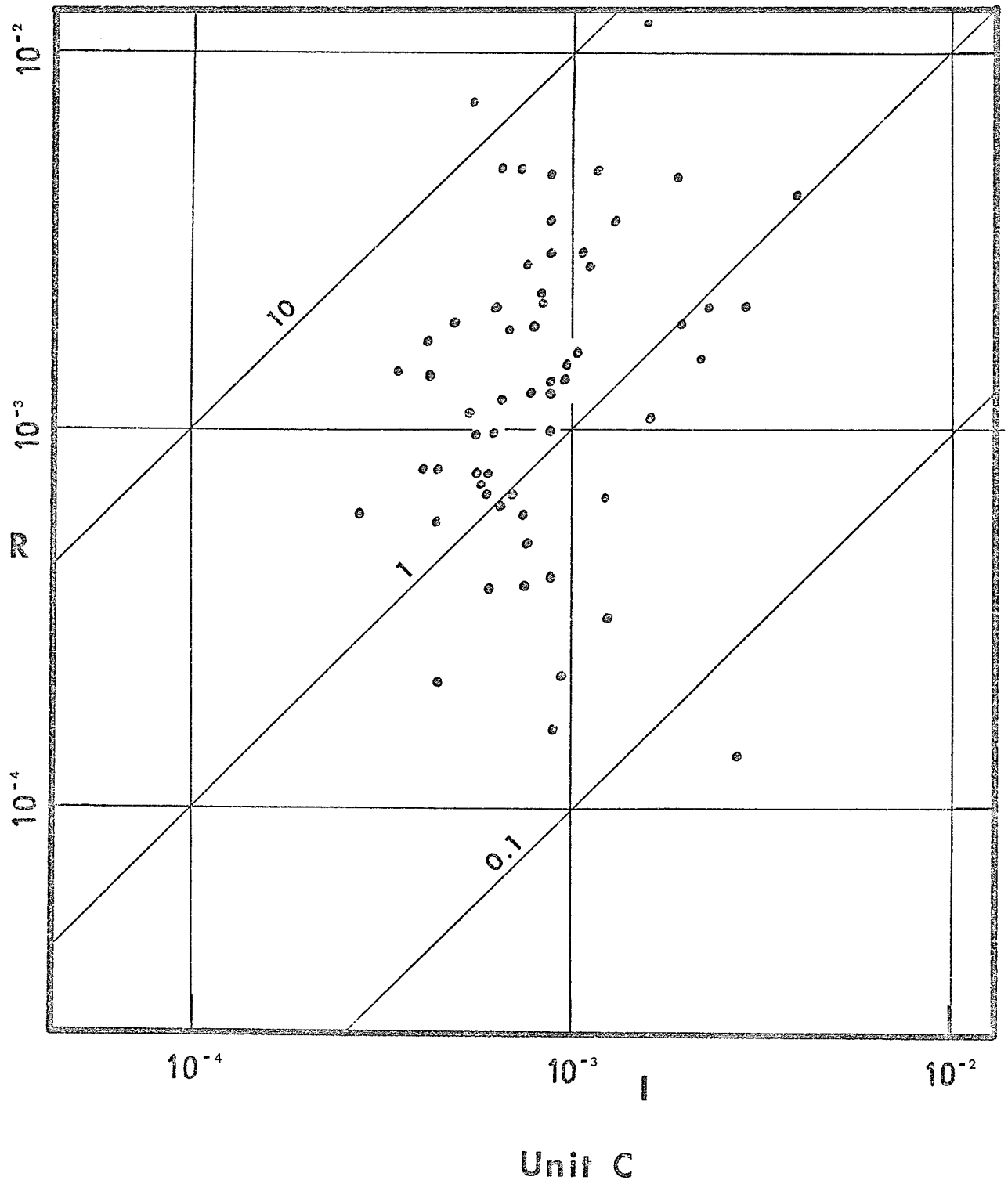

Figure 4.12 Remanent/induced magnetizations.

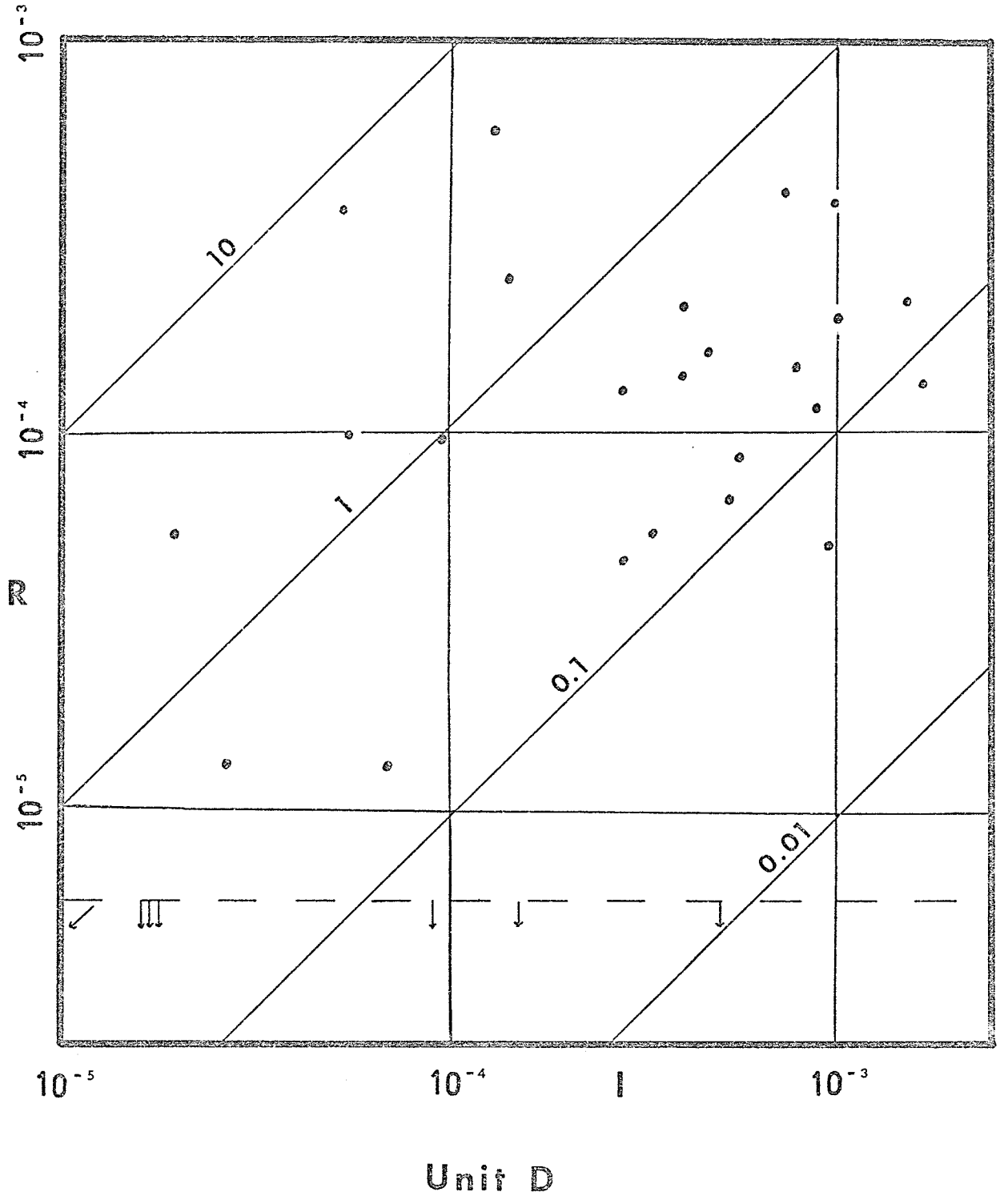

Figure 4.12 Remanent/induced magnetizations.

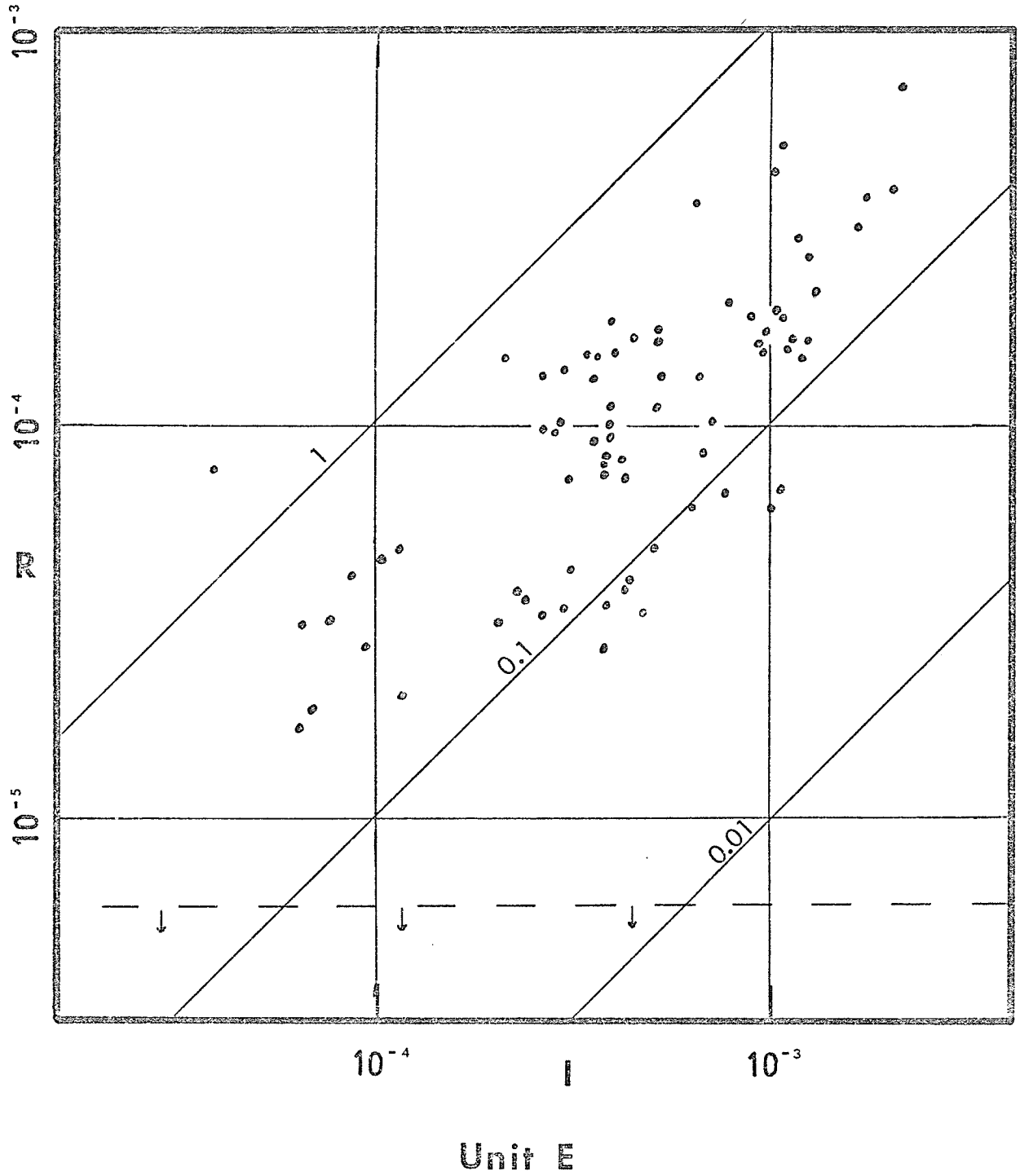

Figure 4.12 Remanent/induced magnetizations.

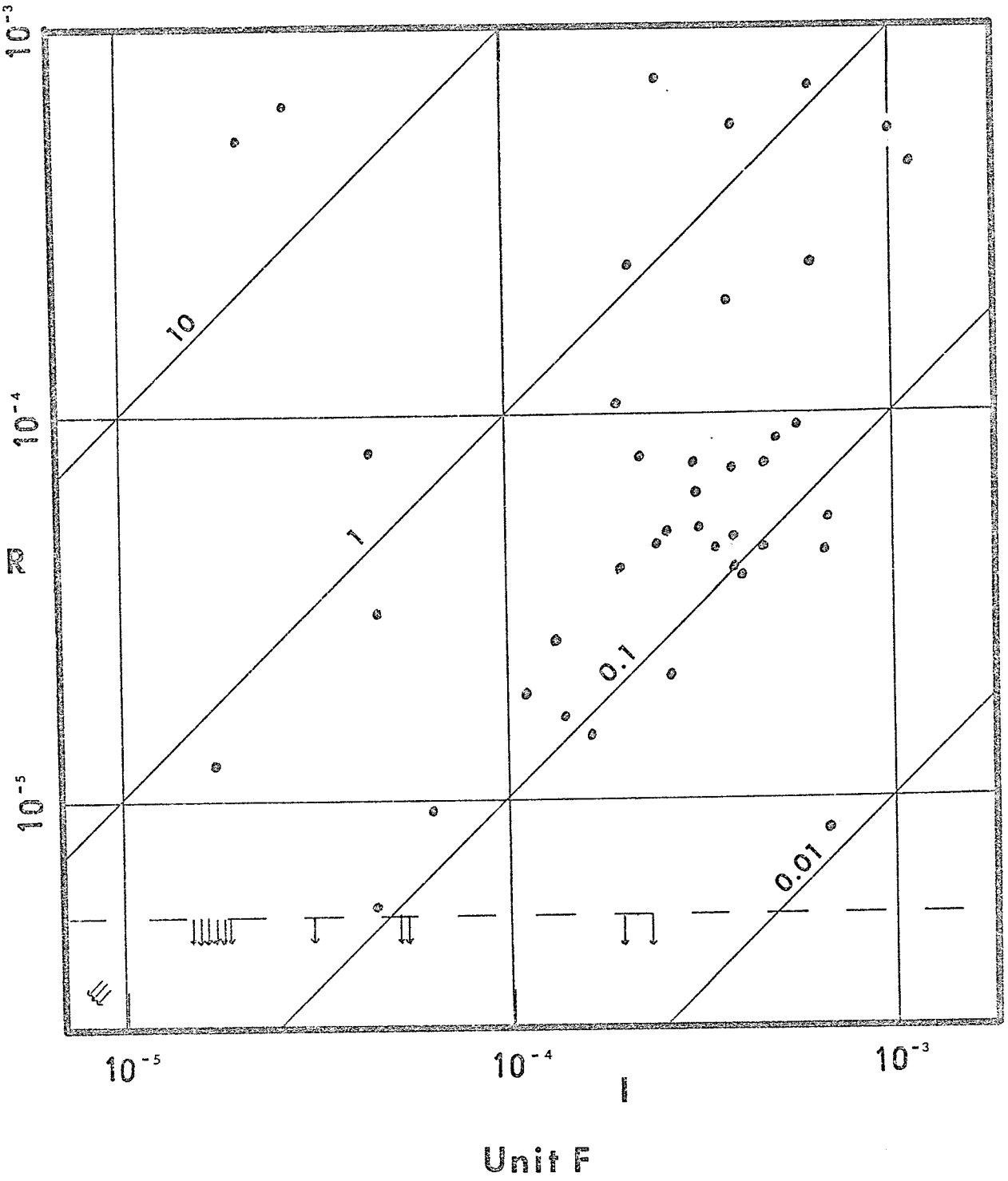

Figure 4.12 Remanent/induced magnetizations.

The divisions between the units D, E, F, are less distinct but comparisons of susceptibilities, remanences and the ratios between these properties do indicate differences in the characters of the magnetizations between the units. The rather tighter grouping of remanence directions in Unit E is noticeable, as is the grouping of remanent/induced magnetization ratios, which though still diffuse for Unit E, is tighter than for Units D and F. Unit E may be considered further as two sub-units. One of these, to the north, is characterized by more widely fluctuating magnetizations over short distances, even within sites. The southerly sub-unit is characterized by more homogeneous magnetizations. Within this second sub-unit, there is still a spatial variation, with a maximum near the centre, but this is of longer wavelength than the variations in sub-unit 1.

Unit G is very distinctive in that most of the magnetizations are less than 6×10^{-6} emu/cm^3. (7.5×10^{-10} Wb/m^2). In most cases, susceptibilities and remanences were not even detectable. In contrast, a few isolated samples were found to have magnetizations comparable with those in the adjacent units.

Unit H is rather vague in its southern boundary, and its northern boundary is not covered by the survey. The magnetizations are higher than in Unit G, and for that reason it is considered as a separate unit.

In addition to these main units, several small areas of different

rock phases are present in Units A, B, C. The corresponding magnetizations are considerably lower, and they generally coincide with small areas of decreased magnetic field. There is also a unit I to the south of Unit A, which is small and too varied to be considered in the various plots. It is characterized by widely separated values of magnetization within a site and between sites, and by scattered remanence directions. It is quite distinct in character from Unit A. Another small group of more highly magnetized samples was found near Point du Bois; the sampling in this region was not detailed enough to determine the full significance of this group, but was sufficient to indicate that these samples could not be satisfactorily grouped with either of the nearby units, D or E.

It has been found, in general, that histogram representations of the susceptibility and remanence data are improved if the logarithm of the property is used in the classification. In some of the units (A, C, E) an approximation to a lognormal distribution is seen, (Fig. 4.8 and Table 4.1). In others, (D, F, G), the distribution is more complex. Units B and H have low populations and may give poorer indications of the actual distributions. For Unit G, the values in Table 4.1 are not fully representative. A very few higher magnetizations affect the mean and standard deviation considerably, and the distribution is very positively skew.

The units as defined are fairly inhomogeneous, as indicated by the relative dispersions s/m in Table 4.1. These values are in general agreement with the results of Puranen et al. (1968), who found that the s/m ratios in the Virrat area of Finland were of the order of 0.5 - 1.0. However, Puranen et al. subdivided their data into specific rock types rather than magnetic units.

4.6 Magnetic Cleaning

Remanent magnetizations in rocks may be acquired by a variety of mechanisms (Irving, 1964). Some of these remanences are stable and not easily removed, whereas others are less stable and more readily removed.

Thermoremanent magnetization (TRM) is acquired by a rock in cooling from an elevated temperature in the presence of a magnetic field (usually the geomagnetic field, for rocks). TRM's are stable at temperatures well below the range of blocking temperatures of grains carrying the TRM.

Chemical remanent magnetization (CRM) is acquired as a magnetic mineral is formed below its Curie temperature during a chemical reaction in the rock, in the presence of a magnetic field. CRM's are also often stable magnetizations.

Isothermal remanent magnetization (IRM) is produced when a rock is subjected to a magnetic field at normal temperature, the field later being removed. Some IRM's are unstable and easily

removed, but others have stable components. This depends on the nature of the magnetic material and on the strength of the applied field.

Natural anhysteretic remanences (ARM) may be produced by lightning strikes; again, these may or may not be easily removed.

Viscous remanent magnetization (VRM) is an isothermal effect produced to a greater or lesser extent in all rocks containing magnetic minerals. For a given grain, VRM is dependent on temperature, time, and the strength and direction of the magnetic field in which the grain is placed. VRM is an effect produced by magnetic transitions across low energy barriers, the transitions are thermally induced. VRM's produced at normal temperatures are generally easily removed; however, they are also easily reacquired. Theoretical studies of VRM have been made, for example, by Neel (1955), Stacey (1963), Sholpo and Belokon (1969), Tropin and Belous (1970).

Detailed studies of remanences in both single and multidomain magnetic grains in rocks have been made by a number of workers (e.g. Stacey, 1963; Dunlop and West, 1969; Dunlop, 1973).

The common presence of more than one type of remanent magnetization in rocks even of paleomagnetic quality has long been recognized, and procedures have been developed to enable the stable component of paleomagnetic significance to be isolated (e.g. Irving, 1964). In fact, magnetic and/or thermal cleaning is considered an

essential step in the processing of samples for this kind of work. Useful discussions of the principles and techniques involved are given by several authors in Chapter 3 of Collinson et al. (1967).

The energy required to change the magnetic state of a specimen may be supplied by a magnetic field, and in this case the coercive force indicates the hardness of magnetic transitions. The average coercive force for a specimen may be measured, but in general the actual magnetic transitions, be they single domain changes or domain wall movements in multidomain grains, will be represented by a wide range of values (microscopic coercivities).

Because of the spectrum of microscopic coercivities, it is possible to progressively demagnetize first softer regions and then harder regions. This may be done by subjecting the sample to a diminishing alternating field such that softer zones are remagnetized into a cancelling configuration, while harder zones are unaffected. This is referred to as magnetic cleaning.

In the context of the present project, magnetic cleaning is important since it is necessary to know the significance of remanences in relation to the induced magnetizations in the production of magnetic anomalies. In some areas, remanence directions have been found to be quite scattered, whereas in others they are somewhat more closely grouped. If remanent

magnetizations are coherent in direction over a considerable region, then they may, if of sufficient intensity, produce a significant part of the total magnetization. Furthermore, if the direction is greatly different from that of the geomagnetic field, then the form of the magnetic anomaly will be greatly affected.

The remanent magnetizations obtained from the uncleaned samples may consist of more than one component. It is quite possible that the open outcrops have been struck by lightning on numerous occasions. It is also possible for samples to have acquired soft magnetizations during storage. To ascertain whether or not there is a significant coherent stable magnetization obscured by secondary magnetizations, it is essential that cleaning procedures be carried out.

An apparatus for performing alternating magnetic field cleaning has been built as part of this project. Details of its design, construction and operation are given in Appendix 2.

A number of pilot runs were made on samples selected from various magnetic units. The peak fields, at which the progressive cleanings were made, were usually at 50 or 100 Oersted intervals up to 200 Oe., and then at 100 or 200 Oe. intervals. (In terms of magnetic induction, 50 Oe. are equivalent to 50 Gauss, or 5 milli-tesla.). Examples of some of these runs are given in Fig. 4.13. The directions are plotted on a lower hemisphere

equal-area projection, and the intensities are normalized to the uncleaned intensity for each sample.

It is immediately apparent that the remanent magnetizations of these samples are in general very soft. In most cases, there is little or no evidence of a stable component of any significance. In a few cases, the levelling of the intensity at intermediate cleaning fields coupled with a temporary halt in the changes of direction suggests a more stable component, but the very soft components are still the most significant.

From the results of these trials, the probability of widespread soft magnetizations appeared great. The intensity and directional plots suggested that 200 Oe. would be a suitable cleaning level to remove the bulk of the soft components. Accordingly, many samples were cleaned at 200 Oe., although some of the weaker ones were also cleaned at the 100 Oe. level prior to this. The general pattern of results confirmed the presence of large proportions of soft magnetization components, and no systematic convergence of directions. In fact, a general divergence occurred in some areas.

Many of the samples were subsequently cleaned at higher fields; convergences were not apparent, but information on the intensity variations was obtained. To give an indication of the changes in intensity with progressive magnetic cleaning, histograms are presented in Fig. 4.14, showing the intensities

Figure 4.13 Examples of Magnetic Cleaning

Intensity plots are normalized to the uncleaned intensity in each case; abscissae are in Oersteds. Directional plots are equal-area projections; dots - lower hemisphere, open circles - upper hemisphere.

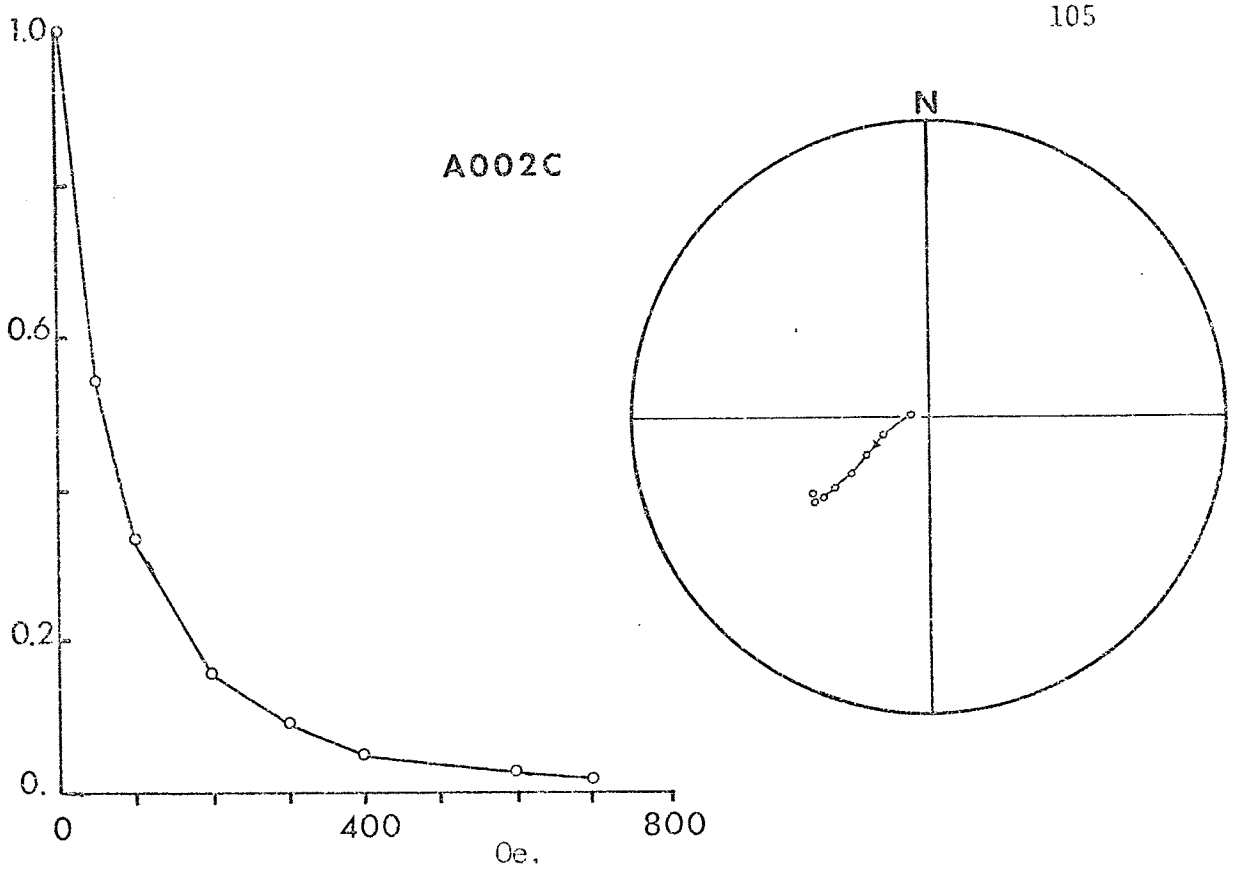

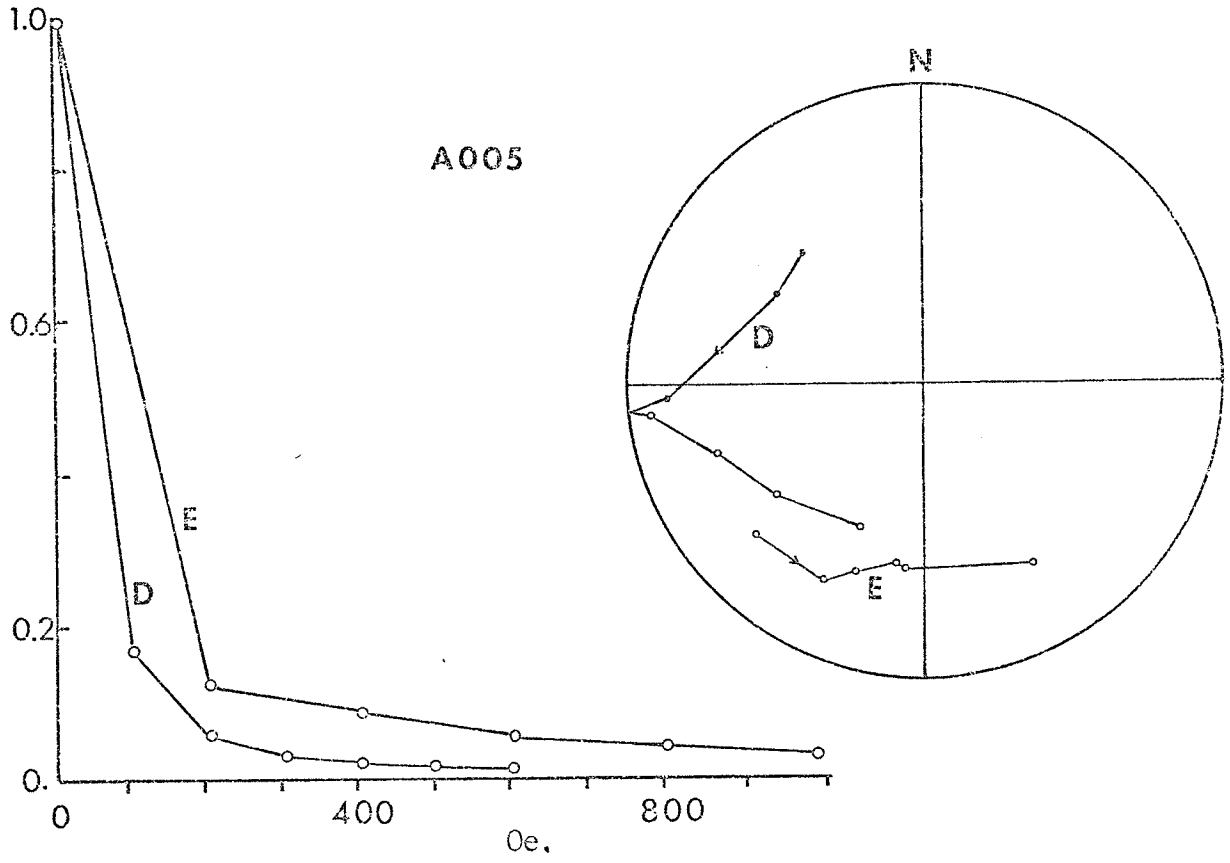

Figure 4.13 Examples of AF cleaning.

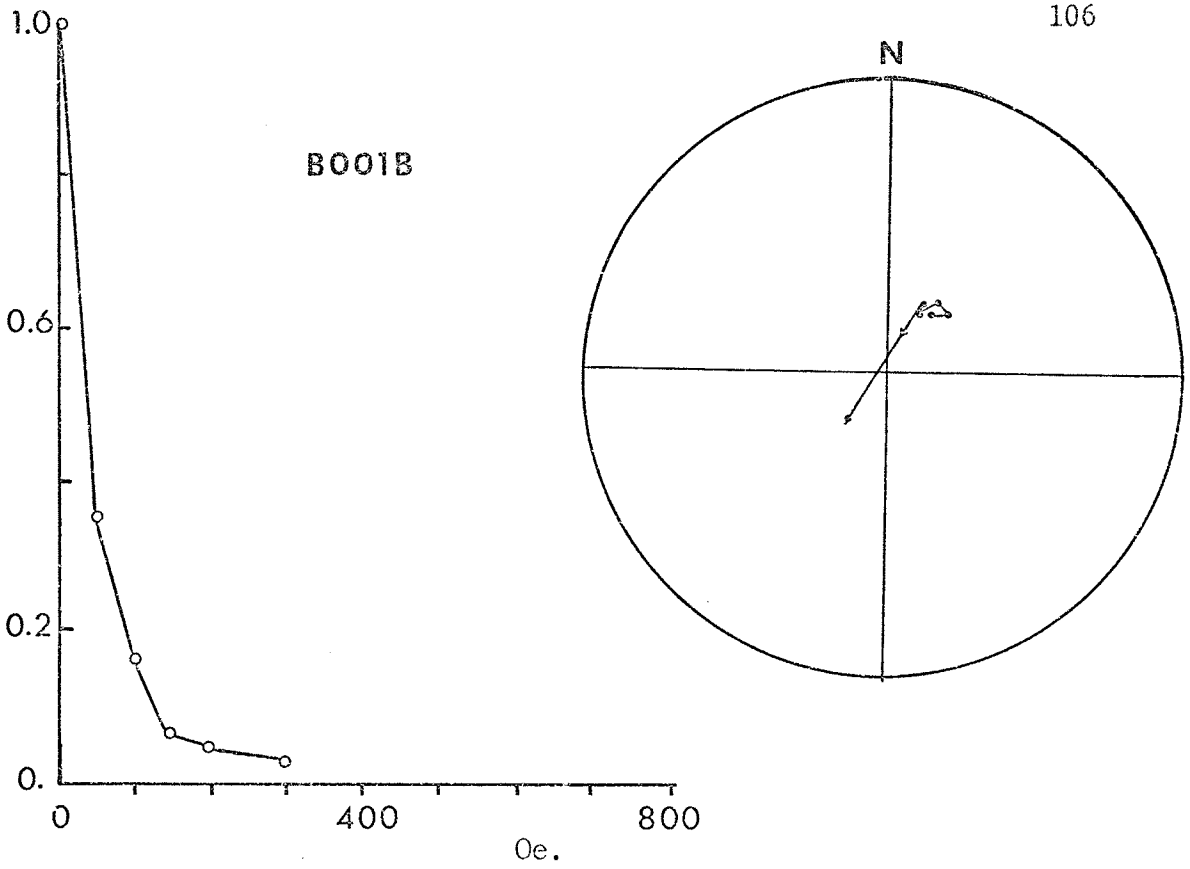

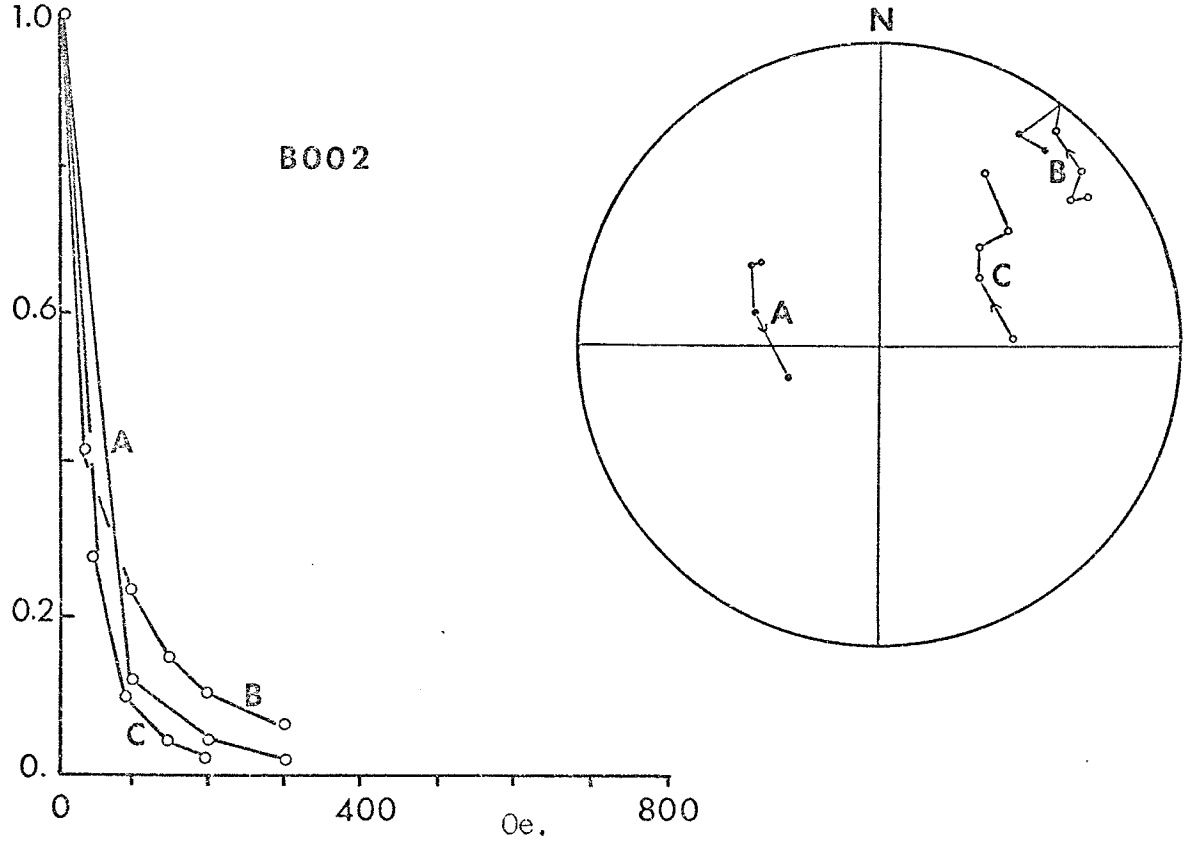

Figure 4.13 Examples of AF cleaning.

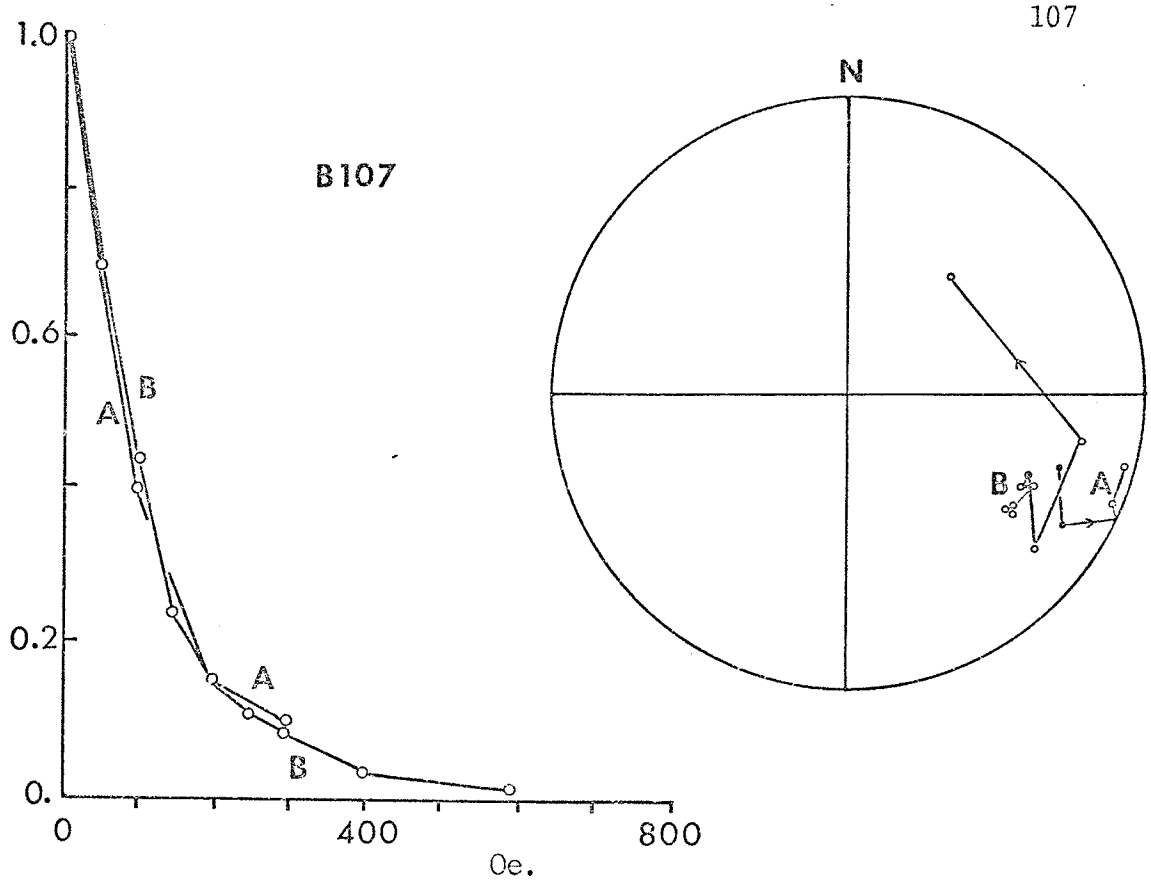

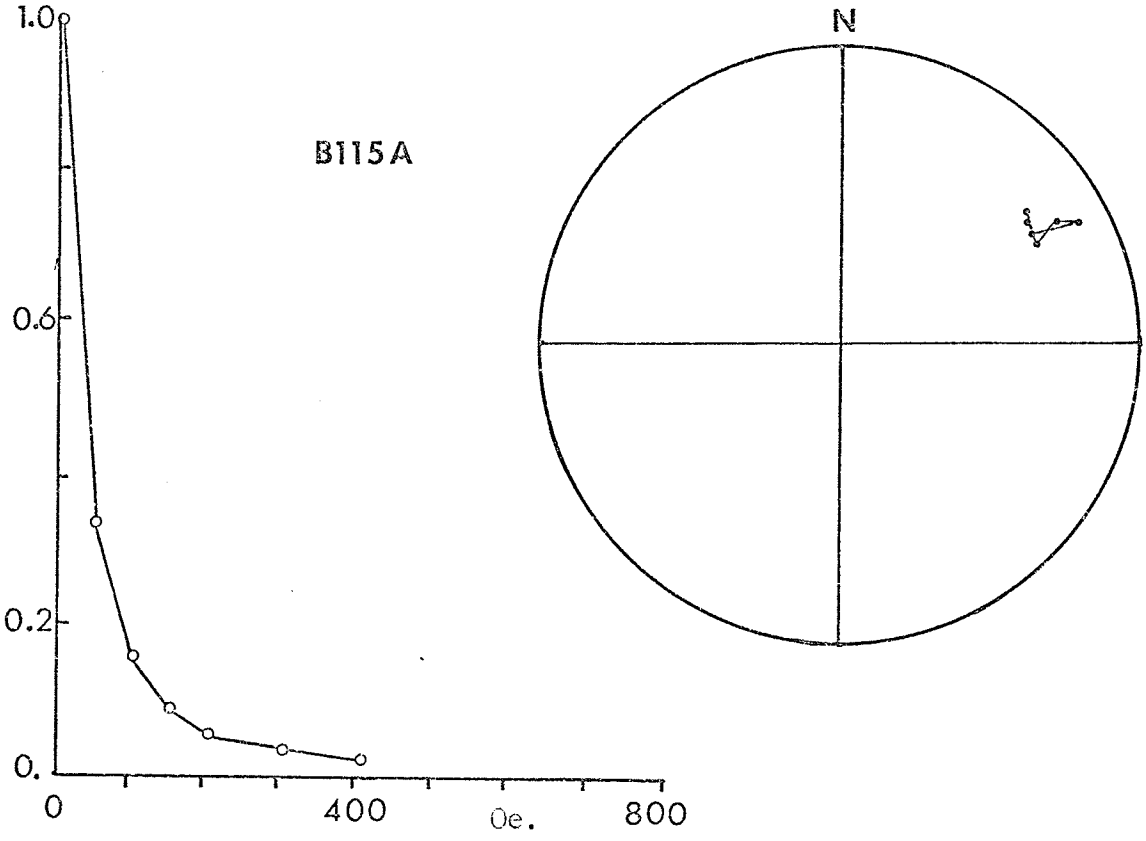

Figure 4.13 Examples of AF cleaning.

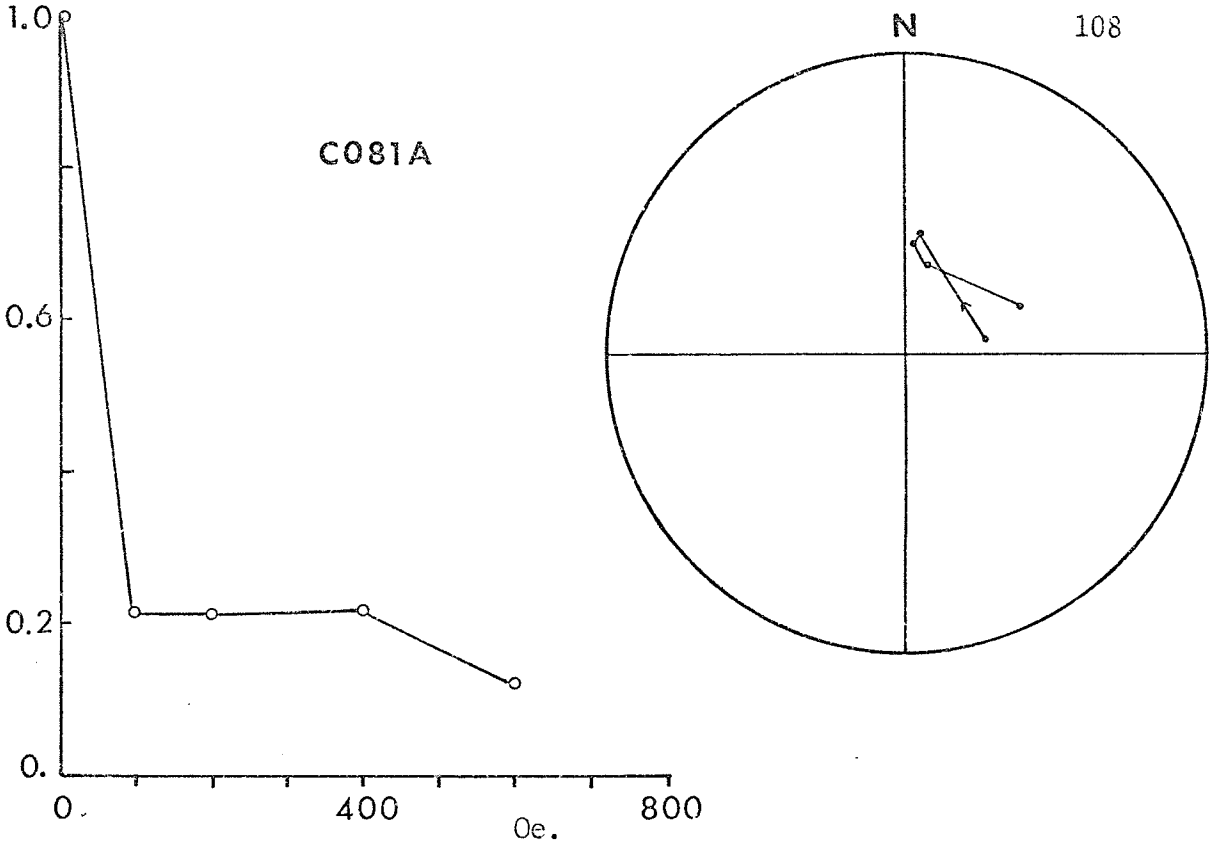

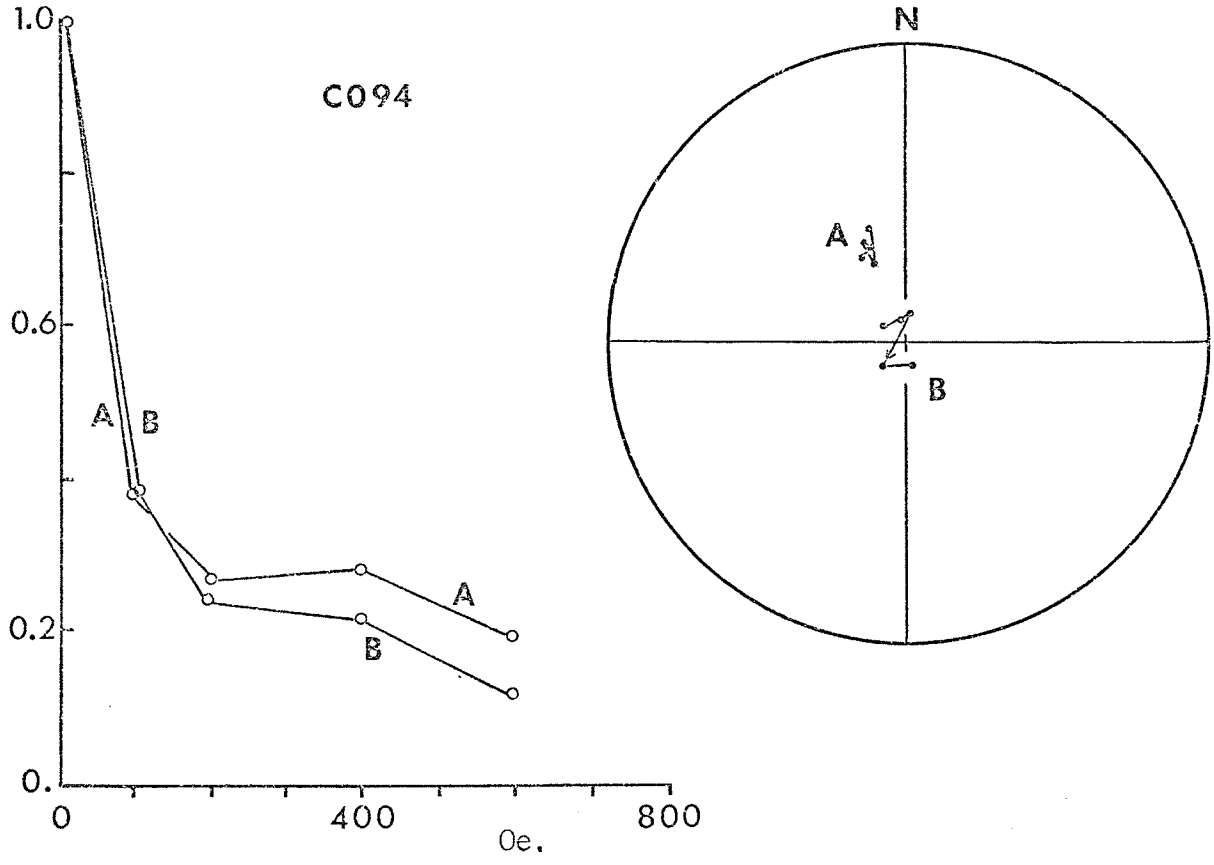

Figure 4.13 Examples of AF cleaning.

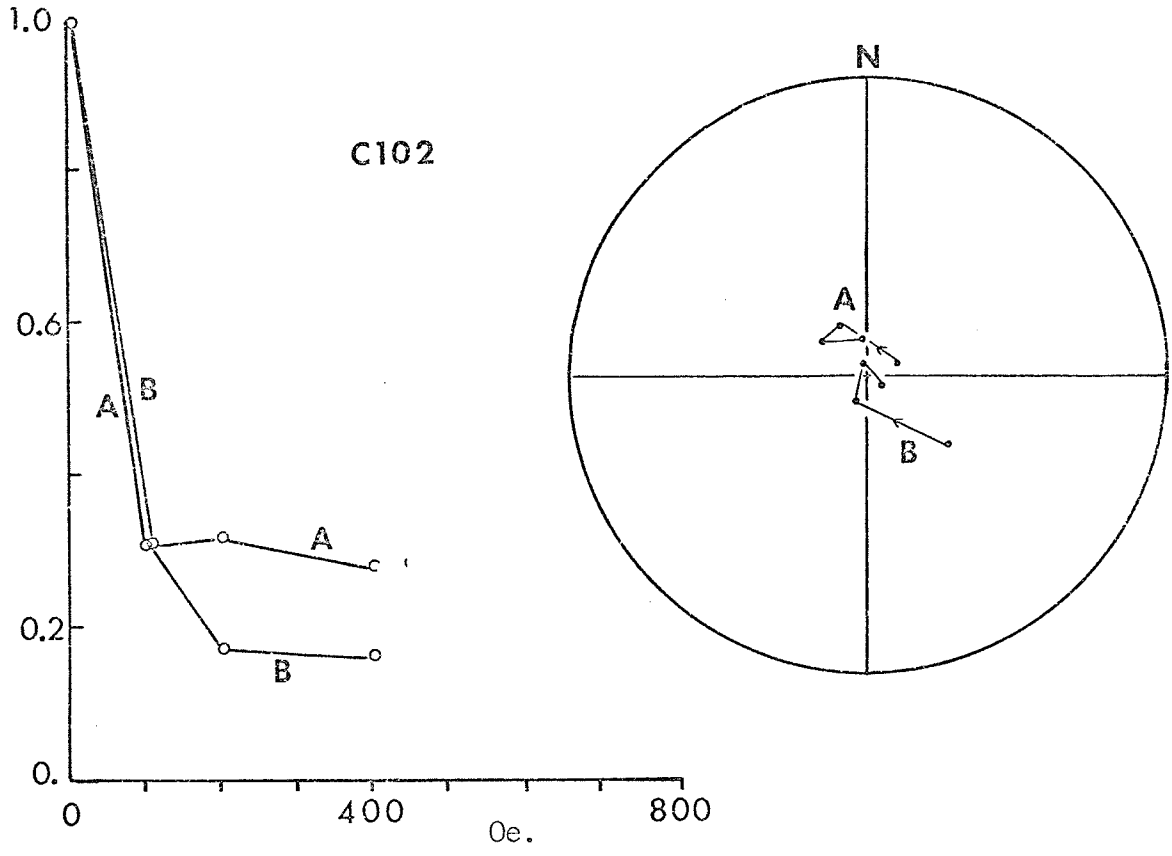

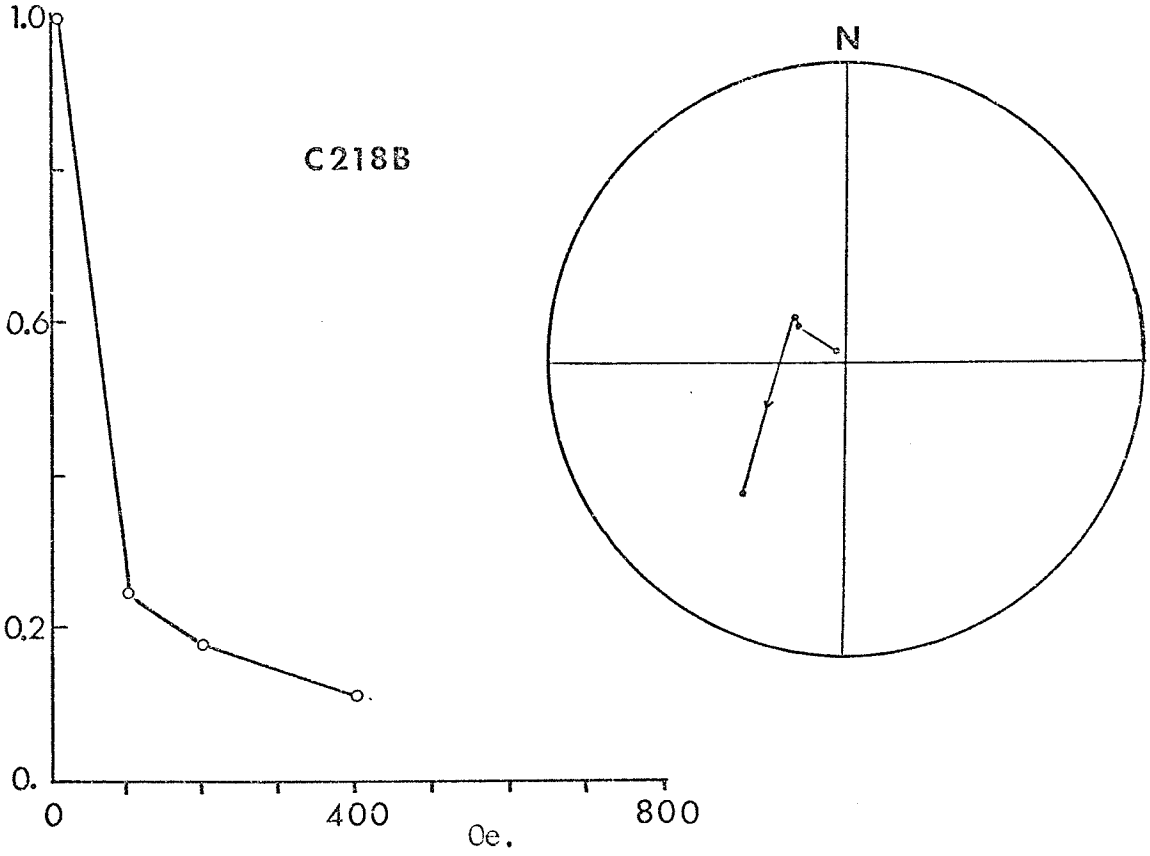

Figure 4.13 Examples of AF cleaning.

for cleaned samples in the two main divisional units, at 200 Oe. and at 400 Oe. The numbers of samples at the 400 Oe. level are less than at the 200 Oe. level for two reasons; firstly, the intensity at the 200 Oe. level may be extremely low, and secondly, the magnetization may have been found to be very unstable at the 200 Oe. level.

This latter point, instability, presented a considerable problem in the measurement of these samples. In some cases, the data on cleaned remanences is not reliable - although all measurements have been made carefully, to the limitations of the instrumentation, it became apparent quite early in the series that many samples were extremely unstable. It was found that repeat measurements were not possible, even over the short time span of about 5 to 10 minutes required to measure the three components of the magnetization. The instrumentation was carefully checked and shown to be stable in calibration.

To verify that the samples were unstable, the following test was devised and applied to a number of the suspected samples (the test is similar to that used in many paleomagnetic laboratories over a longer period of time for testing stabilities). The sample was cleaned in the usual way, and immediately after cleaning (this being the normal procedure) the remanence was measured. However, only one measurement of one component was determined. The sample was then placed, still in the sample

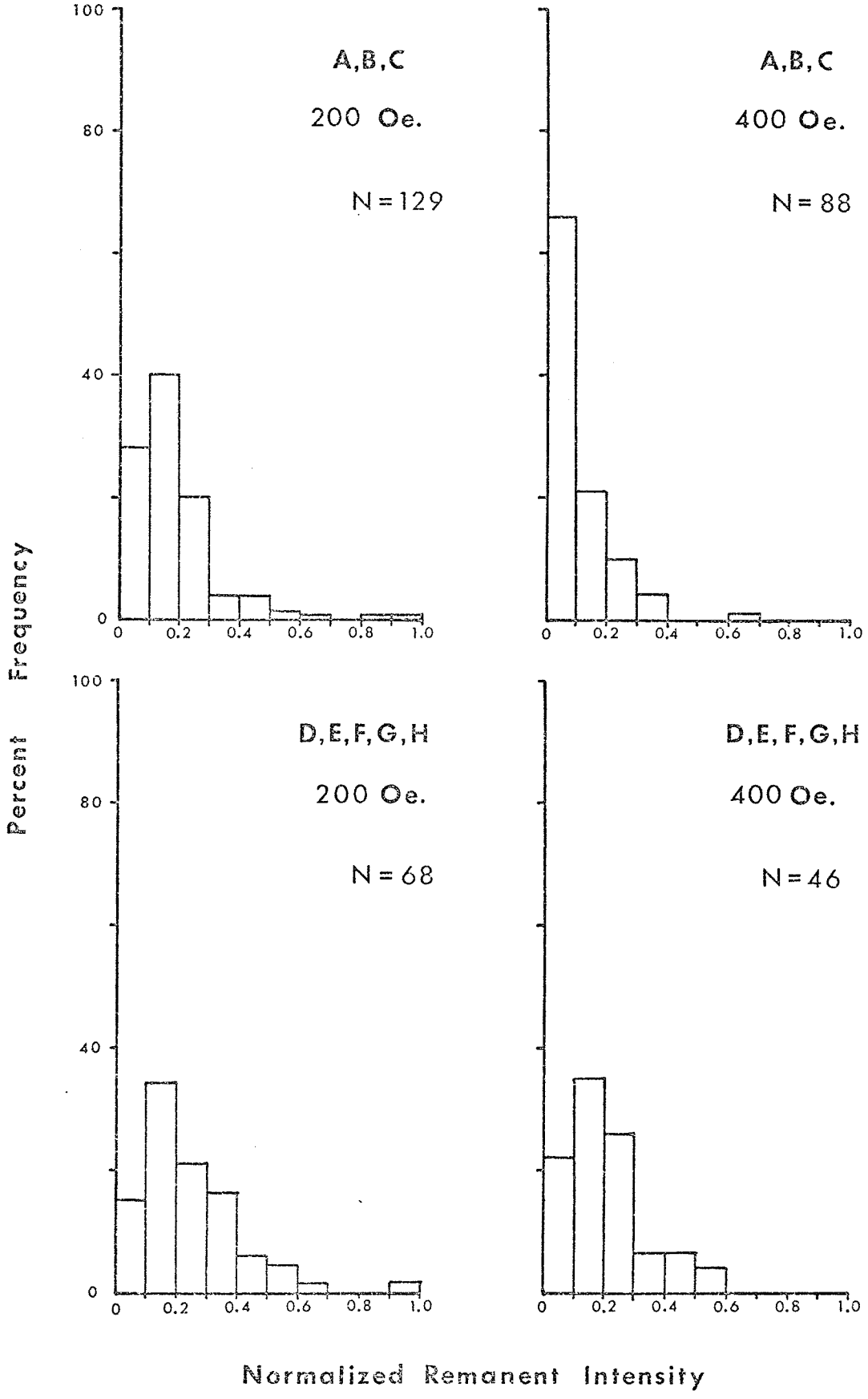

Figure 4.14 Histograms of relative intensities of magnetization after AF cleaning.

holder, on a bench with its +Z axis in the vertical position; it was left there for about 10 minutes. The same measurement of the same component was again determined. The sample, in its holder, was placed on the bench in the same position, but with its +Z axis inverted and left again for 10 minutes. The same component was remeasured again, and the sample placed as before with its +Z axis downwards for 10 minutes. Again the component was measured, the sample left for a further 10 minutes with +Z axis upwards, and finally the component was remeasured. Some typical results are shown in Table 4.2; the notable feature is the correlation of the change in intensity level with the change in +Z axis orientation. It is clear that in these cases, any attempt to measure a remanence accurately will be unsuccessful. In some cases, it was not even necessary to employ a formal test; the intensities changed noticeably whilst being observed in the magnetometer for one or two minutes. Other instances were found wherein the remanence changed quite significantly over a period of several hours.

Subsequently, some of these samples were subjected to another kind of test. They were initially cleaned at the 600 Oe. level (equivalent to 60 millitesla) and immediately afterwards the remanence was measured. The sample was then placed with the Z axis vertical and the X axis in the magnetic meridian. At later times, the remanence was remeasured, with the sample being returned

TABLE 4.2

DEMONSTRATION OF SAMPLE INSTABILITY

Sample inverted between measurements; one component measured.

Sample	Measurement	Intensity (Arb. Scale)	+Z Axis	Interval
B115A	1	1.00	-	10 min.
400 Oe.	2	1.55	D	
	3	1.15	U	
	4	1.40	D	
	5	1.20	U	
C003B	1	0.30	D	10 min.
200 Oe.	2	0.26	U	
	3	0.29	D	
	4	0.26	U	
C098A	1	0.13	-	5 min.
200 Oe.	2	0.16	D	
	3	0.12	U	
	4	0.16	D	
	5	0.14	U	
C117A	1	0.85	D	5 min.
200 Oe.	2	0.62	U	
	3	0.76	D	
	4	0.58	U	

to its same position and orientation after each measurement. The time intervals varied, depending on other activities, but were typically 10 minutes for the first remeasurement, and longer (tens of minutes, hours, days) for the later measurements. Significant changes in remanence occurred in most cases within the first few minutes. However, the observed behaviour with successive measurements was not simple. One of the problems, of course, was the one which had originally been noted, namely, that some remanences change significantly during a measurement. However, it may be concluded that the reacquisition of the soft components of remanence in these rocks appears to be a time-dependent process. Some of the results are given in Fig. 4.15. The intensities and directions are not to be considered accurate, but only indications of trends; the present instrumentation does not permit a closer analysis of this behaviour.

The samples which were subjected to magnetic cleaning were primarily those which were more highly magnetic and had strong remanences, since it is these which might contribute to the anomaly field. Even with investigations of some weak NRM's, no instances of a major remanence masked by soft components were found.

In total, of the samples cleaned, about 45% gave trouble during the measurements and were inherently unstable over very short time periods. The greatest concentration of these was in Unit B, where 80% were very unstable (the rest may be unstable

Sample		Intensity (arb. scale)	Time
B115A	1	0.38	0 min.
	2	1.15	6
1 cot.	3	1.50	12
only	4	1.40	16
	5	0.90	42
	6	1.05	75
	7	1.35	112
	8	1.35	12 hours
	9	1.55	36 hours
B107B	1	0.43	0 min.
	2	0.58	16
total	3	0.82	40
vector	4	0.72	12 hours
	5	0.84	36 hours
	6	1.09	45 hours
A020B	1	0.41	0 min.
	2	0.27	12
total	3	0.18	26
vector	4	0.26	45
	5	0.38	9 hours

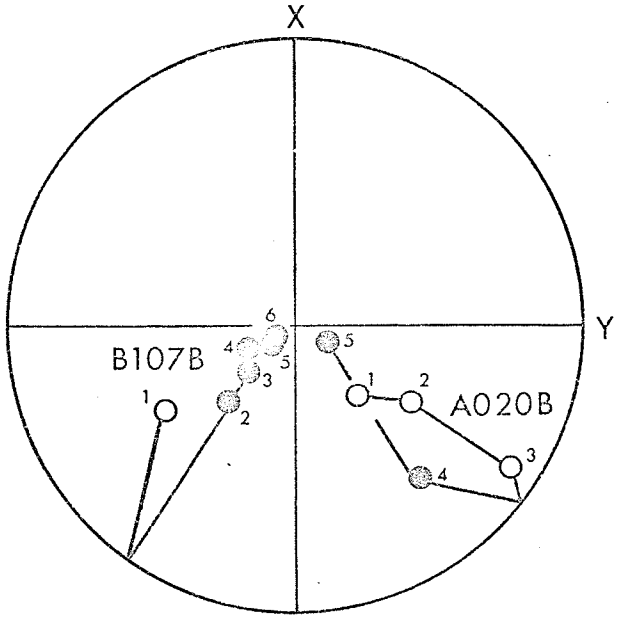

Figure 4.15 Reacquisition of soft remanence.

over longer time periods). Units A and C each contained about 40% very unstable samples. Unit E had the least percentage, about 23%. The remainder, comprising mainly higher magnetizations in other units, amounted to about 55% very unstable samples.

It may be concluded that the samples subjected to magnetic cleaning procedures have shown the presence of a considerable proportion of very low coercivity components contributing to their remanences. Harder components may be present but are very subordinate.

4.7 Opaque Mineralogy

Polished sections have been obtained for a number of samples selected from various magnetic units. They are listed in Table 4.3, and their locations shown in Fig. 3.2. The sections were examined using a Reichert Zeto-pan Large Research Microscope. Reconnaissance surveys were made in air at 132X magnification. The major part of the studies was done with 360X or 540X magnifications with oil immersion, and examination of some detail was made using 1080X magnification in oil. No colour filters were used. The lower magnifications were found to be better for general observation, in view of the nature of the opaques found.

In most of the sections, the opaque minerals were dominated by anhedral, often irregular grains (isotropic, medium to low reflectivity, slightly brownish grey in colour). Following

the descriptions of Ramdohr (1969), this material is interpreted as a magnetite, which may contain unexsolved titanium to some extent. However, as Ramdohr points out, variations in colour are not unequivocally related to chemical composition. The average dimension for these grains varied from 54 μm. to 470 μm. in different sections, (Table 4.3). Individual grains, or possibly clusters in contact, were found with dimensions exceeding 1000 μm. Seven sections contained grains or clusters exceeding 600 μm. in average dimension. In many cases, the intermediate sized grains (100 - 400 μm.) showed no sign of being polycrystalline, but in other cases, as a result of the irregular boundaries of the grains, it was not clear whether adjacent opaque regions were separate grains or were joined below the surface. In yet other cases, there was some evidence of fracturing of larger grains into smaller ones, of sizes ranging up to the order of 100 μm. It should be pointed out that the values in Table 4.3 may be overestimates in some cases, for the above reasons.

In addition to these larger grains, in many of the sections, smaller grains of magnetite were found, ranging in size down to less than 2 μm. (There may be grains much less than 2 μm. but these were not reliably identified). These smaller grains were frequently idiomorphic, often showing octahedral form.

Some of the magnetite grains carried ilmenite exsolution lamellae, generally from 1 to 5 μm. in width, usually only a

TABLE 4.3

AVERAGE GRAIN DIMENSIONS

SAMPLE	MAGNETITE µm	ILMENITE µm	PYRITE µm	PYRRHOTITE µm	HEMATITE µm
A001A	150	20	-	-	-
A005D	80	40	30	-	-
A006B	120	20	5	5	-
A010A	80	20	-	-	-
A013A	90	8	20	20	-
A018B	90	10	10	-	-
A023A	80	100	5	8	-
A027B	320	-	500	-	-
A033A	250	-	-	-	-
B001B	110	20	-	-	-
B002C	190	160	70	40	-
B017A	120	40	-	-	-
B107B	70	130	30	-	-
B111A	210	160	110	60	-
B115A	80	40	7	-	-
B121A	70	60	20	70	-
B133A	70	-	20	-	-
C006B	50	-	-	-	10
C027A	470	20	-	-	-
C052A	60	-	-	-	-
C108A	110	-	20	-	-
C117A	60	-	-	-	15
C117B	70	-	-	-	20
C252B	140	20	50	15	-

small number less than 5 being present in a grain, (Plate 1). Even at the highest magnification available, no evidence of extensive, fine-scale exsolution textures was found.

In some cases, discrete ilmenite grains were found in the same section with magnetite bearing ilmenite lamellae. In other sections, all ilmenite occurred as discrete, usually anhedral grains. These grains are distinctly anisotropic; the colours under partly crossed nicols vary somewhat, but the typical rich red-brown is more apparent in air than in oil. Reflection pleochroism is present, but often difficult to recognize in the absence of a contrasting grain (Plate 2). In several sections from one particular area the amount of ilmenite approached, or exceeded, the amount of magnetite observed (B002C, B107B, B111A, B121A). Grain sizes are extremely varied, but generally smaller on the average than for the magnetite grains (Table 4.3).

In some instances, ilmenite lamellae were seen to be partly or wholly altered to 'leucoxene', a mixture of Ti oxides and hydroxides, (Plate 3). Some discrete ilmenite grains also showed leucoxene coronas, and a few grains appeared to have been almost completely altered to leucoxene, having abundant yellowish internal reflections, with vestiges of opaque polishable surfaces.

Pyrite grains were found in less than 50% of the sections. Generally,the total amounts were small, although in a few cases,

pyrite amounted to about 3% by area of the opaque minerals. In one case, A027B, a single 500 μm. pyrite grain was found, along with a few large magnetite grains.

Pyrrhotite was uncommon, occurring only as isolated grains in a few of the sections. In several cases, replacement by magnetite was evident (Plate 4).

Hematite occurred in a few sections. As blebs in magnetite, it was found around the edges of some grains, and along cracks, (Plate 5). In some cases, associated with these areas, reddish internal reflections were seen in oil. Hematite was occasionally found in magnetite in rather irregular but lamella-like forms; and in others as distinct thin lamellae along the octahedral planes (Plate 6). The host grains in these cases were isotropic, whereas the hematite was much lighter, whiter and distinctly anisotropic.

The areal percentages for the various opaque minerals observed are given in Table 4.4. (These and the data in Table 4.3 were calculated using a computer program developed by Dr. P. Dagley, University of Liverpool).

The procedure followed to obtain these values was to note every grain which passed the field of view during a series of traverses of the section, noting the grain type and estimates of two orthogonal dimensions. The number of traverses varied from specimen to specimen, being dependent on the abundance of

TABLE 4.4

SUMMARY OF PERCENTAGES OF OPAQUE MINERALS

Sample	Magnetite %	Ilmenite %	Pyrite %	Pyrrhotite %	Hematite %	% Area of Major Fraction
A001A	97.52	2.48	-	-	-	0.95
A005D	95.20	4.65	0.15	-	-	0.85
A006B	97.50	2.10	0.15	0.24	-	0.23
A010A	98.50	1.50	-	-	-	0.54
A013A	99.20	0.003	0.51	0.27	-	4.41
A018B	99.70	0.06	0.23	-	-	0.89
A023A	95.90	3.80	0.01	0.20	0.07	0.56
A027B	80.10	-	19.90	-	-	2.31
A033A	100.00	-	-	-	-	1.36
B001B	99.40	0.60	-	-	-	0.91
B002C	67.60	29.00	3.27	0.13	-	8.28
B017A	98.00	2.00	-	-	-	0.74
B107B	55.10	44.30	0.60	-	-	1.55
B111A	58.80	37.80	2.80	0.60	-	4.34
B115A	92.90	7.10	0.02	-	-	1.93
B121A	43.91	52.61	2.99	0.48	-	1.13 *
B133A	96.80	-	3.00	0.20	-	0.82
C006B	99.80	-	-	-	0.20	0.15
C027A	99.99	0.01	-	-	-	(3.68) !
C052A	100.00	-	-	-	-	0.34
C108A	99.80	-	0.20	-	-	0.71
C117A	99.70	-	-	-	0.30	0.32
C117B	96.30	-	-	-	3.70	0.11
C252B	97.90	1.10	0.68	-	0.36	0.41

* Magnetite fraction. ! Only two grains found.

Plate 1. Ilmenite lamellae (dark) in magnetite (light grey).
Sample B001B; magnification 460X; partly crossed nicols, in air.

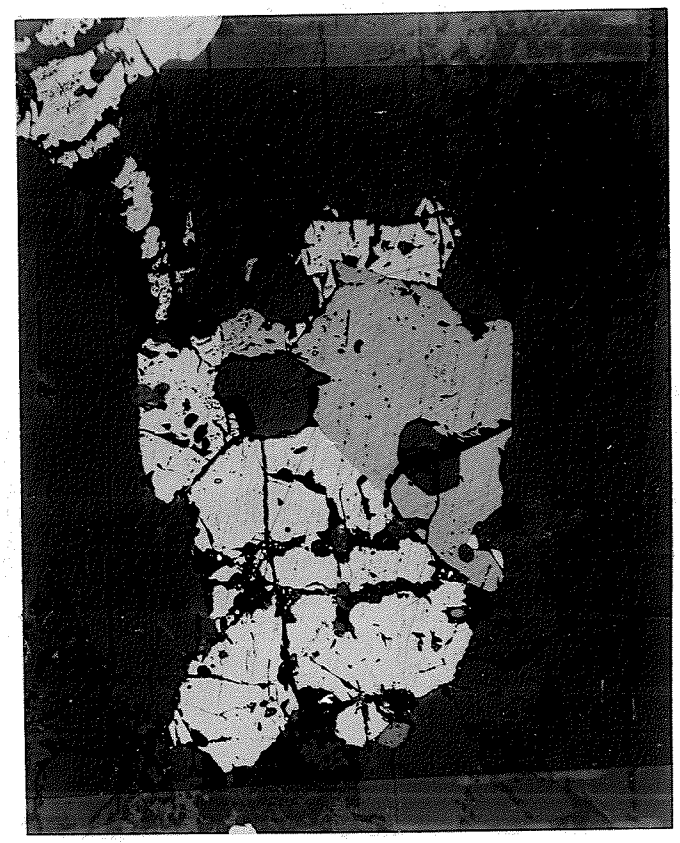

Plate 2. Magnetite (light grey) and ilmenite (medium grey) show a typical association in samples where ilmenite is abundant. Sample B002C; magnification 250X; partly crossed nicols in air.

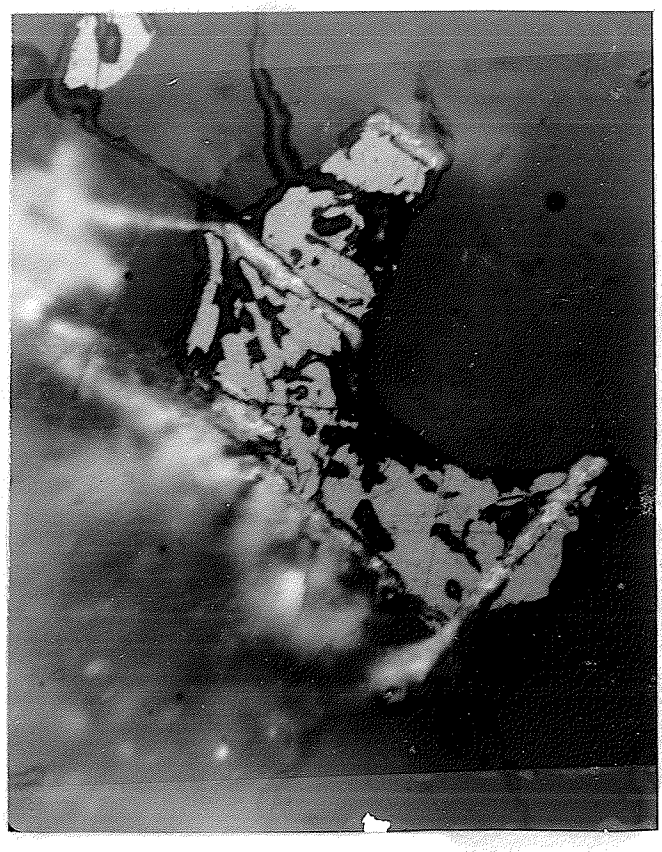

Plate 3. Magnetite grain showing lamellae altered to leucoxene (light, speckled, rather blurred lamella features).
Sample B001B; magnification 490X; partly crossed nicols, in air.

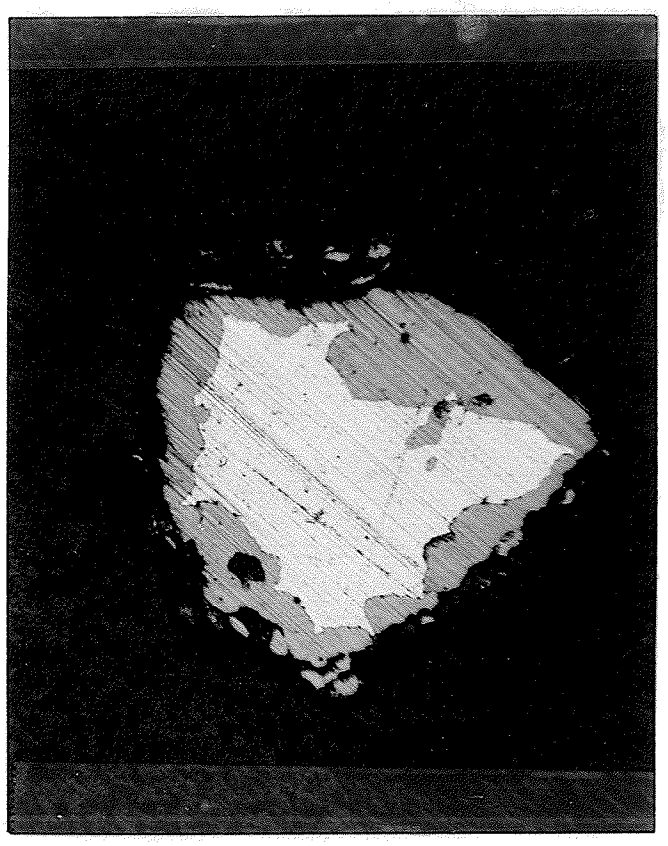

Plate 4. Pyrrhotite (light), partly altered to magnetite (grey). Sample B133A; magnification 490X, in air.

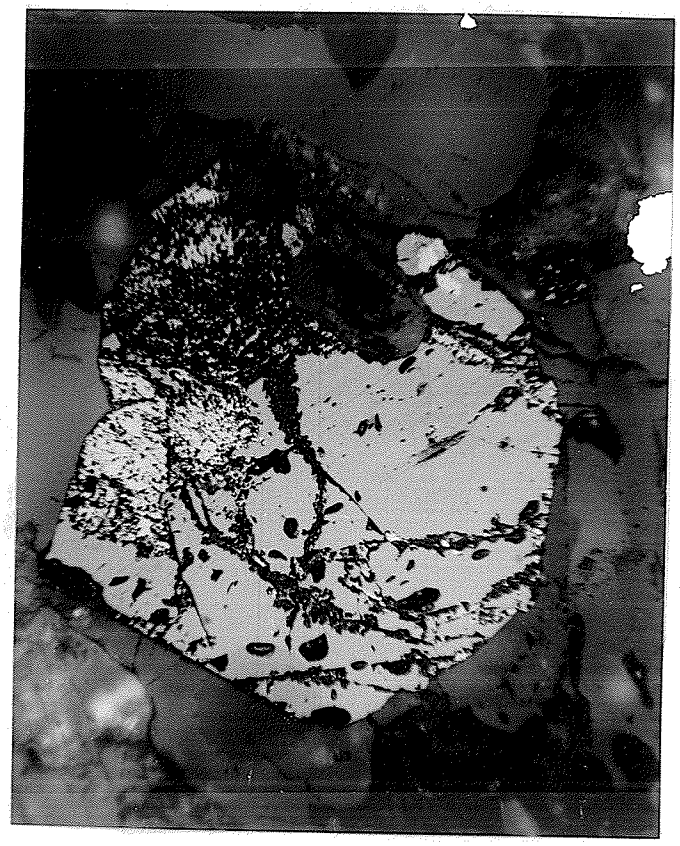

Plate 5. Magnetite (medium grey), showing alteration to hematite (light) along cracks, at edges, with large altered area at left. Sample B017A; magnification 200X, in air.

Plate 6. Magnetite (medium grey) with lamellae of hematite (light). Sample C117B; magnification 340X, in air.

opaques. In some cases, 50 to 100 grains could be found, whereas in others as few as 1 or 2 grains were found. Undoubtedly, only a rough estimate of the distributions of opaque minerals in each sample was obtained.

4.8 Discussion

It is evident from a comparison of Fig. 3.2 and 4.5 with Fig. 4.3 that there is a correlation in gross plan features between the surface magnetic units and the aeromagnetic anomalies. Whether or not the total anomaly amplitudes can be accounted for by the near-surface magnetizations is discussed further in Chapter 5. It is also apparent that there exists a direct correlation between magnetic units and some major geologic units in the area.

The measurements described in this chapter have shown that, in this part of the English River Gneiss Belt, surface magnetizations over much of the area are at quite sufficient levels for the production of aeromagnetic anomalies. It has also been demonstrated that the remanent magnetizations are either extremely soft, or of intermediate to low stability.

The somewhat scattered nature of the remanence directions may be due, in part, to the extreme softness of many of the remanences. Deviations in some cases may be attributable to such processes as lightning strikes, but in others, deviations may be produced during storage. In the storage area, the inclination of the ambient field ranged from about 65° to 80°, owing

to building effects. It was not practically feasible to store several hundred specimens in true orientation relative to the ambient magnetic field vector, and it was decided that measured specimen cylinders would be stored with +Z axes vertically down, but that X axes may be random, since if soft components were present, magnetic cleaning would remove them, leaving any more stable components relatively unaffected. If soft components were predominant, one might expect, at most, a scatter in directions, caused by partial remagnetization of very soft components, amounting to the order of 25° semi-angle, centred on the vertical downward direction. This is in fact observed in Fig. 4.7; however, some directions are outside this range, and may have been acquired 'in situ', in transit, or for one group in the following way. Unit C displays a larger scatter than other units; the bulk of samples from this unit were obtained more than one year before processing equipment was available, and the samples were stored in a random fashion with respect to the X, Y, Z axes. However, the remanences which were subsequently cleaned were found to be soft. One might then postulate only that the character of the 'in situ' directions of remanence might have been similar to those in samples taken later in the program.

The significance of these soft magnetizations is that even if the directional scatter is real (except in Unit C), the contribution of the remanence to the total anomaly field may represent a large fraction of the total magnetization. If the

soft remanences tend to follow the ambient field, the relative contribution of the remanence is governed, in a particular region, by the factor $\overline{Q.\cos\theta}$, where θ is the angle between the geomagnetic field and the remanence vector, and Q is the remanent/induced magnetization ratio. For example, if the angle θ is 30° for all samples, and Q is 1.0, then $\overline{Q.\cos\theta}$ is 0.866. Examination of Fig. 4.9 suggests that in some units, θ is generally of the order of 30° or less from the ambient field. In the southern units, Q is of the order of 1; thus, remanence may be significant in adding a contribution of 50% or more to the total magnetization. In Unit E, Q is lower, but again a contribution of the order of 10 to 20% may be present; here also the observed scatter is less. If in fact the 'in situ' directions were closer to the geomagnetic field direction, then the contribution of the remanent magnetization would be increased.

There is no evidence of strong coherent remanences in directions far removed from the geomagnetic field. The presence of reversely magnetized specimens is attributed mainly to the ease with which the magnetic transitions may occur. As explained above, many of those found in Unit C may be due to storage, whereas in other units, where the relative abundance of reversed directions is small, it is considered that natural 'near-isothermal' remagnetization processes, such as lightning, may be the cause. Natural self-reversals, or effects of geomagnetic field polarity reversals

are considered unlikely, in view of the general low stabilities.

Frolova (1970) has studied the relations between the viscous remanent magnetization (VRM) of magnetite and grain structure, and has indicated that about 50% of the VRM is destroyed in magnetites with ilmenite exsolution textures when placed in fields of about 300 Oe. (or 30 mT), in oxidized magnetites placed in fields of about 100 Oe., and in structurally homogeneous magnetites placed in fields of about 50 Oe. In the samples studied here, the NRM's were reduced to less than 50% by fields less than 200 Oe. in general, and in many cases, less than 50 Oe. This is in keeping with the microscopic observations on polished surfaces, which showed a predominance of optically homogeneous magnetite grains, with a few oxidized (martitized) grains and some with development of ilmenite lamellae.

The microscope studies have indicated considerable inhomogeneity of magnetization within some specimens. This may also be a factor causing some scatter in the remanence directions as measured.

The several tests and observations indicate that the major remanence carried by the samples studied here is probably a VRM, and as such has no paleomagnetic significance. Any other remanences are either randomly oriented IRM's, or are obscured by very soft VRM components, even after cleaning.

Larson et al. (1969) conducted a detailed study into the stability of remanent magnetizations in igneous rocks. They have

shown that a relation between the distribution of grain sizes of magnetic minerals and the spectrum of coercivities exists. They conclude that rocks containing mainly large grains in excess of 10 μm. are magnetically soft. Their results indicate that the carriers of stable components of remanent magnetization reside in actual small grains, rather than in strained regions in larger grains as suggested by Verhoogen (1959). In the present suite of samples, the selected polished sections indicate that, in general, small grains although present are overwhelmed by the quantities of magnetic material in large grains.

Curie temperatures have indicated that the major magnetic mineral in the area is either nearly pure magnetite, or a higher Ti content titanomaghemite which may be very similar in Curie temperature and structural properties to pure magnetite (Larson et al. 1969; Ozima and Larson, 1970). It has not been possible at this stage to distinguish between the two possibilities.

Thus the magnetization variations represent the variations in the distribution of titanomagnetite (in the generalized sense of the term). The mode of origin of the mineral is of interest in this connection, and the correlation of high magnetization with a particular grade or grades of metamorphism or metasomatism may be of significance in the interpretation of other areas, on the basis of magnetic anomalies.

CHAPTER 5

ROCK MAGNETIZATIONS AND MAGNETIC ANOMALIES

5.1 Introduction

Using the results of the measurements discussed in Chapter 4, several models are considered for the magnetization distribution in the area sampled, and the theoretical magnetic anomalies compared with the actual measured field shown in Fig. 5.1a, which is taken from the Four Mile to One Inch series of aeromagnetic maps (G.S.C., 1967, 1969). It is not possible in such an area of rapidly varying magnetizations (spatially), sampled in the manner indicated, to model in great detail the finer points of the anomaly field; neither is this desired at this time. The purpose is rather to consider whether or not the magnetizations of shallow units are capable of producing the total anomaly field observed on the regional scale, or whether these must be extended in depth, or again whether different magnetic units must be inferred at depth.

As was pointed out in Chapter 4, there are correlations between the surface magnetizations and some major lithologic units in the region of study. Magnetic units A, B, and C correspond closely with leucocratic 'granitic' rocks, and Unit B in particular appears to coincide with the Whiteshell Porphyritic Granodiorite of Farquharson and Clark (1971) as discussed in Chapter 3. Unit D agrees closely with the belt of grey granodioritic gneisses along the Winnipeg River near Seven Sisters and Pinawa. Unit E,

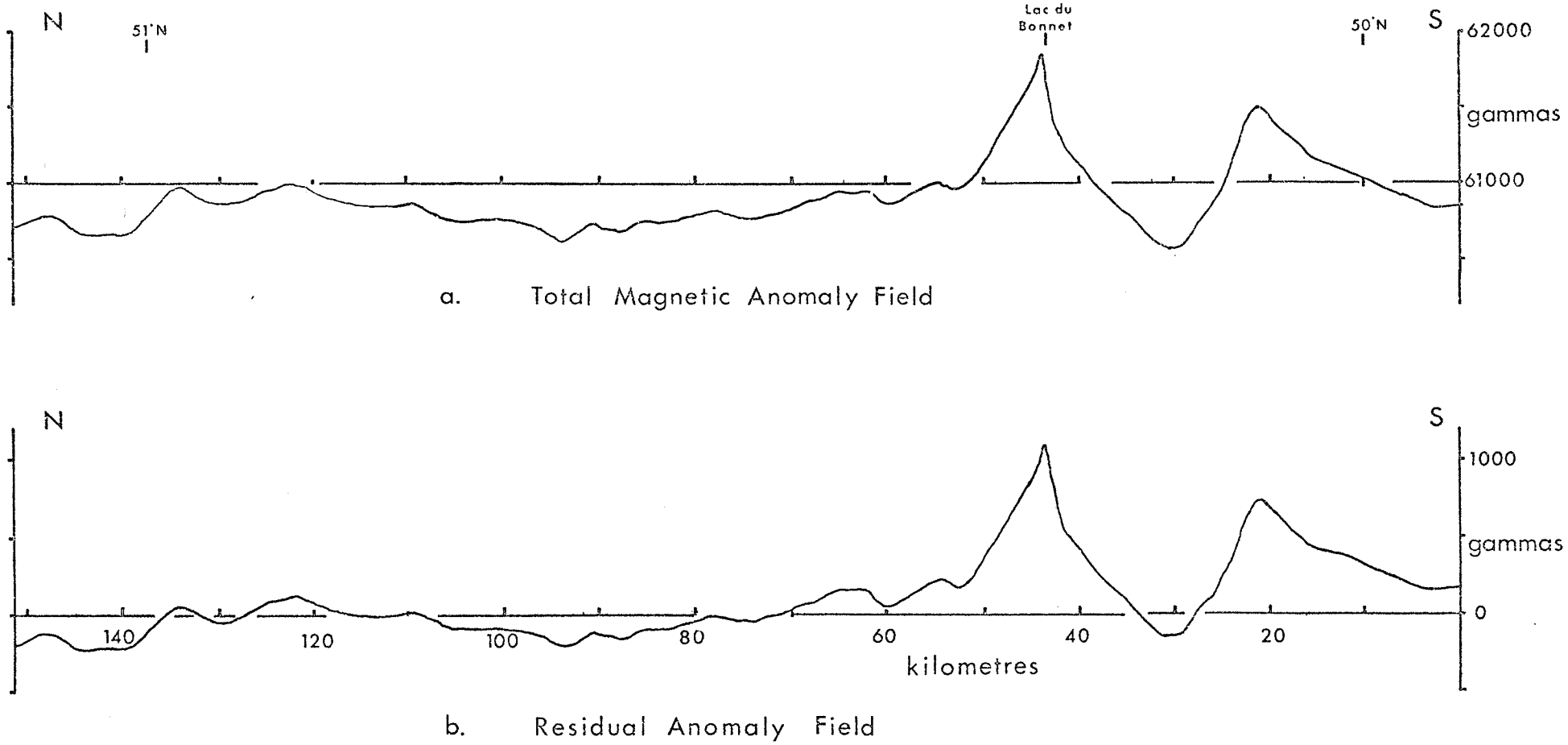

Figure 5.1 Anomaly field profile across sampled region close to Profile XX', (Fig. 4.3).

in the south, corresponds with the Lac du Bonnet pluton of McRitchie (1971), and in the north, with hypabyssal phases of the pluton and quartz dioritic intrusions. The boundary of Unit F with Unit E is indistinct, owing to a shortage of sampling sites, but there is some evidence, from the profile in Fig. 4.2, that an extra unit might be included, of low magnetizations; this unit corresponds with grey granodioritic gneisses. In the bulk of Unit F, magnetizations are higher, and in part at least may correspond with the westward extensions of McRitchie's (1971) Black River Suite. The abrupt change in magnetic character at the northern end of Unit F corresponds with the Black and O'Hanly Rivers fault zone. The mesozonal Manigotagan gneiss belt underlies Unit G, with very low magnetizations.

The correlations between geological units and magnetic units must place some constraints on possible interpretations of the form of the magnetic units, and therefore on their contributions to magnetic anomaly fields.

5.2 Magnetic Units and Anomaly Modelling

In attempting to model anomaly fields using the magnetization data, it is necessary to determine a representative level of magnetization for a particular region of volume. The simplest form is to treat each magnetic unit as a uniformly magnetized block represented by the mean of the magnetizations. In this way,

a gross picture of the general theoretical anomaly levels may be obtained, assuming various depths to the bases of the units.

In Chapter 4, the area was subdivided into a number of magnetic units, and some statistical parameters were quoted in Table 4.1. It is seen that Unit G is characterized by very low magnetizations, in general. It is important from the modelling point of view to know whether or not this unit is likely to have much depth extent.

A semi-quantitative test was described by Puranen et al. (1968). Consider a Model 1, which comprises a number of vertical infinite prisms whose horizontal dimensions are much greater than the flight height. Then over the central regions of prism (i), the total field T_i is given by (following Puranen et al., 1968)

$$T_i = 2\pi k_i T_0$$

assuming induced magnetization only; susceptibility k_i; geomagnetic field T_0. The standard deviations will follow a similar relationship (Puranen et al., 1968),

$$S_T = 2\pi S T_0$$

where S_T is the standard deviation of the anomaly field, and S is the standard deviation of susceptibilities.

Thus,

$$S_T/S = 2\pi T_0$$

Model 2. Here the prisms are finite in depth extent, but still with horizontal dimensions greater than flight height.

Now,

$$T_i < 2\pi k_i T_0$$

and

$$S_T/S < 2\pi T_0$$

Model 3. The prisms are now small in horizontal dimensions, comparable with or smaller than flight height. Owing to interactions with fields due to other prisms

$$T_i < 2\pi k_i T_0$$

and

$$S_T/S < 2\pi T_0$$

Model 4. The prism structure is now overlain by a homogeneous (or nearly so) layer of rock. Since, in surface sampling, it is this top layer which is sampled, S will tend to zero.

Thus,

$$S_T/S \to \infty$$

In the case of unit G, the standard deviation S is 0.2×10^{-3} emu/cm^3 (2.5×10^{-3} SIU), and for the anomaly field sampled close to the sites, the standard deviation S_T is 103 gammas (nanotesla). The ratio S_T/S is $1.39 \times 2\pi T_0$. This is the value obtained when

S includes the effects of the very few isolated more highly magnetic samples; if these are removed, S_T/S will of course increase further. This indicates that the surface magnetic unit G is of very limited depth extent in the form observed. The presence of a few more highly magnetic samples which are similar in character to those found in adjacent units F and H, suggests that the deeper magnetic unit may be similar to these units.

In all the other surface units, there is sufficient variation in magnetization that the ratio S_T/S is always less than $2\pi T_o$. Nothing can therefore be said on this basis, regarding their depth extents.

From a comparison of the anomaly field and the increase in magnetizations at the southern end of Unit F, it is likely that the more magnetic unit F is fairly shallow, at least at the southern end. This magnetization ends abruptly in surface expression at the O'Hanly and Black Rivers fault zone, and as indicated above, it is inferred that this magnetic unit may be present at some depth beneath Unit G.

In view of the interpretations of metamorphic grades placed on these regions by McRitchie (1971), it is also inferred that the higher magnetizations in the south of Unit F may be underlain by lower magnetizations comparable with those of the grey gneisses at the surface, near the boundary region between Units F and E, in the 'katazonal' region.

The anomaly field, Fig. 5.1b, is taken from a profile close to XX' in Fig. 4.3; it is intended only to show the general features of the field. A very large scale trend has been removed, using an expression for a second-order surface for this area, given by McGrath and Hall (1969) and quoted in Chapter 7. This surface is intended to approximate the core-generated field.

An extreme case would be to assume infinite depth extent for the magnetic units; a more realistic case is to consider a level within the crust for the bases of the units. Of course, the units probably extend to different depths, but in the absence of such information, a constant level will be assumed initially, with the exception of part of Unit G.

A simple model is shown in Fig. 5.2. It is evident that fine details cannot be modelled in this way. However, some of the major features of the anomaly field are present. The magnetization levels were based partly on the values in Table 4.1, and partly on the character of the susceptibility profile of Fig. 4.2. A depth to the bases of the units was taken as 20 km., this being an average depth of the major Intermediate seismic interface in the crust in the area (Hall and Hajnal, 1969; Hajnal, 1970; Hall, 1971; Hall and Hajnal, 1973).

If the depth to unit bases is increased, the general level of the anomaly field will increase. As may be seen by a comparison with the residual anomalies in Fig. 5.1b, if the trend surface removal is correct, the general level of the model field

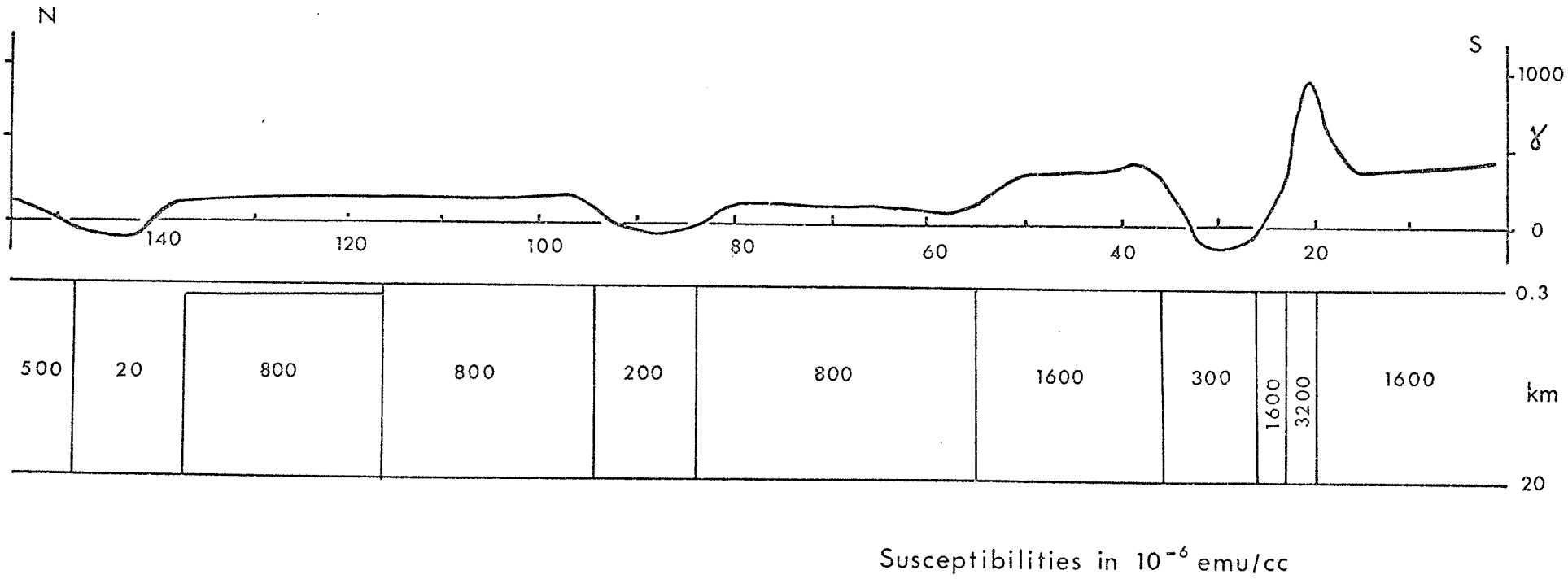

Figure 5.2 Simple model using magnetizations based largely on magnetic unit means.

is already rather too high, with the exception of the area at about 45 km. from the southern end, where the anomaly peak is missing. Only induced magnetization was considered here.

Thus most of the magnetic units as seen at the surface are capable of producing anomalies comparable with the observed field anomalies; their depth extent is not greater than about 20 km. This is in general accord with results of Bhattacharyya and Morley (1965) and Hall (1968) in adjacent areas.

Modelling in this and subsequent sections has used right rectangular prism configurations; the anomaly fields have been calculated using the computer program BLOCK (Chapter 2, section 2.5, and Appendix 3). In profile models, the blocks were normally extended about 30 km. to either side of the profile line. This is reasonable in view of the general form of the anomaly field, and of the known geology in the area.

5.3 Model Syntheses

In order to model the field somewhat more closely, smaller volumes of magnetization are needed. The choice of magnetizations for the blocks is somewhat arbitrary, since the magnetizations are often variable over very short distances. However, values which were interpreted as characteristic of a particular region were used. In most parts of the area, a model profile is considered. The sampling was basically profile in nature, across the general geologic and magnetic strikes.

Southern region

A model profile has been constructed for the southern part of the area close to the profile XX' (Fig. 5.3). Since the choice of block magnetizations is limited by the values obtained from sample measurements, anomaly relief for a given block configuration is governed largely by the depth extent of the blocks. The block magnetizations were interpreted from the profile in Fig. 4.2. The effect of variation of depth for one particular model is shown in Fig. 5.3a, and b.

The general relief is approximately accounted for if the surface units in the southern region extend to about 8 to 10 km. depth. Insufficient relief is produced for smaller depths, using magnetizations no greater than those measured at the surface. Further extension of the block bases beyond 10 km. will of course increase the general level, but the present block form becomes unrealistic.

One model that may be considered is that the more highly magnetized Unit B is relatively shallow, and the larger unit C has a deeper base. A very simple model is to extend the depth by the addition of a generalized region below 8 km., of magnetization of the order of that at the southern end of Unit C. In Fig. 5.3c, this region is extended over the whole area considered. The effect is to raise the level of the field by about 100 gammas, if the unit is extended to about 20 km. depth.

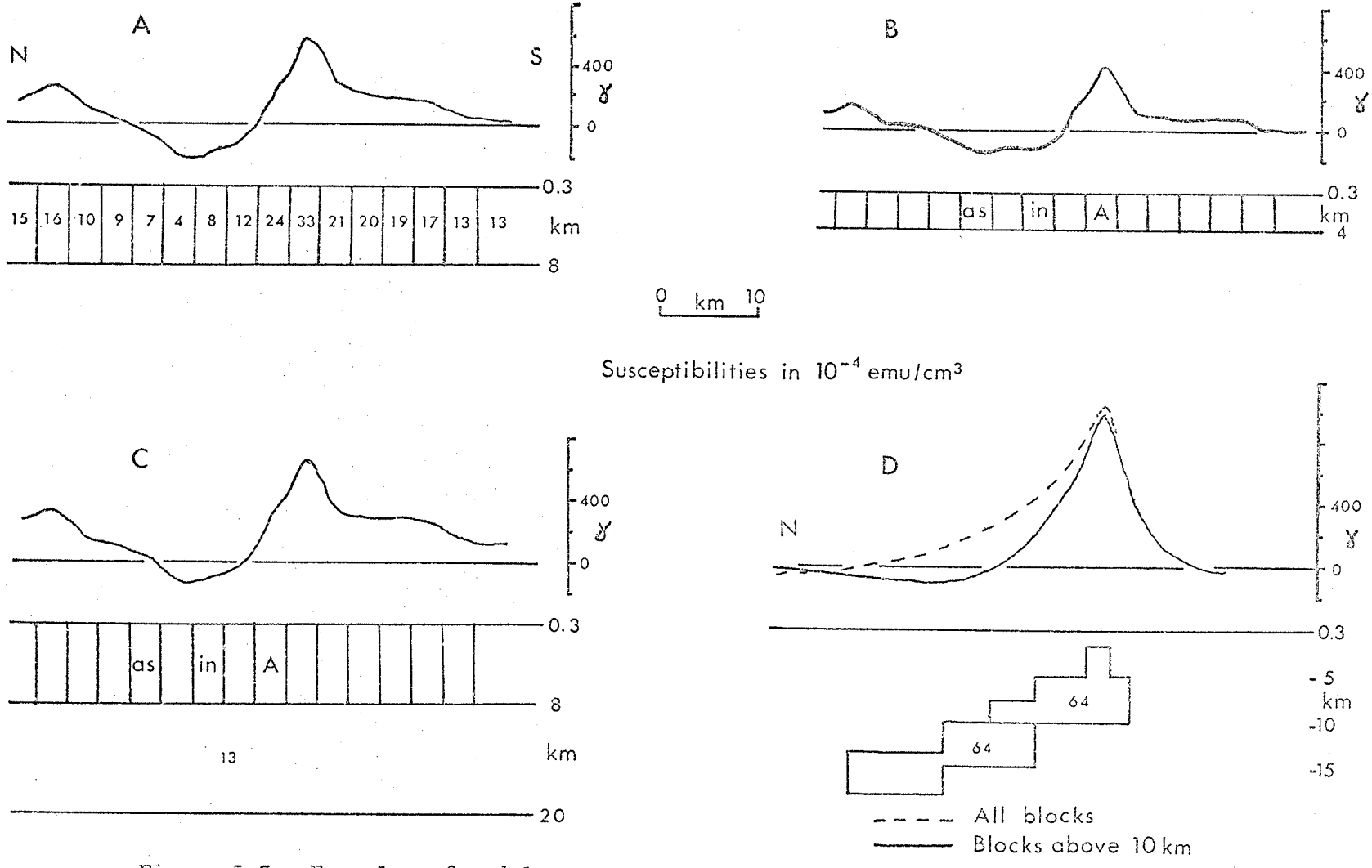

Figure 5.3 Examples of models.

Alternatively, the extent of the magnetization may be restricted to the region underlying its surface expression. Depending on the exact form of the northern boundary, which is indeterminate, the anomaly relief may be increased somewhat as a result.

By using measured sampled magnetizations in the southern area, and considering both their areal distribution and the form of the anomaly field, a model comprising many prisms was constructed. The purpose was not to model definitively or in great detail the anomaly field (this is not possible with the available information), but rather to demonstrate that the observed field in the area may be produced by a simple extension of the surface magnetizations to no more than 10 km. depth. The contoured model field is given in Fig. 5.4a, and the corresponding anomaly field in Fig. 5.4b; this latter is a recognizable portion of the southern part of Fig. 4.3. The model blocks are listed in Table 5.1. Of course, this and the other profile models are but a few of the multitude of possible block arrangements. Any attempt to interpret this area in terms of individual discrete body curve-fitting methods is likely to be unsatisfactory, because of the erratic nature of magnetization distributions. The block magnetizations used in the region where profile XX' lies are similar to those used earlier in the profile model, but not identical. The fields from the two models are comparable in this region.

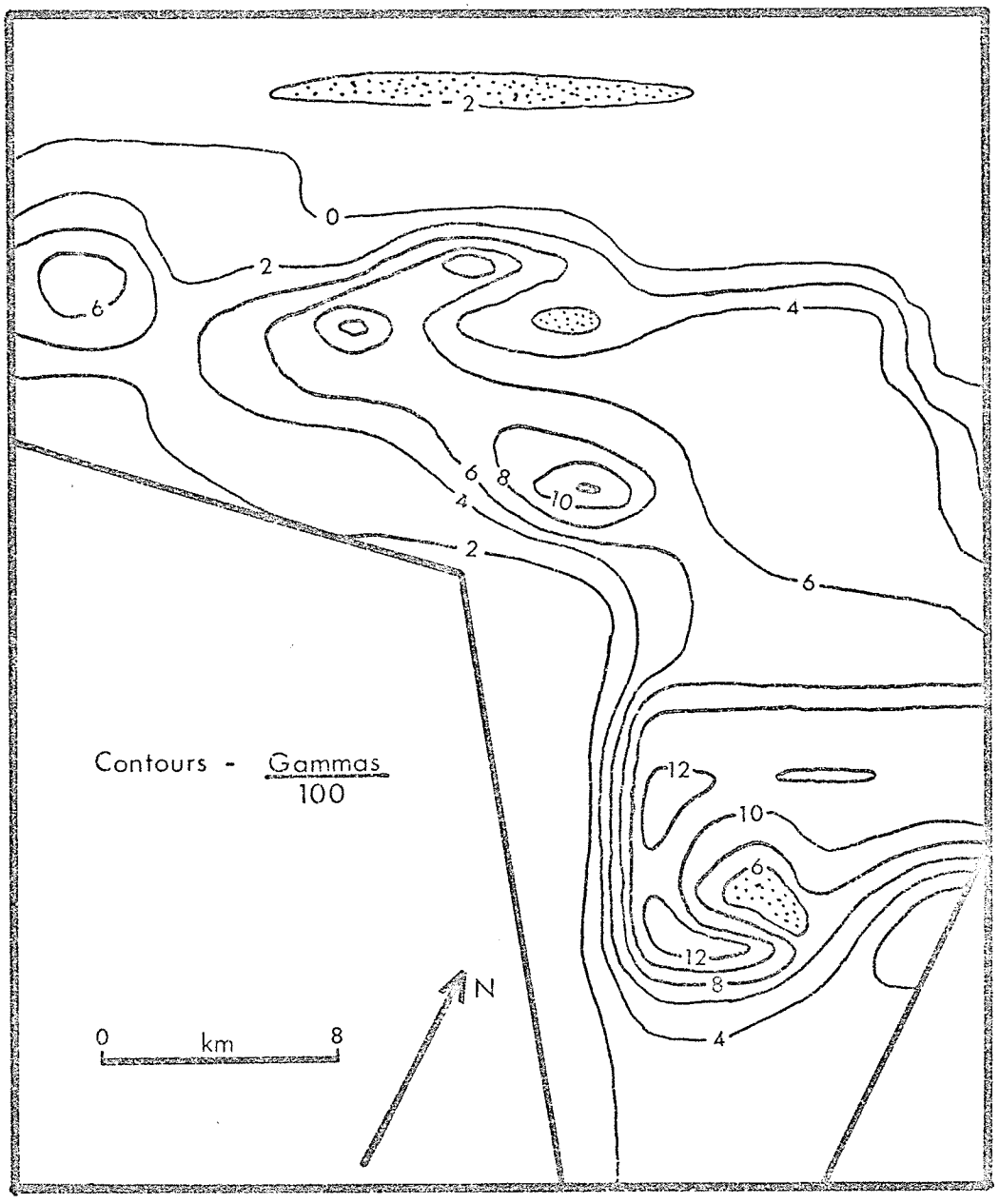

Figure 5.4a A model field in the Southern Region.

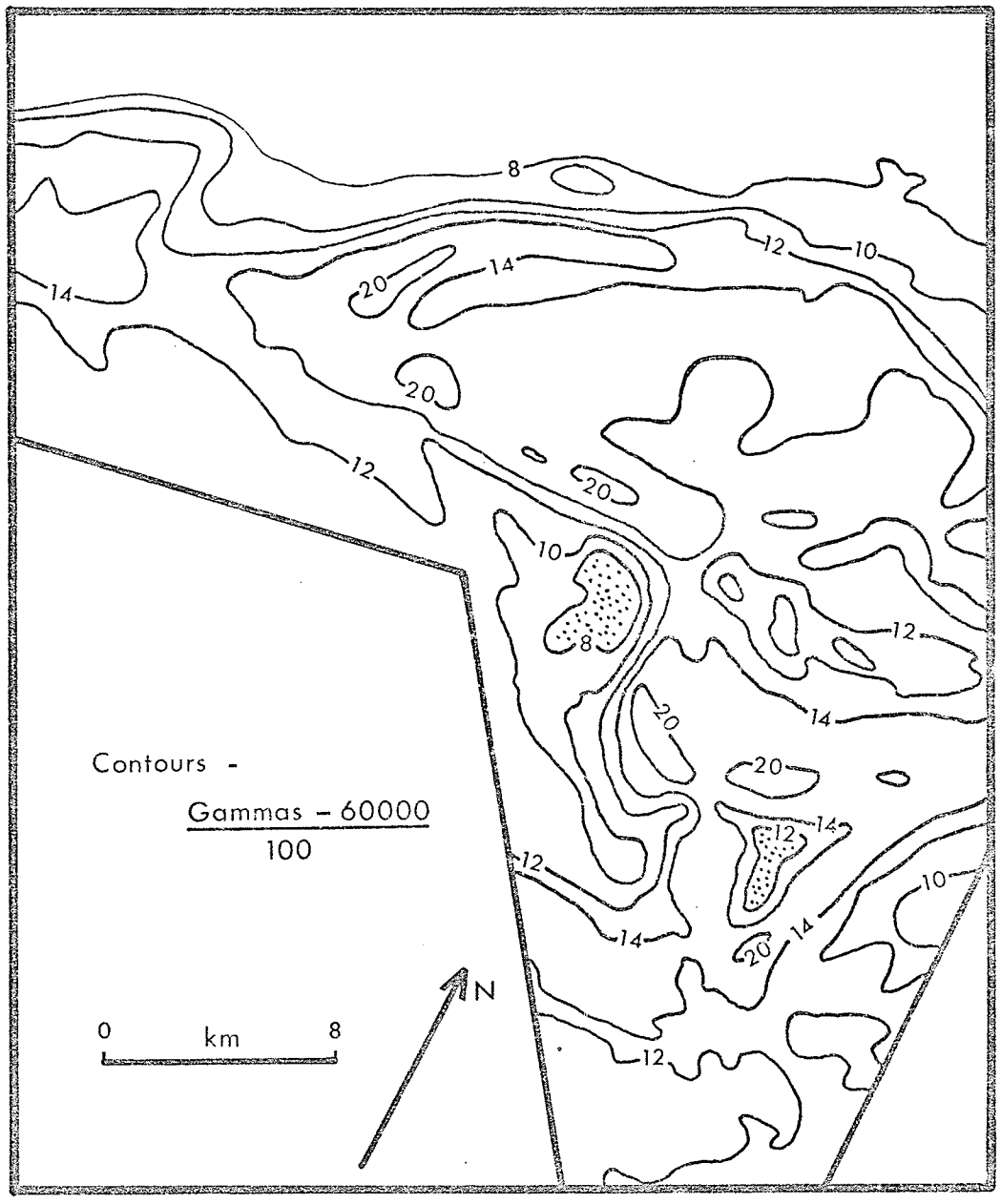

Figure 5.4b Simplified anomaly field in Southern Region. Location shown as Area B in Figure 4.3.

TABLE 5.1

BLOCKS USED IN MODEL OF SOUTHERN REGION

Block	SW. Corner X km.	SW. Corner Y km.	Xlength km.	Ylength km.	Intensity/T_o 10^{-6}emu/cm^3
10	-20.0	-50.0	54.0	86.0	1300
20	34.0	0.0	3.0	7.0	900
30	34.0	-50.0	12.0	100.0	400
50	30.0	0.0	4.0	5.0	2000
60	28.0	5.0	4.0	3.0	700
70	28.0	8.0	4.0	6.0	2000
80	26.0	5.0	2.0	9.0	700
90	27.0	12.0	1.0	2.0	1000
100	31.0	14.0	2.0	4.0	2000
110	31.5	18.0	1.0	3.0	2000
120	26.0	14.0	4.0	8.0	2000
130	24.5	16.0	1.5	2.0	2000
131	24.5	16.0	1.5	2.0	1700*
140	23.5	18.0	2.5	2.0	2000
141	23.5	18.0	2.5	2.0	1700*
150	22.5	20.0	3.5	2.0	2000
151	22.5	20.0	3.5	2.0	1700*
160	22.0	8.0	4.0	14.0	500
180	22.0	22.0	9.0	9.0	2000
190	22.0	31.0	5.0	3.0	1700
200	18.0	22.0	4.0	4.0	2200
210	17.0	26.0	5.0	12.0	2200
220	17.0	21.0	1.0	5.0	3700
230	7.0	21.0	10.0	7.0	3700
240	10.0	24.0	2.0	4.0	-4600
250	12.0	28.0	5.0	12.0	3700
260	9.0	28.0	3.0	2.0	3700
270	-20.0	21.0	27.0	15.0	700
221	17.0	21.0	1.0	5.0	-1500
101	31.0	14.0	2.0	4.0	1700*
71	29.0	11.0	2.0	3.0	1700*
280	34.0	7.0	3.0	32.0	900

Depth to top 0.31 km. Depth to base 10.0 km., except those marked *, where depth to base is 5.0 km.
Induced magnetization only.
Some blocks arranged to overlap to produce required form.

Origin is at S.W. corner of Fig. 5.4a.

The main features of the anomaly field are reproduced by the model, which uses magnetizations no greater than those observed at the surface.

Lac du Bonnet region

Modelling with measured surface-sampled magnetizations has failed to produce the high anomaly peak found in the observed field at about 45 km. north on profile XX', (see Fig. 5.1). Samples have been obtained in the vicinity of the peak, but are only intermediate to low in value. Unfortunately, outcrop is not plentiful in the anomaly high region.

The sharpness of the peak would indicate that the top of the source is not deep, and the magnitude implies considerable depth extent and/or high magnetization.

To the north, and to a lesser extent to the south, of the main anomaly, high localized magnetization peaks were found in the sampling. Yet on examining the original aeromagnetic maps, no evidence of corresponding fine scale anomalies was found; this implies that these magnetizations are localized and fairly shallow in depth extent. If, as McRitchie (1971) suggests, this area is underlain by hypabyssal phases of the pluton which appears to underlie the area of the main anomaly, the high magnetizations may be a result of a contact phenomenon between rock types and may be expected to decrease in number further

from the pluton. McRitchie interpreted the pluton as dipping to the north, based on the form of the anomaly field to the north of the pluton. He attributed this field to the presence of the hypabyssal phases above the main pluton. The predominance in places of the higher magnetizations in the north of Unit E may well be a result of differential erosion of the granodioritic gneissic rocks relative to harder quartz monzonitic or quartz dioritic units. As outcrops are relatively sparse in the area, occurring as hillocks protruding through younger cover, some unevenness in the sampling will inevitably occur as a result. The true abundance of the higher magnetizations may therefore be overestimated; the other magnetizations in the region are low, less than 0.4×10^{-3} emu/cm^3 (often much less).

Although magnetizations do rise to a maximum almost coincident with the high anomaly peak, they cannot produce a sufficient anomaly magnitude even if extended to about 20 km. depth. By taking a grid of data values over the main peak and extending into the region around, a separation of the large scale anomaly and the high peak may be achieved. The grid interval used was 1.6 km.; smaller intervals were rejected because of the noisy nature of the field, and a small amount of manual smoothing was incorporated into the data acquisition. As appears from the map (Fig. 4.3), the larger scale feature is essentially two-dimensional in this region. Accordingly, a surface (in the form

of a curve perpendicular to the major trend) was subtracted from the data values, to give the residual anomaly, Fig. 5.5.

These residual values were then used in the computer program PRISM (Chapter 2 and Appendix 3) to attempt a vertical prism model fit. Because of the rather noisy form of the local field, a good fit was not expected. However, an indication of possible dimensions, depths and magnetizations were obtained. Several starting points were tried; those with intermediate initial magnetizations converged towards very thin, but very deep (order of 20 to 30 km.) prisms, which were rejected as being unrealistic. Higher magnetizations converged towards a smaller shallower body. The model whose curves are shown in Fig. 5.5 was the most reasonable one obtained. The main bulk of the residual peak may be modelled by a body 4.3 km. long by 2.3 km. wide, with depth to top of 1.6 km. and depth to base of 5.0 km. The magnetization is near normal, of inclination 89° and declination from true north of 30°, of intensity 4×10^{-3} emu/cm^3 (3×10^{-7} Wb/m^2). Superimposed again on this anomaly form are two even sharper features which may be interpreted as upward projections from the top of the body. It is quite possible that these may subcrop at the drift-covered Precambrian surface.

However, the nature of this body is not fully defined. There are several peaks similar to this anomaly, along the strike length of the larger scale anomaly. These have not

been subjected to a model fit, but from their forms, similar results to those given above are expected. The suggestion is therefore that these are nearer-surface projections of a deep-lying larger body, of magnetization considerably greater than that observed at the surface. If this is the case, the main broader anomaly will be largely the result of this deeper body.

Alternatives may be considered. These higher magnetized small bodies may be roof pendants similar to the peripheral occurrences of high magnetizations to the north and south of the main surface outcropping pluton, or in a similar manner, may be large xenoliths of stoped material which have undergone metasomatic and/or contact metamorphic effects. However, the intensities of magnetizations found at the surface are still not as high as the model interpretation indicates.

It is also possible that these highly magnetic bodies may be isolated, but in some way were carried upwards in the intrusive phase which produced the surface rock unit.

If these bodies are localized, whatever their mode of origin, one is left with a relatively low magnetization surface unit, and a larger scale anomaly feature which reaches the order of 450 gammas (nanotesla) above base level. Even by extending the surface unit to depths of the order of 20 km. it is not possible to adequately account for the anomaly magnitude.

Figure 5.5 Lac du Bonnet Anomaly - Interpretation of Central Peak.

Profiles were taken at azimuth 150°.

Profile spacing 1.6 km. Station spacing 1.6 km.

Location shown as Area A in Figure 4.3.

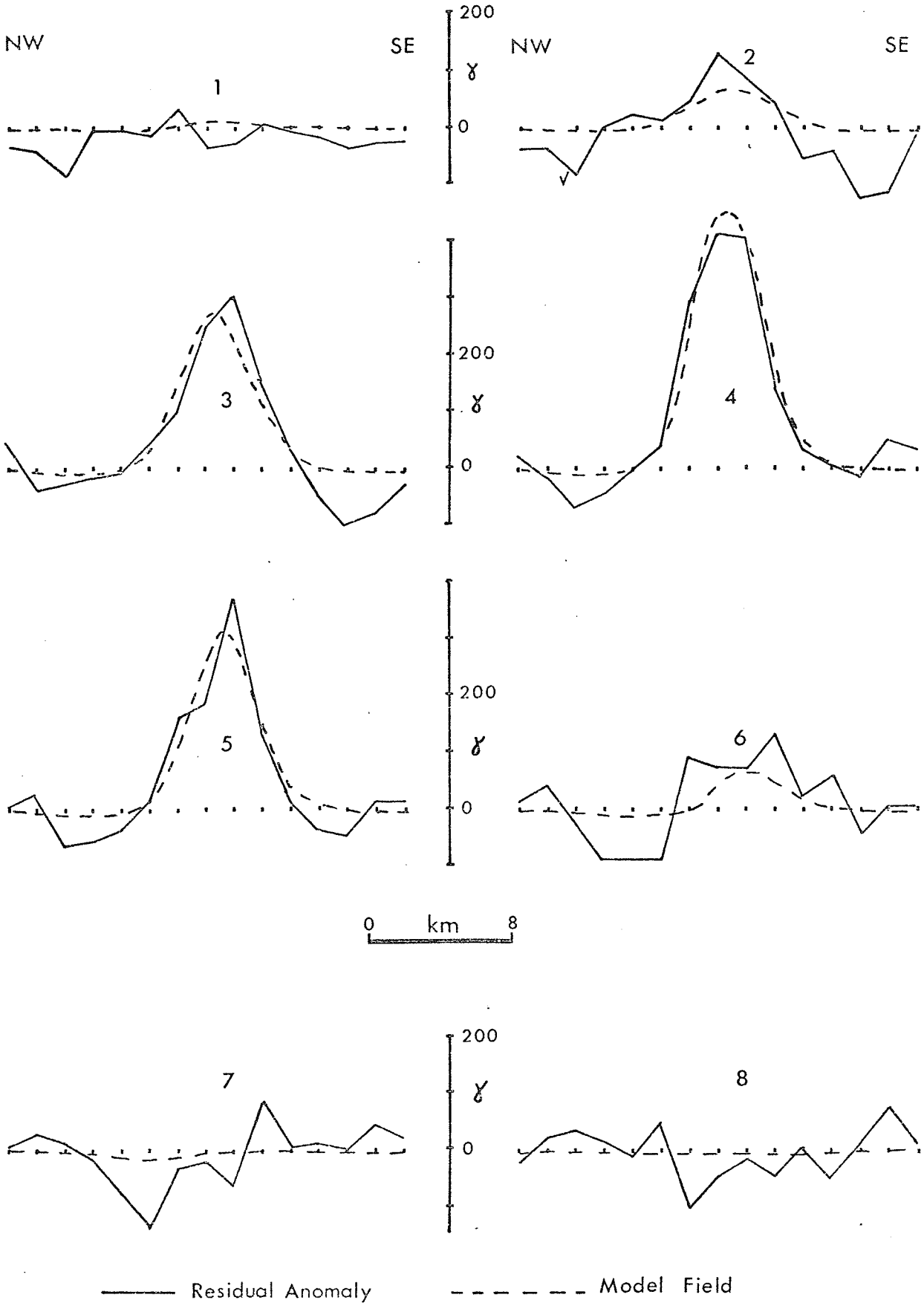
NW
SE
1
200
γ
0
NW
2
SE
3
200
γ
0
4
5
200
γ
0
6
0 km 8
7
200
γ
0
8
Residual Anomaly
Model Field

Figure 5.5

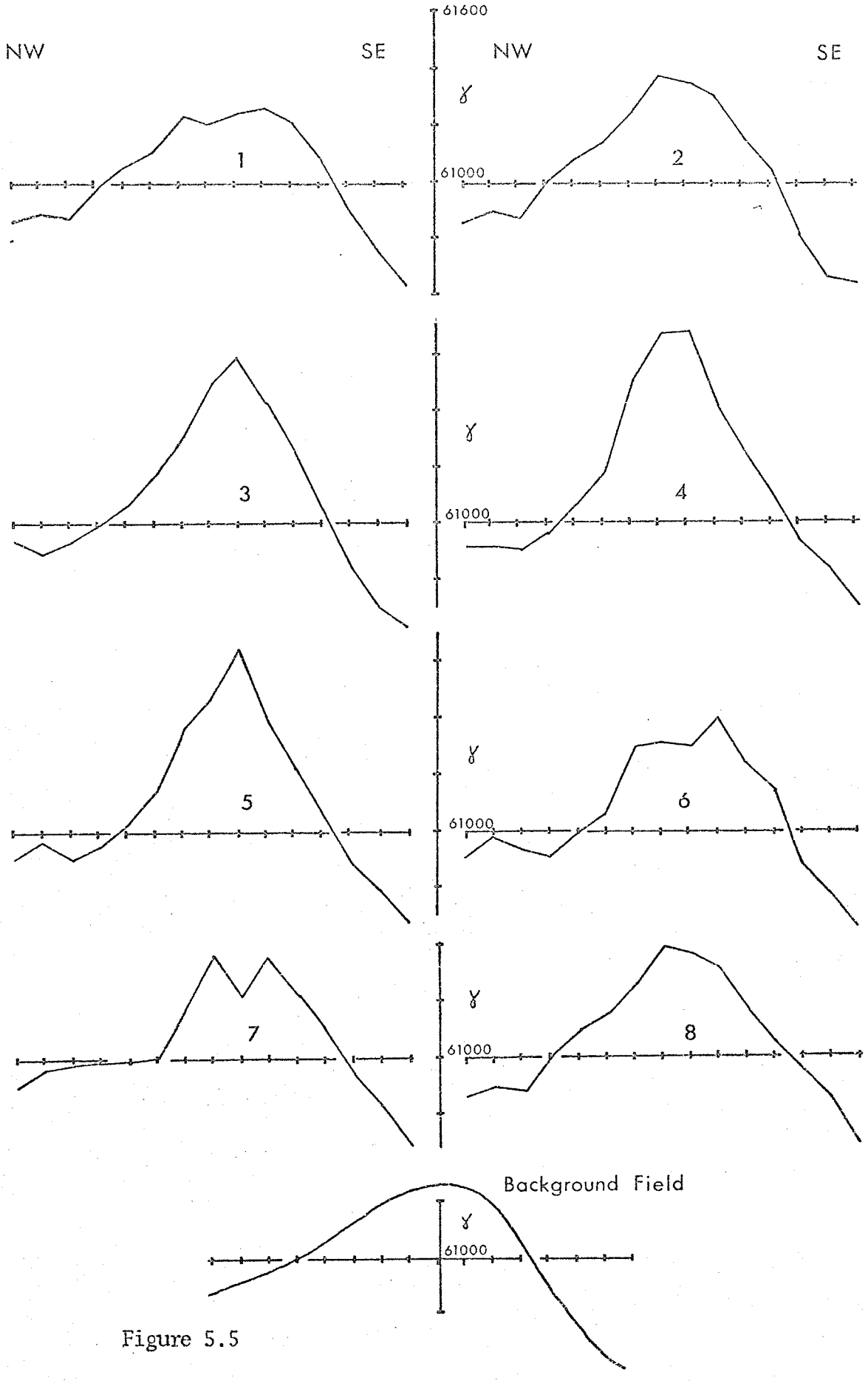

Figure 5.5

It would therefore appear likely that a deeper extensive high magnetization exists below the surface rock and magnetic units in this area, below a depth of about 5 km. If one considers the nature of the anomaly field, a magnetized body dipping to the north is suggested. This has already been proposed for the form of the surface rock unit, the Lac du Bonnet pluton, on geological grounds (McRitchie, 1971). However, as indicated above, it seems that the surface magnetizations are not adequate to account for the main anomaly. It is therefore proposed that the form of the anomaly is a result, not of a unit dipping from the surface, but primarily of an underlying more highly magnetized unit, which also dips to the north. The magnetization may be assumed to be that of the prism interpretation for the high peak. A very simple model, to indicate a possible form, is shown in Fig. 5.3d.

Whereas, in the southern region of the profile XX', surface magnetizations, if extended several kilometres in depth, appear capable of accounting for the anomaly field, in the case of the Lac du Bonnet region, an appeal to deeper, more intense magnetization has to be made.

Northern Region

Further north from the Lac du Bonnet area, the residual anomaly field (Fig. 5.1b) goes below the zero level;

correspondingly there is a region of low magnetizations at the surface. To the north again, the anomaly field rises to slightly above zero and then decreases at the end of the profile to below zero values. The surface magnetizations, as discussed earlier, do not correspond well in the northern part. There is evidence, Section 5.2, that the extremely low magnetization unit G is very shallow, in its southern half, and also that the more magnetic part of Unit F may thicken in depth extent towards the north.

If these units are generally of shallow depth extent, any relief in the anomaly field resulting from them will be small. If, as was shown in the simple model in Fig. 5.2, the depths are extended to 20 km., the field levels are too high.

Geological considerations (McRitchie, 1971) would suggest that surface units F and G are limited in depth to a few kilometres at most. The low magnetizations at the southern end of Unit F are considered to underlie the more northerly parts.

5.4 Evidence for Deep Magnetizations

In the Lac du Bonnet area, recourse has already been made to deeper magnetizations to account for the high anomaly in that region. In other areas, surface magnetizations appear capable in general of producing the level of residual anomaly field (Fig. 5.1b) - or greater.

If the base level as determined is not correct, and there is of course this possibility, there are two possible resultant effects. In view of the method of obtaining the regional surface, by fitting over a very large area to the Dominion Observatory Magnetic F Maps of Canada (McGrath and Hall, 1969), it is considered that the general trend in the present area of study is reasonable; however the absolute level may not be a true representation of the core-generated field, since a uniformly magnetized layer will also contribute to the constant field level.

If the level is accepted as it stands, then it would seem that deeper magnetizations must be invoked in most areas, such that an absence or decrease results in a depression of the general level upon which are superimposed the shorter wavelength variations - in this way, a predominantly negative region may appear.

An alternative is to call for a large extensive body of reversed magnetization. However, it has been found in a number of different Precambrian terrains, of different ages and erosion levels, (e.g. Kornik, 1968; Puranen et al., 1968; Hall, 1968; Chapter 4) that the remanent magnetizations are rarely much greater than the induced magnetizations, are generally near normally magnetized, and as shown in Chapter 4, are mostly of low stability. The prism interpretation for the stronger magnetization under the Lac du

Bonnet area also supports the idea of generally near-normal magnetizations. In the northern two-thirds of the surface sampling area, only an insignificant number of samples were found to be reversely magnetized; they were magnetically soft and the remanent magnetizations generally low in comparison with the induced components. In the south of the area, rather more intermediate or reversed remanences were measured, but as discussed in Chapter 4, these were generally soft and cannot be considered significant over any large area.

It may be suggested that magnetic minerals forming in environments of high temperature and over extended periods of geologic time will tend to form large grains, which may be magnetically unstable, in the absence of fine-scale exsolution textures. In none of the samples studied here was fine-scale exsolution found; the grains indicated a generally soft magnetic behaviour. Stable remanences may be formed by the exsolution of magnetite and hematite in very small grain sizes from silicate minerals. The presence of such exsolution has been noted by McRitchie (1971) in some samples from the Lac du Bonnet pluton. However, in the present study, the occurrence of large homogeneous, or partly martitized, magnetite grains were found in samples from the pluton, carrying a magnetically soft major remanence. If such large grains are present to any extent in a body, they will tend to overshadow any more stable remanence, reversed or otherwise.

Thus, any major body of reversed magnetization must lie at depth, below the zones in which the rocks sampled in this and similar studies were formed.

If the base level, intended here to represent the core-generated field, is too high, this implies that there is more magnetization in the earth's crust and/or upper mantle. In this case, simple extension of surface magnetizations to greater depths to produce the increased residual anomaly field in the present area requires that the units may extend significantly below the 20 km. level. Although there is known structure on the interface, this is a typical level for the Intermediate seismic discontinuity. It would seem unreasonable to attempt to extend the surface units across this distinct boundary. Thus deeper, more intense magnetizations are implied, either above or below the seismic interface.

If the base level is too low, this has the effect of accentuating the need for structure in deep strongly magnetized units, since the northern end of the residual anomaly field (Fig. 5.1b) will become negative. It has been demonstrated that the surface units cannot account for this.

Thus, the need for deep magnetizations is shown. This comparison of surface and shallow magnetizations with anomaly fields has demonstrated the need for a detailed knowledge of shallow magnetizations and their relations with possible geological structures,

when attempting to interpret longer wavelength anomalies. The long wavelength variations in shallow magnetization in the present area will produce components of long wavelength in a filtered map. This is then further confirmation that the 'confidence parameters' for deep interpretation may be low (cf. the simple models in Section 2.4, Chapter 2).

The aim is then to generate the field due to the shallow units and subtract this to obtain the effects of deeper units. Once again, the choice of depth extents for the shallow units is questionable; however, it was indicated earlier that for depths of about 8 to 10 km., the relief in the southern end of the profile could be produced. Furthermore, the bulk of the Lac du Bonnet anomaly may be accounted for by magnetization above 10 km. The depths of all the major blocks was therefore taken as 10 km., with lateral variations according to surface magnetizations.

Any such exercise in 'stripping' is to a greater or lesser extent an arbitrary procedure because little is known of the detailed structures even after a basically one-dimensional surface sampling such as has been undertaken here. Gross assumptions must be made and only gross features can be modelled.

However, a simple model of the topmost 10 km. was produced, which would take into account some of the limitations imposed in the earlier discussion. The model and profile are shown

in Fig. 5.6. Also in Fig. 5.6 is shown the difference, i.e. the 'remaining field', between the residual field, Fig. 5.1b, and the model field. This 'remaining field' must be produced by deep sources.

In the southern half, the remaining field is slightly positive, and in the north, slightly negative, the variation being a feature of long wavelength, perhaps of the order of 150 km. The shorter wavelength features are of course mainly residuals resulting from the model itself.

If the interpretation of the Lac du Bonnet anomaly as caused by a deeper magnetic unit is considered, if it extends below 10 km., or has a greater northward extension above 10 km., the higher field in the 'remaining field' to the north of the Lac du Bonnet area may in fact be removed. Also, if the southern high anomaly sources extend below 10 km., the high remaining in that region may be accounted for. An extension to about 18 km. depth with a magnetization of about 0.8×10^{-3} emu/cm^3 (10^{-7} Wb/m^2) (similar to that of the southern end of unit C) will effectively reduce the remaining field to near zero.

In all of the modelling considered, remanent magnetization has been discussed only insofar as the general absence of significant reverse magnetizations. It was pointed out in Chapter 4 that in the southern units, the remanent intensities were comparable with the induced magnetizations in many cases, and the

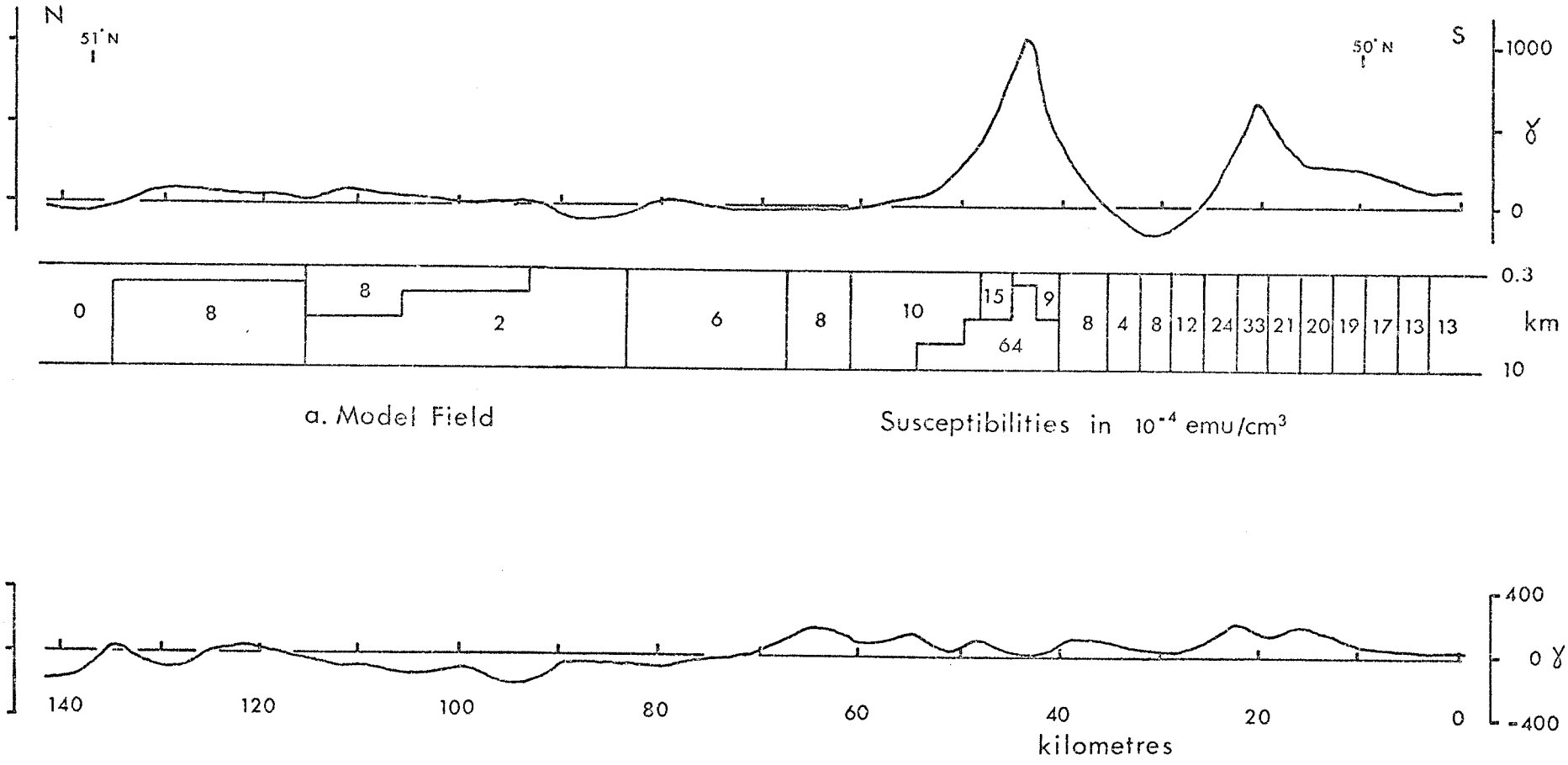

Figure 5.6 Stripping process - a) A model of shallow magnetizations
b) Remaining field after subtraction of shallow effects

directions were predominantly within about 30° of the ambient field. Therefore, remanence may contribute an amount equal to 50% or more of the induced value to the total anomaly, especially in units A and B. In view of the variations within the units, it is not feasible to attempt any form of detailed model synthesis on the basis of the remanence contributions. However, the effect of the remanence may be to reduce the depth extent required in the more highly magnetized parts, i.e. unit B and parts of unit A. In the unit E, over the Lac du Bonnet area, although remanences were soft and close to ambient field, the remanent/induced magnetization ratios were generally low. The small contribution to the anomaly field is not enough to significantly change the earlier arguments.

However, in the low region in the north, no extension in depth of surface units, or appeals to remanent magnetization will reduce the low, but rather will increase the negative values in the 'remaining field'. If the model is made shallower in extent here, the minimum field it will produce is zero, which still leaves a negative 'remaining field'.

Hall (1973) has considered a number of possibilities to account for this and other very long wavelength anomaly features in other areas.

CHAPTER 6

SPECTRAL STUDIES

6.1 Introduction

Studies of the spectra of magnetic anomaly fields may yield some information regarding the structure of the region below the plane of observation. It should be emphasized that there is, in general, no unique solution for an observed anomaly field. This restriction applies even more strongly to the interpretation of functions of the data wherein information carried in the phase is lost. Nevertheless, the use of spectral functions is sometimes advantageous.

In the present work, the interest is primarily in longer wavelength anomaly features, and as such, larger areas of anomaly field are considered, as indicated in Fig. 1.1.

6.2 Data Processing

In obtaining gridded data, a decision has to be made regarding the interval of digitization. There are two conflicting criteria: (1) the digitizing interval should be small enough to avoid significant aliasing at the frequencies of major interest; (2) there exist practical limits to the time and storage available, and cost. The data which has been used in this study was digitized prior to the commencement of the project; that for Area 1 was obtained originally by Bhattacharrya

and Morley (1965), and that for the other areas by McGrath and Hall (1969). These groups were interested in anomaly wavelengths greater than 24 kilometres and 12 kilometres respectively, and the data was obtained at digitizing intervals of 3.2 kilometres and 3 kilometres in the respective cases.

To avoid aliasing completely, the sampling interval should be not greater than one half of the minimum wavelength present in the data. For airborne magnetic data obtained at low altitudes, the minimum wavelength is of the order of 0.5 km. This interval is not practical for magnetic data over very large areas, in view of the large number of data points required. However, a compromise is necessary, and if the contributions from frequencies much greater than the Nyquist frequency $f_n = \frac{1}{2\Delta}$ are relatively small, the level of aliasing may be satisfactorily low.

Second-order polynomial surfaces were removed from the data values, representing the core-generated field. These surfaces were obtained by fitting second-order polynomials to values taken over large areas of the Dominion Observatory Magnetic F Maps of Canada (1955, 1965, 1970). The surface used for Area 1 is given by

$$F(x,y) = 60547 + 6.6953\,x - 1.0951\,y - 0.0045\,xy - 0.0166\,x^2 - 0.0094\,y^2$$

where the origin is at 94°W, 48°45'N, and x and y are in units of 3.2 km.; x is northward and y is eastward.

The surface used for the other areas is the one used by McGrath and Hall (1969) and is

$$F(x,y) = 60898 - 4.1115\,x - 1.4334\,y + 0.0081\,xy - 0.0093\,x^2 - 0.0080\,y^2$$

with x and y axes south and east respectively; the origin is at 93°W, 51°28'N; the units are 3 km.

The residual values thus obtained were then subjected to a screening process which truncated any values which exceeded three times the standard deviation of the data. This removes high intensity local anomalies and reduces aliasing. The removal, by inspection, of remaining isolated peaks had little effect on the spectra.

The estimation of spectra has long been a subject of discussion. Some useful works are by Blackman and Tukey (1958), Jenkins and Watts (1968), together with a collection of papers by prominent workers in the field presented by the IEEE (1967). Other approaches have been considered by Ulrych (1972) and others.

A smoothed spectral estimator of the form

$$C(m\Delta f, n\Delta f) = \frac{\Delta^2}{N^2}\left|\sum_{k=0}^{N-1}\sum_{l=0}^{N-1} w(k,l)\,x(k,l)\,e^{-2\pi i\left(\frac{mk}{N}+\frac{nl}{N}\right)}\right|^2$$

$$m, n = 0, 1, 2 \ldots N-1 \qquad \Delta f = 1/2N\Delta,$$

has been used, where w(k,l) is a window function, and x(k,l) is the data; Δ is the digitizing interval and N the number of data points in the x and y directions.

Spectral estimates were determined for the areas using the computer program POWER, described in Appendix 3. This gives a two-dimensional spectrum estimate. Several data windows were tried, but little difference in the form of the estimate was found; the circular cosine bell window was finally used, over the whole data block in each case.

A second computer program was used to select one-dimensional views of the spectra; the program PROFIL uses a spline interpolation to obtain values on the profile. The assumption of a continuous smooth spectrum is made in doing this. Provision is made for a reduction to the pole of the spectrum. In view of the high magnetic latitudes, little change was produced in the spectra by such a reduction, mainly a slight increase in magnitude. Although remanent magnetization may affect polarization in some cases, it is considered that over the whole area, distortion of the spectrum will be small.

6.3 Spectra of Magnetic Anomaly Fields

The spectral estimates in this section were produced in the manner indicated in the previous section. The two-dimensional estimates were generally quite bumpy in form. The versions

here have been simplified by simple averaging over 9 adjacent spectral points, and by omitting contours enclosing small features at intermediate or higher frequencies. The directions of the corresponding profiles are marked on the plots (a direct comparison of profiles and plots is not possible since the profiles have been reduced to the pole).

The possible existence of aliasing is acknowledged, in view of the digitizing interval. A small area of known higher intensity short wavelength features was available at 1 km. digitizing intervals; a test was made on this data without prescreening, and it was found that aliasing effects were only significant at wavelengths less than about 12 km. (0.08 cyc/km.). Since the present study is concerned mainly with features much larger than this, and since prescreening was normally done, aliasing was not considered of great importance for the longer wavelengths.

The spectral estimates are shown in Fig. 6.1, from areas as indicated in Fig. 1.1. The size of the data blocks was approximately 250 km. in diameter (since the data window is circularly symmetric).

A common feature in many examples of magnetic anomaly spectra has been noted by Spector and Grant (1970), namely that the spectra show a bimodal distribution of power. This

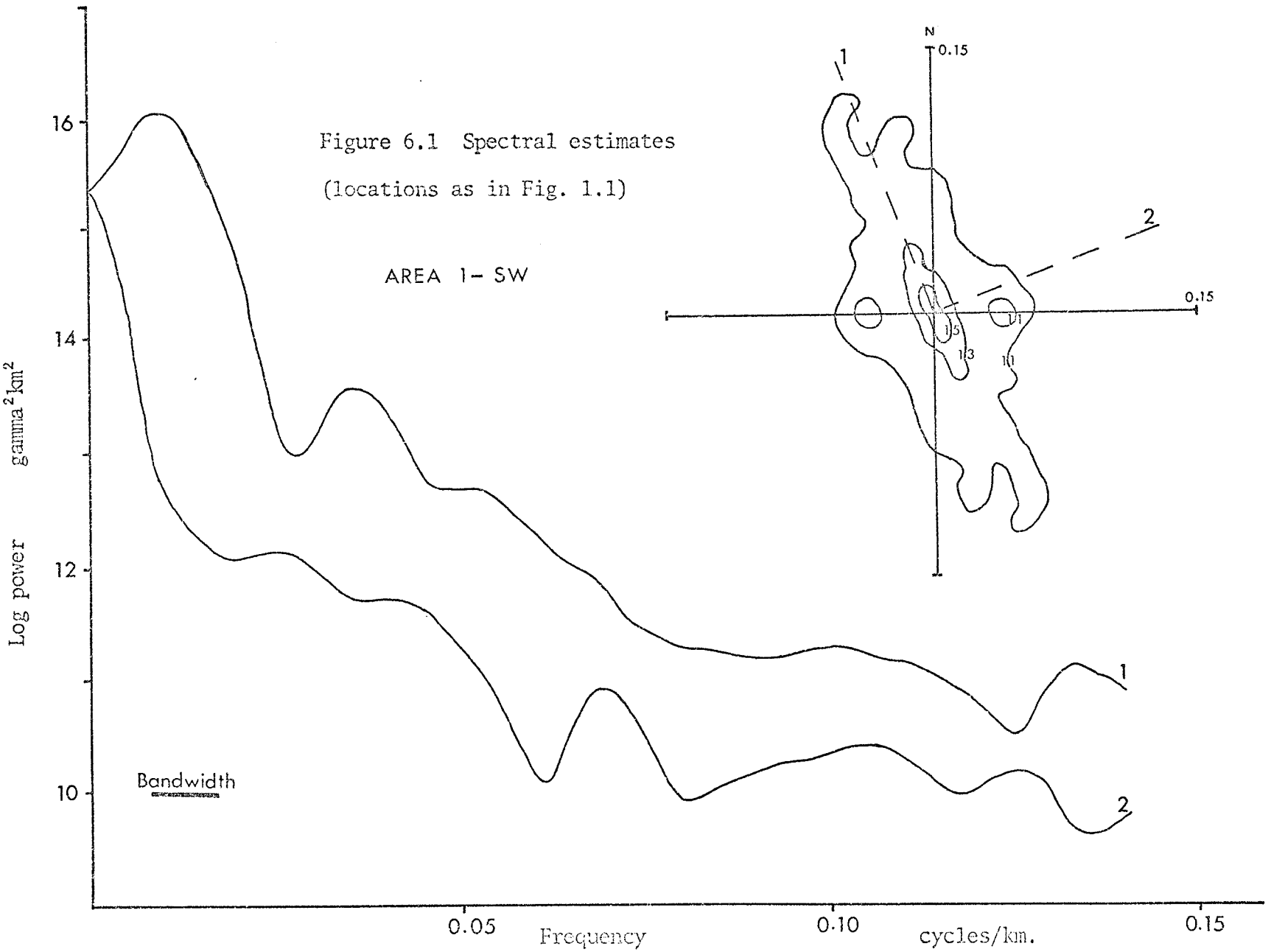
Figure 6.1 Spectral estimates
(locations as in Fig. 1.1)
AREA 1- SW
N
0.15
0.15
1
2
5
3
1
16
14
12
10
Log power gamma^{2}km^2
Bandwidth
1
2
0.05
Frequency
0.10
cycles/km.
0.15

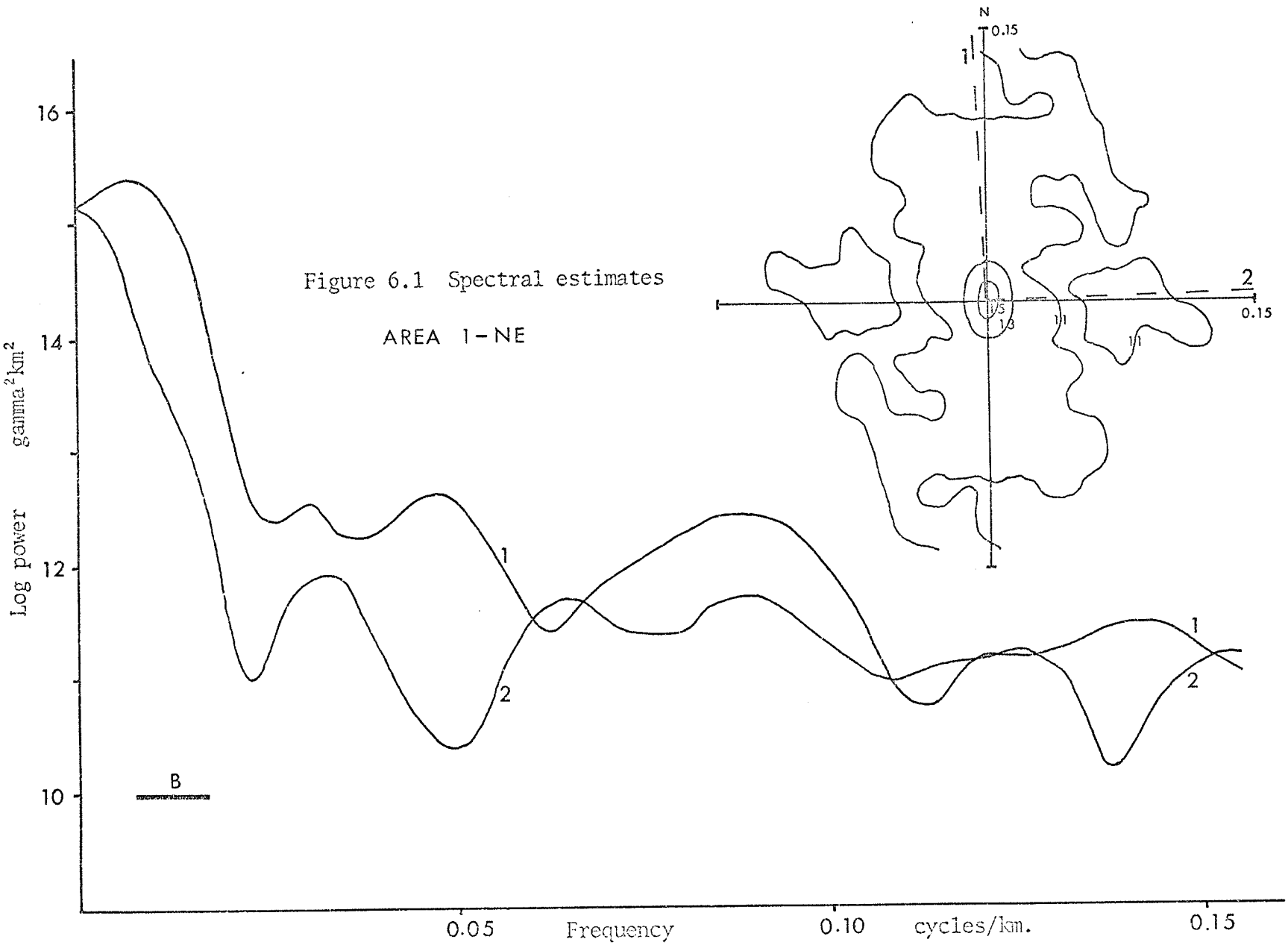

Figure 6.1 Spectral estimates

AREA 1-NE

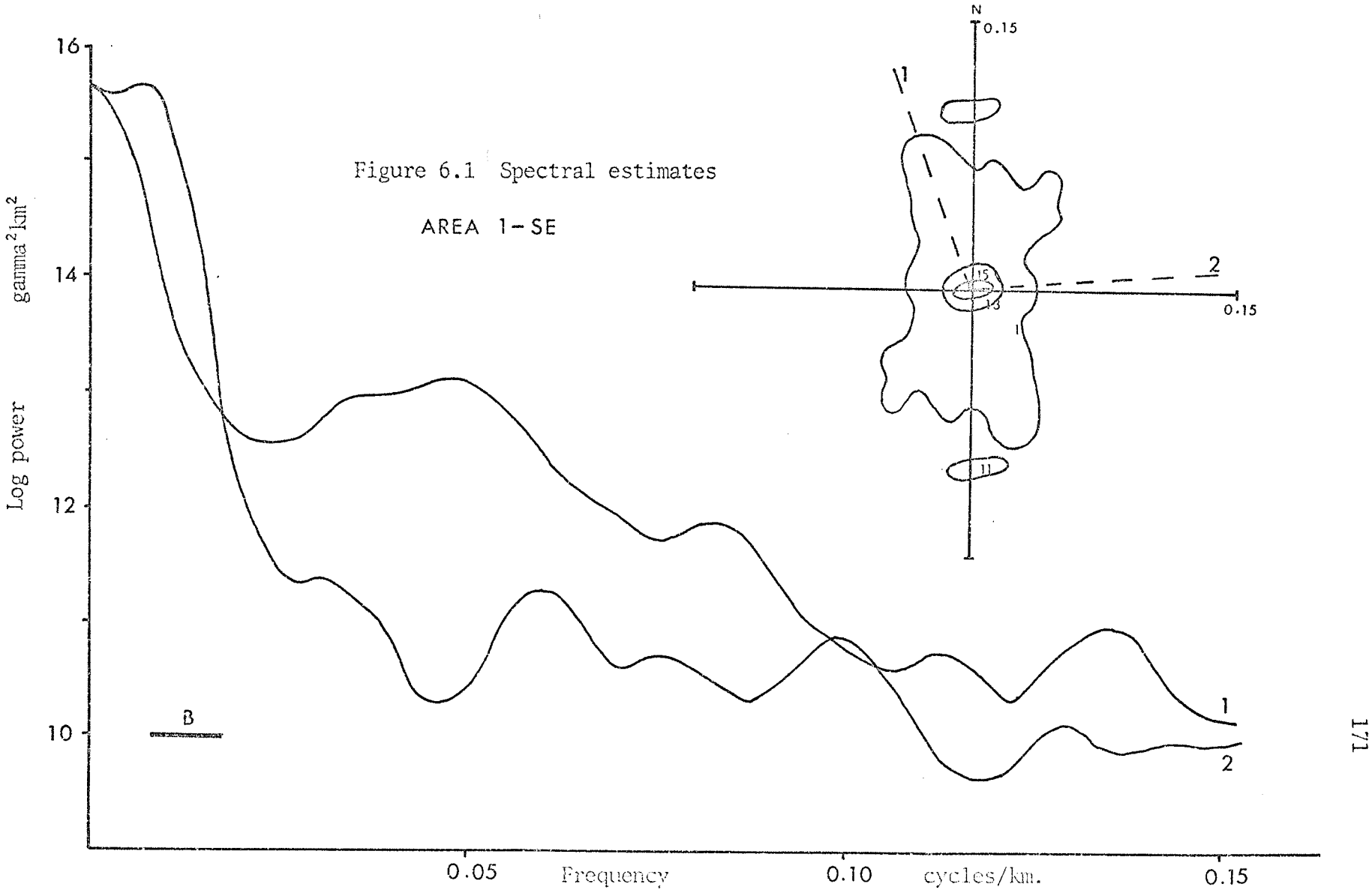

Figure 6.1 Spectral estimates

AREA 1-SE

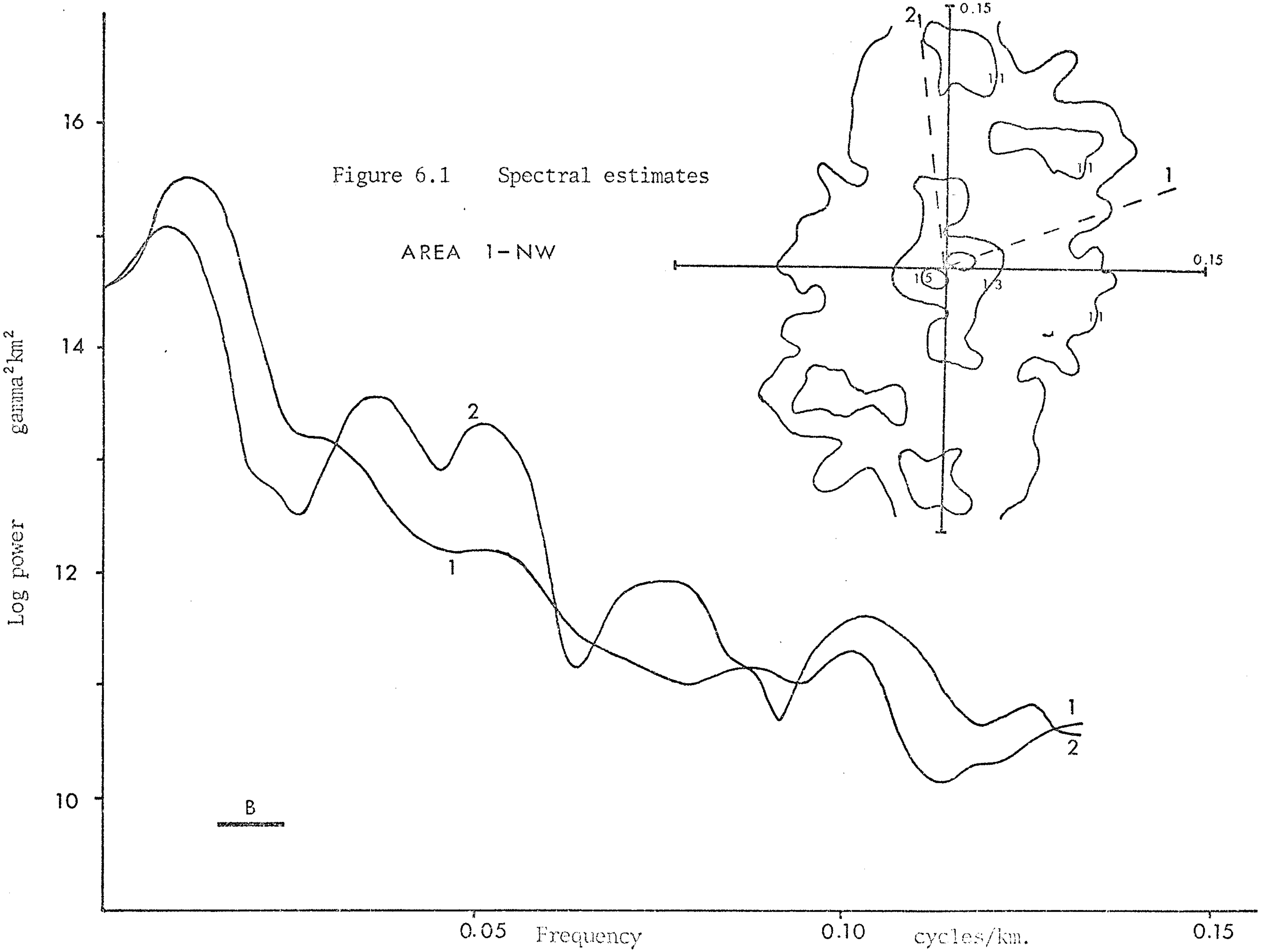

Figure 6.1 Spectral estimates

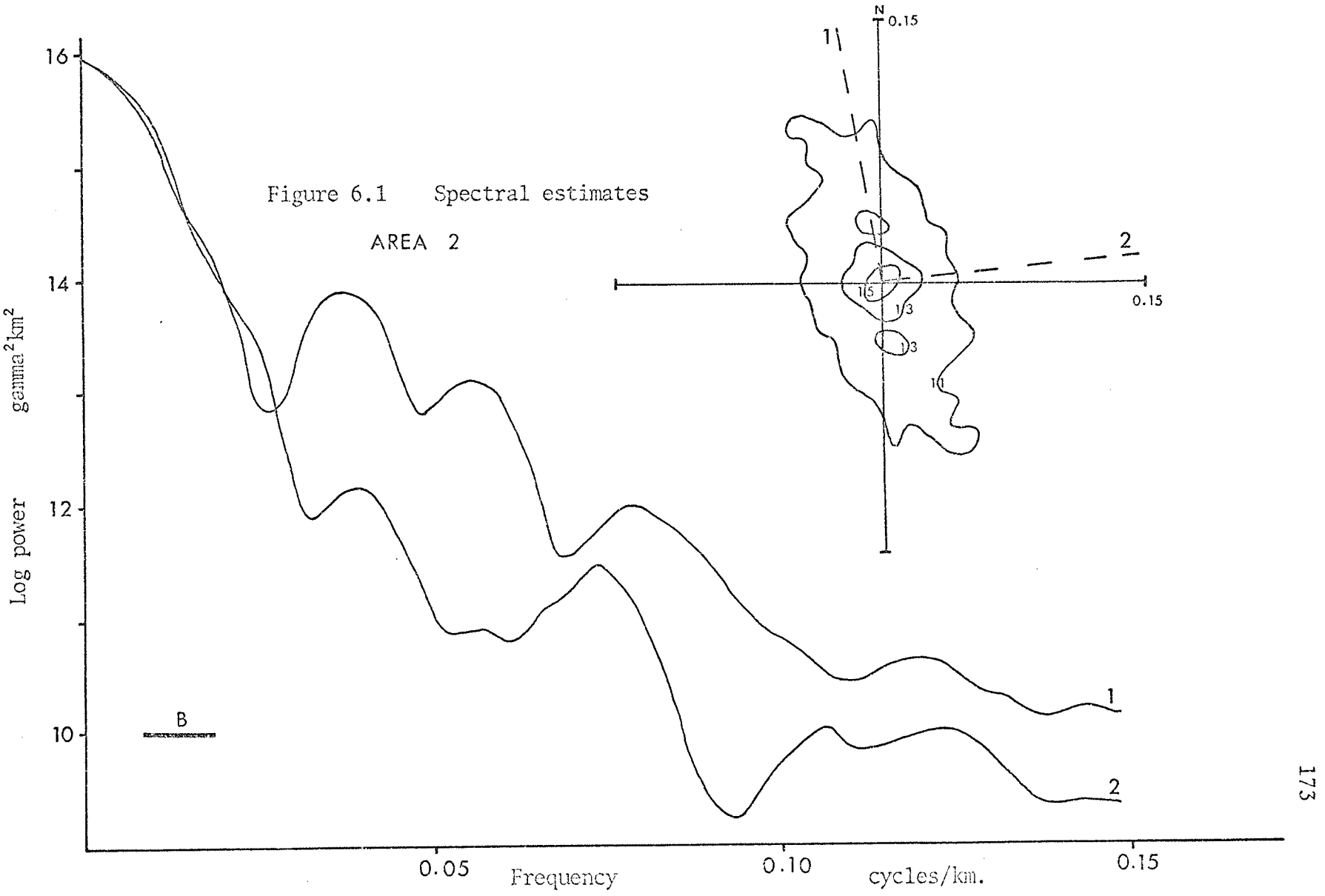

Figure 6.1 Spectral estimates

AREA 2

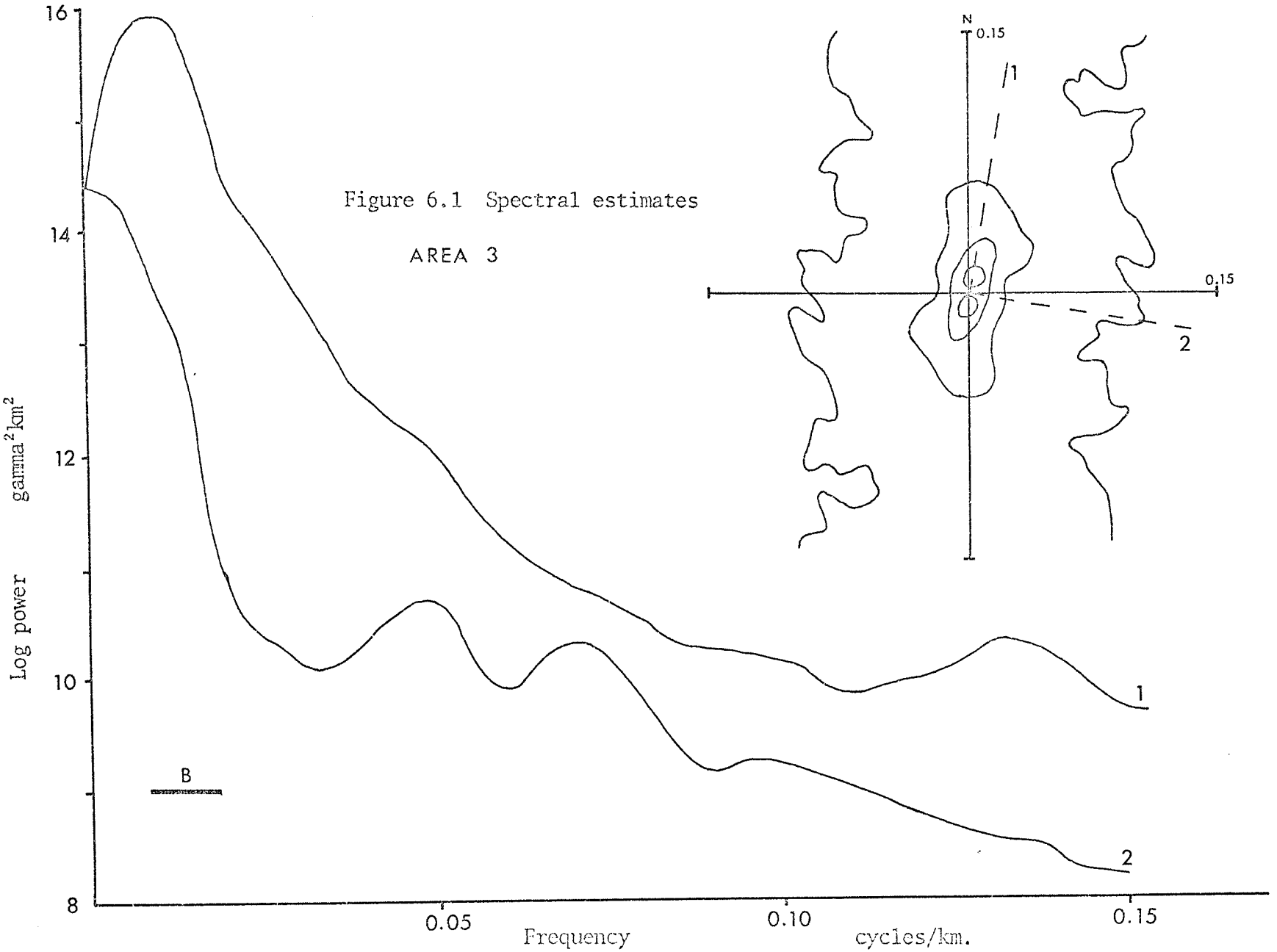

Figure 6.1 Spectral estimates

AREA 3

is significant if any filtering process is to be applied to the data for further interpretation techniques. A bimodal distribution apparently exists in some of the cases in Fig. 6.1. A definite break in the general slope of the spectral curve occurs in the region corresponding to about 40 km. wavelength (0.025 cyc/km). This could indicate that two (at least) processes of differing characteristics are contributing to the anomaly fields, and that to effect a partial separation, a filter cut-off at about this wavelength would be suitable.

Furthermore, as may be seen from the model curves in section 2.4, wavelength components shorter than about 12 km. (0.083 cyc/km) are mainly due to shallow sources. Thus filtering at this wavelength limit removes these shallow effects, leaving the longer wavelengths which may or may not be from deeper sources (e.g. Fig. 2.7).

The choice of optimum filter bandwidth for separation of sources is dependent on the nature of the magnetization distributions present. In section 2.4, several simple models were constructed, to indicate how the signal-to-noise ratios affected the bandwidth. As the magnetic structure in the subsurface is not known a priori, one cannot definitively design a filter by using the structure as a model. However, if one hypothesizes, based on geological and geophysical knowledge

in an area, and constructs an appropriate model, he may choose a filter bandwidth which would enhance particular features of the model. If the form of the measured spectrum is similar to that of the model, there is justification for the choice of filter properties.

There are some similarities between the models in section 2.4 and the spectra in this section. This has implications regarding anomaly interpretations. The filter cut-off of about 40 km. wavelength was chosen as the most suitable compromise value, for enhancing the longer wavelength anomalies for the whole region.

CHAPTER 7

A DISCUSSION OF FILTERED MAGNETIC ANOMALY MAPS AND SPECTRAL ESTIMATES

7.1 Introduction

Magnetic anomaly data have been filtered in many ways and for different purposes. In studies of the whole crust and upper mantle, it is the longer wavelength components which are of prime concern. A number of maps from different areas have been produced by digital filtering (e.g. Bhattacharyya and Morley, 1965; McGrath and Hall, 1969; Hall and Dagley, 1970; Hall, 1971, 1973). The purpose of these is to display in an enhanced form the longer wavelength components in as true a representation as possible.

McGrath and Hall (1969) demonstrated a method based on a classical two-dimensional smoothing operator for removing short wavelengths. Bhattacharyya and Morley (1965) presented a map produced by truncating a double Fourier series expression for the anomaly field.

It has been part of the present project to re-examine this latter area of data. The method of Bhattacharyya and Morley is interesting in its approach; however, a number of relatively intense, but small size, anomalies are apparent in the map, and in some cases appear to be related to the grid directions of the Fourier transformation. A remarkable

result of the interpretations of these and other anomalies was that the directions of polarization were grouped about two diametrically opposite directions, both distant from the ambient field direction. This implies strong remanent magnetizations in all of these bodies. However, such a result may have occurred as an effect of alternating high and low intensities caused by the spurious side lobe effects of an unsuitable window function, namely the data block size.

7.2 Data Processing

The data of Bhattacharyya and Morley (1965) have been filtered using the method of McGrath and Hall (1969), which uses a 17-point smoothing operator to give (for data digitized at 3.2 km.) a cut-off wavelength of about 13 km., and a low distortion for wavelengths greater than 38 km. The data were processed in a manner similar to that described by McGrath and Hall (1969). A second-order surface was removed from the data as described in section 6.3, and the screening and preconditioning procedures carried out as part of the filtering process.

The numerical filter used was the following (McGrath and Hall, 1969)

$$F_0(x,y) = \frac{1}{259}\left[55\, F_i(x,y) + 42\, S_1 + 29\, S_{\sqrt{2}} - 10\, S_{\sqrt{5}} \right]$$

where $F_0(x,y)$ = the filtered value of $F_i(x,y)$

and S_r = the sum of the data falling in circles of radius r centred at $F_i(x,y)$ where r is in sampling units.

The resultant map is shown in Fig. 7.1.

As noted in section 6.4, a filter cut-off at about 40 km. may effect a separation of the long wavelength features. This is the same cut-off as used by Hall (1973). In order to use the method of McGrath and Hall (1969), it is necessary to decimate the previously filtered data to an interval three times the basic interval, i.e. 9.6 km. The new filter cut-off is approximately 38 km., with low distortion beyond about 100 km. After filtering, the data were interpolated back to the original grid interval of 3.2 km. using the computer program SPLINT (Appendix 3), based on bicubic splines. This is possible with this smoothed data. The resultant map is shown in Fig. 7.2.

As indicated in Chapter 2, there is in general a considerable overlap in frequency between different anomaly sources. It is apparent from the spectra that to attempt to isolate the major part of intermediate wavelength anomalies, a bandwidth between about 13 and 50 km. may be better than 13 to 38 km. The 13 km. filtered data were therefore also filtered

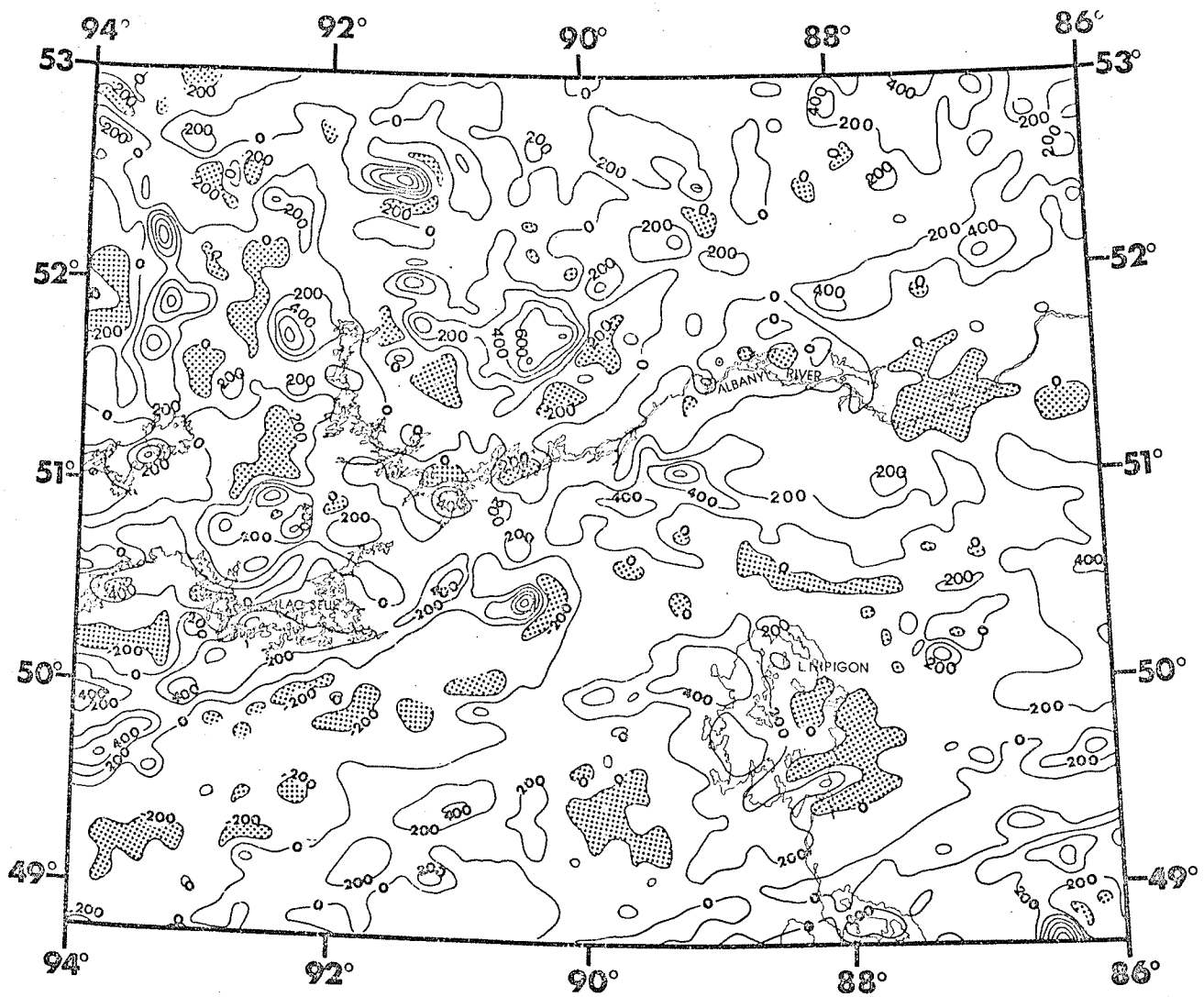

Figure 7.1 Filtered aeromagnetic map - wavelengths 13-1000 km.

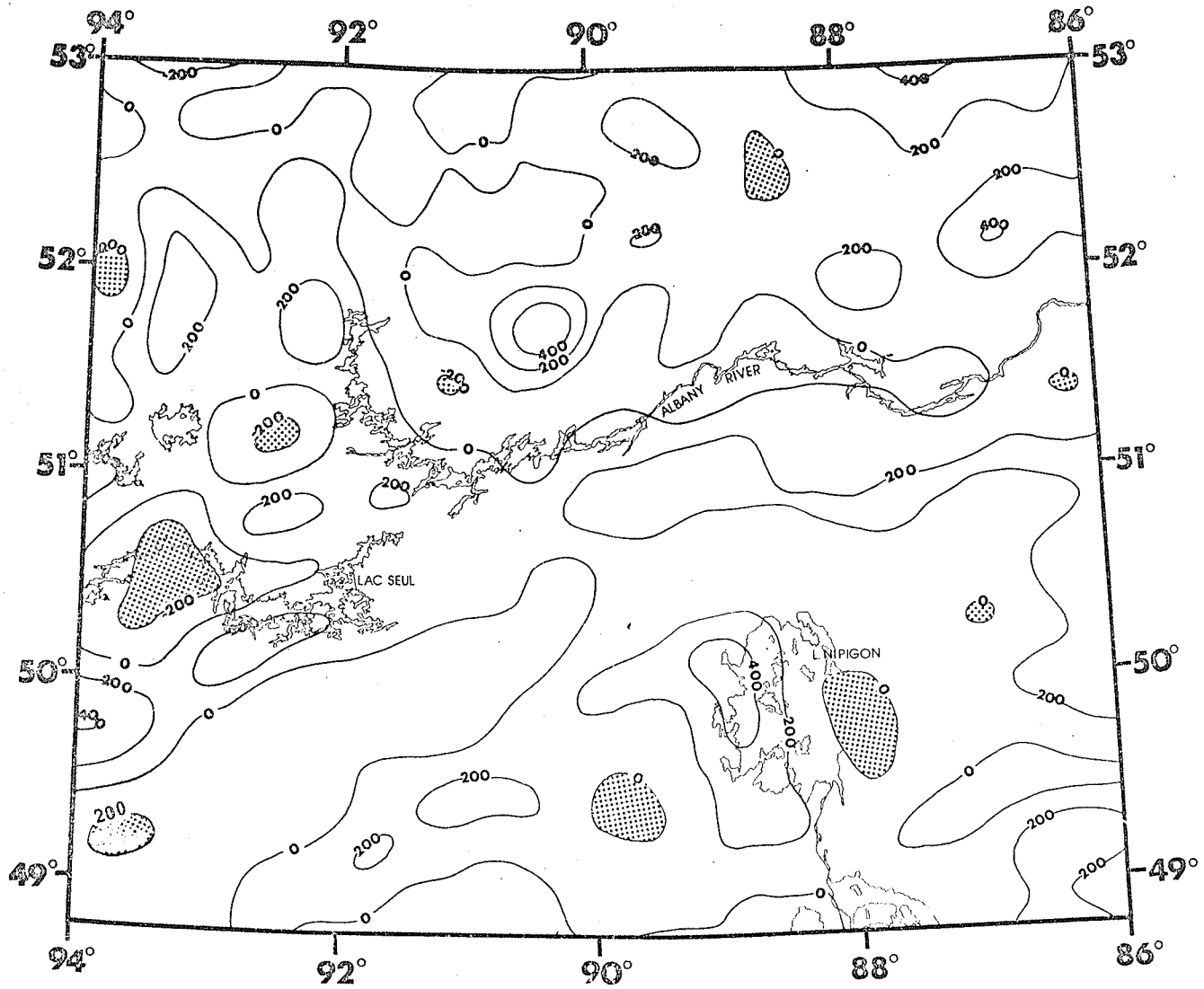

Figure 7.2 Filtered aeromagnetic map - wavelengths 38-1000 km.

again at 52 km. (4 times the basic interval). After interpolation back to the original grid, both this field and the 38 km. field were subtracted from the 13 km. filtered data to give residual intermediate anomalies. The resulting fields contained a few isolated anomalies, but the bulk of residuals followed the main longer wavelength features and were not readily separable into discrete anomalies. This indicates that by filtering at the longer wavelength limits, some information is lost, which may be significant in the interpretation of the anomaly sources.

Spectral estimates were obtained for the filtered data. The data filtered with 13 km. cut-off wavelength was decimated to twice the basic grid interval, giving a Nyquist frequency of 1/12.8 cyc/km.; thus no further aliasing is introduced. The data filtered with 38 km. cut-off wavelength was decimated to six times the basic interval, giving a Nyquist frequency of 1/38.4 cyc/km.; again, no further aliasing is introduced. These processes were performed only for Area 1. The spectral estimates are shown in Figs. 7.3 and 7.4.

7.3 Discussion of Spectra

The same basic features at low frequencies are apparent in the spectra of filtered data as for the unfiltered data.

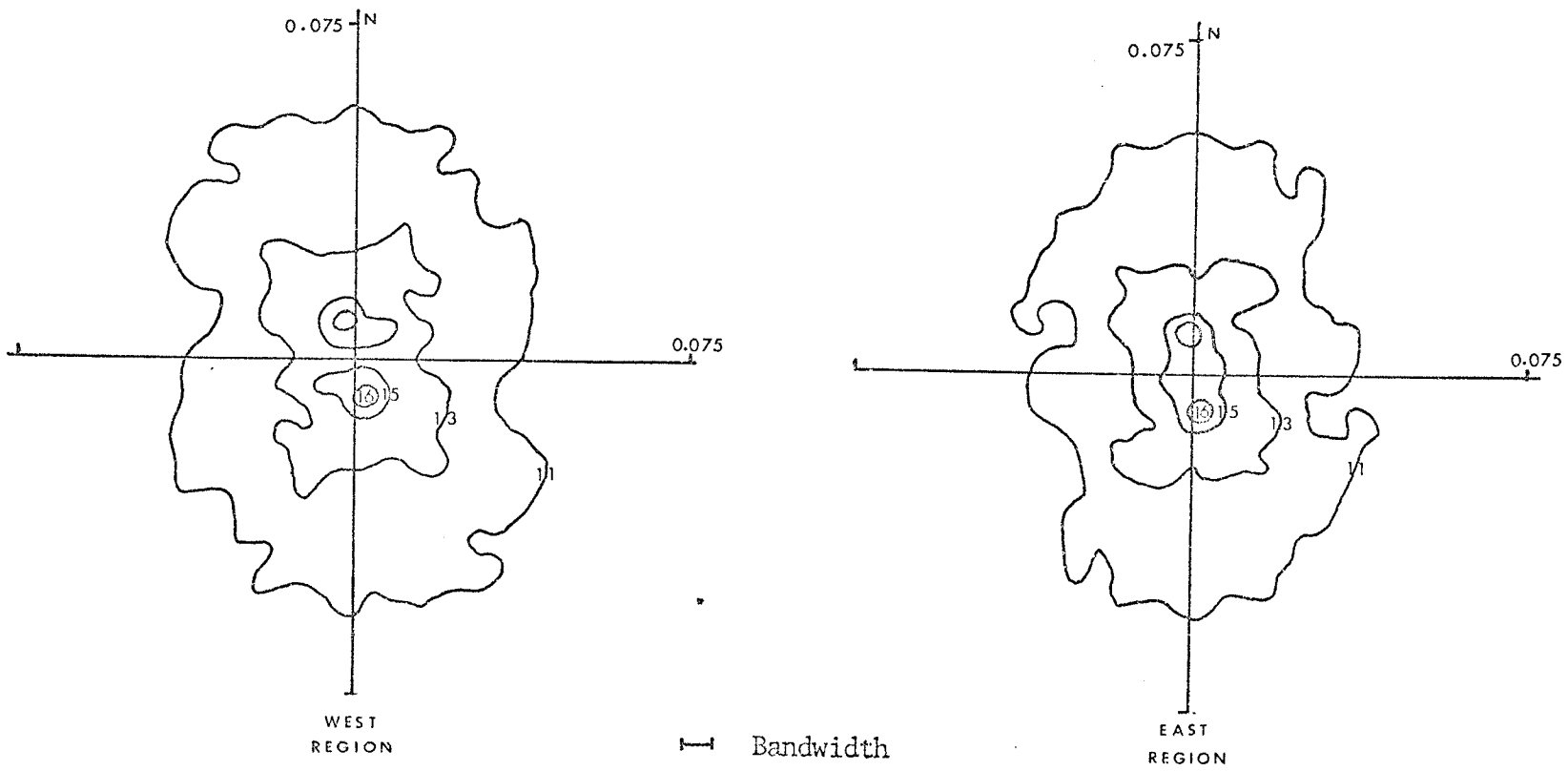

72 x 72 points

Contour levels in log(gamma^{2}km^2)

Figure 7.3 Spectral estimates for Area 1 - wavelength components greater than 13 km.

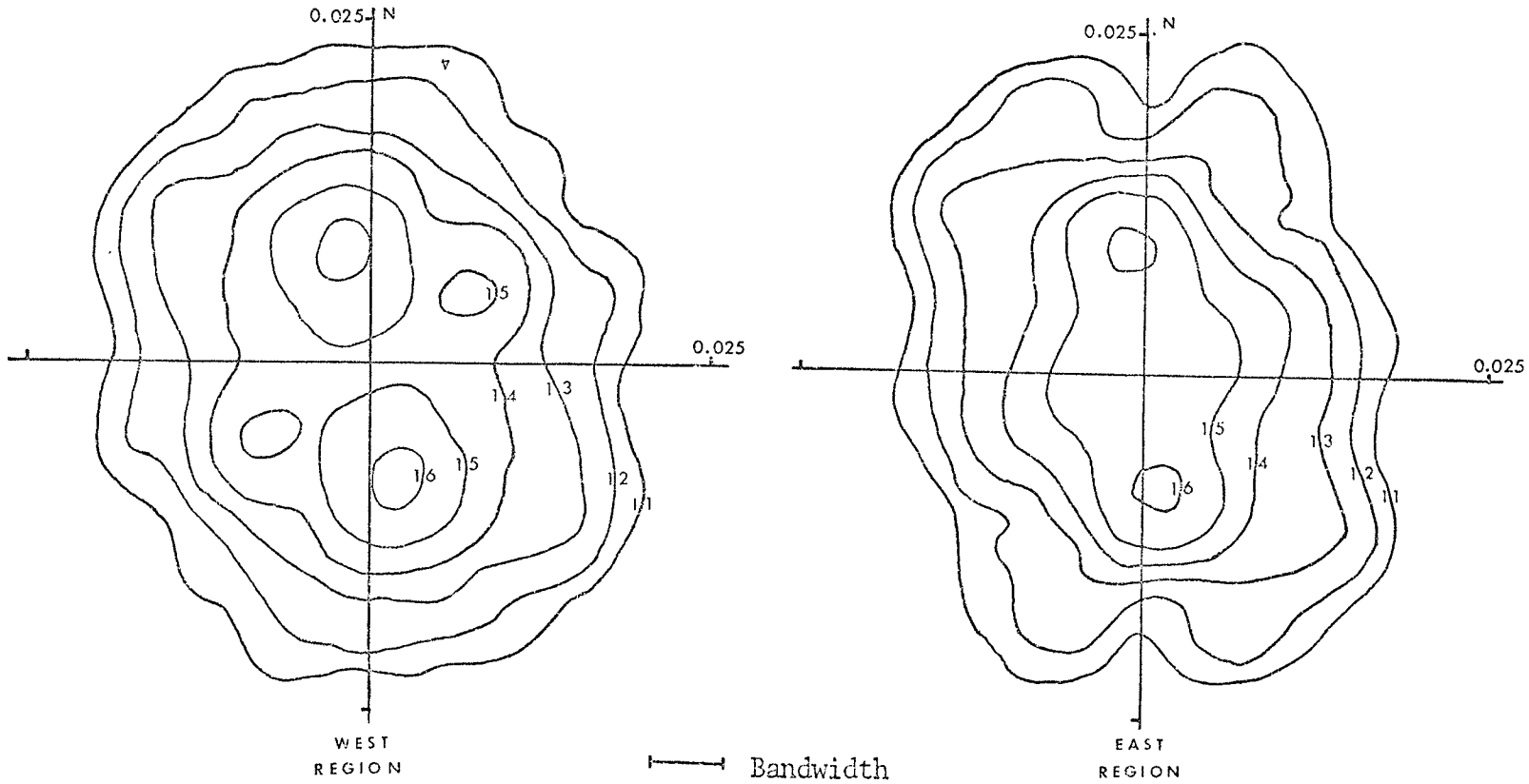

Figure 7.4 Spectral estimates for Area 1 - wavelength components greater than 38 km.

The presence of a peak at wavelengths of the order of 100 km., indicating a dominant ENE trend, points out that this is the main contributor to the longer wavelength anomaly field in the map area.

The nature of the spectral estimates obtained does not permit definitive quantitative interpretations. However, since the anomaly maps show a major trend direction, the assumption of 'flat' magnetization spectra is unreasonable. Furthermore, an interpretation in terms of such a spectrum, with the slope of the logarithm of the spectral estimate representing the depth to the top of the magnetized unit (cf. Spector and Grant, 1970) requires intense magnetization at depths below 20 km.

To demonstrate this, consider Area 1 - SW. The slope of the low frequency spectrum corresponds approximately with that of the 20 km. depth curves (Fig. 2.4). Using the curves in Figs. 2.3 and 2.4, the model spectrum for a random distribution of blocks smaller than 1 km. semi-dimension at a depth of 20 km. was formed for 2 km. and 10 km. layer thicknesses, Fig. 7.5. The model spectra are constructed using an arbitrary amplitude factor of 10^4. The model curve for 2 km. thickness peaks at a log. value of 2.1; the spectral estimate peaks at 16.0. Allowing for the factor of 10^4, the amplitude factor for the spectral estimate is (16 - 2.1 + 9.2)

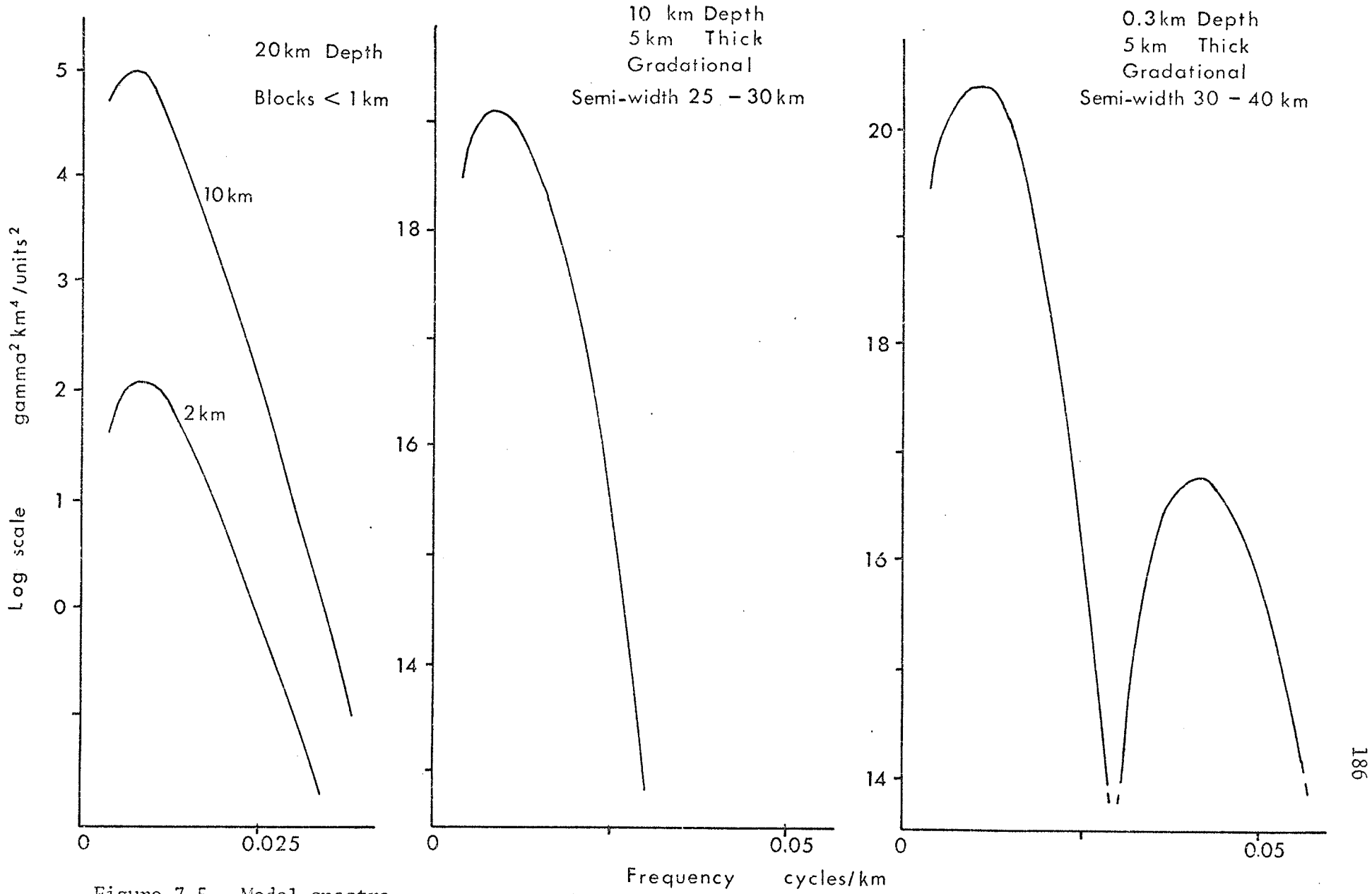

Figure 7.5 Model spectra.

in logarithmic form. The value is approximately 1.1×10^{10} units^2/km^2. If one supposes a distribution as in section 2.4, the number of blocks per unit area is 0.04/km^2. Thus the mean magnetization level is $(1.1 \times 10^{10}/0.04)^{\frac{1}{2}}$ units, which since 1 unit was chosen to be 10^{-6} emu/cm^3., gives a mean level of the order of 0.5 emu/cm^3. (6.5×10^{-5} Wb/m^2). A similar operation for the 10 km. thick layer gives a level of the order of 0.13 emu/cm^3. (1.7×10^{-5} Wb/m^2). The other spectral estimates will give similar high values on this basis. These high magnetizations present problems in the interpretation of the nature of the magnetizations and of the rocks carrying them.

The character of the anomaly field and of the spectra demonstrate that appropriate models to consider may be the 'two-dimensional' forms, viewing rectangular 'block' or 'triangular' magnetizations in a cross-strike direction.

Consider again Area 1 - SW. A model curve for the 'triangular' distribution of semi-dimension 30 - 40 km. with depth extent from surface (0.3 km.) to 5 km. is shown in Fig. 7.5. This is again an approximation to the low frequency spectral estimate. Other magnetization units are undoubtedly present, which may affect the closeness of fit to any particular model.

Using this model, and again allowing for the arbitrary amplitude factor 10^4, the amplitude factor for the spectral

estimate is (16.0 - 20.4 + 9.2) in logarithmic form; the value is about 120. The model curves were calculated for b_{max} = 100 km. and b_{min} = 0. If the value of b_{min} is also taken as 100 km., this is a limiting case, and has the effect of increasing the model curves by a factor 3 (equation (11), section 2.3). Using these latter values, and considering 1 block in 250 x 250 km^2, the number per unit area is 1.6 x $10^{-5}/km^2$. The mean peak magnetization level, at the centre of the variation, is given by ((120 ÷ 3) /1.6 x 10^{-5})$^{\frac{1}{2}}$ units, or the order of 1.6 x 10^{-3} emu/cm^3. This estimate is not truly representative because it has assumed that the spectral estimate is constant over a very large region, enough to contain many such blocks. Bringing a_{min} closer to a_{max} has the effect of slightly increasing the magnitude of the model curves and of increasing their oscillatory nature. In the limit, if only one block size is present, of about 100 km. b-dimension, then the magnetization level is of the order of 1.3 x 10^{-3} emu/cm^3. (1.7 x 10^{-7} Wb/m^2).

Similar block or gradational 'two-dimensional' structures at greater depth will result in higher magnetizations, (by elementary considerations, or by examination of the curves in Figs. 2.4, 2.5, 2.6). Fig. 7.5 also shows a model at 10 km. An analysis similar to that above results in a level of the order of 3 x 10^{-3} emu/cm^3. for the single block situation, or higher values if there are variations in sizes. A variety of

models may be found which are equally satisfactory fits to the spectra. The magnitudes should strictly be only considered as relative, in view of the method of spectral estimation.

Nevertheless, the point is made that shallower, lower intensity magnetizations with longer wavelength components may account satisfactorily for some of the observed spectra, whereas deeper models may require magnetizations whose intensities present difficulties in their interpretation (eg. Serson and Hannaford, 1957). The spectral estimates for the filtered data cover larger areas, but again similar magnitudes are found, with a slightly better statistical population.

It is evident that more than one major magnetic unit (or group of units in the restricted sense of Chapter 4) are contributing to the spectra. In some areas, the lower frequency peak is less evident.

Comparison of the three sets of curves in Fig. 7.5 (which were chosen rather arbitrarily, as having similar low frequency forms) with spectra from areas 1 - NE and 3 shows that these spectra also may be explained largely by shallow (less than 10 km.) magnetization, but that deeper more magnetic units may give similar spectra too.

The spectrum for Area 1 - NW is rather different in that two trends appear. The separation into distinct units, either two-dimensional or isotropic, is not feasible here, although

the form of the curves suggests the presence of considerable effects from shallow sources. The change in character of the spectrum is in keeping with the different nature of the anomaly field.

The spectrum for Area 2 is characterized by a trend which is apparent at intermediate wavelengths in the ENE direction. There are evidently more than one unit contributing to the longer wavelengths, but again they are not separable. A slight long wavelength trend in the WNW direction is apparent, similar to that observed in Area 1 - NW, which partly overlaps Area 2. An examination of the anomaly maps of McGrath and Hall (1969) and Hall (1971) shows that Area 2 encompasses two regions of distinctly different magnetic character. The power increases to zero frequency (to this resolution), which may indicate that deeper magnetizations (greater than 20 km.) may be more significant here than in other regions.

Area 1 - SE again has a different spectrum; the low frequency power increases to a maximum at zero frequency, with a slight peak in a low frequency trend, which contrasts with the major ENE trend in most of the remainder of the map area. Comparison with the anomaly map indicates that this subdued WNW trend is a result of the broad high anomaly feature over the Lake Nipigon region. Consideration of the forms of the model curves in section 2.3 shows that by suitable choice of

dimensions (a_{max} greater than 40 km., for the gradational model), this peak may be explained by shallow magnetization (less than 10 km.).

The presence of deeper sources in the whole area is not excluded, but is indeterminate in view of the inherent ambiguity of interpretation. However, the results in this section, in Section 2.4, and in Chapter 5 imply that deeper effects may be seen with a very low signal-to-noise ratio, and that filtering at any reasonable bandwidth could result in a very low 'confidence parameter' for deep interpretations.

The emphasis above has been on the gradational magnetization model. The relative amplitudes of higher frequency components for the rectangular block forms are higher than in the gradational case, (Figs. 2.5 and 2.6). In attempting to match the observed spectra satisfactorily at low frequencies, blocks at depths greater than about 2 to 5 km. and extending to the order of 20 to 25 km. are necessary for most spectra, with other units producing the bulk of the higher frequency components. A single unit of blocks extending from the surface cannot produce the low frequency peaks adequately and be consistent with the higher frequency portions of the spectra.

A feature of the gradational model approach is that interpretations of the lower frequency portions of the observed spectra may use units extending down from the surface. The

extent to which this actually occurs may be tested by surface studies. Models which must invoke deeper sources cannot be tested in this way directly.

7.4 Magnetic Anomaly Maps, Spectra and Geology

The general geology in the northwestern Ontario map area has been discussed briefly in Chapter 1. Wilson (1971) has presented several maps of the area. One is a magnetic trend map (Wilson's Fig. 3) which delineates part of the English River Gneiss Belt. This belt crosses the present maps between 50° and 51° N in an approximate east-west direction. It corresponds with the intense lows in the western region but becomes more diffuse at about 89°W, where it appears to merge with the southern edge of the anomaly high at 51°N in Fig. 7.1. Between 92° and 94°W, the southern edge of this Gneiss belt is bordered by a region of anomaly high. This high continues to the west, beyond the present map area, to join the high region (Hall, 1971) over which part of the sampling was carried out (Chapters 3 and 4). Hall (1968), as part of a larger survey, has sampled in the region just east of 94°W and just south of 50°N within the present map area. In his whole region, he defined seven magnetic units. Within these units are found some areas of more intense magnetization, related spatially with anomaly highs, and comparable with those in the magnetic units

A, B, C of the present work. The full areal and depth extent of these particular areas is not known, although Hall's sampling suggests that the surface expression in his immediate region may be small. He found the depth extents of certain of his seven defined units to average 17 km.

Careful comparisons of the maps in Figs. 7.1 and 7.2 with Fig. 7.6, and with the Geological Map of Canada, the Tectonic Map of Canada (Douglas, 1970) and the Ontario Geological Maps (Ontario Department of Mines, 1971) show a number of correlations. Wilson (1971) has also discussed areas of greenstone preservation and greenstone destruction.

In the southwest of the maps the northeasterly trending magnetic low overlies a predominantly greenstone area, with diapiric granites. The southernmost belt of magnetic highs overlies a predominantly granitic belt within the major block of greenstone preservation. In the north east of the map area, a region of lows overlies the Albany River belt of greenstones, and another less definite area of irregular highs and lows bears some correlation with the Berens River Block (Wilson, 1971) to the north and west. The anomaly pattern in this northwestern region differs from that in other parts of the maps, as does the surface geology; the spectral estimates for areas 1-SW and 2 also show these different features and trends.

In the south east, a linear belt of lows appears to be

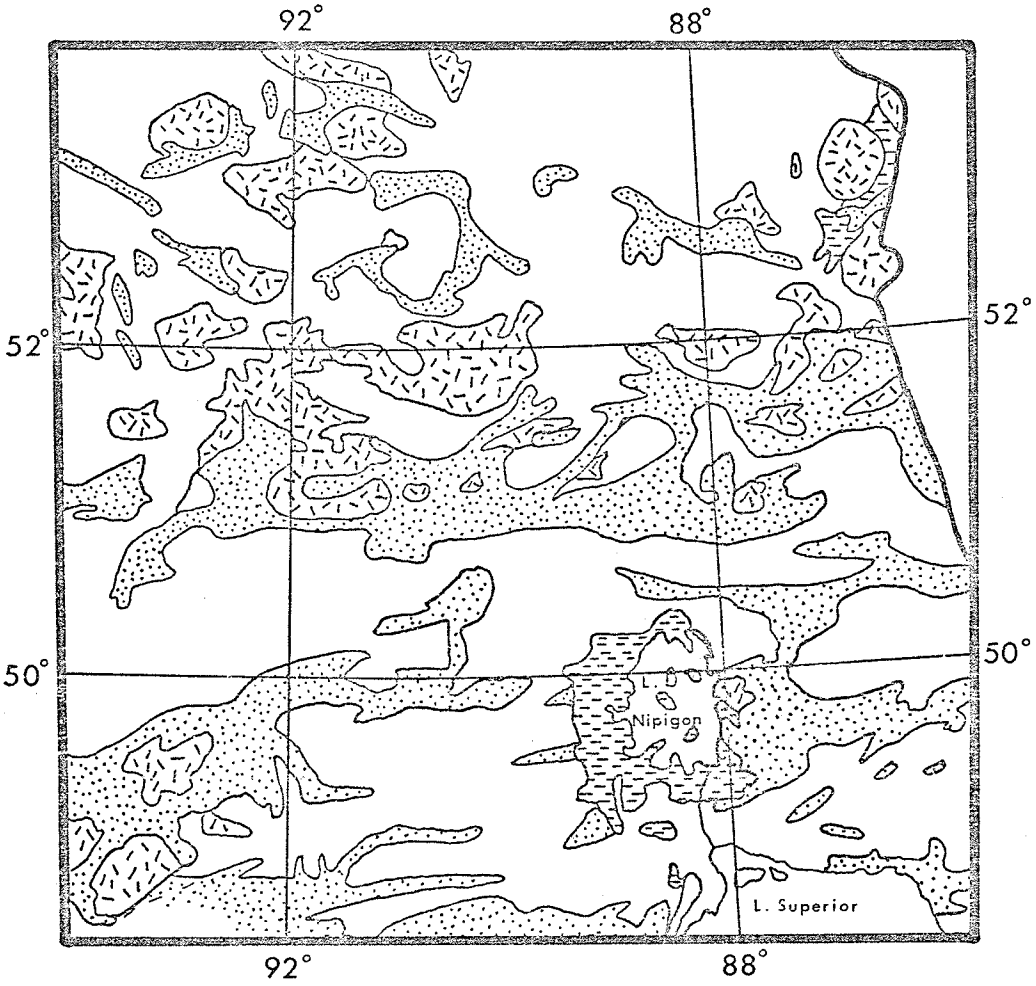

Figure 7.6 Generalized Geology in Area 1

related to the Quetico structural block (Wilson, 1971). Prominent faults in the region bounding this belt of lows suggest a distinct major structure which may extend to depth. An increased occurrence of metasedimentary rocks may be associated with the anomaly lows (Ontario Dept. of Mines, 1971), (cf. the northern part of the sampled region of the English River Gneiss belt, Chapters 3 and 4).

The broad high anomaly around Lake Nipigon coincides well with the geological Nipigon plate (Stockwell et al, 1970), which contains abundant mafic and ultramafic rocks, and is of later age than the Kenoran orogeny. The anomaly and the geological sub-province may be closely related in origin.

Many of the shorter wavelength features of the anomaly map in Fig. 7.1 may be associated with known geological units mapped at the surface. Some of the higher intensity anomalies correspond with carbonatite-alkalic complexes (e.g. in the southeastern corner of the map). In other cases, anomalies may be related to mafic intrusions which partly outcrop at the surface. In other instances, (e.g. the group between 91° and 92°W at about 51.8°N), they may be associated with late felsic and related mafic intrusions.

Some of these shorter wavelength anomalies were subjected to discrete body interpretations, using the computer program PRISM, after subtracting wavelength components greater than

about 50 km. The interpretations resulted in bodies of high magnetizations of 2 to 5 x 10^{-3} emu/cm^3 at depths between about 4 and 10 km. The magnetization directions vary but are generally shallower than the ambient field. The reliability of these interpretations is reduced because of the distortions which may be introduced in the filtering process at these wavelengths. More accurate interpretations would require a more detailed investigation. These bodies do not constitute a major part of the total anomaly field, but do indicate the presence of some higher magnetizations, at least above 10 km.

It is therefore apparent that many of the features of the anomaly maps are related to major surface geological features, although it is possible that the surface geological structure and the magnetics both may reflect deep structure. The interpretation of the spectral estimates shows that models using 'two-dimensional' linear blocks with gradational magnetizations are not incompatible with the spectra. The widths of individual blocks reaching the surface were suggested to be of the order of 60 - 80 km. These dimensions are comparable with those of many of the geological sub-regions. The magnetizations interpreted are of the order of those which have been observed at the surface in similar areas.

The spectra in Areas 2 and 3, which lie within the anomaly map area of Hall (1971), are also compatible with shallow

magnetization interpretations. The anomaly fields in these regions show good correlations with major surface geological units (Wilson, 1971). The forms of the spectra do not show clearly a bimodal type of power distribution, and considerable frequency overlap of the effects from different groups of magnetic sources is implied. This indicates that a separation of anomaly groups may be relatively inefficient.

The spectra from all regions, if interpreted in terms of 'flat', or 'near-flat' magnetization spectra, do indicate a magnetized region below about 15 - 20 km. However, the magnetizations required are high. Direct correlations with such features as the Intermediate seismic discontinuity are not possible with the present spectral estimates, and such correlations with anomaly fields must be treated with the caution necessary in interpreting magnetic field data, in the absence of additional information, such as on shallower magnetizations.

CHAPTER 8

CONCLUSIONS AND COMMENTS

The validity of simple filtering as a means of separating anomalies caused by deep sources is dependent to a considerable degree on the distributions and magnitudes of shallow magnetizations. In situations where prominent shallow magnetic units are evident, filtering of selected wavelength anomalies may not be suitable. Provided sufficient information is available, a 'stripping' process of subtracting the field due to shallow effects (both shorter and longer wavelengths) may be the more satisfactory method.

It has been demonstrated that in the area of sampling, a definite longwavelength variation in measured surface magnetizations is present. For a depth extent of several kilometres for these magnetizations, a significant longwavelength contribution to the total magnetic anomaly field appears.

Remanent magnetizations in the area are dominated by soft components which tend to follow the ambient field direction. These remanences are of sufficient intensity in some areas to give contributions to the anomaly field comparable with those of induced magnetizations. Significant coherent reversed magnetizations have not been found.

The magnetization distributions enable a number of magnetic units to be delineated at the surface. Correspondences also

have been noted between these magnetic units and major geologic divisions. Higher magnetizations are associated on the regional scale with more granitic leucocratic units, whereas metasediments and grey gneissic areas are generally associated with lower magnetizations.

Magnetic minerals in the sampled region are dominated by magnetite. The grain sizes are generally greater than 20 μm., often 100 - 200 μm. The magnetite is generally optically homogeneous, some with slight development of broad ilmenite lamellae, with most ilmenite occurring as discrete grains. The variations in magnetization in the region are governed mainly by variations in the magnetite concentration.

Not all major features of the anomaly field over the sampled region can be satisfactorily accounted for by reasonable depth extension of surface magnetic units. Deeper magnetizations need to be invoked to explain some features of the anomaly field. The anomaly near Lac du Bonnet is of shorter wavelength and a relatively shallow body is proposed. A broader smaller amplitude anomaly remains after the effects of a simple model of shallow magnetizations have been removed over the region. This anomaly is caused by deeper magnetic structure.

In spectrum interpretations, it is shown that models which consider gradational, shallow magnetizations of magnitudes

similar to those observed at the surface are compatible with the measured spectra at longer wavelengths, whereas deeper models require higher magnetizations. It is also possible that both deep and shallow sources are contributing to the spectra at long wavelengths.

A broad comparison of the filtered anomaly maps and the surface geology in the area indicates considerable correlations. Regional anomaly lows are associated with predominantly greenstone areas and areas of metasediments, whereas highs are often associated with granites, granitic gneiss and migmatite areas. This is in general agreement with findings of Hall (1968) and Morley et al. (1967). One large scale anomaly high appears to be related to the younger rocks in the Lake Nipigon region, which contain abundant mafic volcanic units. In order to interpret fully the longer wavelength magnetic anomaly features in the present area of study, it is essential to consider in detail the magnetizations of surface units, by sampling and/or by inference from information gathered in areas which have been shown to be equivalent geologically. The surface geology may be controlled by deep structure, whose magnetic expression may be masked by that of the surface features.

A method of estimating the reliability of separation of an anomaly feature in terms of known, or inferred, magnetization structure, for simple 'rectangular', and 'triangular'

magnetization variations, is presented. A method of selecting appropriate filter bandwidths is indicated.

The data used in the present study do not allow delineation of the form of the deeper magnetizations which have been invoked in at least parts of the area. The study has emphasized the need for knowledge of shallow magnetizations on the large scale prior to considering deeper anomaly sources, since the form and magnitudes of longer wavelength anomalies may be considerably modified by shallow sources, the effects not being efficiently separable by frequency selective filtering.

Ancient shields are good areas for these investigations, since surface sampling is possible, and in many shield areas, geological studies are well advanced.

Recent work on heat flow has given estimates of crustal temperatures (e.g. Cermak and Jessop, 1971), which indicate for shield areas temperatures of the order of 400°C (673 K) at the base of the crust. It is therefore possible for significant magnetizations to exist in the lower crust, and below, provided the Curie temperatures of the magnetic minerals are above the ambient temperature (the Curie temperature of pure magnetite is approximately 581°C (854 K)).

APPENDIX 1

A REMANENCE MAGNETOMETER

A1.1 Introduction

Remanence magnetometers for use in rock magnetism at normal temperatures may be grouped into two general classes: (1) those in which the sample is effectively stationary during measurement; (2) those where the sample must be rotated during measurement. In group (1) are astatic magnetometers of various kinds in use in many laboratories. In some versions, the sample is rotating, but only to average out unwanted components (R.L. Wilson, personal communication, 1971; Collinson, 1970); in others, the sample may be rotated slowly, in order to determine the components in a repetitive manner, for improved reliability. All of these forms, many of which are described in Collinson et al. (1967), are, however, essentially static in their determination of the remanent moment. In group (2) are the spinner, vibration and ballistic magnetometers wherein the sample generates an EMF or charge unbalance by the changing magnetic flux (e.g. Collinson et al. 1967). For these, movement is an essential part of the action, in generating a signal.

In its original conception, the instrument to be described here was a 'static' device, with the sample rotating slowly

(about 0.5 Hz), only a few times for each component; the rate of rotation was unimportant, being governed only by the need for repetition of the measurement. In its later development, the instrument falls into group (2) above, rotation at a fixed rate being an essential part of the measurement.

The magnetometer differs from the conventional dynamo action spinner in that the changing magnetic field produced by the rotating sample is directly measured by a rubidium vapour sensor. In this sense, it is similar to some instruments using fluxgate sensors (e.g. Molyneux, 1971). The prime reasons for the choice of this particular rubidium vapour system were its sensitivity and the possibility of using the gradiometer mode in a noisy environment.

A1.2 Principles of Operation

The gradiometer mode of operation uses two sensors, and the difference between the magnetic fields measured at each is determined as the final output. In its application to rock magnetism, the fact that the response of the gradiometer falls off as $1/r^4$, for r much greater than the separation between the sensors, means that environment magnetic noise from artificial sources can be considerably reduced, and that drifts due to geomagnetic diurnal and other variations are effectively eliminated. With respect to individual sensors, the field due

to the sample falls off as $1/r^3$. The sample is positioned close to one sensor, and the second sensor is placed in a convenient position, far enough away for the effect of the sample to be negligible, yet close enough to allow some reduction of environmental magnetic noise. The change in the difference between the two sensor signals, when the sample is moved, is then a measure of the sample magnetization.

Since the remanences of rocks are generally very weak, high sensitivity is needed. The rubidium vapour optically pumped magnetometer is a total field measuring device capable of measuring to 0.01 gammas (nanotesla). If the disturbing field is small (as is the case for a rock sample in the geomagnetic field), the magnetometer measures in effect the component in the direction of the ambient field. By rotating a sample near the sensor about an axis perpendicular to the ambient field, the component of magnetization in the plane of the sample perpendicular to the axis is measured. This is carried out for three mutually perpendicular planes in the sample.

The final output from the magnetometer is a voltage which is directly proportional to the resultant magnetic field, i.e. that due to the sample, plus a steady bias. In the early 'static' version of the instrument, this voltage was fed to a chart recorder, from which the peak-to-peak amplitudes could be taken to give measures of the magnetizations.

A series of samples for the present work were originally measured using this version in an isolated building in a rural area. However, conditions were not suitable for year-round work, and attempts to use the system in a normal laboratory were unsuccessful as background magnetic noise was too high.

To overcome this problem, and at the same time to eliminate effects of anisotropy, which were not important in the earlier measurements but were anticipated in later work, a modified design was developed. The speed of rotation was raised to approximately 6.45 Hz, and a narrowbandpass 'notch' filter and A.C. meter substituted for the chart recorder. Thus, the emphasis was changed and the instrument became a 'spinner'. The resonant frequency of the filter was the same as the rotation rate of the sample, and the voltage displayed on the A.C. meter was a measure of the component of magnetization.

Initially, both in static and spinner versions, angle measurements were derived from the component intensities, and the correct octant determined by use of a phase marker pulse. In the static version, this pulse was placed on the chart; in the spinner version, the pulse was displayed on a double-beam oscilloscope, the second beam displaying the output waveform from the bandpass filter. In the later development of the instrument, an angle determination facility was incorporated, which is independent of the component intensity measurements.

The phase angle between the reference pulse and the peak of the output waveform is changed mechanically.

A1.3 Details of Instrumentation

The arrangement of the system is shown in Fig. A.1.1. The basic magnetometer consists of the Varian Associates Rubidium Vapour Magnetometer 4938, with additional sensor and sensor coupler for the gradiometer mode of operation. The principles and details of construction are described in the manufacturers' manual. The chart recorder, which is still used in the later versions of the system for calibration, is a Varian Associates Model G-14-A5 modified for use with the 4938 magnetometer. The A.C. voltmeter used as the final readout is the Hewlett-Packard Model 403A, for use from 1 Hz to 1 MHz, and 0.0001 to 300 volts. The double-beam oscilloscope is the Phillips Model PM3230.

The basic active filter section is based on the circuit described by Artusy (1972), and is a modified Wien Bridge oscillator. It is capable of achieving very high stable Q's, and thus narrow bandwidths. It uses a readily available operational amplifier, μA741c, and has separate frequency and bandwidth controls. The filter, Fig. A1.2, is fed by an emitter follower which uses a Darlington type compound transistor, in order to provide a very low source impedance for the filter

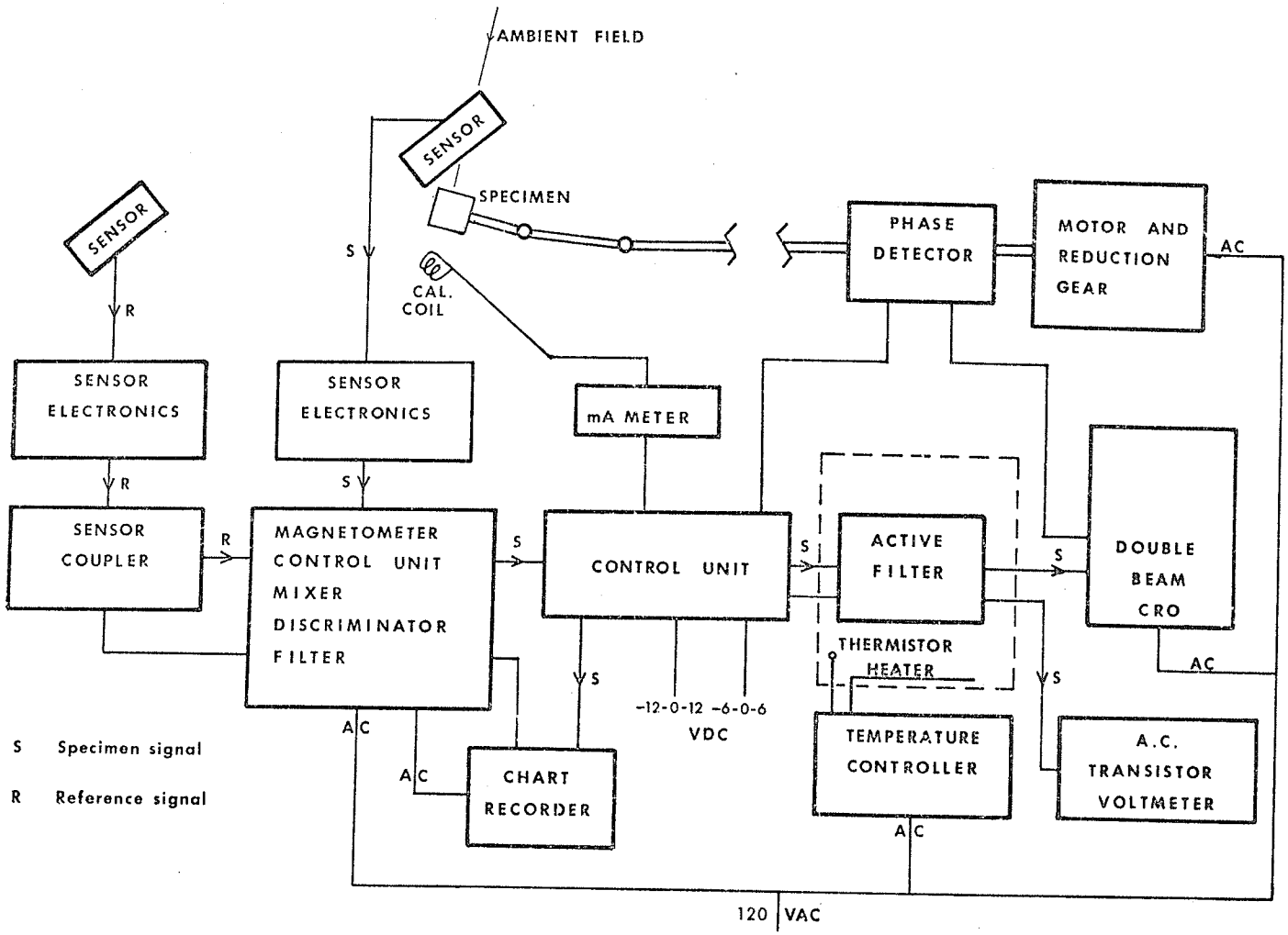

Figure A1.1 Block schematic of magnetometer.

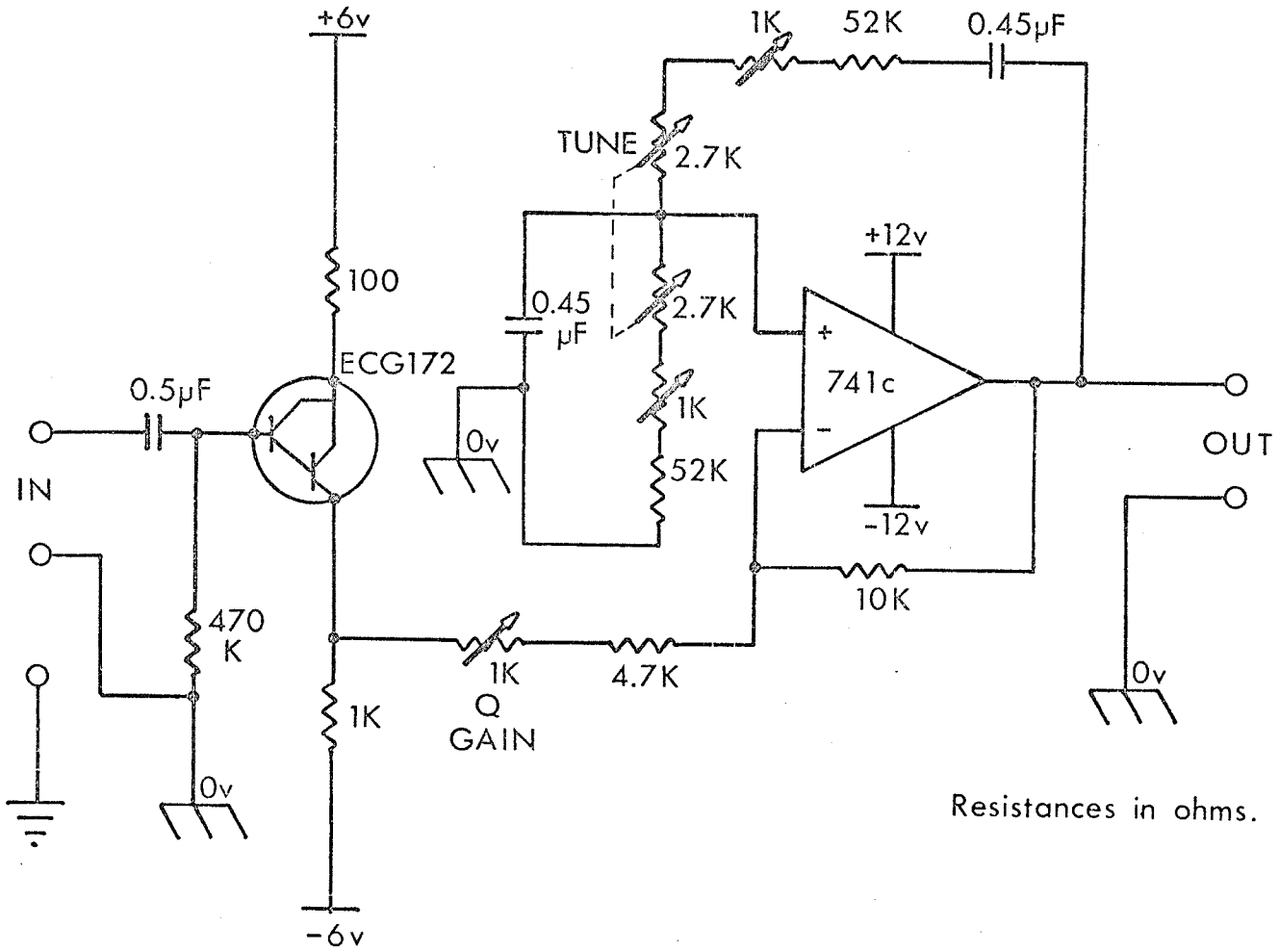

Figure A1.2 Schematic for active filter.

and yet have a high input impedance to prevent appreciable loading of the rubidium magnetometer output.

In working with very high Q's, in order to maintain a stable calibration, an effort has to be made to reduce temperature effects. The whole filter unit including the emitter follower is enclosed in a controlled temperature environment, which consists of a small box built of ¼ inch (0.635 cm.) thick aluminum plate, enclosed in 1 inch (2.54 cm.) thick Styrofoam. A small heater element is embedded in an aluminum block within the box; the temperature sensor is a thermistor attached to the block. The heater is controlled by a circuit external to the box, and the temperature within the box is maintained to within 0.1° of a constant temperature at about 40°C (313 K). This control circuit was designed in the Physics Department, University of Manitoba, and versions of it are in regular use there. The thermistor is in one arm of a bridge connected to a differential amplifier, which controls an SCR, via an unijunction. The SCR passes a portion of the half-wave rectified 120 volt A.C. supply to the heater, which can operate at a maximum of 20 watts. Once equilibrium has been reached in the box (after about a day), the power supplied to the heater is very small.

The sample sensor is mounted on a frame built of Plexiglass, adjustable so that the line joining the centres of the rubidium cell and the sample is coincident with the direction of the

ambient field in the immediate region. The reference sensor is mounted on a wooden frame and positioned a suitable distance away. It is important to ensure that field gradients are not too high at the sensor sites, and that the difference between the two field values is about 250 gammas (nanotesla).

The sample is inserted into a Plexiglass cube-shaped holder, which may be placed in the rotatable holder in the several orthogonal orientations required for the several measurements. The rotation is produced by an induction motor which is about 3 metres away from the sensors. A chain drive from the motor shaft gives a speed reduction of 3:1 to a sectioned brass drive shaft, which extends to about 30 cm. from the sensor. From here to the sample holder, a Plexiglass shaft is used. To allow for imperfect alignment, and for field orientation changes, the drive shaft is in sections, coupled by firm but flexible joints. These transmit the torque satisfactorily, and do not introduce significant errors in the angle measurements. In addition, they help to reduce the transmission of vibrations along the drive shaft to the sensor mount. (The problem of vibrations has given some trouble in maintaining the base noise level of the instrument at a low level.) Bushings support the shaft at intervals.

The magnetometer high frequency cut-off is about 20 Hz, but the present mechanical stability prevented the use of

rotation frequencies above about 10 Hz. In addition, the basic magnetometer has an output filter with a cut-off at 8 Hz, and this would increase the second harmonic rejection and also decrease general higher frequency noise. For frequencies much lower than this, the long time constant of the high Q active filter would introduce excessively long measurement times. The available motor and reduction drive produced a rate of about 6.45 Hz.

The reference pulse is derived from the drive shaft. The shaft carries a disc with a shorting bar, which closes a circuit between two contacts mounted on a plate, concentric with the drive shaft. The plate carries a scale calibrated in degrees. The angular position of the contacts may be changed by rotating the plate, and so the phase of the reference pulse may change relative to the drive shaft and sample. The pulse is used to trigger the oscilloscope timebase, and the effect of rotating the contacts is therefore seen on the oscilloscope as a moving of the filter output waveform relative to reference marks on the graticule.

A proposed improvement to this is to use a light source and photo-cell to produce the pulse. Other, electronic, methods have been considered, but no fully satisfactory one was found.

A1.4 Calibration Procedures

The calibration is based on the known dipole moment of a coil whose dimensions are known. This coil is placed in the sample holder to give maximum signal. A known current is passed through the coil and the corresponding deflection noted on the chart recorder. The coil is then replaced by a secondary standard which is rotated slowly by hand; the corresponding deflection on the chart is noted. This sub-standard is then calibrated in terms of the fundamental measurements. Thus far, the determination is essentially static, and as such constituted the intensity calibration for the early version of the system. Noise is not significant during a calibration. For the spinner mode, the sub-standard is then rotated at the normal operation rate, and the output from the filter read on the A.C. meter. Thus the whole system may be calibrated in terms of the fundamental measurements.

Phase angle calibration is carried out using the sub-standard, which has been positioned in the holder with its remanence vector parallel to an axis of the holder (determined using the chart recorder trace). The angular position of the shorting disk on the drive shaft may then be adjusted so that the waveform peak coincides with a reference mark on the oscilloscope graticule.

The calibration sub-standard is re-inserted at intervals; normally, a check at the beginning and end of a measurement session is sufficient. This serves to check both intensity and direction calibration. The averaging of angles described below in Section A1.5 further removes errors due to any drift in phase angle zero on the instrument.

The sensitivity of the instrument is such that remanences above 6×10^{-6} emu/cm^3. (7.5×10^{-10} Wb/m^2) are considered measurable. The actual sensitivity is about 830 volt/cgs pole.cm. (6.6×10^{11} volt/Wb.m) and is dependent on the Q adjustment. The measurable limit is determined by the noise level, and has been taken as about 10 times the mean noise level. The accuracy is limited primarily by the magnetometer output attenuator and by the output meter, and is taken to be $\pm$ 5%. Repeatability is limited by the filter and can be better than 1%. Second harmonic rejection checks have been made at intervals, and are better than 1000:1, for input supplied to the active filter; the filter in the basic magnetometer increases the rejection further. Even higher rejection has been achieved (exceeding 2000:1 for the active filter) but at the expense of increased filter time constant and thus extended measurement time. Angles may be measured to $\pm$ 2%.

A1.5 Sample Preparation, Data Acquisition and Processing

Immediately after drilling, the rock cores are each given

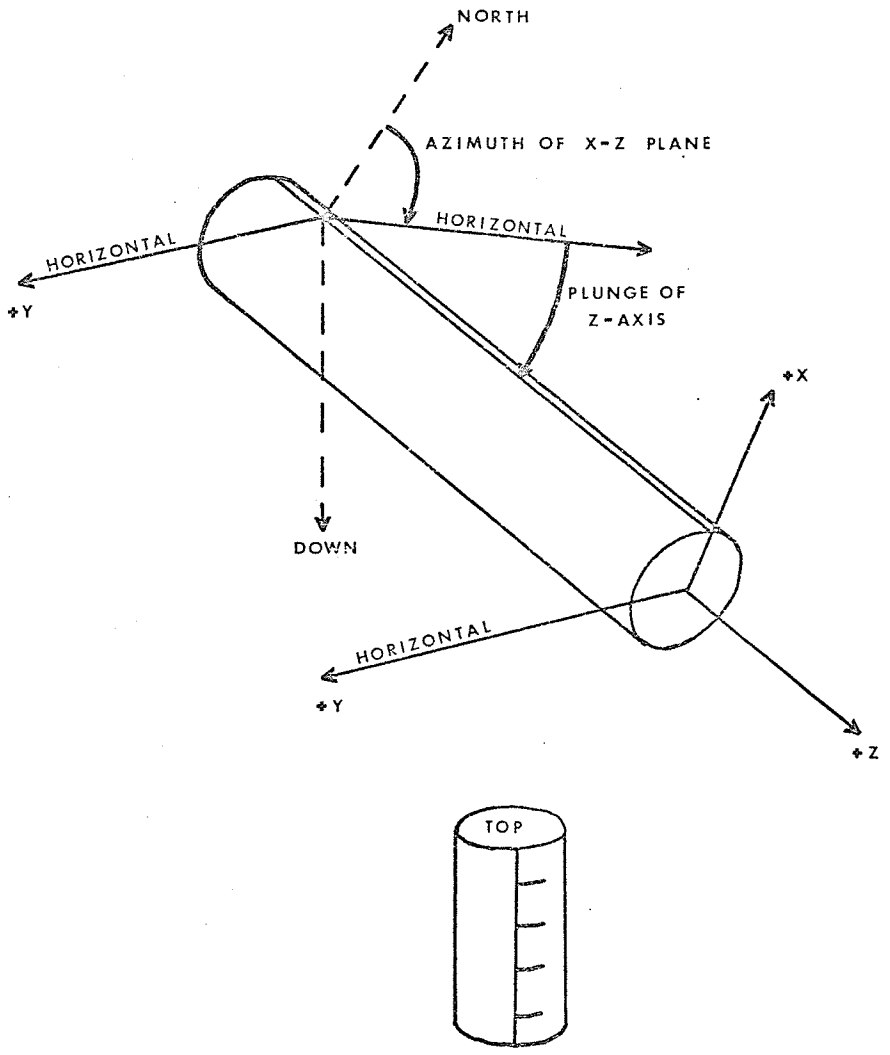

Figure A1.3 Core axes and orientation axes.

an orientation mark corresponding to the position of the X-axis in the core (Fig. A1.3). Using sun sighting (Fraser 1963, Creer and Sanver 1967) or magnetic compass methods, the orientation of the vertical plane containing the X and Z axes of the core is found, as is the inclination of the Z-axis.

The samples to be measured are obtained from the drill cores, and are in the form of short cylinders, whose height to diameter ratio is nominally 0.865, following the recommendations of Noltimier (1971), for minimization of shape anisotropic effects. For the purposes of calculation, the sample magnetization is assumed to be equivalent to a dipole at the sample centre. For a homogeneous sample with the above dimension ratio, this assumption is valid at field measurement points greater than a very few diameters away from the sample centre. Although specifically discussing rock-generator spinner magnetometers, Doell and Cox (1967a) have demonstrated the effectiveness of component averaging in reducing the effects of magnetic inhomogeneities in samples.

The sequence of readings taken is similar to that described by Doell and Cox (1967a). The sequence consists of 12 readings, in three groups of four. In each group, the sample is rotated about one axis, the voltage and component direction being recorded; the sample is then inverted and rotated again about the same axis, the voltage and direction again being noted. The

means of the two voltages and of the two directions are taken. This is repeated for the two other orthogonal axes in the sample.

The component directions are combined graphically using the method described by Doell and Cox (1967a). This is done immediately after the measurements, as a check on validity. The total vector direction, in terms of declination and inclination relative to sample axes, and the component intensities are fed into a computer program which determines the remanence vector in terms of the geographic axes from the field orientation data. A facility for carrying out Fisher statistics (Fisher 1953; Irving 1964) on groups of remanences is also included in the program. Alternatively, the remanence vector may be determined graphically (Doell and Cox, 1967a).

APPENDIX 2

AN ALTERNATING FIELD DEMAGNETIZATION APPARATUS

A2.1 Introduction

Alternating field (AF) demagnetization has become a standard procedure in rock magnetism laboratories as a means of obtaining information about the various remanences carried in rocks, and as a means of separating these remanences, at least partially. There are many variants on the basic principle and some particular systems have been described in the literature (e.g. Creer, 1959; As, 1967; Doell and Cox, 1967b; Pearce, 1967). Doell and Cox gave an analysis of AF demagnetization equipment and point out several factors of importance in the design of such equipment. Pearce has also considered in detail various tests of his equipment.

A2.2 Instrumentation

The system used in this project has been based on the unit in operation at Memorial University of Newfoundland, as described in detail by Pearce (1967). The design was modified insofar as different materials and different electrical arrangements were necessary.

Demagnetization Coils

The basic dimensions of the coils closely follow those of Pearce (1967). The arrangement is a compromise between the finite solenoid and the Helmholtz arrangement, for square section coils; it has in part the greater uniformity of field of the Helmholtz method, and in part the increased specific field (field/current) of the solenoid. Pearce has shown that an optimum shape of winding cross-section is a rectangle 7 units high by 11 units wide, for the following input criteria; (a) the field strength in a space about 3 cm. in diameter, to be occupied by the sample, should not vary by more than 1%; (b) the minimum space required by the tumbler is 12 cm. by 12 cm. at the centre of the coil system, with a separation of 4 cm. between the coils; (c) a specific field of about 250 Oe/amp. is required; (d) 14 swg. varnished copper wire is to be used, to keep the resistance low and allow sufficiently high currents (10 amps. or less) to be used. These criteria agreed closely with the requirements of the proposed unit here.

The actual dimensions of the present system are close to those described by Pearce, who points out that slight variations in dimensions are not critical near the optimum shape. Subsequent checks on the present coils showed that the field varies by less than 1% in the required region. The specifications

of the coils are given in Fig. A2.1.

The coil formers are constructed from plywood and Permawood laminate. The layers of wire are separated from each other by paper insulation which is wrapped around the end turns of each layer, and held by the overlying layer of wire. Although this method reduces slightly the number of layers of wire which may be fitted into a given space, it considerably improves the strength of the coil, placing much less sideways thrust on the former.

Each coil is mounted on a base, which is movable over Teflon strips on a 1 inch (2.54 cm.) plywood platform with supports underneath. Each coil weighs about 34 kg. and is moved by means of a Permawood nut and threaded rod provided with a handle; the movement is necessary to insert and remove the sample from the tumbler, and is rapid and easy with this arrangement. The coils are mounted with their axes in the magnetic east-west direction, so that an uncompensated ambient field component in this direction will be very small.

Power Supply

Several methods for reducing the current from its maximum value are possible. Power units with continuously variable outputs have been produced commercially, and a continuously variable transformer has been built by McElhinny (1966).

Another method which some systems use is the electrolytic resistor (Pearce 1967); this is very susceptible to heating effects, change of resistance characteristics, and is not very safe in operation. Methods where the demagnetization coils themselves are moved are not without problems. A considerable distance of travel is needed at high fields, and the movement of heavy coils may give problems. Furthermore, the uniformity of field at the sample position may deteriorate. As (1967) used autotransformers to control the current.

A variable output transformer was not available; however, it was considered that in the future a smoothly variable power source might be obtained, and the demagnetization unit was built on that basis. But in the present system, two autotransformers were used. A disadvantage in using such an arrangement might be that the field is reduced in finite steps, which become quite large when high initial fields are used.

In the present work, some early runs were made with the demagnetization coils in parallel, to obtain fields up to about 1100 Oe. (induction of 0.11 tesla). A few samples subjected to fields above about 700 Oe. showed some indication that the finite steps were becoming significant - erratic non-repeatable directions were obtained. However, up to about 600 Oe., it appeared from the general behaviour under progressive cleaning that the finite steps were not of major importance in the present work. Most of the magnetic cleaning was done

in fields up to about 400 Oe. However, if in the future higher fields must be used, especially in paleomagnetic work, then a smoothly variable power source will be necessary.

The electrical circuit to provide power for the demagnetization coils is shown in Fig. A2.1. One autotransformer is used to set the maximum initial field, and the second transformer is driven by a synchronous motor via a reduction drive. The time for reduction from maximum to minimum field may be varied between 1 minute and 4 minutes by modification of the reduction drive; usually, a time of about 2 minutes was used. The second harmonic content of the line supply is low and the action of a transformer is to further reject even harmonics. The Q factor of the tuned circuit of capacitors and demagnetizing coils is 34.

Sample Tumbler

Doell and Cox (1967b) have shown that an important factor in demagnetization is the manner in which the sample is rotated within the decreasing alternating field. The tumbler in use in the present system is a three axis one, with the rotation ratios being nominally 1.61:1.21:1.00, as proposed by Doell and Cox. To obtain an efficient coverage of the directions within the sample, it is important that the rates of rotation be commensurate with each other but not simply related.

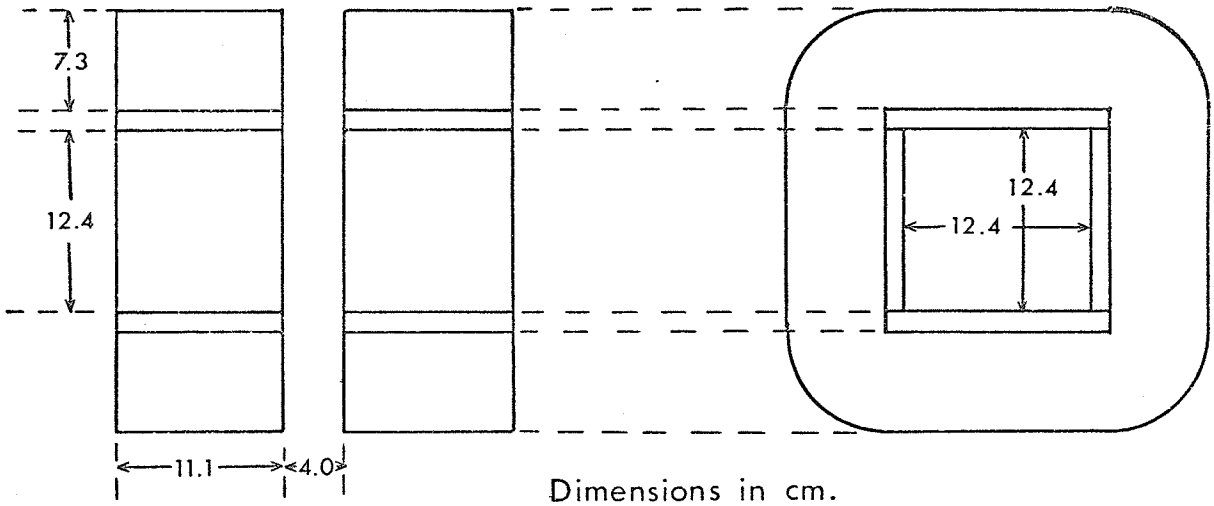

(a) Wiring Section of Coils

(b) Coil Parameters

Resistance Each	Resistance Series	Inductance Series	Turns Each
14.8 ohm	29.6 ohm	2.70 henry	2200

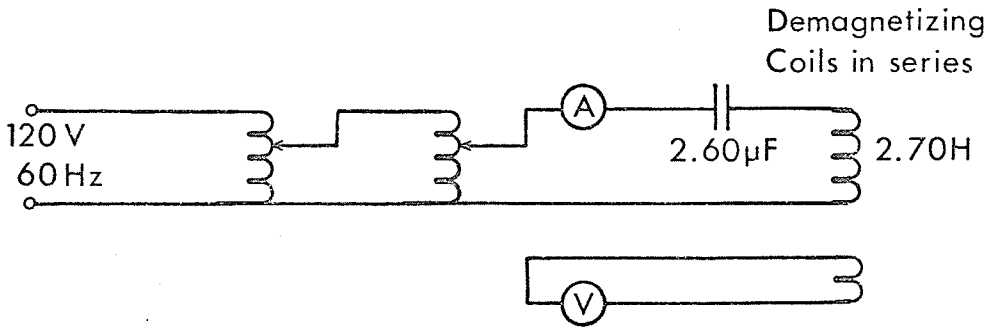

(c) Power Supply Circuit

Figure A2.1 Demagnetizing Coils

The tumbler is constructed from laminated Permawood, with pulleys and shafts of nylon. Drive belts are rubber O-rings. It is designed to take cylindrical specimens up to 1 inch (2.54 cm.) diameter. The tumbler is driven, via a brass shaft 4 feet long, by an A.C. induction motor with a belt reduction drive. The rate of rotation of the outer frame of the tumbler is about 5 Hz.

The average rate of field decrease is about 0.9% per second, during which time the outermost frame (the slowest) has completed about 5 revolutions, and the field passes through about 12 cycles during one rotation of the outer frame. Thus, an effective cancellation should be achieved.

The axis of the outer frame of the tumbler is horizontal and magnetic north-south in direction. The component of the ambient magnetic induction in this direction is small (about 0.1 Gauss, 0.1 millitesla), and with DC cancellation is readily reduced to near zero.

DC Field Compensation

It has been demonstrated by several workers (e.g. Doell and Cox, 1967b; Snape, 1971) that spurious moments may be induced in a specimen if subjected to a decreasing field on which is superimposed a direct steady field. The resulting anhysteretic remanent magnetization (ARM) often is of considerable stability.

This effect has been minimized in the present system by the use of the three-axis tumbler, and by the use of three sets of orthogonal Helmholtz coils arranged to cancel the DC field at the specimen position in the apparatus. The dimensions and electrical circuit arrangements are shown in Fig. A2.2. The coils are powered by three regulated DC power units, N.J.E. Corporation Model PVC-10-2-HP, in constant current mode of operation. The load regulation is 0.01% or 250 microamps. in the High Performance mode; line regulation at constant load is less than 0.01% or 50 microamps. from 105 to 130 volts.

The main source of the field to be eliminated is the geomagnetic field. The vertical component of induction is about 0.6 Gauss (0.6 millitesla) and the horizontal component about 0.1 Gauss. One pair of coils is used to cancel the vertical component, while two orthogonal sets are used to cancel the horizontal component. These latter sets make small angles with the magnetic north-south and east-west directions, respectively. In this arrangement, the system is flexible and may be adjusted easily for any long term drifts in field direction.

The field is uniform to within 0.2% in a region about 10 cm. diameter, and may be reduced to 0 ± 50 gammas (nanotesla), the accuracy being limited by the fluxgate detector used for measuring the field and by the power supply controls. The power supplies can control to about ± 15 gamma.

The alternating field in the main demagnetizing coils induces EMF's in the DC compensation coils. In the NS and vertical sets the net effect is very small, but for the EW pair a large EMF is induced. In order to protect the power supply, and to prevent any spurious alternating currents flowing in the compensation coil, a parallel LC impedance trap is included in the circuit, as shown in Fig. A2.2.

A2.3 Calibration

The field strength produced by the demagnetizing coils is measured in terms of the magnetic induction which produces an EMF in a small coil of several hundred turns permanently fixed in position on the axis of the main demagnetizing coils. The alternating voltage is measured by a voltmeter. This reading in volts is calibrated in terms of field units by placing a second small test coil of known dimensions at the sample position, with its axis aligned with the main field axis. The EMF induced in this coil is measured using a digital voltmeter and the field determined using the known dimensions of the coil, the number of turns and known frequency. The corresponding reading of the regular voltmeter is also noted and a calibration is thereby effected. This procedure is repeated at other field strengths. The calibration accuracy is about 1%, governed mainly by test coil construction and positioning.

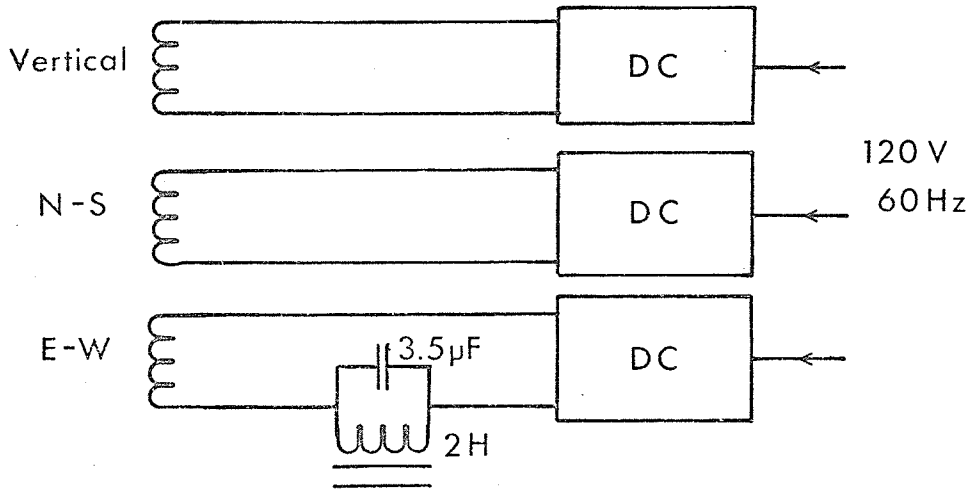

(a) Power Supply Circuits

(b) Coil Parameters

	Mean Radius cm.	Mean Separation cm.	Number of Turns 16 swg.	Current amp.
Vertical	44.7	45.1	30	0.92
N - S	49.9	50.4	25	0.28
E - W	54.6	54.6	15	0.06

Figure A2.2 DC Compensation Coils

The maximum attainable field with the present power supply, and coils in series, is about 800 Oe. peak (or 0.08 tesla induction). However, the coils are capable of carrying higher currents to produce 1500 Oe. with improved power supplies.

A2.4 Operation

In order that the system may stabilize, it was normal to keep the DC field compensation circuits in operation over an extended period. Checks on the effectiveness of the field nulling were made frequently and adjustments made if necessary. Long term drifts in the vertical component were often found, but the horizontal components showed very little change.

A sample is placed in the tumbler, and the coils moved into operating position; the tumbler is then set in rotation. Initially, both autotransformers may be at zero. The motor-driven transformer is then manually turned to maximum position, followed by the setting of the second transformer to produce the required peak field. The sample is tumbled at this field for about 15 seconds, and then the motor drives the transformer, reducing the field to zero. Alternatively, if a series of runs are to be made at the same peak field setting, the field-set transformer may be left at a constant position. In the various plots in this section and in Chapter 4, the peak fields are plotted to an accuracy of about ± 10 Oe. When the field

has reduced to zero, the tumbler is stopped, the coils separated and the sample removed, taking care to avoid the DC compensation coils. The remaining remanence in the sample is measured immediately afterwards. It was found that, especially with the present suite of rocks, significant changes in remanence may occur in a very short time after the cleaning.

To consider the interaction of the system with a sample carrying two distinct remanences, an artificial sample containing magnetite powder in Plaster of Paris was constructed. The grain size was between 177 and 250 μm. The sample was given a total TRM in the earth's field, and its remanence was measured before and during progressive magnetic cleaning, Fig. A2.3. The curve suggests that although a total TRM was imparted to the sample the coercivities were predominantly small (as might be expected from the grain size). After cleaning to 300 Oe., the sample was given an IRM in a DC field of 30 Oe. The behaviour with progressive magnetic cleaning is shown in Fig. A2.3. It is seen that the IRM was effectively removed and the remaining TRM unaffected; this serves also to demonstrate the repeatability of the remanences after successive operations.

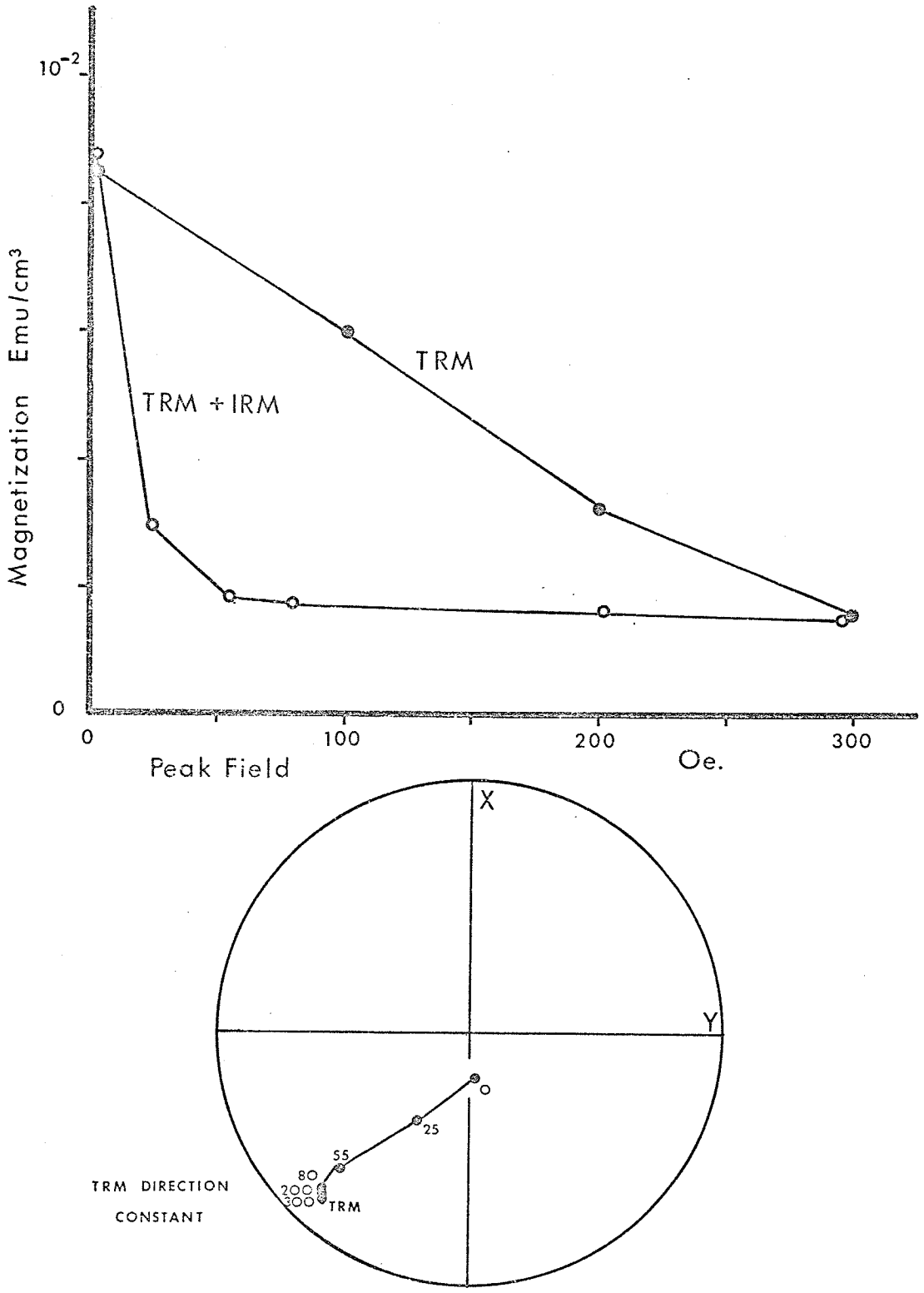

Figure A2.3 Example of Progressive AF cleaning, showing separation of component remanences.

A2.5 Comments

After the tumbler unit had been built, it was pointed out (R.L. Wilson, personal communication, 1971) that there was some evidence that spurious remanences might be produced as a result of slow rotation of ferromagnetic material in alternating fields (Wilson and Lomax, 1972). This has important implications for magnetic cleaning equipment in many laboratories. The effect may be reduced by the two axis tumbler described by Wilson and Lomax.

It has also been shown (e.g. Doell and Cox 1967b; Pearce 1967; Larochelle and Black 1965) that spurious remanences may occur in samples, which are related to the orientation of the tumbler axes, in particular the inner axis, with respect to the sample axes. Attempts were made with the present apparatus, and present suite of rocks, to repeat these tests. However, it was found that in almost all attempts, soft components masked any such effects. One sample, A013A, appeared to have fewer soft components than most samples, but its remanence at 600 Oe was still quite high. An abbreviated test on this sample was made; the X-axis was placed successively in the four positions parallel or perpendicular to the inner tumbler axis, the Z-axis remaining the same throughout. The corresponding changes in remanence direction, when repeatedly

cleaned at 600 Oe. were suggestive of a spurious component parallel to the inner axis, but the changes were of the order of the accuracy of the magnetometer direction determination, and are therefore not conclusive. The attempts to detect an anticipated larger effect with softer samples failed as a result of the very soft components present. Thus, conclusive evidence for or against the effect was not obtained, but it is suggested that it exists, on the basis of the results from A013A.

It is proposed that the present tumbler should be used to investigate the phenomenon described by Wilson and Lomax (1972) and also the three axis behaviour, as and when improved power supplies and suitable samples become available.

APPENDIX 3

Computer Programs

PROGRAM "BLOCK"

1. Identification

Title: Calculations of total field magnetic anomalies due to a series of finite right rectangular prismatic blocks.

Programmer: R. L. Coles

Date: October 1972

Language: Fortran IV

2. Purpose

To calculate the resultant total field anomaly caused by any number of finite right rectangular prisms, of arbitrary sizes and magnetizations, when demagnetization effects are not important.

3. Usage

Operational Procedure: The main program reads the input data. Subroutine PRISM computes the field due to one prism at a time, adding this field to the previous resultant field. The main program prints out the final resultant field, and the input parameters.

Input parameters:

SYMBOL	Identification title
DELT	Grid interval in kilometres
DD	Declination of geomagnetic field, clockwise from x-axis.

DI	Inclination of geomagnetic field
IS,IE,JS,JE	Start and end limits of field array (F)
	Minimum values 1,1,1,1 represent origin of coordinates
LBLOCK	Number of prisms to be added
IADD	= 0 if computing a new model field
	= 1 if modifying a previously computed field which is read into array F
NBLOCK	Number of prisms used previously, if IADD = 1
F	If IADD = 1, field array to be modified, in gammas. If IADD = 0, F is initialized to zero.
ID	Identification number of prism
IP	Magnetization intensity, units of 10^{-6} emu/cc
IREM	= 0 if magnetization parallels ambient field
	= 1 if magnetization non-parallel to ambient field
P(1), P(2)	X,Y coordinates of 'SW' corner of prism
P(3), P(4)	X,Y extents of prism
P(5), P(6)	Top and bottom of prism
	All P(I) in kilometres.
DM	Declination of magnetization, clockwise from x-axis
IM	Inclination of magnetization

Note: DM, IM only required if IREM =1

Calculated parameters:

F Resultant field due to all blocks

Output:

All input parameters, except previous F, are listed, followed by the new resultant field F, in gammas. A facility for placing the F values on disk, tape or cards is included.

4. Comments

The field is computed for one prism at a time. In this way, storage is constant, irrespective of the number of prisms. Time required is closely proportional to the number of prisms, after the basic I/O time, and is about 0.02 seconds per grid point per prism. The facility for modifying a previous field means that if changes are needed, it is not necessary to re-compute the complete field. All parameters pertaining to one prism are on one card. For 3000 data points, 46 K region are required.

5. Input sequence

1. SYMBOL
2. DELT, DD, DI
3. IS, IE, JS, JE, LBLOCK, IADD, NBLOCK

4. Previous field, if IADD = 1. May be on cards or other device.
5. If IADD = 1, NBLOCK cards carrying parameters for previous prisms (ID, IP, IREM, (P(K), K=16), DM, IM) These are normally available from the previous run.
6. LBLOCK cards carrying parameters for new prisms (ID, IP, IREM, (P(K),K=1,6), DM, IM)

Formats as per listing.

6. References:

Bhattacharyya, B.K. 1964 Magnetic anomalies due to prism-shaped bodies with arbitrary polarization; Geophysics, v.29, no. 4, pp. 517-531.

7. Method

As described in Chapter 2, section 2.5

```
      PROGRAM BLOCK(INPUT,OUTPUT,TAPE5=INPUT,TAPE6=OUTPUT,TAPE7)
C******  UNIVERSITY OF MANITOBA  ******
C***  PROGRAM COMPUTES MAGNETIC ANOMALY FIELD ON TWODIMENSIONAL GRID
C***  DUE TO A SERIES OF VERTICAL SIDED PRISMATIC BLOCKS OF FINITE
C***  DEPTH EXTENT
C***  PROGRAMMER  R L COLES OCTOBER 1972
C***  PROGRAM USES THEORY DEVELOPED BY B K BHATTACHARYYA 1964
C   F                FIELD ARRAY
C   IP               POLARIZATION INTENSITY
C   P(1),P(2)        COORDINATES OF SW CORNER OF PRISM
C   P(3),P(4)        X, Y EXTENTS OF BLOCK
C   P(5),P(6)        TOP AND BOTTOM OF PRISM
C   L2, M2, N2       DIRECTION COSINES OF POLARIZATION VECTOR
C   IS,IE,JS,JE      START AND END LIMITS OF F ARRAY
C                    MINIMUM VALUES 1,1,1,1  REPRESENTS ORIGIN OF COORDINATES
C   DELT             GRID INTERVAL
C   DD, DI           DECLINATION, INCLINATION OF GEOMAG FIELD
C                    DECLINATIONS ARE MEASURED CLOCKWISE FROM THE X-AXIS
C   DM,IM            DECLINATION INCLINATION OF BLOCK MAGNETIZATION
C   LBLOCK           NUMBER OF BLOCKS
C   NBLOCK           NUMBER OF BLOCKS USED PREVIOUSLY
C   IREM             IREM.EQ.0 POLARIZATION PARALLELS GEOMAG FIELD
C                    IREM.NE.0 NON-PARALLEL
C   IADD             IADD.EQ.0 COMPUTING NEW MODEL FIELD
C                    IADD.NE.0 MODIFYING EARLIER MODEL FIELD
C
      REAL IO,IM,L1,L2,L3,M1,M2,M3,N1,N2,N3
      COMMON/FIELD/ F(60,1)
      COMMON/LIMIT/ IS,IE,JS,JE
      COMMON/SPECS/ P(6),IP,L2,M2,N2,DM,IM,AIP
      COMMON/ANGLE/ IO,DO,L1,M1,N1,S1,S3,C1,C3
      DIMENSION SYMBOL(80)
9000  CONTINUE
C ---------------------------------------------------------------------
C   INPUT I.D., CONTROL PARAMETERS, GEOMAGNETIC FIELD DATA
      READ(5,2000) (SYMBOL(I),I=1,80)
      READ(5,1000) DELT,DD,DI
      READ(5,1) IS,IE,JS,JE,LBLOCK,IADD,NBLOCK
2000  FORMAT(80A1)
1000  FORMAT(10F8.1)
1     FORMAT(20I4)
C ---------------------------------------------------------------------
      WRITE(6,2001) (SYMBOL(I),I=1,80)
2001  FORMAT("0",80A1)
      WRITE(6,200) DD
200   FORMAT("0","DECLINATION OF MAIN FIELD FROM X-AXIS ",F4.0,
     *" DEGREES")
      WRITE(6,201) DI
201   FORMAT("0","INCLINATION OF MAIN FIELD ",F4.0," DEGREES")
      WRITE(6,202) IS,IE,JS,JE
202   FORMAT("0","GRID SIZE",I4," TO",I4," BY",I4," TO",I4," POINTS")
      WRITE(6,203) DELT
203   FORMAT("0","GRID INTERVAL ",F4.1," KM.")
      IF(IADD) 4000,4000,4001
4000  WRITE(6,600)
```

```
      GO TO 4002
 4001 WRITE(6,601)
 4002 CONTINUE
  600 FORMAT("1","*** THIS IS A NEW MODEL FIELD ***")
  601 FORMAT("1","*** THIS IS A MODIFICATION TO EARLIER MODEL ***")
      WRITE(6,5000)
 5000 FORMAT("0","-----------------------------------------------------
     1-----------------------------------------------")
      WRITE(6,5001)
 5001 FORMAT("0",T2,"BLOCK",T15,"SW.CORNER",T32,"XLENGTH",T45,"YLENGTH",
     1T61,"TOP",T71,"BASE",T89,"POLARIZATION")
      WRITE(6,5002)
 5002 FORMAT(" ",T15,"X",T23,"Y",T82,"DECL.",T91,"INCL.",T100,
     1"INTENSITY")
      WRITE(6,5003)
 5003 FORMAT(" ",T15,"KM.",T23,"KM.",T35,"KM.",T48,"KM.",T62,"KM.",T72,
     1"KM.",T83,"DEG.",T92,"DEG.",T98,"10**-6 EMU/CC.")
      WRITE(6,5000)
      IF(IADD.NE.0) GO TO 500
      DO 3 J=JS,JE
      DO 3 I=IS,IE
    3 F(I,J)=0.
      GO TO 520
  500 CONTINUE
C -----------------------------------------------------------------------
C   INPUT EARLIER FIELD TO BE MODIFIED
      DO 510 J=JS,JE
  510 READ(5,1234) (F(I,J),I=IS,IE)
 1234 FORMAT(6G13.6)
      IR=5
      DO 511 J=1,NBLOCK
      READ(IR,4) ID,IP,IREM,(P(K),K=1,6),DM,IM
      IF(IREM.NE.0) GO TO 512
      DM=DO
      IM=IO
  512 CONTINUE
      WRITE(6,2225) ID,(P(I),I=1,6),DM,IM,IP
  511 CONTINUE
C -----------------------------------------------------------------------
      WRITE(6,5010)
 5010 FORMAT("0","ADDED BLOCKS")
  520 CONTINUE
      DELT=DELT*100000.
      CON=3.14159265/180.
      IO=DI*CON
      DO=DD*CON
      S1=SIN(IO)
      S3=SIN(DO)
      C1=COS(IO)
      C3=COS(DO)
      L1=C1*C3
      M1=C1*S3
      N1=S1
      DO 90 LI=1,LBLOCK
C -----------------------------------------------------------------------
```

```
C   INPUT DATA FOR BLOCK
      READ(5,4) ID,IP,IREM,(P(K),K=1,6),DM,IM
4     FORMAT(I4,I8,I4,8F8.1)
C ---------------------------------------------------------------
      IF(IREM.NE.0) GO TO 30
C ---------------------------------------------------------------
C   POLARIZATION PARALLEL TO AMBIENT FIELD
      L2=L1
      M2=M1
      N2=N1
      DM=DO
      IM=IO
      GO TO 40
30    CONTINUE
C ---------------------------------------------------------------
C   POLARIZATION NON-PARALLEL TO AMBIENT FIELD
      IM=IM*CON
      DM=DM*CON
      L2=COS(IM)*COS(DM)
      M2=COS(IM)*SIN(DM)
      N2=SIN(IM)
40    CONTINUE
      DDM=DM/CON
      DIM=IM/CON
      WRITE(6,2225) ID,(P(I),I=1,6),DDM,DIM,IP
2225  FORMAT("0",T3,I4,T10,F8.2,T20,F8.2,T31,F8.2,T44,F8.2,T58,F8.2,T69,
     1F8.2,T81,F6.1,T90,F6.1,T100,I8)
      DO 45 K=1,6
      P(K)=P(K)*100000.
45    CONTINUE
      AIP=IP/10.

      CALL PRISM(DELT)
50    FORMAT("0",18(F6.0,1X))
90    CONTINUE
      DO 60 I=IS,IE
60    WRITE(6,50) (F(IE+IS-I,J),J=JS,JE)
      IWR=1
      IWR=0
      IF(IWR.EQ.0) GO TO 999
C ---------------------------------------------------------------
C   WRITE OUTPUT ON DISK OR TAPE
      DO 100 J=JS,JE
100   WRITE(7,1234) (F(I,J),I=IS,IE)
999   CONTINUE
      STOP
      END
```

```
      SUBROUTINE PRISM(DELT)
C     CALCULATES FIELD OVER TWODIMENSIONAL GRID DUE TO VERTICAL SIDED PRISM
C     OF FINITE DEPTH EXTENT
      REAL IM,IO,L1,L2,L3,M1,M2,M3,N1,N2,N3
      COMMON/FIELD/ F(60,1)
      COMMON/SPECS/ P(6),IP,L2,M2,N2,DM,IM,AIP
      COMMON/LIMIT/ IS,IE,JS,JE
      COMMON/ANGLE/ IO,DO,L1,M1,N1,S1,S3,C1,C3
      R(A,B)=SQRT(A*A+B*B+H*H)
      F1(A,B)=ALOG((R(A,B)-A)/(R(A,B)+A))
      F2(A,B)=ALOG((R(A,B)-B)/(R(A,B)+B))
      F3(A,B)=ALOG(R(A,B)+H)
      F4(A,B)=ATAN(A*B/(A*A+R(A,B)*H+H*H))
      F5(A,B)=ATAN(A*B/(R(A,B)*H))
      F6(A,B)=A232*F1(A,B)+A132*F2(A,B)-A12*F3(A,B)
      F7(A,B)=ATAN(A*B/(R(A,B)*R(A,B)+R(A,B)*H-A*A))
C     ------------------------------------------------------------------
C     CALCULATE EFFECTS FROM PRISMS WITH TOPS AT P(5) AND P(6), EXTENDING TO
C     INFINITE DEPTH - SUBTRACT TO OBTAIN EFFECT OF FINITE PRISM
      S2=SIN(IM)
      S4=SIN(DM)
      C2=COS(IM)
      C4=COS(DM)
      A12=C2*C1*(C4*S3+S4*C3)
      A132=(C2*C4*S1+S2*C1*C3)/2.
      A232=(C2*S4*S1+S2*C1*S3)/2.
      L3=L2*L1
      M3=M2*M1
      N3=N2*N1
      DO 100 II=5,6
      H=P(II)
      DO 90 J=JS,JE
      Y=(J-1)*DELT
      DO 90 I=IS,IE
      X=(I-1)*DELT
      BL=P(2)-Y
      BU=BL+P(4)
      AL=P(1)-X
      AU=AL+P(3)
      XBLOCK=F6(AU,BU)-L3*F4(AU,BU)+N3*F5(AU,BU)-M3*F7(AU,BU)
      XBLOCK=XBLOCK-F6(AL,BU)+L3*F4(AL,BU)-N3*F5(AL,BU)+M3*F7(AL,BU)
      XBLOCK=XBLOCK-F6(AU,BL)+L3*F4(AU,BL)-N3*F5(AU,BL)+M3*F7(AU,BL)
      XBLOCK=XBLOCK+F6(AL,BL)-L3*F4(AL,BL)+N3*F5(AL,BL)-M3*F7(AL,BL)
      XBLOCK=XBLOCK*AIP
      IF(II.EQ.5) F(I,J)=F(I,J)+XBLOCK
      IF(II.EQ.6) F(I,J)=F(I,J)-XBLOCK
80    CONTINUE
90    CONTINUE
100   CONTINUE
      RETURN
      END
```

PROGRAM "PRISM"

1. Identification

Title: Least-squares fit of finite right rectangular prism to total-field magnetic anomaly.

Programmer: R.L. Coles

Date: March 1973

Language: Fortran IV

2. Purpose

To calculate the parameters of a finite right rectangular prism which produces a best-fit (in the least-squares sense) model field to the total field magnetic anomaly being considered.

3. Usage

Operational Procedure: The main program reads the input data. Subroutine PARAM is called to print out the input parameters. The main program computes derivatives and total field, and sets up normal equations. Subroutine LNEQ, which calls SUBM, is used to solve the equations. Parameters are modified in the main program, and subjected to checks. Iterations proceed until limits are reached, or convergence criteria met. Subroutine PARAM prints the output parameters.

Input Parameters:

LREP	Number of iteration restarts

NOTEST	= 0 if convergence tests are to be applied to each parameter = 1 if no convergence tests
LIMIT	Maximum number of iterations allowed
XLAM	Convergence parameter = LAMDA
IP	Input device number for anomaly field
IS, IE, JS, JE	Start and end limits of anomaly and theoretical field arrays. Minimum values 1,1,1,1 represent origin of coordinates.
DELT	Grid interval in kilometres
IO	Inclination of geomagnetic field
DO	Declination of geomagnetic field, clockwise from x-axis
LCON	= 0 if no constraints on parameters = 1 if constraints applied to parameters (In present form, only applied to top and bottom of prism; others may be included by a simple extension)
ANOM	Array contains input anomaly field, in gammas
SYMBOL	Identification title for model
PMAX(I),PMIN(I)	Maximum and minimum constraints for parameter PA(I)
PB(I),PB(2)	Half X-length, half Y-length

PB(3), PB(4) Top and bottom of prism

PB(5), PB(6) Inclination and declination of prism magnetization, clockwise from X-axis

PB(7) Angle from X-axis to X'-axis

PB(8), PB(9) X,Y coordinates of centre of prism

PB(10) Magnetization intensity

All parameters in degrees or kilometres, except PB(10) which is in units of 10^{-6} emu/cc.

PB(I) is fed to PA(I) in the program.

MJ(I) Control codes I = 1, 10

If MJ(I) =0 Parameter PA(I) is unchanged

If MJ(I) =1 Parameter PA(I) is changed during the iterations.

MJ(I) is fed to MI(I) and N(I) in the program

BASE Lowest base level, in gammas

BINC Base level increment

TOP Highest base level

Calculated Parameters:

All PA(I) may be modified, according to the specified control codes MJ(I).

Output:

The input anomaly field, initial parameters, initial and subsequent model fields at each iteration, the new parameter values at each iteration, and final errors are printed for

each base level iteration.

4. Comments

If certain physically impossible values appear, checks are available which state 'invalid result', and the program proceeds to the next base level iteration. If satisfactory convergence is not reached after a specified number of iterations, the process is stopped and the next base level iteration begun.

The program requires 44 K region for 360 data points; of this more than 20 K are fixed. Time is about 1.5 seconds per individual iteration on 100 points; in many situations, a small number of iterations is adequate.

5. Input Sequence

1. LREP, NOTEST, LIMIT, XLAM, IP
2. IS, IE, JS, JE, DELT, IO, DO, LCON
3. ANOM
4. SYMBOL
5. PMAX(I), PMIN(I), I = 3,4 if LCON = 1

(N.B. If LCON = 0, no card here)

6. PB(I), I = 1,10
7. MJ(I), I = 1, 10
8. BASE, BINC, TOP

Formats as per listing.

6. References:

Bhattacharyya, B. K. 1964 Magnetic anomalies due to prism-shaped bodies with arbitrary polarization; Geophysics, v.29, no. 4, pp. 517-531.

Johnson, W. W. 1969 A least-squares method of interpreting magnetic anomalies caused by two-dimensional structures; Geophysics, v.34, no. 1, pp.65-74.

7. Method

As described in Chapter 2, section 2.6

```
      PROGRAM PRISM(INPUT,OUTPUT,TAPE5=INPUT,TAPE6=OUTPUT,TAPE7)
C*****  UNIVERSITY OF MANITOBA  ******
C***  PROGRAM USES LEAST SQUARES ALGORITHM TO FIT RIGHT RECTANGULAR
C***  PRISM MODEL TO TOTAL FIELD MAGNETIC ANOMALY
C***  PROGRAMMER R.L. COLES MARCH 1973
C***  PROGRAM IS BASED ON FORMULA FOR RIGHT PRISM DEVELOPED BY
C***  B.K. BHATTACHARYYA 1964
C  ANOM              ANOMALY FIELD
C  FIELD             MODEL FIELD
C  IS,IE,JS,JE       START AND END LIMITS OF ANOM AND FIELD ARRAYS
C                    MINIMUM VALUES 1,1,1,1, REPRESENT ORIGIN OF COORD.
C  DELT              GRID INTERVAL
C  I0,D0             DECLINATION, INCLINATION OF GEOMAG. FIELD
C                    DECLINATIONS MEASURED CLOCKWISE FROM X-AXIS
C  BASE              BASE LEVEL STARTING VALUE
C  BINC              BASE LEVEL INCREMENT
C  TOP               BASE LEVEL MAXIMUM
C  PA(1),PA(2)       HALF X"LENGTH, HALF Y"LENGTH
C  PA(3),PA(4)       TOP AND BASE OF PRISM
C  PA(5),PA(6)       INCLINATION,DECLINATION OF PRISM MAGNETIZATION
C  PA(7)             ANGLE FROM X-AXIS TO X"-AXIS
C  PA(8),PA(9)       X,Y COORDS. OF CENTRE OF PRISM
C  PA(10)            INTENSITY OF POLARIZATION
C***  ALL PARAMETERS ARE IN DEGREES OR KILOMETRES, EXCEPT PA(10),
C     WHICH IS UNITS OF (10***-6) EMU/CC.
      DIMENSION F1(8),F2(8),F3(8),F4(8),F5(8),F6(8)
      DIMENSION P1(8),P2(8),P3(8),P4(8),P5(8),P6(8),P7(8),P8(8)
      DIMENSION Q(10),E(24),STORE(10),PB(10)
      DIMENSION PMAX(4),PMIN(4)
      COMMON/SOLVE/ SUM(10,10),VEC(10),IR(10),IC(10)
      DIMENSION ANOM(15,24),FIELD(15,24)
      COMMON PA(10),SYMBOL(80),CON
      REAL I0,IM,LAMDA
      DIMENSION N(10),MI(10),MJ(10)
C ---  EXPRESSIONS USED FREQUENTLY ---
      T1(A,B,H)=SQRT(A*A+B*B+H*H)
      T2(A,B)=A*B
      T3(A,B,H)=A*A+H*H
      T4(A,B,H)=B*B+H*H
      CON=3.14159265/180.
C ---  INPUT DATA ---
      READ(5,7) LREP,NOTEST,LIMIT,XLAM,IP
7     FORMAT(3I4,F8.4,I4)
      READ(5,2) IS,IE,JS,JE,DELT,I0,D0,LCON
2     FORMAT(4I4,3F8.4,I4)
      I0=I0*CON
      D0=D0*CON
      DELT=DELT*100000.
      DO 6 JF=JS,JE
6     READ(IP,5) (ANOM(IF,JF),IF=IS,IE)
5     FORMAT(15F5.0)
      WRITE(6,8)
8     FORMAT("1","ANOMALY FIELD")
      DO 9 JF=JS,JE
9     WRITE(6,9003) (ANOM(IF,JF),IF=IS,IE)
```

```
C --- START OF PROGRAM REPEAT ---
9999  CONTINUE
      READ(5,1) (SYMBOL(I),I=1,80)
1     FORMAT(80A1)
      IF(LCON.EQ.0) GO TO 2999
      READ(5,4) (PMAX(I),PMIN(I),I=3,4)
      WRITE(6,2998) PMAX(3),PMIN(3),PMAX(4),PMIN(4)
2998  FORMAT("0","MAX. TOP",F8.4," MIN. TOP",F8.4," MAX. BASE",F8.4,
     1" MIN. BASE",F8.4)
      DO 2997 I=3,4
      PMAX(I)=PMAX(I)*100000.
      PMIN(I)=PMIN(I)*100000.
2997  CONTINUE
2999  CONTINUE
      READ(5,4) (PB(I),I=1,10)
4     FORMAT(10F8.4)
      READ(5,3) (MJ(I),I=1,10)
3     FORMAT(10I2)
C --- BASE LEVEL ITERATION START
      LCOUNT=0
      READ(5,4) BASE,BINC,TOP
      DO 3000 JF=JS,JE
      DO 3000 IF=IS,IE
3000  ANOM(IF,JF)=ANOM(IF,JF)-BASE
3005  CONTINUE
      IF(LCOUNT.EQ.0) GO TO 3020
      DO 3010 JF=JS,JE
      DO 3010 IF=IS,IE
3010  ANOM(IF,JF)=ANOM(IF,JF)-BINC
      BASE=BASE+BINC
3020  CONTINUE
      WRITE(6,3030) BASE
3030  FORMAT("0","BASE LEVEL ",G13.6)
      LCOUNT=1
      DO 3040 I=1,10
      PA(I)=PB(I)
      MI(I)=MJ(I)
3040  CONTINUE
      PA(1)=PA(1)*100000.
      PA(2)=PA(2)*100000.
      PA(3)=PA(3)*100000.
      PA(4)=PA(4)*100000.
      PA(5)=PA(5)*CON
      PA(6)=PA(6)*CON
      PA(7)=PA(7)*CON
      PA(8)=PA(8)*100000.
      PA(9)=PA(9)*100000.
C --- ALLOWING FOR 10**5 FOR GAUSS TO GAMMAS AND 10**-6 TO EMU/CC
      PA(10)=PA(10)/10.
      MCOUNT=0
3500  CONTINUE
      ICOUNT=0
      NCOUNT=0
      LAMDA=XLAM
      SUMT=1.0E30
```

```
C ---  WRITE INPUT PARAMETERS
      CALL PARAM
      WRITE(6,7008)
7008  FORMAT("0","ANOMALY FIELD")
      DO 7009 JF=JS,JE
7009  WRITE(6,9003) (ANOM(IF,JF),IF=IS,IE)
8000  CONTINUE
      MCOUNT=MCOUNT+1
      DO 8100 I=1,10
8100  N(I)=MI(I)
C ---  START OF ITERATION
5000  CONTINUE
      IF(LCON.EQ.0) GO TO 6155
C ---  TEST FOR CONSTRAINTS
      DO 6150 I=3,4
      IF(PA(I).GE.PMIN(I)) GO TO 6150
      PA(I)=PMIN(I)
      N(I)=0
      WRITE(6,6151) I
6151  FORMAT("0","PARAMETER",I4," CONSTRAINED AT MINIMUM")
6150  CONTINUE
      DO 6152 I=3,4
      IF(PA(I).LE.PMAX(I)) GO TO 6152
      PA(I)=PMAX(I)
      N(I)=0
      WRITE(6,6153) I
6153  FORMAT("0","PARAMETER",I4," CONSTRAINED AT MAXIMUM")
6152  CONTINUE
6155  CONTINUE
      JCOUNT=0
C ---  CALCULATE EXPRESSIONS INDEPENDENT OF X,Y
4000  CONTINUE
      NCOUNT=NCOUNT+1
      DO=DO-PA(7)
      S1=SIN(IO)
      S2=SIN(DO)
      S3=SIN(PA(5))
      S4=SIN(PA(6))
      C1=COS(IO)
      C2=COS(DO)
      C3=COS(PA(5))
      C4=COS(PA(6))
      ALL=C1*C2*C3*C4
      AMM=C1*S2*C3*S4
      ANN=S1*S3
      A12=C1*C3*(C4*S2+S4*C2)
      A23=(C3*S4*S1+S3*C1*S2)/2.
      A31=(C3*C4*S1+S3*C1*C2)/2.
      THOS=SIN(PA(7))
      THOC=COS(PA(7))
      D19=-S3*C1*C4*S2-S3*C1*S4*C2
      D20=-S3*S4*S1+C3*C1*S2
      D21=-S3*C4*S1+C3*C1*C2
      D22=-C1*C2*S3*C4
      D23=-S3*C1*S4*S2
```

```
      D24=C3*S1
      D25=-C3*C1*S4*S1+C3*C1*C4*C2
      D26=C3*C4*S1
      D27=-C3*S4*S1
      D28=-C3*S4*C1*C2
      D29=C3*C4*C1*S2
      D31=-THOC
      D32=-THOS
      D33=THOS
      D34=-THOC
C ---  ZERO MATRIX AND VECTOR FOR NORMAL EQUATIONS
      DO 2000 I=1,10
      DO 2000 J=1,10
2000  SUM(I,J)=0.
      DO 2001 I=1,10
2001  VEC(I)=0.
      SUMSQ=0.
C ---  CALCULATE THEORETICAL FIELD AND DERIVATIVES ---
      DO 6000 IF=IS,IE
      DO 6000 JF=JS,JE
      X=DELT*(IF-1)
      Y=DELT*(JF-1)
      XP=(Y-PA(9))*THOS+(X-PA(8))*THOC
      YP=(Y-PA(9))*THOC-(X-PA(8))*THOS
      AU=PA(1)-XP
      AL=-PA(1)-XP
      BU=PA(2)-YP
      BL=-PA(2)-YP
C ---  EACH CALCULATION IS BROKEN UP INTO SIMPLE SECTIONS ---
      DO 100 J=1,8
      IF(J.GT.1) GO TO 10
      A=AU
      B=BU
      H=PA(3)
      GO TO 80
10    IF(J.GT.2) GO TO 20
      A=AL
      B=BU
      H=PA(3)
      GO TO 80
20    IF(J.GT.3) GO TO 30
      A=AU
      B=BL
      H=PA(3)
      GO TO 80
30    IF(J.GT.4) GO TO 40
      A=AL
      B=BL
      H=PA(3)
      GO TO 80
40    IF(J.GT.5) GO TO 50
      A=AU
      B=BU
      H=PA(4)
      GO TO 80
```

```
50      IF(J.GT.6) GO TO 60
        A=AL
        B=BU
        H=PA(4)
        GO TO 80
60      IF(J.GT.7) GO TO 70
        A=AU
        B=BL
        H=PA(4)
        GO TO 80
70      A=AL
        B=BL
        H=PA(4)
80      CONTINUE
        P1(J)=T1(A,B,H)
        P2(J)=T2(A,B)
        P3(J)=T3(A,B,H)
        P4(J)=T4(A,B,H)
        P5(J)=P1(J)*H
        P6(J)=P1(J)+H
        P7(J)=P3(J)+P5(J)
        P8(J)=P4(J)+P5(J)
        F1(J)=ALOG((P1(J)-A)/(P1(J)+A))
        F2(J)=ALOG((P1(J)-B)/(P1(J)+B))
        F3(J)=ALOG(P1(J)+H)
        F4(J)=ATAN(P2(J)/P7(J))
        F5(J)=ATAN(P2(J)/P8(J))
        F6(J)=ATAN(P2(J)/P5(J))
        IF(NCOUNT.EQ.LIMIT) GO TO 100
        D1=-2./P1(J)
        D2=2.*P2(J)/(P1(J)*P3(J))
        D3=A/(P1(J)*P6(J))
        D4=(B*P7(J)-2.*A*A*B-A*A*B*H/P1(J))/(P7(J)*P7(J)+P2(J)*P2(J))
        D5=(B*P8(J)-A*A*B*H/P1(J))/(P8(J)*P8(J)+P2(J)*P2(J))
        D6=(B*P5(J)-A*A*B*H/P1(J))/(P5(J)*P5(J)+P2(J)*P2(J))
        D7=2.*P2(J)/(P1(J)*P4(J))
        D8=D1
        D9=B/(P1(J)*P6(J))
        D10=(A*P7(J)-A*B*B*H/P1(J))/(P7(J)*P7(J)+P2(J)*P2(J))
        D11=(A*P8(J)-2.*A*B*B-A*B*B*H/P1(J))/(P8(J)*P8(J)+P2(J)*P2(J))
        D12=(A*P5(J)-A*B*B*H/P1(J))/(P5(J)*P5(J)+P2(J)*P2(J))
        D13=2.*A*H/(P1(J)*P4(J))
        D14=2.*B*H/(P1(J)*P3(J))
        D15=1./P1(J)
        D16=-P2(J)*(H*H/P1(J)+P1(J)+2.*H)/(P7(J)*P7(J)+P2(J)*P2(J))
        D17=-P2(J)*(H*H/P1(J)+P1(J)+2.*H)/(P8(J)*P8(J)+P2(J)*P2(J))
        D18=-P2(J)*(H*H/P1(J)+P1(J))/(P5(J)*P5(J)+P2(J)*P2(J))
        E(J)=A23*D1+A31*D2-A12*D3-ALL*D4-AMM*D5+ANN*D6
        E(J+8)=A23*D7+A31*D8-A12*D9-ALL*D10-AMM*D11+ANN*D12
        E(J+16)=A23*D13+A31*D14-A12*D15-ALL*D16-AMM*D17+ANN*D18
100     CONTINUE
C --- INITIALLY ZERO Q(I), TO USE CONTROL PARAMETERS.---
        DO 101 I=1,10
101     Q(I)=0.
        C1=F1(1)-F1(2)-F1(3)+F1(4)-F1(5)+F1(6)+F1(7)-F1(8)
```

```
      C2=F2(1)-F2(2)-F2(3)+F2(4)-F2(5)+F2(6)+F2(7)-F2(8)
      C3=F3(1)-F3(2)-F3(3)+F3(4)-F3(5)+F3(6)+F3(7)-F3(8)
      C4=F4(1)-F4(2)-F4(3)+F4(4)-F4(5)+F4(6)+F4(7)-F4(8)
      C5=F5(1)-F5(2)-F5(3)+F5(4)-F5(5)+F5(6)+F5(7)-F5(8)
      C6=F6(1)-F6(2)-F6(3)+F6(4)-F6(5)+F6(6)+F6(7)-F6(8)
      FIELD(IF,JF)=(A23*C1+A31*C2-A12*C3-ALL*C4-AMM*C5+ANN*C6)*PA(10)
      IF(NCOUNT.EQ.LIMIT) GO TO 210
  110 IF(N(1).EQ.0) GO TO 111
      Q(1)=(E(1)+E(2)-E(3)-E(4)-E(5)-E(6)+E(7)+E(8))*PA(10)
  111 IF(N(2).EQ.0) GO TO 112
      Q(2)=(E(9)-E(10)+E(11)-E(12)-E(13)+E(14)-E(15)+E(16))*PA(10)
  112 IF(N(3).EQ.0) GO TO 113
      Q(3)=(E(17)-E(18)-E(19)+E(20))*PA(10)
  113 IF(N(4).EQ.0) GO TO 114
      Q(4)=(-E(21)+E(22)+E(23)-E(24))*PA(10)
  114 IF(N(5).EQ.0) GO TO 115
      Q(5)=(D20*C1/2.+D21*C2/2.-D19*C3-D22*C4-D23*C5+D24*C6)*PA(10)
  115 IF(N(6).EQ.0) GO TO 116
      Q(6)=(D26*C1/2.+D27*C2/2.-D25*C3-D28*C4-D29*C5)*PA(10)
  116 CONTINUE
      D35=(-E(1)+E(2)+E(3)-E(4)+E(5)-E(6)-E(7)+E(8))*PA(10)
      D36=(-E(9)+E(10)+E(11)-E(12)+E(13)-E(14)-E(15)+E(16))*PA(10)
  117 IF(N(7).EQ.0) GO TO 118
      Q(7)=D35*YP-D36*XP
  118 IF(N(8).EQ.0) GO TO 119
      Q(8)=D35*D34+D36*D33
  119 IF(N(9).EQ.0) GO TO 120
      Q(9)=D35*D32+D36*D31
  120 IF(N(10).EQ.0) GO TO 121
      Q(10)=FIELD(IF,JF)/PA(10)
  121 CONTINUE
C --- SET UP MATRIX AND VECTOR FOR NORMAL EQUATIONS
      DO 200 I=1,10
      DO 200 J=1,I
      DPL=0.
      IF(J.EQ.I) DPL=1.
      SUM(I,J)=SUM(I,J)+Q(I)*Q(J)*(1.+DPL*LAMDA)
      SUM(J,I)=SUM(I,J)
  200 CONTINUE
  210 CONTINUE
      DIFF=FIELD(IF,JF)-ANOM(IF,JF)
      DO 300 J=1,10
      VEC(J)=VEC(J)-Q(J)*DIFF
  300 CONTINUE
      SUMSQ=SUMSQ+DIFF*DIFF
 6000 CONTINUE
      WRITE(6,6002) SUMSQ
 6002 FORMAT("0","SUM OF SQUARES     ",E16.7)
      IF(JCOUNT.EQ.1) GO TO 6005
      WRITE(6,6004)
 6004 FORMAT("0","MODEL FIELD")
      DO 6003 JF=JS,JE
 6003 WRITE(6,9003) (FIELD(IF,JF),IF=IS,IE)
 9003 FORMAT(" ",10G12.5)
C ---  TEST FOR SQUARES REDUCTION
```

```
      IF(SUMSQ.GE.SUMT) GO TO 9500
      WRITE(6,7010) (N(I),I=1,10)
 7010 FORMAT("0","PARAMETER CHANGES  ",10I2)
      IF(ICOUNT.EQ.0) GO TO 6005
      IF(NOTEST.NE.0) GO TO 6005
C --- TESTS FOR CONVERGENCE OF PARAMETERS
      UNDER=5.0E-02
      UNDER=1.0E-2
      DO 6200 I=1,10
      TEMP=ABS(STORE(I)/PA(I))
      IF(TEMP.LE.UNDER) N(I)=0
 6200 CONTINUE
 6005 CONTINUE
      SUMT=SUMSQ
      IF(NCOUNT.NE.LIMIT) GO TO 6010
      WRITE(6,6006)
 6006 FORMAT("0","ITERATION LIMIT REACHED")
      GO TO 9001
 6010 CONTINUE
      DO 5001 J=1,10
      IF(N(J).NE.0) GO TO 5002
 5001 CONTINUE
      IF(MCOUNT.EQ.LREP) GO TO 9001
      GO TO  3500
 5002 CONTINUE
      CALL LNEQ
C --- MODIFY INITIAL VALUES ---
      DO 6050 I=1,10
 6050 PA(I)=PA(I)+VEC(I)
      DO 6100 I=1,10
 6100 STORE(I)=VEC(I)
      ICOUNT=1
      WRITE(6,6998)
 6998 FORMAT("0","-------------------------------------------------")
      WRITE(6,6999)
 6999 FORMAT("0","SOLUTION FOLLOWS")
C ---  WRITE OUTPUT PARAMETERS
      CALL PARAM
      IF(PA(1).LE.0.) GO TO 990
      IF(PA(2).LE.0.) GO TO 990
      IF(PA(3).LE.0.) GO TO 990
      IF(PA(4).LE.0.) GO TO 990
      IF(PA(4).LE.PA(3)) GO TO 990
      LAMDA=LAMDA*0.8
      GO TO 5000
 9500 CONTINUE
      WRITE(6,9501)
 9501 FORMAT("0","SUM OF SQUARES NOT DECREASED")
C ---  RETURN TO PREVIOUS CONSTANTS
      DO 9502 I=1,10
 9502 PA(I)=PA(I)-STORE(I)
C --- INCREASE LAMDA
      LAMDA=LAMDA/0.64
      JCOUNT=1
      IF(NCOUNT.NE.LIMIT) GO TO 4000
```

```
      WRITE(6,9510)
9510  FORMAT("0","NO CONVERGENCE AT ITERATION LIMIT")
      GO TO 9001
990   WRITE(6,991)
991   FORMAT("0","INVALID RESULT")
9001  CONTINUE
      WRITE(6,9005)
9005  FORMAT("0","FINAL ERRORS")
      DO 9002 JF=JS,JE
      DO 9002 IF=IS,IE
9002  FIELD(IF,JF)=ANOM(IF,JF)-FIELD(IF,JF)
      DO 9004 JF=JS,JE
9004  WRITE(6,9003) (FIELD(IF,JF),IF=IS,IE)
      IF(BASE.LT.TOP) GO TO 3005
999   WRITE(6,998)
998   FORMAT("0","END OF EXECUTION")
      STOP
      END
```

```
      SUBROUTINE SUBM(I,J)
      COMMON/SOLVE/ A(10,10),W(10),IR(10),IC(10)
      MA=10
      NA=10
      I=0
      J=0
      TEST=0.0
      DO 5 K=1,MA
      IF(IR(K).NE.0) GO TO 5
      DO 4 L=1,NA
      IF(IC(L).NE.0) GO TO 4
      X=ABS(A(K,L))
      IF(X.LT.TEST) GO TO 4
      I=K
      J=L
      TEST=X
4     CONTINUE
5     CONTINUE
      RETURN
      END
```

```
      SUBROUTINE LNEQ
      COMMON/SOLVE/ A(10,10),W(10),IR(10),IC(10)
      MA=10
      R=MA
      S=0.
      DET=1.0
      DO 2 K=1,MA
      IR(K)=0
2     IC(K)=0
3     CALL SUBM(I,J)
      PIV=A(I,J)
      DET=PIV*DET
      IF(PIV.EQ.0.0) GO TO 16
      IR(I)=J
      IC(J)=I
      PIV=1.0/PIV
      DO6 K=1,MA
6     A(I,K)=A(I,K)*PIV
      W(I)=W(I)*PIV
      DO 10 L=1,MA
      IF(IC(L).NE.0) GO TO 10
      PIV1=A(I,L)
      DO 9 K=1,MA
9     IF(K.NE.I) A(K,L)=A(K,L)-PIV1*A(K,J)
10    CONTINUE
      PIV2=W(I)
      DO 12 K=1,MA
12    IF(K.NE.I) W(K)=W(K)-PIV2*A(K,J)
      S=S+1.
      IF(S.LT.R)GO TO 3
      DO 15 J=1,MA
      K=IC(J)
      L=IR(J)
      IF(K.EQ.J) GO TO 15
      TEMP=W(J)
      W(J)=W(K)
      W(K)=TEMP
      IC(L)=K
      IR(K)=L
      DET=-DET
15    CONTINUE
16    A(1,1)=DET
      RETURN
      END
```

```
      SUBROUTINE PARAM
C --- WRITE INPUT/OUTPUT ---
      COMMON PA(10),SYMBOL(80),CON
      REAL IM
      AX=PA(1)/100000.
      BY=PA(2)/100000.
      HU=PA(3)/100000.
      HL=PA(4)/100000.
      IM=PA(5)/CON
      DM=PA(6)/CON
      THO=PA(7)/CON
      XO=PA(8)/100000.
      YO=PA(9)/100000.
      AIP=PA(10)*10.
      TAX=2.*AX
      TBY=2.*BY
      WRITE(6,7001) (SYMBOL(I),I=1,80)
7001  FORMAT("1",80A1)
      WRITE(6,7002) XO,YO
7002  FORMAT("0","COORDINATES OF CENTRE OF BLOCK  XO=",G13.6," YO=",
     1G13.6)
      WRITE(6,7003) TAX,TBY
7003  FORMAT("0","LATERAL EXTENT,  X ",G13.6," Y ",G13.6)
      ITHO=INT(THO/360.)
      THO=THO-ITHO*360.
      WRITE(6,7004) THO
7004  FORMAT("0","ANGLE FROM GRID X-AXIS TO BLOC X-AXIS ",F6.1,
     1" DEGREES")
      WRITE(6,7005) HU,HL
7005  FORMAT("0"," TOP ",G13.6,10X," BASE ",G13.6)
      WRITE(6,7006) AIP
7006  FORMAT("0","POLARIZATION ",F10.3,"*(10**-6) EMU/CC")
      IDM=INT(DM/360.)
      DDM=DM-IDM*360.
      DDM=DDM+THO
      WRITE(6,7007) IM,DDM
7007  FORMAT("0","INCLINATION ",F6.0," DEGREES",5X,"DECLINATION ",F6.0,
     1" DEGREES")
      RETURN
      END
```

PROGRAM "POWER"

1. Identification

Title: Two-dimensional Spectrum Estimation

Programmer: R.L. Coles, using FFT routines by R.G. Agarwal

Date: June 1972

Language: Fortran IV

2. Purpose

To estimate two-dimensional power spectra using Fast Fourier Transforms (FFT) and a data window.

3. Usage

Operational Procedure: The main program reads the input data, calls subroutines in sequence and produces the output. STATS computes the mean and variance of the data, and removes the mean from the data; TAPER applies a data window; TWODIM calculates two-dimensional Fourier coefficients of the modified data, calling GRIDFT and GRMDFS (FFT routines); RAWPOW squares and adds the real and imaginary parts of the coefficients; FILOUT completes the array; SHIFT moves the frequency origin to the centre of the data block; SMOOTH is an optional extra smoothing for improvement of visual plots; NORM calculates the normalizing factor for normalizing to the variance.

Input Parameters:

SYMBOL	Identification title
NN	Spectrum array size
INT	Data array size
DELT	Grid interval (kilometres)
IDC	= 0 Mean removed
	= 1 Mean not removed
ISM	= 0 Additional smoothing applied
	= 1 No smoothing
XP(I,J)	Input data; I, J = 1,INT

Calculated Parameters:

XP(I,J)	Spectral estimate; I,J = 1,NN
FNYQ	Nyquist frequency
VAR	Variance of data
MEAN	Mean of data
FACTOR	Normalization factor

Output:

The input data, spectral estimate, smoothed estimate and logarithm of estimate are printed, with values of array sizes, Nyquist frequency, mean, variance and normalization factor.

4. Comments

The technique used for the Fourier transform is slightly modified from that of Naidu (1970). The data and spectral

array sizes, INT and NN, must be even, NN greater than or equal to INT, and not contain factors greater than 13. The FFT routines of Agarwal (1968) were modified to accommodate extended precision variables; other FFT routines may be used in their place by calling the variables X, Y and NN where X and Y are extended precision variables containing the data on input and the transform on output. An alternative version of the MAIN program (not listed) is available, for sampling the data in smaller blocks and combining to give the resultant spectrum.

5. Input sequence

   1. SYMBOL
   2. NN, INT, DELT, IDC, ISM
   3. XP(I,J)

   Formats as per listing.

6. References

Agarwal, R.G., 1968. Two-dimensional Harmonic Analysis of Potential Fields; unpublished Ph.D. thesis, University of Alberta, Edmonton, 250 p.

Naidu, P.S., 1970. Fourier Transform of Large-scale Aeromagnetic Field using a Modified Version of Fast Fourier Transform; Pure and Applied Geophysics, v.79, no. 4, p. 17-25.

7. Method

   As indicated in Chapter 6.

```
      PROGRAM POWER(INPUT,OUTPUT,TAPE5=INPUT,TAPE6=OUTPUT,TAPE8,TAPE9)
C****** UNIVERSITY OF MANITOBA ******
C****** DEPARTMENT OF EARTH SCIENCES ******
C*** PROGRAMMER R L COLES MARCH 1972
C*** TWODIMENSIONAL POWER SPECTRUM VERSION 2 JUNE 1972
C*** USING FAST FOURIER TRANSFORM (R.G. AGARWAL 1968)
C*** A DATA WINDOW IS APPLIED, AND SQUARES OF MODIFIED HYPER-FOURIER
C*** COEFFICIENTS COMPUTED
C*** NN,NNN DIMENSIONS OF WORKING ARRAY
C*** INT DIMENSIONS OF DATA SAMPLE ARRAY
C*** DELT DATA POINT SPACING
C*** XT WORK ARRAY FOR TRANSFORMS
C*** XP STORAGE ARRAY
C*** X,Y,S WORK VECTORS FOR TRANSFORMS
      DOUBLE PRECISION XT
      COMMON/ARRAY/ XT(84,84)
      COMMON/STORE/ XP(84,84)
      COMMON/CONST/ NN,NNN,NH,NNH,NI,NNI,NJ,NNJ
      DIMENSION SYMBOL(80)
      READ(5,248) (SYMBOL(I),I=1,80)
248   FORMAT(80A1)
      READ(5,20) NN,INT,DELT,IDC,ISM
20    FORMAT(2I4,F8.4,2I4)
      DO 30 J=1,INT
30    READ(9,1234) (XP(I,J),I=1,INT)
2234  FORMAT(15F5.0,5X)
      NNN=NN
      NH=NN/2
      NNH=NNN/2
      NI=NH+1
      NNI=NNH+1
      NJ=NH+2
      NNJ=NNH+2
      WRITE(6,45)
45    FORMAT("0","DATA VALUES",///)
21    FORMAT("0",I4)
      DO 50 J=1,INT
      WRITE(6,21) J
50    WRITE(6,55) (XP(I,J),I=1,INT)
55    FORMAT(" ",10G13.6)
      CALL STATS(IDC,VAR,INT)
      CALL TAPER(INT,INT)
      DO 460 J=1,NNN
      DO 460 I=1,NN
460   XT(I,J)=0.D0
      DO 480 J=1,INT
      DO 480 I=1,INT
      XT(I,J)=XP(I,J)
480   CONTINUE
      CALL TWODIM
      CALL RAWPOW
      DO 550 J=1,NNN
      DO 550 I=1,NN
      XP(I,J)=SNGL(XT(I,J))
550   CONTINUE
```

```
      CALL SHIFT
C  ALLOW FOR DISCRETE D ATA
C  FORM SPECTRAL ESTIMATOR
      MULT=INT*INT
      DO 10 I=1,NN
      DO 10 J=1,NNN
      XP(I,J)=XP(I,J)*DELT*DELT/MULT
10    CONTINUE
      WRITE(6,70)
70    FORMAT("1","POWER SPECTRUM ESTIMATE")
60    FORMAT("0",10(E10.3,2X))
      DO 80 I=1,NN
80    WRITE(6,60) (XP(I,J),J=1,NNN)
      IF(ISM.GT.0) GO TO 81
      CALL SMOOTH
      WRITE(6,300)
300   FORMAT("1","POWER SPECTRUM ESTIMATE - SMOOTHED",///)
      DO 301 J=1,NNN
301   WRITE(6,60) (XP(I,J),I=1,NN)
81    CONTINUE
      CALL NORM(VAR,NN,DELT)
      WRITE(6,120)
120   FORMAT("1","LOG OF POWER SPECTRUM ESTIMATE",///)
      DO 1000 I=1,NN
      DO 1000 J=1,NNN
      IF(XP(I,J).LE.0.) GO TO 99
1000  XP(I,J)=ALOG(XP(I,J))
      DO 1500 J=1,NNN
1500  WRITE(6,1510) (XP(I,J),I=1,NN)
1510  FORMAT("0",20(F5.1,1X))
C
C  WRITE ON ONE MONTH PACK FOR CONTOUR PLOT
      DO 2000 J=1,NNN
2000  WRITE(8,1234) (XP(I,J),I=1,NN)
1234  FORMAT(6G13.6)
C
99    CONTINUE
      FN=1./(2.*DELT)
      WRITE(6,249) (SYMBOL(I),I=1,80)
249   FORMAT("1",80A1)
      WRITE(6,200) DELT,FN
200   FORMAT("0","DELT=",F10.5,2X,"NYQUIST FREQUENCY=",F10.5," CYCLES PE
     *R KM")
      WRITE(6,220) INT,INT
220   FORMAT("0","DATA SAMPLE ARRAY SIZE",I4," BY ",I4)
      WRITE(6,230) NN,NNN
230   FORMAT("0","SPECTRUM ARRAY SIZE",I4," BY ",I4)
      STOP
      END
```

```
      SUBROUTINE STATS(IDC,VAR,NN)
      COMMON/STORE/ XP(84,84)
      REAL MEAN
      MEAN=0.
      IF(IDC.NE.0) GO TO 15
      DO 10 I=1,NN
      DO 10 J=1,NN
      MEAN=MEAN+XP(I,J)
10    CONTINUE
      MEAN=MEAN/FLOAT(NN*NN)
      WRITE(6,12) MEAN
12    FORMAT("1","MEAN OF DATA",G13.6)
      WRITE(6,13)
13    FORMAT("0","DC HAS BEEN REMOVED")
15    CONTINUE
      DO 20 I=1,NN
      DO 20 J=1,NN
      XP(I,J)=XP(I,J)-MEAN
20    CONTINUE
      IF(IDC.NE.0) WRITE(6,21)
21    FORMAT("1","DCHAS NOT BEEN REMOVED")
C***  COMPUTE VARIANCE
      VAR=0.
      DO 30 I=1,NN
      DO 30 J=1,NN
30    VAR=VAR+XP(I,J)*XP(I,J)
      VAR=VAR/FLOAT(NN*NN-1)
      WRITE(6,31) VAR
31    FORMAT("0","VARIANCE OF DATA ",G13.6)
      RETURN
      END
```

```
      SUBROUTINE NORM(VAR,NN,DELT)
      COMMON/STORE/ XP(84,84)
      SUM=0.
      DELTN=DELT*FLOAT(NN)
      DELTNS=DELTN*DELTN
      DO 10 I=1,NN
      DO 10 J=1,NN
10    SUM=SUM+XP(I,J)/DELTNS
C***  THE SPECTRUM ESTIMATE IS NORMALIZED TO THE VARIANCE
      FACTOR=VAR/SUM
      WRITE(6,30) FACTOR
30    FORMAT("0","NORMALIZATION FACTOR ",G13.6)
      RETURN
      END
```

```
      SUBROUTINE TAPEP(NN,NNN)
      COMMON/STORE/ XT(84,84)
      REAL K,L
      T(K,L)=0.5*(1+COS(CX*SQRT(K*K+L*L)))
      PI=3.14159265
      IN=NN/2
      INN=NNN/2
      XN=FLOAT(IN*IN)
      CX=PI/FLOAT(IN)
      DO 120 I=2,IN
      K=FLOAT(IN+1-I)
      XK=K*K
      TX=T(K,0.)
      II=NN-I+2
      XT(I,(INN+1))=XT(I,(INN+1))*TX
      XT(II,(INN+1))=XT(II,(INN+1))*TX
      DO 120 J=2,INN
      JJ=NNN-J+2
      L=FLOAT(INN+1-J)
      IF(I.GT.2) GO TO 110
      XK=L*L
      TY=T(0.,L)
      XT((IN+1),J)=XT((IN+1),J)*TY
      XT((IN+1),JJ)=XT((IN+1),JJ)*TY
  110 CONTINUE
      XK=K*K+L*L
      TXY=T(K,L)
      IF(XK.GE.XN) TXY=0.
      XT(I,J)=XT(I,J)*TXY
      XT(I,JJ)=XT(I,JJ)*TXY
      XT(II,JJ)=XT(II,JJ)*TXY
      XT(II,J)=XT(II,J)*TXY
  120 CONTINUE
      DO 130 I=1,NN
      XT(I,1)=0.
  130 CONTINUE
      DO 135 J=1,NNN
      XT(1,J)=0.
  135 CONTINUE
      RETURN
      END
```

```
      SUBROUTINE TWODIM
      DOUBLE PRECISION XT,X,Y,S
      COMMON/ARRAY/ XT(84,84)
      COMMON/VECT/ X(200),Y(200),S(200)
      COMMON/CONST/ NN,NNN,NH,NNH,NI,NNI,NJ,NNJ
      L=0
C     TRANSFORM J ROWS IN PAIRS
10    CONTINUE
      J=L+1
      JJ=L+2
      DO 15 I=1,NN
      X(I)=XT(I,J)
      Y(I)=XT(I,JJ)
15    CONTINUE
      CALL GR 1D FT(NN)
      CALL GRMDFS(NN)
      XT(1,J)=X(1)
      XT(1,JJ)=Y(1)
      XT(NI,J)=X(NI)
      XT(NI,JJ)=Y(NI)
      DO 20 I=2,NH
      II=NN-I+2
      XT(I,J)=(X(I)+X(II))/2.D0
      XT(II,J)=(Y(I)-Y(II))/2.D0
      S1=(X(I)-X(II))/2.D0
      S2=(Y(I)+Y(II))/2.D0
      XT(I,JJ)=S2
      XT(II,JJ)=-S1
20    CONTINUE
      L=L+2
      NNL=NNN-1
      IF(L.LE.NNL) GO TO 10
C     TRANSFORM I COLUMNS
      DO 25 J=1,NNN
      X(J)=XT(1,J)
      Y(J)=XT(NI,J)
25    CONTINUE
      CALL GR 1D FT(NNN)
      CALL GRMDFS(NNN)
      XT(1,1)=X(1)
      XT(NI,1)=Y(1)
      XT(1,NNI)=X(NNI)
      XT(NI,NNI)=Y(NNI)
      DO 30 J=2,NNH
      JJ=NNN-J+2
      XT(1,J)=(X(J)+X(JJ))/2.D0
      XT(1,JJ)=(Y(J)-Y(JJ))/2.D0
      S1=(X(J)-X(JJ))/2.D0
      S2=(Y(J)+Y(JJ))/2.D0
      XT(NI,J)=S2
      XT(NI,JJ)=-S1
30    CONTINUE
      DO 40 I=2,NH
      II=NN-I+2
      DO 50 J=1,NNN
```

```
      X(J)=XT(I,J)
      Y(J)=XT(II,J)
50    CONTINUE
      CALL GR1D FT(NNN)
      CALL GRMDFS(NNN)
      DO 60 J=1,NNN
      XT(I,J)=X(J)
      XT(II,J)=Y(J)
60    CONTINUE
40    CONTINUE
      RETURN
      END


      SUBROUTINE RAWPOW
      DOUBLE PRECISION X
      COMMON/ARRAY/ X(84,84)
      COMMON/CONST/ NN,NNN,NH,NNH,NI,NNI,NJ,NNJ
C   SQUARE ARRAY
      X(1,1)=X(1,1)*X(1,1)
      X(1,NNI)=X(1,NNI)*X(1,NNI)
      DO 10 J=2,NNH
      X(1,J)=X(1,J)*X(1,J)+X(1,(NNN-J+2))*X(1,(NNN-J+2))
      X(1,(NNN-J+2))=X(1,J)
10    CONTINUE
      X(NI,1)=X(NI,1)*X(NI,1)
      X(NI,NNI)=X(NI,NNI)*X(NI,NNI)
      DO20 J=2,NNH
      X(NI,J)=X(NI,J)*X(NI,J)+X(NI,(NNN-J+2))*X(NI,(NNN-J+2))
      X(NI,(NNN-J+2))=X(NI,J)
20    CONTINUE
      DO 30 I=2,NH
      II=NN-I+2
      DO 30 J=1,NNN
      X(I,J)=X(I,J)*X(I,J)+X(II,J)*X(II,J)
30    CONTINUE
      CALL FILOUT
      RETURN
      END


      SUBROUTINE FILOUT
      DOUBLE PRECISION XT
      COMMON/ARRAY/ XT(84,84)
      COMMON/CONST/ NN,NNN,NH,NNH,NI,NNI,NJ,NNJ
      DO 50 I=2,NH
      NL=NN-I+2
      XT(NL,1)=XT(I,1)
      DO 50 J=2,NNN
      NNL=NNN-J+2
      XT(NL,J)=XT(I,NNL)
50    CONTINUE
      RETURN
      END
```

```
      SUBROUTINE SHIFT
C  SHIFT ARRAY
      COMMON/STORE/ XT(84,84)
      COMMON/CONST/ NN,NNN,NH,NNH,NI,NNI,NJ,NNJ
      DO 40 I=1,NI
      IR=NN-I+1
      IS=NI-I+1
      DO 40 J=1,NNI
      JR=NNH+J-1
      XT(IR,JR)=XT(IS,J)
      IF(J.GT.(NNH-1)) GO TO 40
      XT(IR,J)=XT(IS,(JR+2))
40    CONTINUE
      NG=NH-1
      DO 50 I=1,NG
      NL=NN-I
      XT(I,NNN)=XT(NL,NNN)
      NNM=NNN-1
      DO 50 J=1,NNM
      NNL=NNN-J
      XT(I,J)=XT(NL,NNL)
50    CONTINUE
      RETURN
      END


      SUBROUTINE SMOOTH
C     SMOOTHED ESTIMATE
C     NEGLECT SMOOTHING OF EDGES
      DOUBLE PRECISION XT
      COMMON/ARRAY/ XT(84,84)
      COMMON/STORE/ X(84,84)
      COMMON/CONST/ NN,NNN,NH,NNH,NI,NNI,NJ,NNJ
      IR=1
      IRR=IR+1
      NMI=NN-IR
      IRT=2*IR+1
      MULT=IRT*IRT
      DO 20 J=IRR,NMI
      DO 20 I=IRR,NMI
      XT(I,J)=X(I,J)
      DO 30 K=1,IR
30    XT(I,J)=XT(I,J)+X(I+K,J)+X(I-K,J)
      DO 40 L=1,IR
40    XT(I,J)=XT(I,J)+X(I,J+L)+X(I,J-L)
      DO 50 K=1,IR
      DO 50 L=1,IR
50    XT(I,J)=XT(I,J)+X(I+K,J+L)+X(I+K,J-L)+X(I-K,J-L)+X(I-K,J+L)
      XT(I,J)=XT(I,J)/MULT
20    CONTINUE
      DO 200 J=IRR,NMI
      DO 200 I=IRR,NMI
200   X(I,J)=SNGL(XT(I,J))
      RETURN
      END
```

PROGRAM "PROFIL"

1. Identification

Title: Profiles across two-dimensional spectra, using bicubic splines.

Programmer: R.L. Coles, with some subroutines based on work by M.T. Holroyd.

Date: October 1972

Language: Fortran IV

2. Purpose

To calculate values along profiles across two-dimensional spectra. A facility for reduction to the pole is included.

3. Usage

Operational Procedure: The main program reads the input data, and performs the reduction to the pole, if requested. DERIV calculates the derivatives of the data for each spline cell. MAIN program considers each required data point on the profile in turn, the spline coefficients are calculated by COEFF, and the data point value obtained using Function SPLINE. Profiles may be added and averaged, if requested.

Input Parameters:

SYMBOL	Identification title
NN	Data block size (square)

NQ	Ratio of interpolated interval to grid interval (integral)
FNYQ	Nyquist Frequency
IRED	= 0 for no reduction to the pole
	= 1 for reduction to the pole
GI, GD	Inclination, declination of geomagnetic field clockwise from x-axis
XP(I,J)	Spectral data I,J = 1,NN
PHI	Angle between x-axis and profile (counter-clockwise)
IAV	= 0 no averaging
	= 1 add to previous profile
	= 2 add to previous profile, output averaged profiles and zero store.

Calculated Parameters:

G(I)	Profile data
STORE(I)	Averaged profile data

Output:

Identification, Nyquist frequency, frequency increment. Each profile is listed, with angle identification; each average is listed, with identification.

4. Comments

The purpose of the program in this form is to examine a

two dimensional spectrum in profile form. The spectral values have not been actually determined at the frequency points on these profiles; the assumption of a smooth spectrum is made. This program is readily converted to a general profiling program, by omitting the reduction to the pole and averaging procedures, and adding a facility for variable profile origins.

5. Input sequence

    1. SYMBOL
    2. NN, NQ, FNYQ
    3. IRED, GI, GD
    4. XP(I,J)
    5. PHI, IAV

    Formats as per listing.

6. References:

Holroyd, M.T. and Bhattacharyya, B.K. 1970 Automatic contouring of Geophysical data using bicubic spline interpolation; Geological Survey of Canada, Paper 70-55, 40p.

```
      PROGRAM PROFIL(INPUT,OUTPUT,TAPE5=INPUT,TAPE6=OUTPUT,TAPE9)
C---  PROFILES ACROSS TWO DIMENSIONAL GRIDDED DATA, USING BICUBIC SPLINES
C---  BASED ON WORK BY BHATTACHARYYA AND HOLROYD
      COMMON/BLOCK/ XP(84,44),P(84,44),Q(84,44),S(84,44),A(4,4),
     1G(84),XC(84),XD(84),YX(84),GG1(2),GG2(2),GX1(2),GX2(2),GY1(2),
     2GY2(2),GZ1(2),GZ2(2)
      COMMON/CONST/ NN,NH,NJ,NM
      DIMENSION SYMBOL(80),STORE(84)
      READ(5,1000) (SYMBOL(I),I=1,80)
 1000 FORMAT(80A1)
 1001 FORMAT("1",80A1)
      WRITE(6,1001) (SYMBOL(I),I=1,80)
      READ(5,1002) NN,NQ,FNYQ
 1002 FORMAT(2I4,F8.4)
      READ(5,1003) IRED,GI,GD
 1003 FORMAT(I4,2F8.4)
      NH=NN/2
      NJ=NH+2
      NM=NH-1
      NP=NH*NQ-NQ+1
      DO 1004 J=1,NJ
 1004 READ(9,1234) (XP(I,J),I=1,NN)
 1234 FORMAT(6G13.6)
      CON=3.14156265/180.
      FYNC=FNYQ/NH
      FINC=FYNC/NQ
      WRITE(6,1005) FNYQ
 1005 FORMAT("0","NYQUIST FREQUENCY  ",F10.6)
      WRITE(6,1006) FINC
 1006 FORMAT("0","FREQUENCY INCREMENT  ",F10.6)
      IF(IRED.EQ.0) GO TO 3100
C***  REDUCTION TO THE POLE IN FREQUENCY DOMAIN
      WRITE(6,3001)
 3001 FORMAT("0","SPECTRUM IS REDUCED TO THE POLE")
      GI=GI*CON
      GD=GD*CON
      DL=COS(GI)*COS(GD)
      DM=COS(GI)*SIN(GD)
      DN=SIN(GI)
      DO 3000 KI=2,NH
      K=NH+KI-1
      KK=NH-KI+1
      IK=(KI-1)
      DO 3000 LJ=2,NH
      L=NH+LJ-1
      LL=NH-LJ+1
      JL=(LJ-1)
      R=SQRT(FLOAT(IK*IK+JL*JL))
      DIR=DL*IK/R+DM*JL/R
      FACTOR=DIR*DIR+DN*DN
      REDUCE=FACTOR*FACTOR
      REDUCE=ALOG(REDUCE)
      XP(KK,LL)=XP(KK,LL)-REDUCE
      XP(K,LL)=XP(K,LL)-REDUCE
      IF(L.GT.NJ) GO TO 3000
```

```
      XP(K,L)=XP(K,L)-REDUCE
      XP(KK,L)=XP(KK,L)-REDUCE
3000  CONTINUE
      REDUCE=DL*DL+DN*DN
      REDUCE=ALOG(REDUCE)
      DO 3010 K=1,NN
3010  XP(K,NH)=XP(K,NH)-REDUCE
      REDUCE=DM*DM+DN*DN
      REDUCE=ALOG(REDUCE)
      DO 3020 L=1,NJ
3020  XP(NH,L)=XP(NH,L)-REDUCE
3100  CONTINUE
C---  CALCULATE DERIVATIVES
      CALL DERIV
4000  CONTINUE
      N=0
      DO 4001 I=1,NP
4001  STORE(I)=0.
6000  CONTINUE
      I=NH
      J=NH
      READ(5,6001) PHI,IAV
6001  FORMAT(F8.4,I4)
      PHI=PHI*CON
      CPHI=COS(PHI)
      SPHI=SIN(PHI)
      G(1)=XP(I,J)
      DO 5000 K=2,NP
      KI=K-1
      X=KI*CPHI/NQ
      Y=KI*SPHI/NQ
      XX=FLOAT(I)+X
      IX=INT(XX)
      YY=FLOAT(J)-Y
      JY=INT(YY)
C---  CALCULATE COEFFICIENTS FOR CELL(IX,JY)
      CALL COEFF(IX,JY)
      X=XX-IX
      Y=YY-JY
      G(K)=SPLINE(X,Y,A)
5000  CONTINUE
      PHI=PHI/CON
      WRITE(6,5001)
5001  FORMAT("1","----------------------------------------------------")
      WRITE(6,5002) PHI
5002  FORMAT("0","PROFILE AT  ",F6.0,"  DEGREES COUNTERCLOCKWISE FROM
     1+IX AXIS")
      WRITE(6,5003) (G(I),I=1,NP)
5003  FORMAT(" ",6G13.6)
      IF(IAV.EQ.0) GO TO 4000
      N=N+1
      DO 5004 I=1,NP
5004  STORE(I)=STORE(I)+EXP(G(I))
      IF(IAV.EQ.1) GO TO 6000
      DO 5005 I=1,NP
```

```
      STORE(I)=STORE(I)/FLOAT(N)
      STORE(I)=ALOG(STORE(I))
 5005 CONTINUE
      WRITE(6,5001)
      WRITE(6,5006) N
 5006 FORMAT("0","SIMPLE AVERAGE OF THE PREVIOUS ",I4," PROFILES")
      WRITE(6,5003) (STORE(I),I=1,NP)
      IF(IAV.LT.3) GO TO 4000
 9000 CONTINUE
      STOP
      END

      SUBROUTINE COEFF(IK,JL)
      COMMON/BLOCK/ GP(84,44),P(84,44),Q(84,44),S(84,44),A(4,4),
     1G(84),XC(84),XD(84),YX(84),GG1(2),GG2(2),GX1(2),GX2(2),GY1(2),
     2GY2(2),GZ1(2),GZ2(2)
      COMMON/CONST/ NN,NH,NJ,NM
      J=JL
      JP=JL+1
      DO 27 ID=1,2
      I=IK+ID-1
      GG1(ID)=GP(I,J)
      GX1(ID)=P(I,J)
      GY1(ID)=Q(I,J)
      GZ1(ID)=S(I,J)
      GG2(ID)=GP(I,JP)
      GX2(ID)=P(I,JP)
      GY2(ID)=Q(I,JP)
   27 GZ2(ID)=S(I,JP)
      I=1
      IP=2
      A(1,1)=GG1(I)
      A(2,1)=GX1(I)
      A(1,2)=GY1(I)
      A(2,2)=GZ1(I)
      G1=GG1(IP)-GG1(I)
      G2=GX1(IP)-GX1(I)
      G3=GY1(IP)-GY1(I)
      G4=GZ1(IP)-GZ1(I)
      A(3,1)=3.*G1-(GX1(I+1)+2.*GX1(I))
      A(4,1)=GX1(I+1)+GX1(I)-2.*G1
      A(3,2)=3.*G3-GZ1(I+1)-2.*GZ1(I)
      A(4,2)=(GZ1(I+1)+GZ1(I))-2.*G3
      A(1,3)=3.*(GG2(I)-GG1(I))-(GY2(I)+2.*GY1(I))
      A(2,3)=3.*(GX2(I)-GX1(I))-(GZ2(I)+2.*GZ1(I))
      A(1,4)=GY2(I)+GY1(I)-2.*(GG2(I)-GG1(I))
      A(2,4)=GZ2(I)+GZ1(I)-2.*(GX2(I)-GX1(I))
      P1=GG2(I+1)-GG2(I)-G1+GX1(I)-GX2(I)-G3+GZ1(I)
      P2=GX2(I+1)-GX2(I)-G2-G4
      P3=GY2(I+1)-GY2(I)-G3+GZ1(I)-GZ2(I)
      P4=GZ2(I+1)-GZ2(I)-G4
      A(4,4)=P4-2.*P3-2.*P2+4.*P1
      A(3,3)=9.*P1-3.*P2-3.*P3+P4
      A(4,3)=-P4+2.*P3+3.*P2-6.*P1
      A(3,4)=3.*P3-P4-6.*P1+2.*P2
      RETURN
      END
```

```
      SUBROUTINE DERIV
      COMMON/BLOCK/ GP(84,44),P(84,44),Q(84,44),S(84,44),A(4,4),
     1G(84),XC(84),XD(84),YX(84),GG1(2),GG2(2),GX1(2),GX2(2),GY1(2),
     2GY2(2),GZ1(2),GZ2(2)
      COMMON/CONST/ NN,NH,NJ,NM
      M=NN
      N=NJ
41    CONTINUE
      DO 21 KKK=1,3
      IF(KKK-2)2,3,4
2     L2=N
      LL2=1
      GO TO 5
3     L2=M
      LL2=1
      GO TO 5
4     L2=N
      LL2=N-1
5     DO 21 KK=1,L2,LL2
      IF(KKK-2)6,8,10
6     L1=M
      DO 7 K=1,L1
7     G(K)=GP(K,KK)
      GO TO 12
8     L1=N
      DO 9 K=1,L1
9     G(K)=GP(KK,K)
      GO TO 12
10    L1=M
      DO 11 K=1,L1
11    G(K)=Q(K,KK)
12    XC(1)=0.5
      XD(1)=1.5*(G(2)-G(1))
      IXX=L1-1
      DO 13 K=2,IXX
      KP=K+1
      KM=K-1
      XS=3.0*(G(KP)-G(KM))-XD(KM)
      XC(K)=1.0/(4.0-XC(KM))
13    XD(K)=XS*XC(K)
      XS=3.0*(G(L1)-G(IXX))-XD(IXX)
      XT=2.0-XC(IXX)
      YX(L1)=XS/XT
      K=L1
      DO 14 K1=2,L1
      K=K-1
      KP=K+1
14    YX(K)=XD(K)-XC(K)*YX(KP)
      IF(KKK-2)15,17,19
15    DO 16 K=1,M
16    P(K,KK)=YX(K)
      GO TO 21
17    DO 18 K=1,N
18    Q(KK,K)=YX(K)
      GO TO 21
```

```
 19     DO 20 K=1,M
 20     S(K,KK)=YX(K)
 21     CONTINUE
        IT=N-2
        DO 26 I=1,M
        DO 22 J=1,N
 22     YX(J)=P(I,J)
        XC(2)=0.25
        XD(2)=(3.0*(YX(3)-YX(1))-S(I,1))*0.25
        DO 23 K=3,IT
        KP=K+1
        KM=K-1
        XS=3.0*(YX(KP)-YX(KM))-XD(KM)
        XC(K)=1.0/(4.0-XC(KM))
 23     XD(K)=XS*XC(K)
        IX=N-1
        K=IX
        XS=3.0*(YX(N)-YX(IT))-S(I,N)-XD(IT)
        XT=4.0-XC(IT)
        S(I,IX)=XS/XT
        DO 24 K1=3,IX
        K=K-1
        KP=K+1
 24     S(I,K)=XD(K)-XC(K)*S(I,KP)
 26     CONTINUE
        RETURN
        END


        FUNCTION SPLINE(X,Y,A)
C---
C---    CALC. VALUE OF BICUBIC AT POINT WITHIN SPLINE CELL
C---
        DIMENSION A(4,4),AB(4)
        IF(X.EQ.0.0.AND.Y.EQ.0.0) GO TO 4
        Y2=Y*Y
        Y3=Y2*Y
        IF(X.EQ.0.0) GO TO 2
        X2=X*X
        X3=X2*X
        IF(Y.EQ.0.0) GO TO 3
        DO 1 IY=1,4
 1      AB(IY)=A(IY,1)+A(IY,2)*Y+A(IY,3)*Y2+A(IY,4)*Y3
        SPLINE=AB(1)+AB(2)*X+AB(3)*X2+AB(4)*X3
        RETURN
 2      SPLINE=A(1,1)+A(1,2)*Y+A(1,3)*Y2+A(1,4)*Y3
        RETURN
 3      SPLINE=A(1,1)+A(2,1)*X+A(3,1)*X2+A(4,1)*X3
        RETURN
 4      SPLINE=A(1,1)
        RETURN
        END
```

PROGRAM "SPLINT"

1. Identification

Title: Interpolation of gridded data to finer grid

Programmer: R. L. Coles, based on subroutines by M. T. Holroyd

Date: March 1973

Language: Fortran IV

2. Purpose

To interpolate gridded data to finer grid, on submultiples of basic grid interval.

3. Usage

Operational Procedure: MAIN program reads the input data, and subdivides the basic unit. Derivatives are calculated by DERIV (see PROFIL). The interpolated values are calculated in profiles parallel to the x-axis. Cell coefficients are calculated by COEFF and the interpolated values by SPLINE

Input Parameters:

SYMBOL	Identication title
NN, NJ	X, Y, data array size
NQ	Subdivisor for interpolation (integral)
IX, JY	X, Y interpolated data array size
X, Y	Starting point (origin) for interpolated data

XP(I,J) Input data

Calculated Parameters:

XQ(I,J) Interpolated data

Output:

An alphanumeric display is printed, with the interpolated data and identification title.

4. Comments

The program has been used to interpolate back to original grid after decimation and smoothing.

5. Input sequence

1. SYMBOL
2. NN, NJ, NQ, IX, JY, X, Y
3. XP(I,J)

6. References:

Holroyd, M. T. and Bhattacharyya, B. K. 1970 Automatic contouring of Geophysical data using bicubic spline interpolation; Geological Survey of Canada, Paper 70-55, 40p.

```
      PROGRAM SPLINT(INPUT,OUTPUT,TAPE5=INPUT,TAPE6=OUTPUT,TAPE8,TAPE9)
C---  PROFILES ACROSS TWO DIMENSIONAL GRIDDED DATA, USING BICUBIC SPLINES
C---  BASED ON WORK BY BHATTACHARYYA AND HOLROYD
C---  INTERPOLATION TO FINER GRID
C---
      COMMON/BLOCK/ XP(50,65 ),P(50,65),Q(50,65),S(50,65),A(4,4),
     1G(90),XC(84),XD(84),YX(84),GG1(2),GG2(2),GX1(2),GX2(2),GY1(2),
     2GY2(2),GZ1(2),GZ2(2)
      COMMON/CONST/ NN,NH,NJ,NM
      DIMENSION XQ(86,182)
      DIMENSION SYMBOL(80)
      READ(5,1000) (SYMBOL(I),I=1,80)
 1000 FORMAT(80A1)
 1001 FORMAT("1",80A1)
      WRITE(6,1001) (SYMBOL(I),I=1,80)
      READ(5,1002) NN,NJ,NQ,IX,JY,X,Y
 1002 FORMAT(5I4,2F8.6)
      DO 1004 J=1,NJ
 1004 READ(9,1234) (XP(I,J),I=1,NN)
 1234 FORMAT(6G13.6)
      DO 1010 J=1,NJ
      XP(NN+1,J)=XP(NN,J)+XP(NN,J)-XP(NN-1,J)
 1010 CONTINUE
      NM=NN+1
      DO 1020 I=1,NM
      XP(I,NJ+1)=XP(I,NJ)+XP(I,NJ)-XP(I,NJ-1)
 1020 CONTINUE
C---  SUBDIVISION OF BASIC UNIT
      DINC=1./FLOAT(NQ)
      CALL DERIV
      XX=X
      DO 4000 J=1,JY
      JL=INT(Y)+1
      DO 3000 I=1,IX
      IK=INT(X)+1
      XL=X-INT(X)
      YL=Y-INT(Y)
      CALL COEFF(IK,JL)
      G(I)=SPLINE(XL,YL,A)
      X=X+DINC
 3000 CONTINUE
      DO 3100 I=1,IX
 3100 XQ(I,J)=G(I)
      X=XX
      Y=Y+DINC
 4000 CONTINUE
      DO 5000 J=1,JY
      DO 5100 I=1,IX
      K=XQ(I,J)/100.
 5100 G(I)=SYMBOL(K+10)
      WRITE(6,5150) (G(I),I=1,IX)
 5150 FORMAT(" ",120A1)
 5000 CONTINUE
      DO 5200 J=1,JY
 5200 WRITE(8,1234) (XQ(I,J),I=1,IX)
```

```
      DO 5300 J=1,JY
      WRITE(6,5301) J
 5301 FORMAT(2I4)
 5300 WRITE(6,2234) (XQ(I,J),I=1,IX)
 2234 FORMAT(" ",6G13.6)
      STOP
      END
```

BIBLIOGRAPHY

Agarwal, R.G., 1968. Two-dimensional Harmonic Analysis of Potential Fields, unpublished Ph.D. thesis, University of Alberta.

Artusy, M., 1972. Tunable Active Filter Has Controllable High Q; Electronics, 45, no. 2, 57.

As, J.A., 1967. The A.C. Demagnetization Technique, 221-223, in Collinson et al., 1967.

Baranov, V., 1957. A new method for interpretation of aeromagnetic maps, pseudo-gravimetric anomalies, Geophysics, 22, 359-383.

Baranov, V., and H. Naudy, 1964. Numerical Calculation of the Formula of Reduction to the Magnetic Pole, Geophysics, 29, 67-79.

Bhattacharyya, B.K., 1964. Magnetic Anomalies due to Prism-shaped Bodies with Arbitrary Polarization, Geophysics, 29, no. 4, 517-531.

Bhattacharyya, B.K., and L.W. Morley, 1965. The Delineation of Deep Crustal Magnetic Bodies from Total Field Aeromagnetic Anomalies, J. Geomagn. Geoelectr., 17, no. 3-4, 237-252.

Blackman, R.B., and J.W. Tukey, 1958. The Measurement of Power Spectra, Dover, New York, 190 p.

Brillouin, L., 1956. Science and Information Theory, Academic Press, New York, 320 p.

Brown, H.C., and M.A. Kahn, 1967. Portable apparatus for collecting small oriented cores, 31-35, in Collinson et al., 1967.

Cermak, V., and A.M. Jessop, 1971. Heat Flow, Heat Generation and Crustal Temperature in the Kapuskasing Area of the Canadian Shield, Tectonophysics, 11, 287-303.

Coles, R.L., 1970. A thermomagnetic analysis of rocks (20-700°C): the design and construction of measuring apparatus, and its application to rocks from the Whiteshell area, Manitoba, M.Sc. thesis, University of Manitoba, 85 p.

Collinson, D.W., K.M. Creer, and S.K. Runcorn, 1967. Methods in Paleomagnetism, Proc. of NATO Adv. Study Inst. on Paleomagnetic Methods 1964, Elsevier, New York, 609 p.

Collinson, D.W., 1970. An astatic magnetometer with rotating sample, Geophys. J.R. astr. Soc., 19, no. 5, 547-549.

Creer, K.M., 1959. A.C. demagnetization of unstable Triassic Keuper marls from S.W. England, Geophys. J.R. astr. Soc., 2, 261-275.

Creer, K.M., and M. Sanver, 1967. The use of the Sun Compass, 11-15, in Collinson et al., 1967.

Delury, J.S., 1946. Boundary Area, Southeastern Manitoba, Man. Mines Br., Map 37-4, Winnipeg.

Doell, R.R., and A. Cox, 1967a. Analysis of spinner magnetometer operation, 196-206, in Collinson et al., 1967.

Doell, R.R., and A. Cox, 1967b. Analysis of alternating field demagnetization equipment, 241-253, in Collinson et al., 1967.

Dominion Observatory, 1955, 1965, 1970. Magnetic F charts, Division of Geomagnetism, Earth Physics Branch, Department of Energy, Mines and Resources, Ottawa.

Douglas, R.J.W., 1970. Geology and Economic Minerals of Canada, Economic Geology Report No. 1, Geol. Surv. Canada, 838 p., Vol. 1, Text; Vol. 2, Maps and Charts.

Dunlop, D.J., and G.F. West, 1969. An experimental evaluation of single domain theories, Rev. Geophys., 7, no. 4, 709-757.

Dunlop, D.J., 1973. Superparamagnetic and single-domain threshold sizes in magnetite, J. Geophys. Res., 78, no. 11, 1780-1793.

Dwibedi, K., 1966. Petrology of the English River gneissic belt, Northern Ontario and Southeastern Manitoba, Ph.D. thesis, University of Manitoba.

Erdelyi, A., 1954. Ed. Bateman Manuscript Project - Tables of Integral Transforms, Vol. I and II, 451 p and 391 p.

Ermanovics, I.F., 1971. 'Granites', 'Granite Gneiss' and Tectonic Variation of the Superior Province in Southeastern Manitoba, in 'Geoscience Studies in Manitoba', ed. A.C. Turnock, G.A.C. Special Paper No. 9, 77-81.

Ermanovics, I.F., 1972. Precambrian Geology of the Norway House and Grand Rapids Map-Area, Geol. Surv. Canada, Paper 72-29, 27 p.

Farquharson, R.B., and G.S. Clark, 1971. Rb-Sr Geochronology of Some Granitic Rocks in Southeastern Manitoba, in 'Geoscience Studies in Manitoba', ed. A.C. Turnock, G.A.C. Special Paper No. 9, 111-117.

Fisher, R.A., 1953. Dispersion on a sphere, Proc. Roy. Soc. (London), Ser. A., 217, 295-305.

Fraser, D.C., 1963. Sun chart compass corrections for reconnaissance mapping and geophysical prospecting in areas of magnetic disturbance, Econ. Geol., 58, 131-137.

Frolova, O.M., 1970. Viscous magnetization of magnetite - A structurally sensitive parameter of inhomogeneous grain structure, [English Translation], Akad, Nauk SSSR Izv. Fizika Zemli, no. 2, 113-117.

Geological Survey of Canada, 1967, 1969. Aeromagnetic Maps, Geophysics Papers 7106, 7124, 7301, 7692, 7706.

Haines, G.V., W. Hannaford, and R.P. Riddihough, 1971. Magnetic anomalies over British Columbia and the adjacent Pacific Ocean, Can. J. Earth Sci., 8, 387-391.

Hajnal, Z., 1970. A continuous deep crustal seismic refraction and near-vertical reflection profile in the Canadian Shield interpreted by digital processing techniques, Ph.D. thesis, University of Manitoba.

Hall, D.H., 1968. Regional magnetic anomalies, magnetic units, and crustal structure in the Kenora District of Ontario, Can. J. Earth Sci., 5, 1277-1296.

Hall, D.H., and Z. Hajnal, 1969. Crustal structure of Northwestern Ontario: Refraction Seismology, Can. J. Earth Sci., 6, 81-99.

Hall, D.H., and P. Dagley, 1970. Regional magnetic anomalies: An analysis of the smoothed aeromagnetic map of Great Britain and Northern Ireland; Inst. Geol. Sci. London, Rept. 70/10.

Hall, D.H., 1971. Geophysical determination of deep crustal structure in Manitoba in 'Geoscience Studies in Manitoba', ed. A.C. Turnock, G.A.C. Special Paper No. 9, 83-88.

Hall, D.H., and Z. Hajnal, 1973. Deep seismic crustal studies in Manitoba, Bull. Seism. Soc. Amer., 63, 885-910.

Hall, D.H., 1973. Long-wavelength anomalies - magnetizations in the lower crustal layer; to be presented at the Second General Scientific Assembly of the International Association of Geomagnetism and Aeronomy, Kyoto, Japan, September 1973.

Helsley, C.E., 1967. Advantages of field-drilling of samples for paleomagnetic studies, 31-35, in Collinson et al., 1967.

Holroyd, M.T., and B.K. Bhattacharyya, 1970. Automatic contouring of geophysical data using bicubic spline interpolation, Geol. Surv. Canada, Paper 70-55, 40 p.

IEEE, 1967. Special Issue on the Fast Fourier Transform, IEEE Transactions on Audio and Electroacoustics, AU-15, no. 2.

Irving, E., 1964. Paleomagnetism and its application to geological and geophysical problems, Wiley, New York, 399 p.

Jenkins, G.M., and D.G. Watts, 1968. Spectral Analysis and its Applications, Holden-Day, San Francisco, 525 p.

Johnson, W.W., 1969. A least-squares method of interpreting magnetic anomalies caused by two-dimensional structure, Geophysics, 34, no. 1, 65-74.

Kornik, L.J., 1968. Regional magnetic susceptibility survey in Manitoba and Saskatchewan, Geol. Surv. Canada, Paper 68-18, 18-22.

Krutikhovskaya, Z.A., I.K. Pashkevich, and T.N. Simonenko, 1973. Magnetic anomalies of Precambrian shields and some problems of their geological interpretation, Can. J. Earth Sci., 10, 629-636.

Larochelle, A., and R.F. Black, 1965. The design and testing of an alternating-field demagnetizing apparatus, Can. J. Earth Sci., 2, 684-696.

Larson, E., M. Ozima, M. Ozima, T. Nagata, and D. Strangway, 1969. Stability of remanent magnetization of igneous rocks, Geophys. J.R. astr. Soc., 17, no. 3, 263-292.

Lidiak, E.G., 1973. Relation of magnetic anomalies and rock types for selected areas in the US; abstract, EOS Trans. AGU, 54, no. 4, p. 246.

Marquardt, D.W., 1963. An algorithm for least-squares estimation of non-linear parameters, J. Soc. Indust. Appl. Math., 11, no. 2, 431-441.

McElhinny, M.W., 1966. An improved method for demagnetizing rocks in alternating magnetic fields, Geophys. J.R. astr. Soc., 10, 369-374.

McGrath, P.H., and D.H. Hall, 1969. Crustal structure in Northwestern Ontario: Regional magnetic anomalies, Can. J. Earth Sci., 6, no. 1, 101-107.

McGrath, P.H., and P.J. Hood, 1970. The dipping dyke case - A computer curve-matching method of magnetic interpretation, Geophysics, 35, no. 5, 831-848.

McGrath, P.H., and P.J. Hood, 1973. An automatic least-squares multimodel method for magnetic interpretation, Geophysics, 38, no. 2, 349-358.

McRitchie, W.D., 1971. The petrology and environment of the acidic plutonic rocks of the Wanipigow-Winnipeg Rivers Region, Southeastern Manitoba, in McRitchie and Weber, 1971, 7-61.

McRitchie, W.D., and W. Weber, 1971. Geology and geophysics of the Rice Lake Region, Southeastern Manitoba (Project Pioneer), Manitoba Dept. Mines and Nat. Res. Publ. 71-1, Winnipeg, 430 p.

Molyneux, L., 1970. A complete result magnetometer for measuring the remanent magnetization of rocks, Geophys. J.R. astr. Soc., 24, 429-433.

Morley, L.W., A.S. Maclaren, and B.W. Charbonneau, 1967. Magnetic anomaly map of Canada, Geol. Surv. Canada, Map 1255A, 1:5,000,000.

Mundt, W., 1969. Depth determination of magnetization and density contrasts in the Earth's crust, Phys. Earth Planet. Int., 2, no. 2, 115-122.

Naidu, P.S., 1968. Spectrum of the potential field due to randomly distributed sources, Geophysics, 33, no. 2, 337-345.

Naidu, P.S., 1970. Fourier transform of large scale aeromagnetic field using a modified version of a fast Fourier transform, Pure and Appl. Geophys., 79, 17-25.

Neel, L., 1955. Some theoretical aspects of rock magnetism, Advan. Phys., 4, 191-243.

Noltimier, H.C., 1971. Magnetic rock cylinders with negligible shape anisotropy, J. Geophys. Res., 76, no. 17, 4035-4037.

Ontario Department of Mines, 1971. Ontario Geological Maps 2199, 2201, Toronto.

Opdyke, N., 1967. A large sampling drill, 41-43, in Collinson et al., 1967.

Ozima, M., and E.E. Larson, 1970. Low- and high-temperature oxidation of titanomagnetite in relation to changes in the magnetic properties of submarine basalts, J. Geophys. Res., 75, no. 5, 1003-1017.

Papoulis, A., 1962. The Fourier Integral and its Applications, McGraw-Hill, New York, 318 p.

Pearce, G.W., 1967. Design and Calibration of Apparatus for the Alternating Field Demagnetization of Rocks; M.Sc. thesis, Memorial University of Newfoundland.

Penner, A.P., and G.S. Clark, 1971. Rb-Sr Age Determinations from the Bird River area, Southeastern Manitoba: in 'Geoscience Studies in Manitoba', ed. A.C. Turnock, G.A.C. Special Paper no. 9, 105-109.

Puranen, M., V. Marmo, and V. Hämäläinen, 1968. On the geology, aeromagnetic anomalies and susceptibilities of Precambrian rocks in the Virrat region (Central Finland), Geoexploration, 6, 163-184.

Ramdohr, P., 1969. The Ore Minerals and Their Intergrowths, Pergamon Press, Toronto, 1174 p.

Riddihough, R.P., 1972. Regional magnetic anomalies and geology in Fennoscandia: A discussion, Can. J. Earth Sci., 9, no. 3, 219-232.

Riddihough, R.P., G.V. Haines, and W. Hannaford, 1973. Regional magnetic anomalies of the Canadian Arctic, Can. J. Earth Sci., 10, 157-163.

Roy, A., 1962. Ambiguity in geophysical interpretation, Geophysics, 27, 90-99.

Sax, R.L., 1966. Application of filter theory and information theory to the interpretation of gravity measurements, Geophysics, 31, no. 3, 570-575.

Serson, P.H., and W. Hannaford, 1957. A statistical analysis of magnetic profiles, J. Geophys. Res., 62, 1-17.

Shannon, C.E., 1963. The Mathematical Theory of Communication, University of Illinois Press, Urbana, 117 p.

Sharma, P.V., 1966. Rapid computation of magnetic anomalies and demagnetization effects caused by bodies of arbitrary shape, Pure and Appl. Geophys., 64, 89-109.

Sholpo, L.Y., and V.I. Belokon, 1969. Investigation of the relationship between hysteresis and thermal activation processes of rock magnetization at different temperatures [English Translation], Akad. Nauk SSSR Izv. Fizika Zemli, no. 8, 70-80.

Skeels, D.C., 1947. Ambiguity in gravity interpretation, Geophysics, 12, 43-56.

Snape, C., 1971. An example of anhysteretic moments being produced by A.C. field demagnetization apparatus, Geophys. J., 23, 361-364.

Spector, A., and F.S. Grant, 1970. Statistical models for interpreting aeromagnetic data, Geophysics, 35, no. 2, 293-302.

Springer, G.D., 1952. Geology of the Rennie-West Hawk Lake Area, Man. Mines Br. Publ. 50-6, Winnipeg.

Stacey, F.D., 1963. The physical theory of rock magnetism, Adv. in Phys., 12, 45-133.

Stockwell, C., J. McGlynn, R. Emslie, B. Sanford, A. Norris, J. Donaldson, W. Fahrig, and K. Currie, 1970. Geology of the Canadian Shield, 43-150, in 'Geology and Economic Minerals of Canada', ed. R.J.W. Douglas, Geol. Surv. Canada, Ottawa, 838 p.

Talwani, M., 1965. Computation with the help of a digital computer of magnetic anomalies caused by bodies of arbitrary shape, Geophysics, 30, 797-817.

Tropin, Y.D., and I.M. Belous, 1970. Physical mechanism of magnetic viscosity in multidomain rock grains [English Translation], Akad. Nauk SSSR Izv. Fizika Zemli, no. 2, 67-74.

Turner, F.J., and L.E. Weiss, 1963. Structural Analysis of Metamorphic Tectonites, McGraw-Hill, New York, 545 p.

Ulrych, T.J., 1972. Maximum entropy power spectrum of truncated sinusoids, J. Geophys. Res., 77, no. 8, 1396-1400.

Verhoogen, J., 1959. Origin of thermoremanent magnetism, J. Geophys. Res., 64, 2441-2449.

Wilson, H.D.B., 1971. The Superior Province in the Precambrian of Manitoba, in 'Geoscience Studies in Manitoba', ed. A.C. Turnock, G.A.C. Special Paper No. 9, 41-49.

Wilson, H.D.B., and W.C. Brisbin, 1963. Nature of the granitic crust in the Superior Province, Bull. Geol. Soc., 74, p. 175.

Wilson, R.L., and R. Lomax, 1972. Magnetic remanence related to slow rotation of ferromagnetic material in alternating magnetic fields, Geophys. J., 30, no. 3, 295-303.

Wright, J.V., 1932. Geology and mineral deposits of a part of Southeastern Manitoba, Geol. Surv. Canada Memo. 169.